"COMBINED CONVECTION AND OTHER EFFECTS IN HEAT TRANSFER IN HORIZONTAL FLOWS"

Thesis submitted for the Degree of Doctor of Philosophy

by

Giovanni Sebastiano Barozzi

Department of Mechanical Engineering and Aeronautics

Thermo-fluids Engineering Research Centre

CITY University

SCHOOL OF ENGINEERING

August 1993

ABSTRACT

For many internal flow situations the effect of buoyancy is to cause significant modifications of the internal flow field and heat transfer rate.

The present study focuses on combined forced and free convection under laminar flow conditions in horizontal cylindrical ducts. There, the superposition of secondary, buoyancy induced circulations to the basic forced flow, and the presence of peripheral and axial conduction in the duct wall, give rise to a three-dimensional conjugate heat transfer problem. Such a combined convection feature had not been investigated previously. A novel parallel predictive and experimental study of combined convection for laminar flow in cylindrical ducts is carried out here.

The finite volume code FLOW3D from Harwell is used to treat the fully elliptic three-dimensional thermal-flow problem. The choice derives from a complete and detailed survey of the numerical techniques used in the context of combined convection.

The predictive work relates specifically to a new experimental study, which has the object of obtaining fresh data for combined convection in horizontal duct flow. A 3 m long, 16 mm I.D. copper pipe is used, with uniform peripheral electrical heating. Wall temperature measurements are taken at twelve axial positions. The experiment covers the range of stable mixed convection and strictly laminar flow conditions, with the Reynolds number ranging from 500 to 1000, and the modified Rayleigh number, Ra_q, from $1x10^5$ to $5x10^6$. The scope of the experiment is to provide data for comparison with numerical predictions. These, in turn, are designed to model the experimental conditions very accurately, including, in particular, the effects of peripheral and axial wall conduction.

The study is complemented with various analyses intended to understanding properly both pure forced and natural convection modes. These are investigated separately in the first part of the work.

Overall, this work provides fresh experimental and predictive evidence on various features relevant to the onset and the development of buoyancy induced secondary flows in round ducts under heating conditions. More specifically, the effects of conduction in the duct wall are highlighted, and demonstrated to have a definite influence on wall temperature, and Nusselt number distributions, even in the case of long, thin-walled ducts.

ACKNOWLEDGEMENTS

I would like to express my gratitude to my research supervisor, Prof. Michael W. Collins, from the Mechanical Engineering and Aeronautics Department of City University. He gave initial motivation to the research program, and sustained me with constant advice and encouragement all along the development of the project.

All co-Authors of the papers published in the framework of this Thesis are warmly acknowledged. I take the opportunity for addressing special thanks to Prof. Antonio Carlos M. Sousa, from the Department of Mechanical Engineering, University of New Brunswick, Canada, and to Dr. Enrico Nobile, from the Istituto di Fisica Tecnica, Università di Trieste, Italy, for six years of intense and fruitful cooperation. My present knowledge of numerical techniques is largely due to their internationally recognized competence in that field.

I feel indebted to Prof. Sandro Salvigni, Director of the Istituto di Fisica Tecnica, Università di Bologna, Italy, for permitting the free use of labs and facilities at IFTB.
I wish to extend my appreciation to the administrative and technical staff of that Institute, with a very special mention to Mr. Maurizio Chendi, whose help was providential in more than one critical circumstance, and to Mr. Carlo M. Carlino.

I would like to thank Dr. Stefano Piva, from the Istituto di Fisica Tecnica, Università di Bologna, Italy, for his essential support in both experimental and numerical activities.

Prof. Gian Carlo Pellacani, Dean of the Faculty of Engineering, and Prof. Angelo O. Andrisano, Director of the Istituto di Disegno, Università di Modena, Italy, provided funding for most of the facilities used in the experimental part of the work. Their help is appreciated.

The technical support offered by CINECA, Centro di Calcolo Interuniversitario dell' Italia Nord-Orientale, Casalecchio, Italy, was excellent, and is highly appreciated.
Specifically, I wish to acknowledge the courtesy of Dr. Sanzio Bassini, Responsible for the Visualization Section, Ing. Antonella Guidazzoli, and Dr. Marco Voli. Dr. Chiara Levoni, introduced me to the use of FLOW3D. Her enthusiasm and dedication were of critical importance for me.

The promptness and expertise of the Consultancy Service of AEA Technology, Computational Fluid Dynamics Services, Harwell, UK, has also been appreciated in the course of the numerical activity.

Most of the research funding was from MURST (Ministero dell' Università e della la Ricerca Scientifica e Tecnologica), and C.N.R. (Consiglio Nazionale delle Ricerche) of Italy.

The Thermo-fluids Engineering Research Centre of City University, School of Engineering, also gave partial support.

CINECA Computer Centre made available some free computer time on their CRAY YMP supercomputer.

A final 'Thank You' is due to all my family, for having supported me with their patience and tolerance, during the completion of this work.

DECLARATION

"I grant powers of discretion to the University Librarian to allow this thesis to be copied in whole or in part without further reference to me. This permission covers only copies made for study purposes, subject to normal conditions of acknowledgement."

Signed .....

Date .....29 July 1994.....

CONTENTS

LIST OF TABLES

LIST OF FIGURES

NOMENCLATURE

Dimensional quantities

A	Cross-sectional area of the duct	(m^2)
A_T	Constant in boundary condition eqn.(6.2)	(W/m^2K)
$\boldsymbol{B}$	Buoyancy force	(N/m^3)
B_T	Constant in boundary condition eqn.(6.2)	(-)
$C_{A,B,C,D}$	Coefficients in eqn.(5.15)	
C_T	Constant in boundary condition eqn.(6.2)	(W/m^2)
c	Speed of sound	(m/s)
c_p	Specific heat (fluid)	(J/kgK)
c_{pa}	Specific heat (air)	(J/kgK)
c_{pw}	Specific heat (wall)	(J/kgK)
D	Diameter (circular ducts) [$D = D_h$]	(m)
D_h	Hydraulic diameter $\left[D_h = 4A/\Gamma\right]$	(m)
D_{out}	Outer diameter (circular ducts)	(m)
D_{in}	Inner diameter (circular ducts)	(m)
D_{is}	Outer diameter of insulation(circular ducts)	(m)
$\boldsymbol{g}$	Gravitational acceleration vector	(m/s^2)
g	Gravitational acceleration intensity	(m/s^2)
H	Height (rectangular ducts and cavities)	(m)
h_a	External heat transfer coefficient	(W/Km^2)
h_{fd}	Asymptotic heat transfer coefficient	(W/Km^2)
h_l	Local heat transfer coefficient	(W/Km^2)
h_m	Average heat transfer coefficient (from 0 to z')	(W/Km^2)
h_z	Mean heat transfer coefficient (at z')	(W/Km^2)
I	Electric current	(A)
k, k_f	Thermal conductivity (fluid)	(W/mK)
k_a	Thermal conductivity (air)	(W/mK)
k_i	Thermal conductivity (insulating material)	(W/mK)
k_p	Thermal conductivity (acrylic material)	(W/mK)
k_w	Thermal conductivity (wall)	(W/mK)
L_b	Scale length for buoyancy driven effects [$L_b = D_h$]	(m)
L_f	Scale length for forced flow effects $\left[L_f = D_h\,Re\,Pr\right]$	(m)
L_{ht}	Heat transfer length	(m)
L_{hy}	Hydrodynamic development length	(m)
L_{th}	Thermal entrance length	(m)
$\mathbf{n}'$	Unit vector	(m)
n'	Normal coordinate	(m)

P_o	Reference value for the mean motion pressure over the duct cross-section [$P_o = \mu\alpha Re^2 Pr^2/D_h^2$]	(Pa)
p_o	Reference value for the deviation of the motion pressure from the average [$p_o = \mu\alpha Ra^{1/2}/D_h^2$]	(Pa)
P'_m	Average motion pressure (at z')	(Pa)
p'	Static pressure	(Pa)
p'_o	Reference value for pressure	(Pa)
p'_z	Mean static pressure (at z')	(Pa)
p'_h	Hydrostatic pressure	(Pa)
p'_m	Motion pressure	(Pa)
p'_{mb}	Buoyancy-induced motion pressure	(Pa)
Q_m	Mass flow rate	(kg/s)
$\dot{Q}_{el}$	Electric power	(W)
$\dot{Q}_{lt,is}$	Power loss (heat loss estimate)	(W)
$\dot{Q}_{lt,w}$	Power loss (energy balance estimate)	(W)
$\dot{Q}_w$	Net power input	(W)
q'_{go}	Reference heat dissipation rate	(W/m^3)
q'_g	Volumetric energy generation rate	(W/m^3)
q'_w	Heat flux density (general)	(W/m^2)
q'_{wl}	Local heat flux density	(W/m^2)
q'_{wz}	Mean heat flux density (at z')	(W/m^2)
R_{el}	Electric resistance	(Ω)
$R_{T,i}$	Wall-to-air thermal resistance from z'_{i-1} to z'_i	(mK/W)
$R_{is-a,i}$	Convective thermal resistance from z'_{i-1} to z'_i	(mK/W)
R_{w-is}	Conductive thermal resistance	(mK/W)
r'	Cylindrical radial coordinate	(m)
T'	Fluid temperature	(K)
T'_o	Reference temperature (at z'=0)	(K)
T'_a	Ambient temperature	(K)
T'_c, T'_h	Cold and hot surface temperatures in a differentially heated cavity	(K)
T'_{is}	Outer surface temperature of insulation (at z')	(K)
T'_m, T'_{mz}	Bulk fluid temperature (at z')	(K)
T'_{out}	Outlet fluid temperature	(K)
T'_w	Wall temperature (general)	(K)
T'_{wl}	Local wall temperature	(K)

$T'_{wl,i}$	Local wall temperature (at z'_i)	(K)
T'_{wz}	Mean wall temperature (at z')	(K)
$T'_{wz,i}$	Mean wall temperature (at z'_i)	(K)
$\Delta T'_o$	Reference temperature difference	(K)
	$[\Delta T'_o = T'_w - T'_o]$ (case **T**)	
	$[\Delta T'_o = q'_{wz} D_h/k]$ (case **H**)	
	$[\Delta T'_o = T'_a - T'_o]$ (case **T3**)	
t	Wall thickness	(m)
t'	Time	(s)
t'_o	Time scale $[t'_o = L_b/U_b]$	(s)
U_b	Scale velocity for buoyancy-driven flows	
	$\left[U_b = (g\beta\Delta T_o L_b \alpha/\nu)^{1/2}\right]$	(m/s)
u'	Velocity vector	(m/s)
u'	Cartesian velocity (x-component)	(m/s)
u'_r	Radial velocity component	(m/s)
u'_θ	Tangential velocity component	(m/s)
V	Electric voltage	(V)
v'	Cartesian velocity (y-component)	(m/s)
W	Width (rectangular ducts and cavities)	(m)
w'	Axial velocity	(m/s)
w'_{fd}	Fully developed axial velocity	(m/s)
w'_m	Scale velocity for forced flow; mean velocity at the inlet section (z'=0)	(m/s)
w'_{td}	Thermally developed axial velocity	(m/s)
x', y'	Cartesian cross-stream coordinates	(m)
z'	Axial coordinate	(m)
z'_i	Axial coordinate at station i (i=1÷13)	(m)
α	Thermal diffusivity (fluid) $[\alpha = k/c_p\rho'_o]$	(m^2/s)
α_a	Thermal diffusivity (air) $[\alpha_a = k_a/c_{pa}\rho'_a]$	(m^2/s)
β	Isobaric thermal expansion coefficient (fluid)	(K^{-1})
β_a	Isobaric thermal expansion coefficient (air)	(K^{-1})
Γ	Wetted duct perimeter	(m)
γ	Inclination angle over the horizontal	(rad)
θ	Cylindrical tangential coordinate	(rad)

κ	Temperature-viscosity coefficient $\left[\kappa = -\frac{1}{\mu}\left(\frac{d\mu}{dT'}\right)\right]$	(K^{-1})
μ	Dynamic fluid viscosity	(kg/ms)
μ_m	Dynamic fluid viscosity at bulk fluid temperature	(kg/ms)
μ_w	Dynamic fluid viscosity at wall temperature	(kg/ms)
ν	Kinematic fluid viscosity (fluid)	(m^2/s)
ν_a	Kinematic fluid viscosity (air)	(m^2/s)
ξ'	Dummy axial coordinate	(m)
Ξ	General function for temperature-dependent properties	
ρ'	Density (fluid)	(kg/m^3)
ρ'_o	Reference value for density (at z'=0)	(kg/m^3)
ρ'_a	Density (air)	(kg/m^3)
ρ'_h	Hydrostatic density	(kg/m^3)
ρ'_m	Motion density	(kg/m^3)
ρ'_w	Density (wall)	(kg/m^3)
σ	General diffusion coefficient	
τ'_{wl}	Local wall shear stress	(N/m^2)
τ'_{wm}	Average wall shear stress (from 0 to z')	(N/m^2)
τ'_{wz}	Mean wall shear stress (at z')	(N/m^2)
Φ'	Dissipation function	(m/s^2)
φ'	General variable	
χ	Isothermal compression factor	(Pa^{-1})
ψ'	Stream function	(m^2/s)
ω'	Vorticity	(s^{-1})

Non-dimensional quantities

A_e	Cell-side area in SIMPLE discretization
AR	Aspect ratio (rectangular ducts and cavities)
a_e, a_p, a_{nb}	Influence coefficients in SIMPLE discretization
B	Buoyancy term in SIMPLE discretization
Be	Bergles number $\left[Be = \kappa(T'_w - T'_m)\right]$
Br	Brinkman number $\left[Br = \mu w'_m / k\Delta T'_o\right]$
b	Mass residual in SIMPLE discretization
DR	Diameter ratio (round ducts) $\left[DR = D_{out}/D_{in}\right]$
d_e	Modified influence coefficient in SIMPLE discretization $\left[d_e = A_e/a_e\right]$
f_{app}	Apparent Fanning friction factor $\left[f_{app} = D_h \Delta P'_m / 2z'\rho' w'^2_m\right]$
$f_{app,cp}$	Apparent Fanning friction factor for constant properties
f_m	Length average Fanning friction factor (from 0 to z') $\left[f_m = \tau'_{wm}/(\rho' w'^2_m/2)\right]$
f_z	Mean Fanning friction factor (at z') $\left[f_z = \tau'_{wz}/(\rho' w'^2_m/2)\right]$
Gr	Grashof number $\left[Gr = g\beta\Delta T_o D_h^3/\nu^2\right]$ (general definition) $\left[Gr = g\beta(T'_{wz} - T'_m)D_h^3/\nu^2\right]$ (operative definition for ducts)
Gr_o, Gr_e	Grashof number at inlet/outlet conditions
Gr_c	Grashof number (operative definition for vertical cavities) $\left[Gr_c = \beta g H^3 (T'_h - T'_c)/\nu^2\right]$
Gr_q	Modified Grashof number $\left[Gr_q = g\beta q'_{wz} D_h^4/(k\nu^2)\right]$
Gr_{qo}, Gr_{qe}	Modified Grashof number at inlet/outlet conditions
Gz	Graetz number $\left[Gz = Re\ Pr\ \Gamma/4z'\right]$
K	Wall to fluid conductivity ratio $\left[K = k_w/k_f\right]$
K_d	Momentum flux correction factor
L^*	Heat transfer length $\left[L^* = L_{ht}/D_h\ Re\ Pr\right]$
L^*_{th}	Thermal entrance length
Ma	Mach number $\left[Ma = w'_m/c\right]$
N_A	Non dimensional group $\left[N_A = \beta\Delta T'_o\right]$

N_B	Non dimensional group $\left[N_B = g\rho'\chi L_b\right]$
N_C	Non dimensional group $\left[N_C = g\beta L_b / c_p\right]$
N_D	Non dimensional group $\left[N_D = q_{go}D_h/k\Delta T'_o\right]$
Nu_a	External Nusselt number $\left[Nu_a = h_a D_{is}/k_a\right]$
Nu_l	Local Nusselt number $\left[Nu_l = h_l D_h/k\right]$
Nu_N	Mean Nusselt number for pure natural convection
Nu_m	Length average Nusselt number (from 0 to z') $\left[Nu_m = h_m D_h/k\right]$
$Nu_{z,cp}$	Mean Nusselt number (at z') for constant properties
Nu_z	Mean Nusselt number (at z') $\left[Nu_z = h_z D_h/k\right]$
Nu_{fd}	Asymptotic Nusselt number
$Nu_{fd,cp}$	Asymptotic Nusselt number for constant properties
P	Average motion pressure $\left[P = P'_m/P_o\right]$
Pw	Tube wall parameter $\left[Pw = h_{fd}D^2/k_w t\right]$
Pw^*	Modified tube wall parameter $\left[Pw^* = kD/k_w t\right]$
Pe	Péclet number [Pe = Re Pr]
Pe_o, Pe_e	Péclet number at inlet/outlet conditions
Pr	Prandtl number (fluid) $\left[Pr = \nu/\alpha\right]$
Pr_o, Pr_e	Prandtl number at inlet/outlet conditions
Pr_a	Prandtl number (air) $\left[Pr_a = \nu_a/\alpha_a\right]$
p	Buoyancy-induced motion pressure $\left[p = p'_{mb}/p_o\right]$
p^*	Guessed pressure field in SIMPLE discretization
$\hat{p}$	Pressure correction field in SIMPLE discretization
p_P, p_E	Nodal pressures in SIMPLE discretization
$\hat{p}_P$, $\hat{p}_E$, $\hat{p}_{nb}$	Nodal pressure corrections in SIMPLE discretization
Ra	Rayleigh number $\left[Ra = g\beta\Delta T_o D_h^3/(\alpha\nu)\right]$ (general) $\left[Ra = g\beta\left(T'_{wz} - T'_m\right)D_h^3/(\alpha\nu)\right]$ (operative definition for ducts)
Ra_o, Ra_e	Rayleigh number at inlet/outlet conditions
Ra_a	Rayleigh number (operative definition for horizontal cylinders) $\left[Ra_a = \beta_a g D_{is}^3\left(T'_{is} - T'_a\right)/\alpha_a\nu_a\right]$
Ra_c	Rayleigh number (operative definition for heated vertical cavities) $\left[Ra_c = \beta g H^3\left(T'_h - T'_c\right)/\alpha\nu\right]$

Ra_{c1}, Ra_{c2}	Critical Rayleigh numbers for heated vertical cavities
Ra_q	Modified Rayleigh number $\left[Ra_q = g\beta q'_{wz} D_h^4/(k\alpha\nu)\right]$
Ra_{qo}, Ra_{qe}	Modified Rayleigh number at inlet/outlet conditions
$Ra_{q,ob}$	Critical Ra_q-value for the onset of buoyancy
Re	Reynolds number $\left[Re = w'_m D_h/\nu\right]$
Re_o, Re_e	Reynolds number at inlet/outlet conditions
Re_{cr1}, Re_{cr2}	Critical Reynolds numbers
r	Radial coordinate $\left[r = r'/L_b\right]$
T	Temperature $\left[T = (T' - T'_o)/\Delta T'_o\right]$
T_P, T_{nb}	Nodal temperatures in SIMPLE discretization
t	Time $\left[t = t'/t'_o\right]$
u, v	Cross-stream velocity components (Cartesian coordinates) $\left[u, v = (u', v')/U_b\right]$
u_r, u_θ	Cross-stream velocity components (cylindrical coordinates) $\left[u_r, u_\theta = (u'_r, u'_\theta)/U_b\right]$
$\hat{u}$, $\hat{v}$	Velocity correction field in SIMPLE discretization
u^*, v^*	Guessed velocity field in SIMPLE discretization
u_e, u_w, u_{nb}	Nodal velocities in SIMPLE discretization
v_s, v_n	
$\hat{u}_e$	Nodal velocity correction in SIMPLE discretization
u^*_e	Nodal guessed velocity in SIMPLE discretization
w	Axial velocity $\left[w = w'/w'_m\right]$
w_b	Deviation from fully developed velocity $\left[w_b = w - w_{fd}\right]$
w_{fd}	Fully developed axial velocity
x, y	Cross-stream coordinates $\left[x = x'/L_b\,,\ y = y'/L_b\right]$
z^*	Axial coordinate $\left[z^* = z'/(D_h\,Re\,Pr)\right]$
ξ	Transformed axial coordinate
ρ	Density $\left[\rho = \rho'/\rho'_o\right]$
ψ	Stream function
ω	Vorticity

List of subscripts

A	Integration to be performed over A
nb	Neighbouring grid points of point P in control-volume disctretization
wl	Local value at the duct wall
wz	Mean value at the duct wall (at z')
z'	Integration to be performed up to z'
Γ	Integration to be performed along Γ

COMBINED CONVECTION AND OTHER EFFECTS IN HEAT TRANSFER IN HORIZONTAL FLOWS

CHAPTER 1: INTRODUCTION

1.1 - Generalities of Mixed Convection Flows

The name convection is given to the general category of flows with externally introduced temperature variations.
The two basic modes of convective transport are forced and natural convection, and, generally, transport rates are estimated by considering one of these modes to be dominant. In forced convection flows, the fluid motion is promoted by some external source (e.g. a fan, a blower, a pump or a moving surface/object in an otherwise still fluid). Superimposed temperature gradients do not affect the flow field, apart from the possible effect of temperature-dependent properties. In the absence of significant externally-induced flow, the case may be studied as a pure natural convection, or free convection circumstance. In a flow of this nature, temperature induced density variations constitute the only driving force in the flow. For that reason, natural convection flows are also termed thermogravitational or buoyancy induced flows [1](pp.2-4).

In many cases, the effect of buoyancy is assumed to be negligible in comparison to the forced convection effects, because of the small temperature differences and/or length scales involved. The problem is then treated as a forced convection case, which implies several simplifications, such as the decoupling of the velocity field from the temperature field, other fluid properties, apart from density, being constant. However, in any forced convection flow, temperature differences exist, at least in the boundary region near a heated or cooled surface, and, in the presence of the gravitational field, they necessarily produce buoyancy effects. Thus, in any forced convection circumstance, natural convection effects are also likely to be present. Looked at in this light, mixed convection is the most general case of convection problems, of which pure forced and free convection are only, strictly speaking, limiting cases.
Mixed convection flows are alternatively termed combined free and forced convection flows, buoyancy-affected flows, or viscous-gravitational flows.

From the engineer's standpoint, the important question is how large buoyancy effects are, and under what conditions they may be neglected, compared to the forced convection effects. More specifically, it is the effect on performance parameters, essentially mean heat transfer and friction factor, that is of interest. In turn, if the buoyancy effects are of greater relative magnitude, the question is when forced convection may be neglected. Finally, when the two effects are of comparable order, the question is how to account for both in the prediction of the friction factors and heat transfer coefficients.

Mixed convection processes may either be considered in terms of (a) external flows, ie over surfaces or in free-boundary flows, such as plumes, wakes and buoyant jets, or (b) internal flows in tubes, channels and in enclosed fluid regions. The external flow problems have received much greater attention because of greater simplicity in analysis and in experimentation, as compared to internal flows. However, internal mixed convection flows are of concern in many important engineering applications, and recent years have seen a growing interest in this area of mixed convection.

In this work, attention is specifically focused upon mixed convection in horizontal duct flows.

1.2 - Applications

Mixed convection duct flow is relevant to most engineering applications where fluids are circulated.
Just to mention a few, buoyancy effects are always present in heating, cooling and air conditioning plants, where energy is transferred by the heat carrying fluid through a network of ducts or pipes. Heat exchangers in the chemical, mechanical and food industries very often work in the viscous regime, and are subject to considerable buoyancy effects. A variety of duct geometries and orientations is possible in those applications. Buoyancy effects are also present in heat rejection and energy storage systems.
The cooling of electronic circuitry by means of fans, or through cold plate heat exchangers is always influenced by free convection effects superimposed on the basic forced flow.
Sometimes a slow forced flow is superimposed on the basic free convection mechanism. Examples of this kind are found in the thermal control of huge electronic equipment, such as supercomputers, and in the cooling system of nuclear reactors.

From the above non-exhaustive list, it should be evident that combined free and forced convection in ducts is relevant to a variety of applications. In many of them, buoyancy appears as a modifying effect, in the sense that it simply affects the heat transfer rate intensity, usually improving the forced flow performance. In many circumstances, however, the presence of buoyancy completely changes the flow structure. A well-known example in this class is the occurrence of flow reversal, and transition to turbulence observed with laminar opposing flow in vertical and inclined ducts.

1.3 - Combined Convection Phenomena in Horizontal Duct Flows

Consideration will be given here to mixed convection in straight ducts and pipes, with horizontal or inclined orientation.

The distinctive characteristic of internal flows in those cases is that the buoyancy and pressure forces are not parallel, as they are in the case of vertical ducts, resulting in the loss of symmetry (rotational symmetry for axisymmetric geometries, or about the mid-plane for parallel plate ducts, and so forth). The buoyancy forces generate a secondary cross-flow pattern superimposed on the main flow, whose axial velocity and pressure gradient distributions are thereby modified. For a straight circular tube, the secondary motion is a pair of horizontal helical circulations, while it consists of pairs of counter-rotating longitudinal rolls in the case of parallel-plate ducts. The resulting flow and temperature fields are very complex and three-dimensional in nature, even in the case of laminar flow. Two sample cases are given in Figs.1.1 and 1.2. Streamlines and isotherms on a section of a circular duct are shown in Fig.1.1. The trajectories of two fluid particles in an annular duct are shown in Fig.1.2.

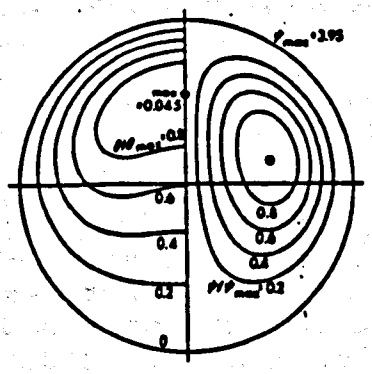

Fig.1.1 - Streamline patterns and isotherms for a circular duct with uniform wall temperature ($z^* = 0.1$; $Ra = 6.25 \times 10^3$) [2]

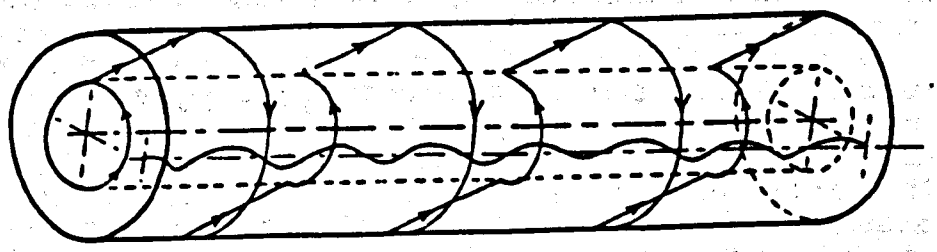

Fig.1.2 - Trajectories of two fluid particles in an annular duct [3]

In terms of the most important engineering parameters - friction factor, Nusselt number, thermal inlet length - the effects of buoyancy may be very pronounced. These effects increase as the relative importance of buoyancy increases compared with the forced flow inertia.

Further effects may superimpose and add complexity to the investigation of this, already complex, thermal and dynamic structure; these are:

- axial diffusion of heat and momentum: theoretical and experimental investigations indicate that axial diffusion of heat and momentum can be important under many circumstances, e.g. for low Re flows, and/or low Pr fluids (see eg [4] and related references);

- wall conduction: in almost all the cases of practical concern, the effect of conduction in the wall is important, and should not be disregarded. Peripheral and axial wall conduction affect the distribution of temperature and heat flux density. The thermal boundary condition at the outer face of the wall is thus transferred in a modified manner to the solid-to-fluid interface, giving rise to a conjugate heat transfer problem (see e.g. [5] and related references);

- viscous dissipation and/or internal heat generation: these effects can also be present and may affect the heat transfer process under special circumstances [4];

- temperature-dependent properties: the density-temperature relationship is usually assumed linear, based on the assumption of small temperature changes, but sometimes non-linear temperature-dependent density must be considered. Water at about 4 °C is a standard example of this kind. The viscosity of liquids changes rapidly with temperature, and its effect interacts with that of density in a complex way. The variations of other fluid properties, such as thermal conductivity and specific heat, are usually assumed to have a minor effect on heat transfer and fluid flow (but note that k increases with about the 0.8 power of the absolute temperature for gases). A complete review, treating either experimental or numerical aspects of variable-property effects, has been given by Bergles [7]. Allen, Collins and Szpiro [8] showed that at first approximation, the effects on Nusselt number were additive;

- compressibility effects: the effect of pressure on density is commonly assumed to be minor, and is overlooked in the analysis of buoyancy induced/affected flows;

- effects of orientation: the inclination of the duct further complicates the consideration of mixed convection flows. Two configurations are possible for inclined ducts, namely: aiding flow, where the axial component of the buoyancy force is in the same direction as the forced flow - this is the case of heating with ascending flow, or cooling with descending flow - and opposing flow, where the buoyancy force is opposite to the forced

flow direction, as in the case of cooling in ascending flow, or heating in descending flow. In both the cases the possibility exists of flow reversal. When buoyancy counteracts the flow, a reduction of the heat transfer rate results, and, possibly, separation occurs. Such an occurrence has been experimentally investigated for vertical ducts, but information relevant to opposing flow in inclined ducts is very limited. Flow reversal is also possible with aiding flow conditions [9];

- non-Newtonian properties: many fluids showing a complex, non-linear shear rate-shear stress relationship are subject to heating/cooling processes in the chemical and food industries. The effects of buoyancy for such fluids are almost completely uninvestigated, particularly for horizontal duct flow conditions;

- turbulence: a firm opinion persists that no substantial thermogravitational effect can occur in turbulent channel flows. However, such effects have now been demonstrated in a number of cases, as a consequence of developing new branches of modern technology, and the increased power densities of the apparatus they use. The interaction between the process of turbulence generation due to the gradients of averaged velocity and the work of buoyancy forces is now the subject of intensive investigation [10].

In the light of the above considerations, it is not surprising that several important issues in mixed convection duct flow still remain widely unexplored, even for the basic case of laminar duct flow in horizontal pipes.
Some of the major issues are:

- Onset of the mixed convection flow regimes: the onset of mixed convection is recognized to depend on the flow geometry, thermal boundary conditions, the Prandtl number, and the relative magnitude of the Grashof and Reynolds numbers. An exhaustive analysis of this is far from complete.

- Limits of the flow regimes: a very important consideration in the study of mixed convection is the determination of the limits of the flow region over which neither forced nor natural convection mechanisms are dominant and both need to be considered. In situations where both free and forced convection are present, an indication of the relative magnitude of the two effects may be obtained from a study of the non-dimensional parameters appearing in the governing equations. However, some situations are encountered where a clear distinction between the two types of flow is difficult to make. This results in a somewhat arbitrary designation of the heat transfer regime boundaries. Metais and Eckert [11] related these to engineering performance, that is where the heat transfer coefficient is 10% higher than the corresponding heat transfer coefficient for either pure free or forced convection. The concept is of practical value, but has no sound basis and leaves unanswered the essential question of the limits of the flow regimes for most flow situations.

- Flow stability and transition: buoyancy also affects the stability and transition to turbulence in a complex and controversial manner. The most important parameters governing the physics of the problem are Grashof (or Rayleigh), Reynolds, and Prandtl numbers. These not only determine the onset and strength of secondary flow, but also the stability of laminar flow, and its transition to turbulence. The possible occurrence of laminar bifurcations is also regulated by those parameters. Bifurcations correspond to the coexistence of two distinct stable solutions for the same thermo-fluid problem. These are respectively obtained by progressively reducing the value of the leading independent group, the Rayleigh number in the present case, starting from a previous solution in the high-Ra range, or by increasing progressively Ra, starting from a low-Ra solution. Bifurcated solutions have been theoretically predicted for various geometries [12], but their existence still remains to be confirmed experimentally.

Other than its practical importance, mixed convection in horizontal ducts is interesting because it represents a typical situation where most of the basic numerical problems are encountered, in connection with a geometrically simple and experimentally documented problem. Whereas in fact the numerical techniques and computational resources available excluded until recently the possibility of predicting either 3D or transient flows, many commercial CFD codes are now available, and new techniques are constantly under development, aimed to handle very complex thermo-fluid problems, including irregular geometries and turbulence. In many cases, however, the declared capabilities of the code are not fully validated, in the sense that the comparison with available experimental/numerical data is limited to very simple flow conditions. The case of laminar mixed convection in horizontal ducts could thus represent a very good reference case for code validation. Some basic combined convection heat transfer cases have been widely investigated, either experimentally or theoretically, and substantial data for heat transfer/fluid flow are now available for a few laminar flows.

From the above, it is quite clear that the prediction of mixed convection flows is a very difficult task. Despite this, there is a great practical need for it. This consideration is at the origin of the great amount of research effort which has been performed through the world, aimed to obtain reliable theoretical predictions of these thermo-fluid problems. It may also be pointed out that no real progress can be achieved on the predictive (numerical) side, without concurrent experimental validation and experience-led direction. So, in this research area, the development of new numerical tools does not tend to offset, but rather to stress the importance of experimentation.

1.4 Objectives and Limitations of the Study

The first purpose of this study is to obtain an updated and, possibly, complete picture of the state of the art in the domain of mixed convection heat transfer in horizontal and inclined ducts. To achieve such a perspective, the literature survey is not restricted

to the case treated later in this study or the parameter range explored numerically and experimentally in it. It is rather directed to give a self-contained presentation of the topic, with no limitation on the duct geometry, the thermal boundary conditions, or the duct orientation. However, for the sake of brevity and coherence, attention is limited to steady laminar flow conditions and excludes non-Newtonian effects, and irregularities in geometry (the presence of internal obstructions, obstacles, and cross-sectional variations). Horizontal and inclined duct flows being the concern of this work, the vertical orientation is not considered. A complete review of that case has been presented in [13].

A second aspect of this study is the analysis of a few thermal effects which may be present in combined convection experiments, and be a source of uncertainty in their interpretation. These have been listed in § 1.3. Of special concern are: (a) axial diffusion of heat and momentum in the fluid; (b) conjugate conduction and convection; (c) the influence of different thermal boundary conditions; (d) the effect of property variations; and (e) the case of purely natural convection, and of purely forced convection, the latter for Newtonian and non-Newtonian fluids.
Here, it is important to stress that the various effects have been isolated in the analysis, so as to obtain a good (qualitative/quantitative) appreciation of their importance in absolute terms. It is obvious that they are all present at a time in real world experience, and must be considered at the best in the prediction practice.

In this part of the work different numerical methods are tried, in combination with Finite Difference, Finite Element, and Finite Volume discretizations.
Past experience in the numerical modelling of mixed convection duct flows is of special concern in this thesis. This is critically reviewed.

From those analyses and observations, the conclusion is drawn that accurate predictions of mixed convection in horizontal duct flow can only be achieved by treating the inherently three-dimensional, and elliptic nature of the problem. The adoption of the computer program FLOW3D Release 3, from Harwell Laboratory, for treating the fully elliptic three-dimensional thermal-flow problem, follows as a direct and natural consequence.
HARWELL-FLOW3D algorithm is based on a Finite Volume Method - FVM - discretization of the governing p.d.e.s', and is particularly suitable for computing fluid flows in three dimensional geometries [14]. The method uses a general non-orthogonal boundary-fitted coordinate system, and, in contrast with most CFD codes, makes use of co-located, i.e. non-staggered, grids, for either the velocity components, or pressure and other scalar variables. The code has a poly-algorithmic structure, in that different solution algorithms can be specified such as SIMPLE [15], and SIMPLE-derived schemes. Various linear algebra solvers are also available for selection.
The program allows the treatment of many of the peculiar aspects that a specific CFD problem may present, such as variable fluid properties, turbulent regimes, and conduction in solid regions.

FLOW3D has been widely used in the prediction of very complex thermal-fluid circumstances (see e.g. [16,17]); however, it has not been applied previously to the case of concern.

Aside from the use of FLOW3D, an original algorithm is also developed for the numerical solution of problems in a three-dimensional feature. Also in this case a FVM discretization is used. However, the method is specifically directed to deal with the numerical solution of incompressible flow problems, when a strong inter-equation coupling exists. This is the case in mixed convection flows, where the momentum and energy equations are coupled through the temperature-dependent buoyancy term in the momentum equations, and the convective terms in the energy equation. As discussed by Galpin and Raithby [18], the treatment of the inter-equation coupling becomes critical for increasing the values of the Rayleigh and Prandtl numbers. In current practice, use is made of segregated algorithms, where the coupling is treated by 'freezing' the coupled terms at the previous iteration. The Symmetrically Coupled Gauss-Seidel - SCGS - algorithm is based on ideas given by Vanka [19]. In this scheme, the variables associated with any single cell in the computational grid are all computed at the same time, using most recently updated values of the discretization coefficients. This allows the stability/convergence constraints of segregated methods to be overcome. Use is also made of a multigrid technique, to improve the convergence and accuracy.

The final use of all the computational work is the direct numerical simulation of the experiment. This is probably the most original part of the work, in that CFD is not simply used *a posteriori*, to compare the experimental outcome with theoretical predictions. It is rather employed as a full part of the experiment itself. In fact, the experiment is numerically simulated in full, on account of the geometrical details of the test section, and the properties of the operating fluid and the duct wall, with the thermal boundary condition applied.

Experimental runs are performed with a purpose built hydraulic loop, in a 3 m long 16 mm I.D. copper pipe, under the uniform heat flux boundary condition. Water is used as the working fluid.

As consequences of this study:
- a clear-cut insight of the present knowledge is obtained for mixed convection in horizontal duct flow;
- a new application is documented for FLOW3D computer code;
- a new numerical algorithm is available and tested, to be extended to more complex situations;
- fresh experimental data on mixed convection through horizontal circular ducts, are presented for the uniform heat flux b.c. Conductive effects in the duct wall are accounted for in the data reduction;
- areas of future development are indicated.

1.5 Outline of this Thesis

A general introduction to buoyancy affected duct flows is given in the present Chapter (Ch.1).

The basic differential equations and boundary conditions are presented in Chapter 2. The mathematical formulation of the problem precedes the literature survey, in this case, rather than following it, as it is usual. This is because it provides the basis for the subsequent subdivision, presentation and discussion of the material. Non-dimensional forms of the equations are derived in this section, and the basic non-dimensional parameters governing the problem defined. It is also important to treat the theory beforehand in that different definitions are found in the literature for the same parameter, an obvious source of confusion. Results from the open literature are presented in a unified and conformal format.

Chapter 3 is dedicated to the literature survey. The main consequences and well established results are collated and presented for the basic duct geometries: circular, parallel plate, and annular duct. When established, limits of laminar stability and transition, onset values for the buoyancy effects, correlations for the inlet length, the friction factors and the Nusselt numbers, are presented and discussed. Areas of future research are indicated. The performance of the numerical methods used to date to tackle mixed convection problems in internal duct flow are reviewed, and their performance discussed. An alternative numerical approach is also presented, based on a non-segregated procedure, which has been devised to deal with the problem of inter-equation coupling at high Ra-values. The performance of the code is demonstrated by various numerical experiments.

Chapter 4 synthesizes the main research information obtained by the candidate in the framework of this Thesis, and already published in Journal or Conference Proceedings. This part of the work is devoted to the analysis of some of the effects, mentioned in Ch.1.3, which may well be present in combined convection, and should either be eliminated beforehand, or accommodated. Specifically, the issues of axial diffusion, conduction conjugate with the convection and variable properties were raised. Some numerical aspects of Control-Volume SIMPLE-like equations are also investigated, with reference to the basic case of natural convection in a differentially heated cavity.
Publications themselves are a part of this Thesis and are presented in Appendix I.

The experimental rig and procedure are described in Chapter 5. The heat transfer section is made with a 16/18 copper pipe, 2.80 m long. It is preceded by an unheated development section, 1.30 m long. Wall temperature values at 12 axial positions are measured by 22 Copper-Constantan thermocouples, welded on the pipe wall. A uniform heat flux boundary condition is provided by six AC-powered electrical resistances. These are helically wired along the heating section. Wall and fluid temperatures, and the flow rate are automatically collected by a computerized data acquisition system. The measuring

procedure and the treatment of data are described, with error estimates. Experimental results are presented for preliminary runs and the final data set.

Chapter 6 describes the algorithms adopted for the numerical solution of the mixed convection problem. The schemes are based on the control volume approach in connection with a primitive-variable formulation of the equations, in their fully elliptic 3D form. Main features, and operative characteristics of HARWELL-FLOW3D CFD code are summarized, with specific reference to the case of concern. Details are only presented as for the treatment of thermal boundary conditions at the wall, and thermal and flow b.c.s' at the inlet/outlet sections. Results of preliminary accuracy tests and grid-refinement experiments are reported.
The geometrical details of the experimental set up are simulated numerically, and the effects of heat conduction in the wall are fully accounted for in the analysis. Numerical predictions are presented for five experimental runs, and results compared with experimental data. Possible sources of disagreement are discussed. The effects of heat conduction in the duct wall under combined convection circumstances are finally demonstrated.

In Chapter 7, the main conclusions of the work are summarized and the perspectives for future research are indicated.

References

1. B. Gebhart, Y. Jaluria, R.L. Mahajan, and B. Sammakia - *'Buoyancy-Induced Flows and Transport'*, Hemisphere pub. Co., Washington D.C., 1988.
2. J-W. Ou, and K.C. Cheng - Natural Convection Effects on Graetz Problem in Horizontal Isothermal Tubes - Int. J. Heat Mass Transfer, 20, 1977; 953-960.
3. A. Mojtabi, and J.- P. Caltagirone - Analyse du Transfert de Chaleur en Convection Mixte Laminaire Entre Deux Cylindres Coaxiaux Horizontaux - Int. J. Heat Mass Transfer, 23, 1980; 1369-1375.
4. R.K. Shah, and A.L. London - *'Laminar Flow Forced Convection in Ducts'*, Supplement 1 - Advances in Heat Transfer, T.J. Irvine, Jr., and J.P. Hartnett, eds., Academic Press, NY, 1978.
5. G.S. Barozzi, G. Pagliarini - A Method to Solve Conjugate Heat Transfer Problems: the Case of Fully Developed Laminar Flow in a Pipe - ASME, J. Heat Transfer, 107, 1985; 77-83.
6. M.W. Collins - Viscous Dissipation Effects on Developing Laminar Flow in Adiabatic and Heated Tubes - Proc. Inst. Mech. Eng., 189 15/75, 1975; 129-137.
7. A.E. Bergles - Prediction of the Effect of Temperature-Dependent Fluid Properties on Laminar Heat Transfer - *and* - Experimental Verification of Analyses and Correlation of the Effects of Temperature-Dependent Fluid Properties on Laminar Heat Transfer - in *'Low Re Number Heat Exchangers'*, S. Kacac, R.K. Shah, and A.E. Bergles, eds., Hemisphere pub. Co., Washington D.C., 1983; 451-486.

8 O. Szpiro, M.W. Collins, and P.H.G. Allen - The Influence of Temperature Dependence of Thermophysical Properties on the Prediction Accuracy in Laminar Mixed Convection Heat Transfer in Vertical Tubes - Procs. '*6th Int. Heat Transfer Conf.*', Toronto, Canada, 1978; Pap. MC-6, 31-36.

9. K.C. Cheng, and S.W. Hong - Combined Free and Forced Laminar Convection in Inclined Tubes - Appl. Sc. Res., 27, sec. A, 1972; 19-38.

10. A.E. Polyakov - Mixed Convection in Single-Phase Flows - in '*Heat Transfer: Soviet Reviews, Convective Heat Transfer*', Vol. 1; O.G. Martynenko, and A.A. Zukauskas, eds., Hemisphere pub.. Co., Washington D.C., 1989; 1-95.

11. B. Metais, and E.R.G. Eckert - Forced, Mixed and Free Convection Regimes - Trans. ASME, J. Heat Transfer, 86, 1964; 295-296.

12. K. Nandakumar, J.H. Masliyah, and H-S. Law - Bifurcation in Steady Laminar Mixed Convection Flow in Horizontal Ducts - J. Fluid Mech., 152,1985; 145-161.

13. J.D. Jackson, M.A. Cotton, and B.P. Axcell - Studies of Mixed Convection in Vertical Tubes - Int. J. Heat and Fluid Flow, 10, 1989; 2-15.

14. A.D. Burns, and N.S. Wilkes - A Finite Difference Method for the Computation of Fluid Flows in Complex Three Dimensional Geometries - Harwell Report AERE-R 12342., Harwell, Oxfordshire, U.K., 1987.

15. S.V. Patankar - '*Numerical Heat Transfer and Fluid Flow*', Hemisphere pub. Co., Washington D.C., 1983.

16. M.W. Collins - Heat Transfer Predictions for Turbulent Flow Downstream of an Abrupt Pipe Expansion - Report HTFS RS477, July 1983.

17. M. Ciofalo, and M.W. Collins - k-ε Predictions of Heat Transfer in Turbulent Recirculating Flows Using an Improved Wall Treatment - Num. Heat Transfer, part B, 15, 1989; 21-47.

18. P.F. Galpin, and G.D. Raithby - Numerical Solution of Problems in Incompressible Fluid Flow: Treatment of the Temperature-Velocity Coupling - Num. Heat Transfer, 10, 1986; 105-129.

19. S.P. Vanka - A Calculation Procedure for Three-Dimensional Steady Recirculating Flows Using Multigrid Methods - Comp. Meth. Appl. Mechanics and Engineering, 55, 1986; 321-338.

CHAPTER 2: **Mathematical Formulation**

2.1 - General Statements and Definitions

The following statements and definitions apply to any combined convection problem in duct flow, once applied to the case of present concern.

General description of the problem

The general features of the thermo-fluid problem are presented. With reference to Fig.2.1, we consider a fluid flowing through a duct, under laminar flow conditions and at a constant mass flow rate, Q_m. The duct is straight, with constant cross-section, A. There is no limitation regarding the shape of the section. Most common shapes are: parallel-planes, rectangular, circular, and annular ducts. Other geometries are however of interest, and are considered in the heat transfer literature (see Ch.3).

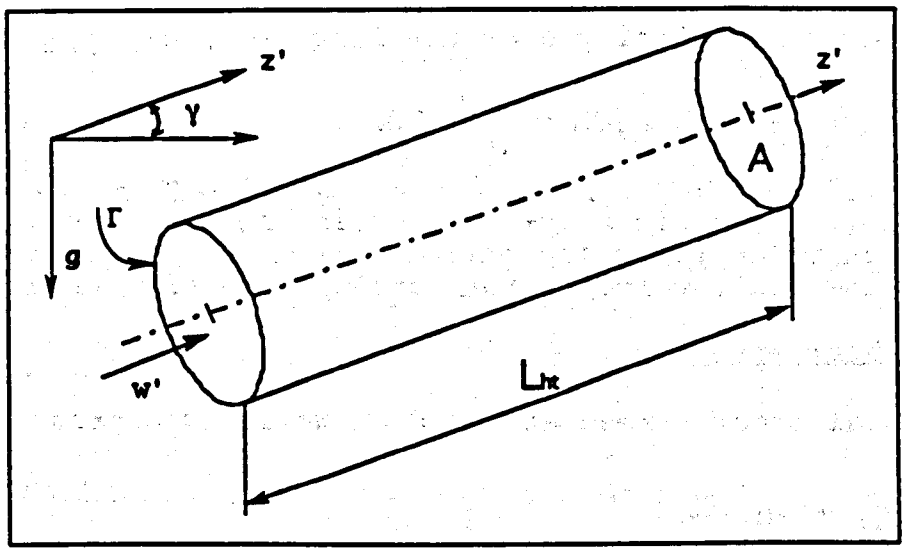

Fig.2.1 - General scheme of the thermo-fluid problem

The fluid interacts with the external environment along the heat transfer length, L_{ht}. This may or may not be preceded and/or followed by an adiabatic calming length, of the same cross-section. The inner duct perimeter is designated as Γ. The axial coordinate is z', and originates at the upstream extremity of the heat transfer length (inlet section). The axial velocity component is designated as w'. Possibly, the duct axis is inclined at an angle γ to the horizontal. Dependent variables for the problem are: density, ρ', velocity, $\mathbf{u}'$, pressure, p', temperature, T'.

Reference conditions

If not otherwise specified, the reference conditions for the fluid are specified at the inlet section, z'= 0, where all the thermodynamic properties of the fluid are assumed uniform:

$$\rho' = \rho'_o$$
$$p' = p'_o \qquad \text{at } z' = 0$$
$$T' = T'_o$$

Hydraulic diameter

The hydraulic diameter is a characteristic length for the geometry of the duct cross-section. It is defined as

$$D_h = 4\frac{A}{\Gamma} \tag{2.1}$$

Mean fluid velocity

The mean axial velocity of the fluid is defined as the integrated average axial velocity over the flow area, A:

$$w'_m = \frac{1}{A}\int_A (\mathbf{u}'.\mathbf{n}')dA = \frac{1}{A}\int_A w'dA \tag{2.2}$$

In eqn.(2.2), $\mathbf{n}'$ is a unit vector in the flow direction.
The mean velocity at the entrance section (z'= 0) is usually assumed to be the scale velocity for forced convection flows.

Wall shear stress

The local shear stress at the duct walls is expressed as

$$\tau'_{wl} = -\mu\left(\frac{\partial w'}{\partial n'}\right)_{wl} \tag{2.3}$$

n' designates the outward normal to the wall.
The axially local wall shear stress is defined as the average wall shear stress with respect to the wetted perimeter of the duct:

$$\tau'_{wz} = \frac{1}{\Gamma}\int_{\Gamma}\tau'_{wl}d\Gamma = -\mu\left(\frac{\partial w'}{\partial n'}\right)_{wz} \qquad (2.4)$$

The flow length average wall shear stress is then defined as

$$\tau'_{wm} = \frac{1}{z'}\int_{o}^{z'}\tau'_{wz}d\xi' \qquad (2.5)$$

where ξ' is a dummy axial variable.

Fanning friction factor

The ratio of wall shear stress to the flow kinetic energy per unit volume is defined as the Fanning friction factor.
The peripheral average, axially local, friction factor is:

$$f_z = \frac{\tau'_{wz}}{\rho' w'^2_m/2} \qquad (2.6)$$

The mean, or flow length average, friction factor is:

$$f_m = \frac{1}{z'}\int_{o}^{z'} f_z d\xi' = \frac{\tau'_{wm}}{\rho' w'^2_m/2} \qquad (2.7)$$

The *apparent* Fanning friction factor is often preferred in engineering applications. This is based on the ratio of the total pressure drop - from the entrance section (z'= 0) to the general axial section at z' - to the flow kinetic energy per unit volume:

$$f_{app}\frac{z'}{D_h/4} = \frac{p'_z - p'_o}{\rho' w'^2_m/2} \qquad (2.8)$$

Mean wall temperature

The general symbol adopted for the wall temperature is T'_w. In the case where this quantity is not uniform, its local value is indicated as T'_{wl}. The peripheral mean wall temperature, T'_{wz}, at an arbitrary cross section z', is then defined as:

$$T'_{wz} = \frac{1}{\Gamma}\int_{\Gamma} T'_{wl}d\Gamma \qquad (2.9)$$

Bulk fluid temperature

The fluid bulk, or mean, temperature, T'_m, at an arbitrary cross

section z', is defined as:

$$T'_m = \frac{\int_A \rho' c_p T' (\mathbf{u}' \cdot \mathbf{n}') dA}{\int_A \rho' c_p (\mathbf{u}' \cdot \mathbf{n}') dA} = \frac{\int_A T' w' dA}{w'_m A} \qquad (2.10)$$

The second equality only holds for constant ρ', and c_p.

Heat transfer coefficient

The local heat transfer coefficient relates the local heat flux density at the wall, q'_{wl}, and the temperature difference $(T'_{wl} - T'_m)$:

$$q'_{wl} = h_l (T'_{wl} - T'_m) \qquad (2.11)$$

The peripherally average, axially local, heat transfer coefficient, h_z, is defined by

$$q'_{wz} = h_z (T'_{wz} - T'_m) \qquad (2.12)$$

The flow length average coefficient, h_m, is the integrated average of h_z from 0 to z':

$$h_m = \frac{1}{z'} \int_0^{z'} h_z d\xi' \qquad (2.13)$$

Nusselt number

The Nusselt number represents the ratio of the convective heat transfer coefficient, to the molecular thermal conductance. The local definition of the Nusselt number for ducts is:

$$Nu_l = \frac{h_l D_h}{k} = \frac{q'_{wl} D_h}{k(T'_{wl} - T'_m)} = \frac{(\partial T'/\partial n')_{wl} D_h}{k(T'_{wl} - T'_m)} \qquad (2.14)$$

The peripheral average local Nusselt number is based on h_z, and is defined as:

$$Nu_z = \frac{h_z D_h}{k} = \frac{q'_{wz} D_h}{k(T'_{wz} - T'_m)} = \frac{(\partial T'/\partial n')_{wz} D_h}{k(T'_{wz} - T'_m)} \qquad (2.15)$$

The mean, or flow length average, Nusselt number is based on h_m, and is defined as

$$Nu_m = \frac{h_m D_h}{k} = \frac{1}{z'} \int_0^{z'} Nu_z d\xi' \qquad (2.16)$$

Non-dimensional axial distance and Graetz number

In the heat transfer literature, the non-dimensional axial distance from the thermal inlet section (z'=0) is defined as

$$z^* = \frac{z'}{D_h \, Re \, Pr} \tag{2.17}$$

This quantity is related to the Graetz number, Gz, defined as:

$$Gz = \frac{Re \, Pr \, \Gamma}{4z'} \tag{2.18}$$

by the equation

$$z^* = \frac{\Gamma}{4 D_h Gz} \tag{2.19}$$

For a circular duct this reduces to:

$$z^* = \frac{\pi}{4Gz} \tag{2.20}$$

Consistently, the non-dimensional heat transfer length is

$$L^* = \frac{L_{ht}}{D_h \, Re \, Pr} \tag{2.21}$$

In the above, Re and Pr respectively are the Reynolds and Prandtl numbers, as defined later.

Hydrodynamic entrance length

For isothermal conditions, the hydrodynamic entrance length, L_{hy}, is defined as the duct length required to achieve a duct section maximum velocity of 99% of the corresponding fully developed magnitude, when the entering flow is uniform. The fully developed velocity profile for this situation is designated as w'_{fd}. This definition can be extended to combined convection circumstances, where the flow development takes place even if the velocity profile is initially fully developed. We indicate the thermally developed profile with w'_{td}.

Thermal entrance length

The thermal entrance length is defined as the duct length required to achieve a value of the local Nusselt number, Nu_z, 5% higher than the asymptotic, fully developed, value, Nu_∞. The non-dimensional

thermal entrance length is expressed as

$$L^*_{th} = \frac{L_{th}}{D_h Pe} \tag{2.22}$$

Reynolds number

For internal duct flows, the Reynolds number is defined as

$$Re = \frac{w'_m D_h}{\nu} \tag{2.23}$$

Prandtl number

The Prandtl number is the ratio of momentum diffusivity to thermal diffusivity of the fluid:

$$Pr = \frac{\nu}{\alpha} = \frac{\mu c_p}{k} \tag{2.24}$$

Péclet number

The Péclet number represents the relative magnitude of the thermal energy convected to the fluid to the thermal energy conducted within the fluid. It is defined as

$$Pe = \frac{w'_m D_h}{\alpha} = Re\, Pr \tag{2.25}$$

Brinkman number

The Brinkman number is the non-dimensional group accounting for the effect of viscous dissipation; it is defined as:

$$Br = \frac{\mu w'_m}{k \Delta T'_o} \tag{2.26}$$

Here, $\Delta T'_o$ designates a characteristic temperature difference for the problem considered.

Grashof number

The Grashof number appears in any natural or combined convection circumstance. Under purely natural convection conditions it represents the ratio of the inertia to the viscous forces.
The general definition that is used here is

$$Gr = \frac{g\beta \Delta T'_o D_h^3}{\nu^2} \tag{2.27}$$

Here, $\Delta T'_o$ designates a characteristic temperature difference for the problem considered.

Rayleigh number

The Rayleigh number appears in any natural or combined convection circumstance. In purely natural convection it represents the ratio of the convective to the conductive terms, in the energy equation. The general definition that is used here is

$$Ra = \frac{g\beta\Delta T'_o D_h^3}{\nu\alpha} = Gr\ Pr \qquad (2.28)$$

Here, $\Delta T'_o$ designates a characteristic temperature difference for the problem considered.

Basic thermal boundary conditions

While the thermal boundary conditions at the walls might assume many different forms, in actual fact only three basic conditions have been considered in the context of combined convection. Conforming to Shah and London's notations [1], these are:

Case **T**: the wall temperature, T'_w, is assigned and uniform.

Case **H**: the heat flux density, q'_w, is assigned at the wall. Usually the averaged value of q'_{w1} over the duct periphery , q'_{wz}, (in other terms the heat supply per unit length) is assumed constant. Two extreme cases are however considered as for the distribution of q'_{w1} along the section contour [2]:
- in case **H1** the peripheral wall temperature is uniform. This corresponds to the extreme case of infinite wall conductivity in the cross-stream direction;
- in case **H2**, the heat flux density is uniform along the periphery of the duct. This corresponds to the case of zero wall conductivity.

The case of finite wall conductivity is obviously closer to the experimental conditions, and is intermediate between the two. Thermal conduction in the duct wall must be considered in this case, giving rise to a conjugate conduction-convection problem. We designate this as case **HCj**.

Case **T3**: the temperature of the external environment, T'_a, and an external heat transfer coefficient (from the wall to the ambient), h_a, are specified. The effect of the thermal resistance of the wall can also be treated in this feature (see [1], pp.23-24). Both h_a and T'_a are usually assumed uniform.

Characteristic temperature difference

The scale temperature difference is indicated as $\Delta T'_o$; its definition differs from case to case, on account of the thermal condition at the wall-boundary. Most common choices are:

Case **T**: $$\Delta T'_o = T'_w - T'_o \tag{2.29}$$

Case **H**: $$\Delta T'_o = \frac{q'_{wz}}{k/D_h} \tag{2.30}$$

Case **T3**: $$\Delta T'_o = T'_a - T'_o \tag{2.31}$$

Temperature differences in eqns.(2.29) and (2.31), and the heat flux density in eqn.(2.30), are assumed to be positive.

2.2 - Basic Conservation Equations

The general equations of fluid transport for buoyancy-induced, or buoyancy-affected flows, are derived from the general equations of fluid mechanics. Without force-producing electrical, magnetic or rotational effects, and for a Newtonian, chemically and physically homogeneous fluid, these are written with vector form notation:

- continuity

$$\frac{\partial \rho'}{\partial t'} + \overline{\nabla}'.(\rho' \mathbf{u}') = 0 \tag{2.32}$$

- momentum

$$\rho' \frac{D\mathbf{u}'}{Dt'} = +\rho' \mathbf{g} - \overline{\nabla}' p' + \mu \overline{\nabla}'^2 \mathbf{u}' + \frac{1}{3} \mu \overline{\nabla}' \left(\overline{\nabla}'. \mathbf{u}'\right) \tag{2.33}$$

- energy

$$\rho' c_p \frac{DT'}{Dt'} = \overline{\nabla}'. \left(k \overline{\nabla}' T'\right) + \beta T' \frac{Dp'}{Dt'} + \mu \Phi' + q'_g \tag{2.34}$$

The following local quantities arise in eqns.(2.32)-(2.34): velocity, $\mathbf{u}'$; absolute temperature, T'; static pressure, p'; gravity acceleration, $\mathbf{g}$; dissipation function, Φ'; volumetric energy generation rate, q'_g. The local fluid properties are: density, ρ', dynamic viscosity, μ, specific heat at constant pressure, c_p, coefficient of thermal expansion, β, and thermal conductivity, k. Viscosity is assumed constant in eqn.(2.33). For the case of variable viscosity, and using the index notation (i, j, k = 1, 2, 3) with Cartesian coordinates, eqn.(2.33) can be expressed [3]:

$$\rho'\left(\frac{\partial u_i'}{\partial t'} + u_j'\frac{\partial u_i'}{\partial x_j'}\right) = +\rho' g_i - \frac{\partial p'}{\partial x_i'} + \frac{\partial}{\partial x_i'}\left(\mu\left(\frac{\partial u_i'}{\partial x_j'} + \frac{\partial u_j'}{\partial x_i'}\right) - \frac{2}{3}\mu\,\delta_{ij}\frac{\partial u_k'}{\partial x_k'}\right) \quad (2.35)$$

The viscous dissipation term, $\mu\Phi'$, in eqn.(2.34) is the volumetric rate of flow energy dissipation into thermal energy. This term is approximately the difference between the total mechanical power input by the stress system and the smaller amount of the total power input that produces thermodynamically reversible effects, such as increases in potential and kinetic energy. As an example, the dissipation function, Φ', is written in orthogonal Cartesian coordinates:

$$\Phi' = 2\left(\left(\frac{\partial u'}{\partial x'}\right)^2 + \left(\frac{\partial v'}{\partial y'}\right)^2 + \left(\frac{\partial w'}{\partial z'}\right)^2\right) + \left(\frac{\partial v'}{\partial x'} + \frac{\partial u'}{\partial y'}\right)^2 + \left(\frac{\partial w'}{\partial y'} + \frac{\partial v'}{\partial z'}\right)^2 + \left(\frac{\partial u'}{\partial z'} + \frac{\partial w'}{\partial x'}\right)^2 - \frac{2}{3}\left(\overline{\nabla'}.\,\mathbf{u}'\right)^2 \quad (2.36)$$

The specific character of the equations governing the flows affected by buoyancy is that the body force per unit volume, $\rho'\mathbf{g}$, is locally changing, and participates in the driving mechanism of the flow. The net body force, or buoyancy force, is expressed [4]

$$\boldsymbol{B} = \mathbf{g}\left(\rho' - \rho_o'\right) \quad (2.37)$$

where, ρ' is the point-variable fluid density, and ρ_o' is the density at some reference level, (p_o', T_o'), which must be properly defined. The buoyancy force $\boldsymbol{B}$ appears in the momentum balance as follows. Assume

$$p' = p_o' + \Delta p_h' + \Delta p_m' \quad (2.38)$$

$$T' = T_o' + \Delta T' \quad (2.39)$$

$$\rho' = \rho_o' + \Delta\rho_h' + \Delta\rho_m' \quad (2.40)$$

where, $\Delta p_m'$, $\Delta T'$, and, $\Delta\rho_m'$, respectively are pressure, temperature, and density variations related to the fluid motion; $\Delta p_h'$, $\Delta\rho_h'$, are the hydrostatic variations of pressure, and density, respectively. These are functions of the vertical coordinate only. With no flow, one therefore has $p' = p_o' + \Delta p_h'$.

The hydrostatic pressure field, $\Delta p_h'$, which would result in a fluid at rest, is given by:

$$\overline{\nabla'}\left(\Delta p_h'\right) = \left(\rho_o' + \Delta\rho_h'\right)\mathbf{g} \quad (2.41)$$

Under condition (2.46)[5] this can be approximated as:

$$\overline{\nabla}'(\Delta p_h') = \rho_o' \mathbf{g} \tag{2.42}$$

The body force and the pressure field terms in eqn.(2.33) are now written as:

$$\rho' \mathbf{g} - \overline{\nabla}' p' = (\rho_o' + \Delta\rho_m')\mathbf{g} - \overline{\nabla}'(p_o' + \Delta p_h' + \Delta p_m') = (\Delta\rho_m')\mathbf{g} - \overline{\nabla}'(\Delta p_m') \tag{2.43}$$

where: $\mathbf{g}(\Delta\rho_m') = (\rho' - \rho_o) = \boldsymbol{B}$; $\overline{\nabla}'(\Delta p') = \overline{\nabla}'(p_m' - p_h')$

and p_h' is the hydrostatic pressure: $p_h' = p_o' + \Delta p_h'$

Denoting now $\Delta p_m'$ with p_m', the motion pressure, eqn.(2.33) becomes:

$$\rho' \frac{D\mathbf{u}}{Dt'} = +\mathbf{g}(\rho' - \rho_o') - \overline{\nabla}' p_m' + \mu \overline{\nabla}'^2 \mathbf{u}' + \frac{1}{3}\mu \overline{\nabla}'(\overline{\nabla}' . \mathbf{u}') \tag{2.44}$$

For the case of pure free convection the necessary conditions for reducing the equation set (2.32), (2.34), (2.44), to the Boussinesq form are [5]:

$$N_A = \beta \Delta T_o' << 1 \tag{2.45}$$

$$N_B = g\rho'\chi L_b << 1 \tag{2.46}$$

$$N_C = g\beta L_b / c_p << 1 \tag{2.47}$$

Here χ is the isothermal compression factor, L_b is a characteristic length for buoyancy effects in the problem of concern, and $\Delta T_o'$ an appropriate temperature difference.
For the case of combined convection in ducts, the standard incompressibility condition for isothermal flows, and conditions for overlooking viscous heating and internal heat generation terms in the energy equation, should be added to conditions (2.45)-(2.47). These respectively are:

$$Ma^2 = \frac{w_m'^2}{c^2} << 1 \tag{2.48}$$

$$Br = \frac{\mu w_m'}{k\Delta T_o'} << 1 \tag{2.49}$$

$$N_D = \frac{q_{go}' D_h}{k\Delta T_o'} << 1 \tag{2.50}$$

Ma designates the Mach number, Br is the Brinkman number; c, and q'_{go}, respectively indicate the sonic speed in the fluid, and a reference quantity for the volumetric heat dissipation rate.

Subject to the above conditions, the governing conservation equations assume what is termed the Boussinesq form [6]:

continuity

$$\overline{\nabla'}.\mathbf{u}' = 0 \tag{2.51}$$

momentum

$$\rho'_o\left(\frac{\partial \mathbf{u}'}{\partial t'} + \mathbf{u}'.\overline{\nabla'}\mathbf{u}'\right) = -\overline{\nabla'}p'_m - \rho'_o\beta(T' - T'_o)\mathbf{g} + \mu\overline{\nabla'^2}\mathbf{u}' \tag{2.52}$$

energy

$$\frac{\partial T'}{\partial t'} + \mathbf{u}'.\overline{\nabla'}\mathbf{u}' = \alpha\overline{\nabla'^2}T' \tag{2.53}$$

Eqn.(2.53) is written for constant fluid properties. When the temperature-dependent character of k is retained, the energy equation is written:

$$\rho'_o c_p\left(\frac{\partial T'}{\partial t'} + \mathbf{u}'.\overline{\nabla'}\mathbf{u}'\right) = \overline{\nabla'}\left(k\overline{\nabla'}T'\right) \tag{2.54}$$

The second term on the r.h.s. of eqn.(2.52) is the buoyancy term, expressed according to the Boussinesq approximation (incompressible fluid, except in this term).

In conjugate problems, the conductive wall interacts with the fluid, and the temperature distribution inside it must be determined. The energy equation for the wall is:

$$\rho'_w c_{pw}\left(\frac{\partial T'_w}{\partial t'}\right) = k_w\overline{\nabla'^2}T'_w \tag{2.55}$$

In eqn.(2.55), the suffix w distinguishes the properties of the wall; the thermal conductivity k_w is assumed as temperature-independent.

2.3 - Boundary Conditions

Eqns.(2.51)-(2.53), with the possible addition of eqn.(2.55), are subject to boundary conditions at the periphery of the cross-stream section, and at the open (inlet/outlet) sections. Initial conditions are also to be specified for unsteady problems.

Solid boundaries

a. flow conditions
The condition of adherence (non-slip condition) applies at the solid walls:

- B.C.1 - $\mathbf{u}' = 0$ at the solid walls.

b. thermal conditions:
The basic thermal boundary conditions, already mentioned in § 2.1, are:

Case **T**: the wall temperature T'_w is assigned:

- B.C.2 - $T' = T'_w$ at the solid walls.

Case **H1**: the mean heat flux density, q'_{wz}, is given; the wall temperature, T'_{wl}, is uniform along the duct perimeter. Neither T'_{wz} nor q'_{wl} is given:

- B.C.3 - $T' = T'_{wz}$
  - $q'_{wz} = \text{cons.}$ at the solid walls.

Case **H2**: the heat flux density at the wall, q'_w, is assigned.

- B.C.4 - $q'_{wl} = q'_{wz} = -k(\partial T'/\partial n')_{wl}$ at the solid walls.

Here, n' indicates the direction of the outward normal to the wall; usually q'_{wz} is assumed uniform.

Case **HCj**: the heat flux density, q'_{wz}, is assigned at the outer surface of the wall.

- B.C.5 - $q'_w = -k_w(\partial T'_w/\partial n')_{wl}$ at the outer surface of the solid walls.

  $-k_w(\partial T'_w/\partial n')_{wl} = -k(\partial T'/\partial n')_{wl}$ at the fluid-solid interfaces.
  $T' = T'_{wl}$

Here, n' indicates the direction of the outward normal to the wall.

Case **T3**: the temperature of the external environment, T'_a, and the external heat transfer coefficient, h_a, are specified.

- B.C.6 - $-k(\partial T'/\partial n')_{wl} = h_a(T'_{wl} - T'_a)$ at the solid walls.

Here, n' indicates the direction of the outward normal to the wall. Both h_a and T'_a are usually assumed uniform.

Peripheral fluid boundaries

When the section is partially bounded by fluid, as in the case of flow between parallel plates, and where the domain of interest is artificially limited by planes which give periodic or symmetrical fluid behaviour, a symmetry condition applies at those fluid boundaries.

- B.C.7 - $\partial \mathbf{u}'/\partial n' = \partial T'/\partial n' = 0$ at fluid boundaries.

Open boundaries

Thermal and fluid flow conditions must be specified at the inlet section. Such specifications are also needed at the end of the thermally active region (outlet section) when the problem is treated as fully elliptic.
Two basic flow conditions are commonly employed at the entrance; these are: i. fully developed velocity profile, and, ii. uniform velocity profile. The fluid temperature is usually assumed uniform.
The outlet conditions are commonly specified as corresponding to thermally developed flow conditions.

- B.C.8 - $\mathbf{u}' \equiv w'_{fd}$ at the inlet section.
- B.C.9 - $\mathbf{u}' \equiv w'_m$ at the inlet section.
- B.C.10 - $T' = T'_o$ at the inlet section.
- B.C.11 - $\partial \mathbf{u}'/\partial z' = \partial T'/\partial z' = 0$ at the outlet section.

Here, w'_m and w'_{fd}, respectively designate the mean fluid velocity at the inlet, and the fully-developed velocity profile for isothermal conditions.

2.4 - Non-Dimensional Forms

Dimensional analysis is of great help in the physical interpretation and correlation of the results, either experimental or numerical. Equations (2.51)-(2.53) are now reduced to their non-dimensional forms by dividing the primed variables by appropriate scale quantities. The choice of these is crucial not only for a correct estimate of the leading terms in the equations, but also because an improper choice of scale quantities can be detrimental for accuracy, and even stability, of numerical methods, as discussed by Ostrach [7]. As a rule, a scale quantity is meant to represent the variable it scales by some order of magnitude. The choice of scale quantities is however non-unique, and various alternatives are of common use in the present context. In this context, it is worth mentioning that Hellums and Churchill [8] have proposed a general method to identify

automatically the arbitrary scale quantities; however, the validity of their assumptions remains undemonstrated.

For combined convection problems, reference quantities must be defined for length, time, velocity, pressure and temperature. Guiding criteria for the choice of these are now discussed.

Length scales

- We assume that a reference length is properly defined if non-dimensional temperature and velocity vary by an order of magnitude over a distance of the order of the scale length itself. As a consequence, buoyancy-induced and forced flows will not have, in general, coincident scales.
- In the case of combined convection in horizontal ducts, buoyancy forces act over a length which is of the order of the vertical extent of the duct itself. For most common geometries, this is proportional to the hydraulic diameter, D_h , by an order one factor (then, the choice of D_h might become questionable for inclined/vertical ducts). For the sake of generality we leave it provisionally indicated as L_b.
- The standard choice for L_f, the scale length of forced convection flows, is the hydraulic diameter, D_h. However, under laminar forced flow conditions, variations of axial velocity of the order of the mean velocity, occur over the hydrodynamic entrance length, which is proportional to D_hRe , and thermal entrance effects cover a length proportional to D_hRePr. The order of magnitude of the proportionality factor, ranges from 1 to $1x10^{-2}$ for the various geometries [1]. This latter figure is not completely satisfactory for scale analysis purposes, nonetheless we set the forced flow length scale, L_f , equal to D_hRePr.

Velocity scales

- In horizontal ducts, flow is usually promoted by external sources, since buoyancy is not effective in inducing a bulk flow motion in a horizontal duct. While it is a rare, but of course possible, case where a forced flow is just a small perturbation of buoyancy-induced flow[1], the reverse is a standard case in combined convection in ducts. Scale velocity for buoyancy-induced and forced flow effects are then not coincident. This implies that the velocity components lying over the plane of the duct section are only a small fraction of the axial component.
  The situation may be quite different in a vertical duct, where the bulk effect of buoyancy may be comparable with, or even stronger than, the one associated with the forced flow.
- We define the scale velocity for forced flow as the mean velocity at the inlet section of the duct, w'_m. This is assumed to be known in most theoretical analyses of combined convection flows, as it is for forced flows. It should be considered, however, that the

---

1 A clear example, however, is that of accident-type reactor core flows in Magnox nuclear reactors.

effect of buoyancy is to modify the friction factor, and the pressure drop, in respect to a corresponding forced flow occurrence - i.e., a case where the same flow rate is obtained without buoyancy. For this reason some authors prefer to define a reference pressure gradient, from which the scale velocity is implicitly or explicitly defined (see e.g. [9,10]). There is actually no special advantage in such a choice, apart from the conceptual fact that, the basic situation chosen to compare buoyancy-affected results is a forced flow giving the same pressure drop, rather than one having the same flow rate.

- The choice of the scale velocity for buoyancy-induced flows is non-unique in the literature. The following reference quantities have been proposed for the buoyancy scale velocity, U_b:

$$U_b = \nu/L_b \quad ; \quad U_b = \alpha/L_b \tag{2.55}$$

$$U_b = g\beta\Delta T'_o L_b^2/\nu = Gr(\nu/L_b) \tag{2.56}$$

where, Gr designates a Grashof number based on L_b.

Use and appropriateness of these definitions is discussed by Ostrach [11,12] in the context of buoyancy driven flows in cavities. The first two alternatives correspond to molecular diffusion velocity of momentum and heat, respectively. Usually, they are several orders of magnitude lower than buoyancy-induced velocity components, and are not adequate as reference quantities. Eqn.(2.56) derives from an order of magnitude balance of the buoyancy and viscous terms in the momentum equation, and is appropriate at low Rayleigh and Grashof numbers ($Ra \leq 1$; $Gr \leq 1$).

For the high-Gr range, Ostrach [12] indicates the thermal boundary layer thickness, of order $L_b(U_b L_b\, Pr/\nu)^{-1/4}$, as the length over which the buoyancy forces act. Use of this length scale makes the convection and diffusion terms of the same order in the energy equation. For small Pr, the balance between buoyancy and inertia forces in the momentum equation gives:

$$U_b = (g\beta\Delta T'_o L_b)^{1/2} = Gr^{1/2}(\nu/L_b) \tag{2.57}$$

For large Pr, the appropriate balance is between buoyancy and viscous forces in the momentum equation. This yields the following definition for the scale velocity:

$$U_b = (g\beta\Delta T'_o L_b\alpha/\nu)^{1/2} = (Gr/Pr)^{1/2}(\nu/L_b) \tag{2.58}$$

Eqn.(2.57) is valid at high Gr and low Pr values ($Pr < 1$), while eqn.(2.58) holds for high Gr and Pr values. Both have been derived in the context of pure natural convection.

Eqn.(2.58) is used here in the context of combined convection problems, apparently for the first time. Note that for fluids having $Pr \sim 1$, eqn.(2.58) coincides with eqn.(2.57), and is therefore adequate for both gases and liquids, with the exception of liquid metals. For low-Pr fluids eqn.(2.57) should be more appropriate.

The ranges of low and high Gr and Ra values, however, remain rather undefined for the case of concern, and eqn.(2.56) is also used in the literature [13].

Pressure scales

- We define the motion pressure, p'_m , as the sum of two terms as follows:

$$p'_m = P'_m + p'_{mb} \tag{2.59}$$

Here, P'_m is the result of averaging the motion pressure over the duct section, and p'_{mb} is the deviation from that average. Such a choice is dictated by the consideration that the two terms have different origins, and must be scaled differently. In fact, the axial gradient of P'_m mainly depends on the viscous resistance to the forced flow, consistently with the assumption that buoyancy produces just *second order* effects. On the other hand, deviations from P'_m are either associated with buoyancy-induced secondary circulation, or to hydraulic entrance phenomena. As a rule, these effects do not overlap, since the action of buoyancy starts becoming effective at a certain distance from the hydraulic entrance section. Therefore, in most combined convection circumstances, the gradient of p'_{mb} is related to the strength of the buoyancy term in the momentum equation.

- We derive the mean pressure scale, P_o, by an order of magnitude balance of the viscous term and the mean pressure gradient, in the axial momentum equation. The forced flow length scale is used to scale this pressure gradient.
- The scale pressure for the buoyancy-induced term, p_o, is obtained by an order of magnitude balance of the viscous and pressure gradient terms over the cross section.

- The resulting pressure scales are:

$$P_o = \mu\alpha Re^2 Pr^2/D_h^2 \tag{2.60}$$

$$p_o = \mu\alpha Ra^{1/2}/L_b^2 \tag{2.61}$$

Note that in neither case a scale level of the type $p_{ref} = \rho_o U_o^2$ is invoked. That pressure scale, even if widely used in the analysis of laminar combined convection, is not really relevant to it, but is rather concerned with high-Re, viscosity-free circumstances.

Time scale

- The reference time scale , t'_o, is defined as the ratio of L_b to U_b, under the argument that possible unsteadiness is related to the onset or the disturbance of the buoyancy-induced motion.

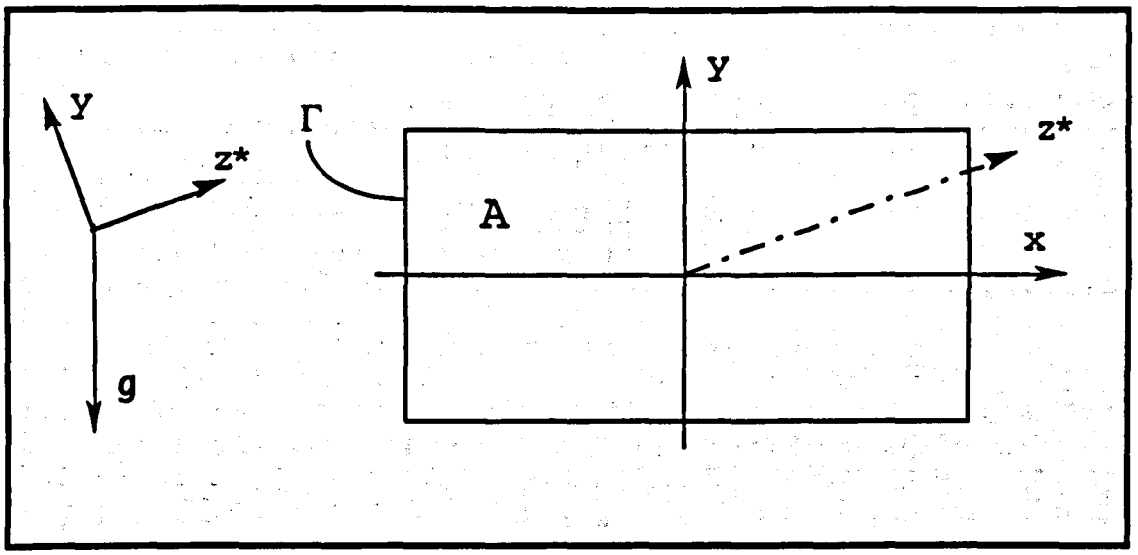

Fig.2.2 - Scheme for orthogonal Cartesian coordinates

Temperature scale

- We scale the temperature differences by the general $\Delta T_o'$ temperature difference, related to the thermal boundary condition for the problem at hand.

Cartesian coordinates

Using the above definitions, and symbols as in Nomenclature, eqns.(2.51)-(2.53) are written with orthogonal Cartesian coordinates (x,y,z*). Reference is made to the scheme in Fig.2.2.

continuity

$$Ra^{1/2}\left(\frac{\partial u}{\partial x}+\frac{\partial v}{\partial y}\right)+\left(\frac{D_h}{L_b}\right)^2\frac{\partial w}{\partial z^*}=0 \qquad (2.62)$$

x-momentum

$$\frac{Ra^{1/2}}{Pr}\left(\frac{\partial u}{\partial t}+u\frac{\partial u}{\partial x}+v\frac{\partial u}{\partial y}\right)+\frac{1}{Pr}\left(\frac{L_b}{D_h}\right)^2\left(w\frac{\partial u}{\partial z^*}\right)= -\frac{\partial p}{\partial x}+\left[\left(\frac{\partial^2 u}{\partial x^2}+\frac{\partial^2 u}{\partial y^2}\right)+\frac{(L_b/D_h)^2}{(Re\,Pr)^2}\left(\frac{\partial^2 u}{\partial z^{*2}}\right)\right] \qquad (2.63)$$

y-momentum

$$\frac{Ra^{1/2}}{Pr}\left(\frac{\partial v}{\partial t} + u\frac{\partial v}{\partial x} + v\frac{\partial v}{\partial y}\right) + \frac{1}{Pr}\left(\frac{L_b}{D_h}\right)^2\left(w\frac{\partial v}{\partial z^*}\right) = Ra^{1/2}T\cos(\gamma) + \\ -\frac{\partial p}{\partial y} + \left[\left(\frac{\partial^2 v}{\partial x^2} + \frac{\partial^2 v}{\partial y^2}\right) + \frac{(L_b/D_h)^2}{(Re\ Pr)^2}\left(\frac{\partial^2 v}{\partial z^{*2}}\right)\right] \qquad (2.64)$$

z-momentum

$$\frac{Ra^{1/2}}{Pr}\left(\frac{\partial w}{\partial t} + u\frac{\partial w}{\partial x} + v\frac{\partial w}{\partial y}\right) + \frac{1}{Pr}\left(\frac{L_b}{D_h}\right)^2\left(w\frac{\partial w}{\partial z^*}\right) = \frac{Ra}{Re\ Pr}\left(\frac{D_h}{L_b}\right)T\sin(\gamma) + \\ -\frac{Ra^{1/2}}{(Re\ Pr)^2}\left(\frac{\partial p}{\partial z^*}\right) - \left(\frac{L_b}{D_h}\right)^2\frac{dP}{dz^*} + \left[\left(\frac{\partial^2 w}{\partial x^2} + \frac{\partial^2 w}{\partial y^2}\right) + \frac{(L_b/D_h)^2}{(Re\ Pr)^2}\left(\frac{\partial^2 w}{\partial z^{*2}}\right)\right] \qquad (2.65)$$

energy

$$Ra^{1/2}\left(\frac{\partial T}{\partial t} + u\frac{\partial T}{\partial x} + v\frac{\partial T}{\partial y}\right) + \left(\frac{L_b}{D_h}\right)^2\left(w\frac{\partial T}{\partial z^*}\right) = \\ = \left[\left(\frac{\partial^2 T}{\partial x^2} + \frac{\partial^2 T}{\partial y^2}\right) + \frac{(L_b/D_h)^2}{(Re\ Pr)^2}\left(\frac{\partial^2 T}{\partial z^{*2}}\right)\right] \qquad (2.66)$$

The following comments are relevant to eqns.(2.62)-(2.66):

- For generality, Gr and Ra are defined with reference to L_b, the characteristic length for buoyancy, rather than to D_h. For mild inclinations to the horizontal, L_b is of the same order of magnitude as the hydraulic diameter. We then set $L_b/D_h = 1$ in all the equations, leaving open the question whether this assumption is still correct for vertical, or close to vertical, orientations.
- For horizontal ducts, the first term at the r.h.s. of eqn.(2.65) drops out.
- Under steady conditions, all time derivatives are zero.
- In the diffusive terms, in square brackets at the r.h.s. of eqns.(2.63)-(2.66), axial derivatives can be dropped if the Péclet number, $Pe = RePr$, is sufficiently high (see [1]).
- For $Ra \to 0$, the continuity equation reduces to $\partial w/\partial z^* = 0$, and eqn.(2.65) gives:

$$0 = -\frac{dP}{dz^*} + \left[\left(\frac{\partial^2 w}{\partial x^2} + \frac{\partial^2 w}{\partial y^2}\right)\right] \qquad (2.67)$$

This is the well-known Stokes' equation for fully developed flow conditions. The energy equation, eqn.(2.66), in turn simplifies into:

$$\left(w\frac{\partial T}{\partial z^*}\right) = \left[\left(\frac{\partial^2 T}{\partial x^2} + \frac{\partial^2 T}{\partial y^2}\right)\right] \qquad (2.68)$$

Eqns.(2.67) and (2.68) represent the thermal inlet problem for forced convection.
This indicates that the above non-dimensional forms are particularly suitable for cases where the velocity profile is fully developed at the inlet of the heat transfer zone ($z^*=0$), the *Graetz problem* in ducts. They are less informative for simultaneously developing flow conditions.

- Cheng *et al.* [14] introduce the *large Prandtl number assumption* to reduce the originally 3D Graetz problem with buoyancy to a 2D situation. The simplification consists in assuming $Pr\to\infty$, and, as pointed out by Chou and Hwang [13], also $Gr\to 0$. In considering the above non-dimensionalization, we specify that the two conditions must combine to give out Ra of order one. Under these assumptions, and the large-Pe hypothesis, the above set of equations reduces as follows:

$$0 = -\frac{\partial p}{\partial x} + \left[\left(\frac{\partial^2 u}{\partial x^2} + \frac{\partial^2 u}{\partial y^2}\right)\right] \qquad (2.69)$$

$$0 = Ra^{1/2} T\cos(\gamma) - \frac{\partial p}{\partial y} + \left[\left(\frac{\partial^2 v}{\partial x^2} + \frac{\partial^2 v}{\partial y^2}\right)\right] \qquad (2.70)$$

$$Ra^{1/2}\left(u\frac{\partial T}{\partial x} + v\frac{\partial T}{\partial y}\right) + \left(w\frac{\partial T}{\partial z^*}\right) = \left[\left(\frac{\partial^2 T}{\partial x^2} + \frac{\partial^2 T}{\partial y^2}\right)\right] \qquad (2.71)$$

In eqn.(2.71), w indicates the axial velocity, which remains unaffected by buoyancy, and is then determined from eqn.(2.67). The equation set (2.69)-(2.71) is similar to the one presented in [14], but is not coincident with it, due to the different definition of the scale quantities.

Cylindrical coordinates

Use of cylindrical coordinates (r, θ, z^*) is beneficial in the approach of problems presenting an axis-symmetrical geometry, such as round and annular ducts. We then present the non-dimensional conservation equations in cylindrical coordinates, as derived by direct substitution of the above non-dimensional quantities into the dimensional forms (see e.g., [15]). Reference is made to the scheme in Fig.2.3.

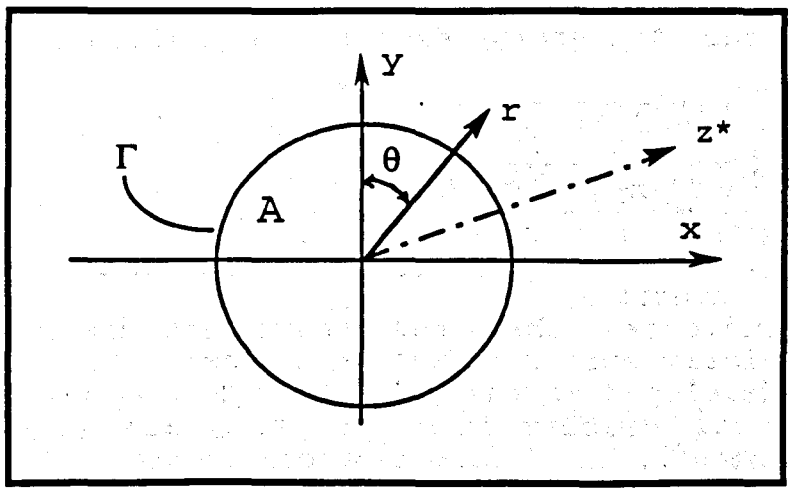

Fig.2.3 - Scheme for cylindrical coordinates

continuity

$$Ra^{1/2}\left(\frac{1}{r}\frac{\partial(ru_r)}{\partial r}+\frac{1}{r}\frac{\partial u_\theta}{\partial \theta}\right)+\left(\frac{D_h}{L_b}\right)^2\frac{\partial w}{\partial z^*}=0 \qquad (2.72)$$

r-momentum

$$\frac{Ra^{1/2}}{Pr}\left(\frac{\partial u_r}{\partial t}+u_r\frac{\partial u_r}{\partial r}+\frac{u_\theta}{r}\frac{\partial u_r}{\partial \theta}-\frac{u_\theta^2}{r}\right)+\frac{1}{Pr}\left(\frac{L_b}{D_h}\right)^2\left(\frac{\partial u_r}{\partial z^*}\right)=Ra^{1/2}T\cos(\theta)\cos(\gamma)+$$
$$-\frac{\partial p}{\partial r}+\left[\frac{\partial}{\partial r}\left(\frac{1}{r}\frac{\partial(ru_r)}{\partial r}\right)+\frac{1}{r^2}\frac{\partial^2 u_r}{\partial \theta^2}-\frac{2}{r^2}\frac{\partial u_\theta}{\partial \theta}+\frac{(L_b/D_h)^2}{(Re\,Pr)^2}\left(\frac{\partial^2 u_r}{\partial z^{*2}}\right)\right] \qquad (2.73)$$

θ-momentum

$$\frac{Ra^{1/2}}{Pr}\left(\frac{\partial u_\theta}{\partial t}+u_r\frac{\partial u_\theta}{\partial r}+\frac{u_\theta}{r}\frac{\partial u_\theta}{\partial \theta}\right)+\frac{1}{Pr}\left(\frac{L_b}{D_h}\right)^2\left(w\frac{\partial u_\theta}{\partial z^*}\right)=-Ra^{1/2}T\sin(\theta)\cos(\gamma)+$$
$$-\frac{1}{r}\frac{\partial p}{\partial \theta}+\left[\frac{\partial}{\partial r}\left(\frac{1}{r}\frac{\partial(ru_\theta)}{\partial r}+\frac{1}{r^2}\frac{\partial^2 u_\theta}{\partial \theta^2}+\frac{2}{r^2}\frac{\partial u_r}{\partial \theta}\right)+\frac{(L_b/D_h)^2}{(Re\,Pr)^2}\left(\frac{\partial^2 u_\theta}{\partial z^{*2}}\right)\right] \qquad (2.74)$$

z-momentum

$$\frac{Ra^{1/2}}{Pr}\left(\frac{\partial w}{\partial t}+u_r\frac{\partial w}{\partial r}+\frac{u_\theta}{r}\frac{\partial w}{\partial \theta}\right)+\frac{1}{Pr}\left(\frac{L_b}{D_h}\right)^2\left(w\frac{\partial w}{\partial z^*}\right)=\frac{Ra}{Re\,Pr}\left(\frac{D_h}{L_b}\right)T\sin(\gamma)+$$

$$-\frac{Ra^{1/2}}{(Re\,Pr)^2}\left(\frac{\partial p}{\partial z^*}\right)-\left(\frac{L_b}{D_h}\right)^2\frac{dP}{dz^*}+\left[\frac{1}{r}\frac{\partial}{\partial r}\left(r\frac{\partial w}{\partial r}\right)+\frac{1}{r^2}\frac{\partial^2 w}{\partial \theta^2}+\frac{(L_b/D_h)^2}{(Re\,Pr)^2}\left(\frac{\partial^2 w}{\partial z^{*2}}\right)\right] \qquad (2.75)$$

energy

$$Ra^{1/2}\left(\frac{\partial T}{\partial t}+u_r\frac{\partial T}{\partial r}+\frac{u_\theta}{r}\frac{\partial T}{\partial \theta}\right)+\left(\frac{L_b}{D_h}\right)^2\left(w\frac{\partial T}{\partial z^*}\right)=$$

$$=\left[\frac{1}{r}\frac{\partial}{\partial r}\left(r\frac{\partial T}{\partial r}\right)+\frac{1}{r^2}\frac{\partial^2 T}{\partial \theta^2}+\frac{(L_b/D_h)^2}{(Re\,Pr)^2}\left(\frac{\partial^2 T}{\partial z^{*2}}\right)\right] \qquad (2.76)$$

Here, the velocity components, and the dimensional coordinates are u_r', u_θ', w' and r', θ, z', respectively. Their non-dimensional counterparts are:

$$r=\frac{r'}{D_h};\ z^*=\frac{z'}{D_h\,Re\,Pr};\ u_r=\frac{u_r'}{U_b};\ u_\theta=\frac{u_\theta'}{U_b};\ w=\frac{w'}{w_m'}$$

Comments ,on eqns.(2.62)-(2.66) also apply to eqns.(2.72)-(2.76).

References

1. R.K. Shah, and A.L. London - *Laminar Flow Forced Convection in Ducts* - Academic Press, NY, 1978.
2. P.H. Newell, and A.E. Bergles - Analysis of Combined Free and Forced Convection for Fully Developed Laminar Flow in Horizontal Tubes - Trans. ASME, J. Heat Transfer, 92, 1970; 83-93.
3. H. Schlichting - *Boundary Layer Theory* - 6th ed., McGraw-Hill, N.Y.,1968.
4. B. Gebhart, Y. Jaluria, R.L. Mahajan, and, B. Sammakia - *Buoyancy-Induced Flows and Transport* - Hemisphere pub. Co., Washington, 1988.
5. D.J. Tritton - *Physical Fluid Dynamics* - 2nd ed., Clarendon Press, Oxford, UK, 1988.
6. D.D. Gray, and A. Giorgini - The Validity of the Bussinesq Approximation for Liquids and Gases - Int. J. Heat Mass Transfer, 19, 1976; 545-551.
7. S. Ostrach - Natural Convection in Cavities and Cells - Procs. '*7th Int. Heat Transfer Conf.*', Munich, D, 1982, Vol. 1; 365-379.
8. J.D. Hellums, and S.W. Churchill - Dimensional Analysis and Natural Circulation - Chem. Eng. Progress. Symp. Ser., Vol. 57, No.32, 1961; 75-80.

9 G.J. Hwang, and K.C. Cheng - Boundary Vorticity Method for Convective Heat Transfer with Secondary Flow - Application to Combined Free and Forced Laminar Convection in Horizontal Tubes - '*4th Int. Heat Transfer Conf.*', Paris, F, 1970; Vol.4, pap. NC3.5.
10. G.J. Hwang, and F.C. Chou - Effect of Wall Conduction on Combined Free and Forced Laminar Convection in Horizontal rectangular Channels - Trans. ASME, J. Heat Transfer, 109, 1987; 936-942.
11. S. Ostrach - Low-Gravity Fluid Flows - Ann. Rev. Fluid Mech., 1982, Vol. 14; 313-345.
12. S. Ostrach - Natural Convection in Enclosures - ASME, J. Heat Transfer, 110, 1988; 1175-1190.
13 F.C. Chou, G.J. Hwang - Vorticity-Velocity Method for the Graetz Problem and the Effect of Natural Convection in a Horizontal Rectangular Channel with Uniform Wall Heat Flux - ASME, J. Heat Transfer, 109, 1987; 704-710.
14 - K.C. Cheng, S.W. Hong, and G.J. Hwang - Buoyancy effects on Laminar Heat Transfer in the Thermal Entrance Region of Horizontal Rectangular Channels with Uniform Heat Flux for Large Prandtl Number Fluid - Int. J. Heat Mass Transfer, 15, 1972; 1819-1836.
15 - R.B. Bird, W.E. Stewart, and E.N. Lightfoot - '*Transport Phenomena*'- J. Wiley & S. Inc., NY, 1960.

COMBINED CONVECTION AND OTHER EFFECTS IN HEAT TRANSFER IN HORIZONTAL FLOWS

CHAPTER 3: REVIEW OF RELEVANT LITERATURE

3.1 - Introduction

This literature survey is restricted to laminar combined convection in horizontal or inclined ducts. As mentioned in Ch.1, other items are dealt with in the Thesis, such as wall conduction effects, and pure natural convection in cavities. Most of that work has been published in Journals and Conference proceedings, and is discussed in Ch.4. The appropriate references are given in the papers, which are enclosed as Appendix I.

The amount of the literature relevant to combined convection in ducts is very large. However, in view of the fact that the objective of the review is to present the complete state of the art in that area, no restriction has been imposed on duct geometry or thermal boundary conditions. The reference collection includes about 160 papers, published up to early 1992. It is worthy of note that about half the literature has been published in the last decade.

Besides the scope of updating the state of the art, there is here a specific interest in estimating the possible performance of the numerical schemes/approaches which have been tried with combined convection problems in horizontal duct flow. Therefore, the review work is organized into two parts. The first is exclusively dedicated to the numerical work, and is directed to identifying the performance of the various techniques in the context of the combined convection problems. As already noted, combined convection with horizontal flows offers peculiar difficulties, which can severely reduce the capabilities of otherwise well-performing techniques, in terms of convergence, accuracy, and, robustness. A part of the work has been presented in a Conference paper (included in Appendix A). This is re-assessed and completed in ≅ 3.3.
In the second part of the review (≅ 3.4), all the experimental, analytical, and numerical work is considered. The subdivision of material is based on duct geometry. Results on uniformly heated circular ducts are discussed in detail, and areas of future work are indicated.

One major problem arising in the interpretation of results on combined convection, derives from the fact that different definitions are used by different authors for Rayleigh and Grashof numbers, but confusingly designated by the same symbol and name.
As far as possible, all the data have been converted to the following definitions:

Grashof number (operative definition)

$$Gr = g\beta\left(T'_{wz} - T'_{m}\right)D_h^3/\nu^2 \qquad (3.1)$$

Modified Grashof number for B.C. **H**

$$Gr_q = g\beta q'_{wz}D_h^4/\left(k\nu^2\right) \qquad (3.2)$$

Rayleigh number (operative definition)

$$Ra = Gr\ Pr = g\beta\left(T'_{wz} - T'_{m}\right)D_h^3/(\alpha\nu) \qquad (3.3)$$

Modified Rayleigh number for B.C. **H**

$$Ra_q = Gr_q\ Pr = g\beta q'_{wz}D_h^4/(k\alpha\nu) \qquad (3.4)$$

Gr, Gr_q, Ra, and Ra_q, are related as follows:

$$Gr = Gr_q/Nu_z \ , \text{ and } Ra = Ra_q/Nu_z \qquad (3.5)$$

A comprehensive list of definitions and equivalences is given in [9].

3.2 - General References

Previous review work on combined convection in horizontal ducts is summarized in this section.

Earliest experimental data were collected by Metais and Eckert [1]. Tentative graphs were produced, to identify regions of free, forced, and combined convection, and areas of laminar, transitional, and turbulent flow, for either horizontal or vertical ducts.
Bergles has summarized the theoretical work on the effects of temperature-dependent properties in buoyancy affected duct flows [3], and the relevant experimental work [2]. Mixed convection in horizontal parallel-plate channels has been reviewed by Incropera [4]. Recent Soviet literature has been summarized by Petukhov et al. [5] and by Polyakov [6].

A general review of internal and external combined convection flows is given in [7]. Selected equations for heat transfer engineering applications are reported in [8,9].

Research needs and perspectives in natural and combined convection were identified by Jaluria et al. [10].

3.3 - Review of Numerical Analyses

Most of the contents of this paragraph has been the subject of a paper presented at the 1991 U.I.T. annual meeting on heat transfer [11]. As part of this Thesis' work, the paper is reproduced in Appendix I. Here, only the general lines of the work are presented, with additional references and comments.

In [11], the relevant literature is reviewed, subdivided into five groups, corresponding to the fundamental mathematical formulation of the problem. Results are collected into two tables, where, whenever possible, the maximum value of Ra (or Ra_q) for which converged results are obtained, and the grid size employed are mentioned. Those quantities are assumed to characterize adequately the numerical method in terms of stability.

In its complete form the problem of combined convection in horizontal/inclined ducts, can only be described by the fully 3D elliptic formulation expressed by the equation set (2.62)-(2.66), or (2.72-2.76). Different simplifying assumptions can however be considered, under which the problem becomes more tractable. These have been grouped as follows:

i. Fully developed flow: the establishment of fully developed, ie axially invariant, thermal and flow conditions is assumed to occur at some distance from the start of heating. Since velocity and temperature are invariant with the axial coordinate the problem is reduced to the coupled solution of 2D momentum and energy equations over the duct section. The axial component of velocity is obtained from the z-momentum equation, as reduced under f.d. assumptions. This type of problem is fully developed in the z-direction and two-dimensional elliptic over the cross-section. We designate it (2DE.fdz).

ii. Thermal inlet region with buoyancy effects: in plane or axisymmetric geometries, the thermal inlet region can be analyzed as a 2D feature. Only one cross-stream velocity component is present, and buoyancy interacts with the thermohydraulic inlet process through the presence of buoyancy terms in the y- or r-momentum equations. The problem is still elliptic, but usually weakly so, the flow field tending to become parabolic for increasing Re and z. Solutions of this type are restricted to the region preceding the onset of thermally induced instabilities. These are 3D in nature, and lead to circulations in the cross-stream section. This problem is two-dimensional over (y,z) or (r,z) planes, and is indicated by (2Dyz).

iii. High Prandtl number fluids: in the limit of $Pr \rightarrow \infty$, not only second order axial derivatives are dropped in the momentum equations, but also the inertia terms vanish. The problem remains elliptic in the cross-stream section, but axial velocity is as for fully developed isothermal flow. The solution is employed to deal with the Graetz problem with buoyancy, and is designated as (2DE.tdz).

iv. Axially parabolic flow: axial diffusion of heat and momentum are ignored. The problem is thus reduced to a parabolic form, as far as the development of axial velocity and temperature are concerned. The elliptic nature of the flow and thermal fields is retained over the duct section, however. This type of solution is designated as two-dimensional elliptic with (parabolic) hydraulic development (2DE.hdz).

v. Fully elliptic flow: the original three dimensional elliptic problem is indicated as (3DE).

For any of the above choices, several formulations of the flow problem are possible. While in fact, the energy and axial momentum equations remain unchanged, the following are viable formulations of the flow problem over the cross-stream section:

i. primitive variables (pv): the solution is in terms of velocity and pressure. The two momentum equation components are left unchanged (conservative and/or transient forms are eventually used), and coupled with the continuity equation. The latter can be substituted with a Poisson-like equation for pressure, as in MAC-derived methods [12]. Alternatively, discretized pressure and/or pressure correction equations are directly obtained, as in SIMPLE [13] and SIMPLE-derived [14] approaches ;

ii. stream function-vorticity ($\psi\omega$): the two momentum equations are cast into a single convection-diffusion equation for vorticity(ω), eliminating pressure by cross-differentiation. The continuity equation is substituted by a Poisson equation for the stream function (ψ). Both equations are eventually given a transient form;

iii. biharmonic stream function equation ($\psi 4$): vorticity is eliminated from the above equations, to give a single 4th order p.d.e. for the stream function.

Discretization schemes for p.d.e.'s of current use in CFD fall into three main families. These are: Finite Difference Methods (FDM) [12]; Finite or Control Volume Methods (CVM) [13,14]; Finite Element Methods (FEM)[14,15]. The Boundary Element Method (BEM)[16] is also gaining favour in CFD analyses. In principle, all of them can apply to any of the above problem formulations.

While reference is made to [11] for (2DE.fdz), (2Dyz), and (2DE.tdz) solutions, the discussion of axially parabolic (2DE.hdz), and fully elliptic (3DE) solutions is extended and completed here.

3.3.1 - Axially parabolic flow solutions

When approaching (2DE.hdz)-problems, the governing equations are derived by dropping 2nd-order diffusive terms, and upstream propagation of downstream pressure effects ($\partial p/\partial z^*=0$) in eqns.(2.63)-(2.66), or (2.73)-(2.76). Non-dimensional forms of the equations

indicate that the validity of these assumptions is respectively subject to conditions:

$$Pe^2 = (Re\ Pr)^2 >> 1 \qquad (3.1)$$

$$Pe^2 = (Re\ Pr)^2 >> Ra^{1/2} \qquad (3.2)$$

It is important to stress that, contrary to condition (3.1), condition (3.2) may not be fulfilled in many circumstances of practical interest.

A primitive-variable formulation - The case of a circular duct with B.C.**T**, and a fully developed entry velocity profile was considered by Kato et al. [17], either numerically or experimentally. Primitive-variable equations were discretized into FD form, using the 'upwind method' [12]. A regular 10x20 (r,θ) mesh was used. The axial step, Δz^*, ranged from 2.5×10^{-6}, to 4×10^{-5}. Results for air were presented up to $Ra = 1.4\times10^6$.
Kato et al. simplified the problem by assuming:

$$\frac{\partial u_r}{\partial z^*} = \frac{\partial u_\theta}{\partial z^*} = \frac{\partial w}{\partial z^*} = 0 \qquad (3.3)$$

and

$$\frac{dP}{dz^*} = \text{const.} \qquad (3.4)$$

The constant in eqn.(3.4) was estimated as for isothermal Poiseuille flow. This is physically inconsistent for low Pr-fluids, and is presumably at the root of the poor agreement observed with experimental data.

Velocity-Vorticity Method (VVM) - This method has been applied by Chou and Hwang to the square, rectangular and circular duct geometries under b.c.**H2** [18-20]. Velocity was assumed fully developed at $z = 0$ $(w = w_{fd})$, and expressed as:

$$w = w_{fd} + w_b \qquad (3.5)$$

Here, w_b is the buoyancy-induced deviation from the constant-property f.d. solution.
The derivation of the working equations is rather complex in this method, where the solution is worked out in terms of u,v,w,T, and ω. The basic p.d.e.'s are transformed into the following form (note that the non-dimensionalisation process used in [18-20] is different from the one presented in Ch.2; non-dimensional groups are however defined in the same way):

$$Gr\left(u\frac{\partial\omega}{\partial x} + v\frac{\partial\omega}{\partial y} + w_b\frac{\partial\omega}{\partial z^*} + \omega\frac{\partial u}{\partial x} + \omega\frac{\partial v}{\partial y} + \frac{\partial w_b}{\partial y}\frac{\partial u}{\partial z^*} - \frac{\partial w_b}{\partial x}\frac{\partial v}{\partial z^*}\right) +$$

$$+\frac{1}{Pr}\left(\frac{\partial w_{fd}}{\partial y}\frac{\partial u}{\partial z^*} - \frac{\partial w_{fd}}{\partial x}\frac{\partial v}{\partial z^*} + w_{fd}\frac{\partial\omega}{\partial z^*}\right) = \nabla^2\omega - \frac{\partial T}{\partial x} \qquad (3.6)$$

$$\nabla^2 u = \frac{\partial\omega}{\partial y} - \frac{\partial^2 w_b}{\partial x \partial z^*} \qquad (3.7)$$

$$\nabla^2 v = -\frac{\partial\omega}{\partial x} - \frac{\partial^2 w_b}{\partial y \partial z^*} \qquad (3.8)$$

Here, ω is the axial component of vorticity:

$$\omega = \frac{\partial u}{\partial y} - \frac{\partial v}{\partial x} \qquad (3.9)$$

and ∇^2 is defined:

$$\nabla^2 = \frac{\partial^2}{\partial x^2} + \frac{\partial^2}{\partial y^2} \qquad (3.10)$$

Eqn.(3.6) is the Velocity-Vorticity Equation; it is derived by cross-differentiation of x- and y-momentum equations. Eqns.(3.7) and (3.8), are obtained by a combination of the continuity equation and the differentiation of the vorticity function, eqn.(3.9). These, with z-momentum and energy equations, form the set of p.d.e.'s to be solved. As discussed in [21-24], this formulation is advantageous compared to classic $\psi\omega$-formulations, particularly for doubly-connected domains, and in cases where the flow rate is not known in advance. In comparison with primitive-variable segregated techniques, VVM does not need pressure to be solved over the duct cross-section, thereby avoiding the solution of pressure and pressure-correction equations, and the associated problem of defining appropriate boundary conditions for them. However, there is still the need of determining vorticity at the solid walls. When used in its 2-D aspect, the method is suitable for a fully implicit solution. Stone's strongly implicit algorithm was used in [21]. Instead, a block tridiagonal system is derived in the method presented in [22-24], and all variables are determined at the grid points at the same time. This interesting possibility was not exploited in combined convection solutions [18-20], where a more traditional sequential solution was employed. The FDM discretization uses backward differences axially, and centred differences in the transverse directions. The solution advances following the DuFort-Frankel scheme [12], i.e., all information being available at z*, and (z*-&z*), w,ω, and T are estimated explicitly at (z*+&z*), from z-momentum, velocity-vorticity, and energy equations, respectively. Iteration is needed to estimate $\therefore p/\therefore z^*$, so as to conserve the mass flow-rate. Cross-stream velocity components, u,v, are determined from the Poisson-like eqns.(3.7) and (3.8). In the

solution of these equations, vorticity at the solid walls is implicitly determined at any iteration. A special discretized expression for ω_w was presented in [18].
Grid-dependency experiments were reported [18], and demonstrate the insensitivity of the local Nusselt number on the axial step size. The regular rectangular mesh (x,y) varied from 16x80 (AR=0.2) to 40x16 (AR=5), and was 14x28 for the square duct. The axial step varied from $\Delta z^*=1x10^{-4}$ to $4x10^{-4}$; the lower values were found to be necessary for increasing Ra, and reducing Pr. The results, in terms of Nu_z, compared satisfactorily with the results obtained by Cheng et al. [25] under the high-Pr assumption.

SIMPLE - The problem of combined convection in square and rectangular ducts was considered by Abou-Ellail and Morcos [26-28], using SIMPLE. The effects of inclination and a uniform entry velocity profile were included, for B.C. **H2**.
The Semi-Implicit Method for Pressure-Linked Equations [13] is a control-volume based segregated technique used for the numerical approach of thermal-flow problems with primitive variables. The discretization entails the subdivision of the domain into a number of finite volumes or cells each of which encloses an imaginary grid node, at which all variables are stored, while the velocity components are chosen to lie on the cell boundaries, where they are needed for mass flow computations. The pressure difference between two adjacent grid points is used to estimate the pressure gradient for the velocity component located between them. Therefore, the pressure gradient is discretized over a mesh of the same size as the one used for velocity, and the "checkerboard problem" discussed in [13] is avoided. In SIMPLE and SIMPLE-derived methods, the computations proceed to convergence via a series of continuity-satisfying velocity fields. The advantages arising from this important characteristic are discussed in [14].

A brief description of the method follows. The 2D staggered rectangular mesh shown in Fig.3.1 is used for reference.
The governing p.d.e.'s are integrated over a typical cell &x&y&z* to give finite-difference forms.
The energy equation is given the form:

$$a_P T_P = \sum_{nb} a_{nb} T_{nb} \qquad (3.11)$$

The influence coefficients, a_{nb}, represent the total transport by convection and diffusion across each cell boundary. The subscript nb denotes neighbouring grid points of P, and the summation is to be taken over all neighbours. For each variable one has:

$$a_P = \sum_{nb} a_{nb} \qquad (3.12)$$

The staggered locations for the velocity components determine the corresponding C.V.s' to be used for the discretized momentum equations. For example, two faces of the C.V. for the velocity component u_e in Fig.3.1, pass through the grid points P and E. The corresponding momentum equation can be written as

$$a_e u_e = \sum_{nb} a_{nb} u_{nb} + B + A_e(p_P - p_E) \qquad (3.13)$$

where B accounts for the possible presence of the temperature-dependent buoyancy term, A_e is the area over which the pressure force acts, and a's are the appropriate influence coefficients. A similar equation can be written for y- and z-directions. The discretized equations are modified for the boundary cells, to embody thermal and flow boundary conditions.

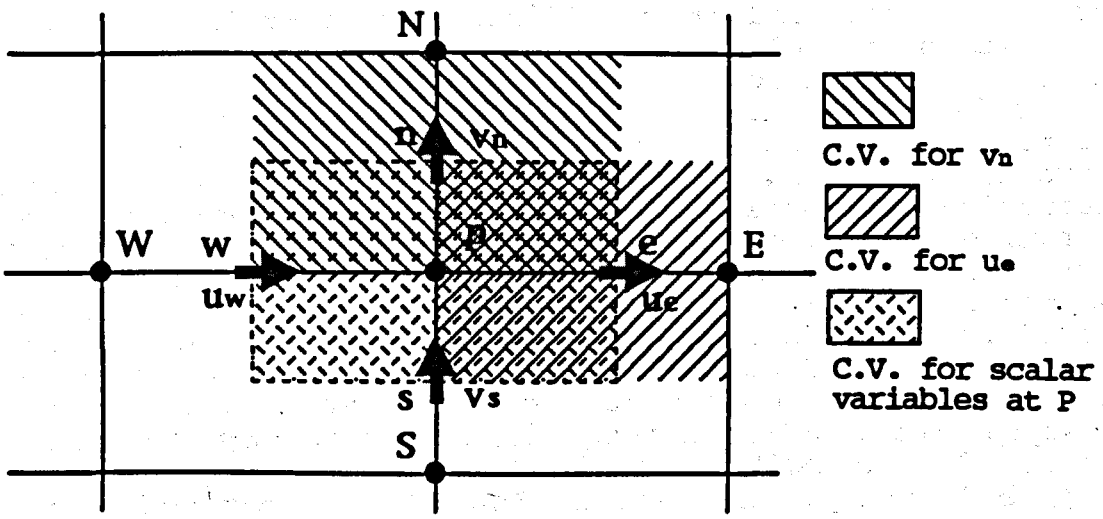

Fig.3.1 - Basic control volume grid, and staggered x and y-momentum grids.

The continuity equation is not used directly in SIMPLE procedures. It is rather employed to derive a 'pressure correction' equation. In fact, eqn.(3.13) can be solved for an estimated pressure field p*. Denoting as u* the velocity field obtained, these will satisfy eqns.(3.13), but, in general, they will not satisfy the continuity equation. Corrections to p* are sought such that the resulting corrections to the velocity field ensure satisfaction of the continuity equation. Denoting by p, and p*, respectively, the updated and guessed pressure fields, and by $\hat{p}$, the pressure correction field, one has

$$p = \hat{p} + p^* \qquad (3.14)$$

Setting $d_e = A_e/a_e$, the 'velocity correction equation' for u_e is:

$$\hat{u}_e = u_e^* + d_e(\hat{p}_P - \hat{p}_E) \qquad (3.15)$$

Similar equations can be written for other u,v components.
The pressure correction equation is obtained by substituting the velocity-correction formulae into the discretized form of the continuity equation, to give:

$$a_P\hat{p}_P = \sum_{nb} a_{nb}\hat{p}_{nb} + b \qquad (3.16)$$

where b represents the residual in the continuity equation when the starred velocities are employed.

A SIMPLE procedure is constituted by the following main steps:

1. Guess an initial pressure field, p*.
2. Using the guessed p*, solve the momentum equations, such as (3.13), to obtain u*,v*.
3. Solve the pressure correction equation, eqn.(3.16), for $\hat{p}$.
4. Calculate p by adding $\hat{p}$ to p*, as from eqn.(3.14) (underrelaxation is necessary to retain convergence).
5. Calculate u, v, from their starred values, using the velocity correction equations such as eqn.(3.15).
6. Solve the energy equation for T.
7. Treat the corrected pressure field (step 4.) as the guessed field for the next iteration, return to step 2., and repeat the whole process up to the pre-defined level of convergence.

In [26-28], the above solution procedure was modified to take advantage of the axially-parabolic nature of the problem, which allows the use of a marching procedure. Note that the influence coefficients in the z-momentum and energy equations are estimated according to a first order upwind or a hybrid scheme, so that the downstream influence coefficients were all automatically set to zero. In this way, no information is transmitted upstream from a downstream cell. The axial pressure difference is assumed uniform over the cross-section and equal to its upstream value. Eqn.(3.14) is solved for the axial velocity field at the specified cross-section. The solution is obtained by a line-by-line Gaussian-elimination method with an alternating direction algorithm. The computed axial velocity field will not in general satisfy the overall mass continuity. The difference between the computed and the true mass flow rate across the section is used to correct simultaneously the axial pressure difference and the axial field. The above SIMPLE cycle is then repeated up to convergence. It was observed in [26-28] that the number of iterations needed reduces with a reduction in the forward axial step, &z*. The forward step size was chosen so that axial convection was greater than cross-stream diffusion.
In non-dimensional terms this leads to the condition:

$$\Delta z^* < (w\Delta y\delta y) / Pr \qquad (3.17)$$

where, &y is the cell height, and δy is the vertical distance of two grid nodes.

The accuracy of the solution was checked versus asymptotic Nu-values for forced convection. However, the comparison with Chou and Hwang results [18] indicates qualitative and quantitative discrepancies with results. In fact, in [28] Nu decreases for increasing Pr, approaching from above the high-Pr solution [25] - but with poor agreement even at Pr=20. In [18] Nu steadily increases with Pr (at equal Ra_q), and approaches the high-Pr solution from below. Furthermore, all Nu-curves at equal Ra_q and different Pr-values, converge at a unique asymptote, contrary to the results in [18], to the experimental evidence [29], and the result of dimensional analysis. In fact, the fully developed form of eqns.(2.62)-(2.66), indicates a dependence of Nu_{fd}, on either Ra_q or Pr. Quantitatively, the asymptotic Nusselt number differs in the two solutions by about 10%.
It is worth noting that the upwind scheme used is only first order accurate, and is prone to produce 'artificial diffusion' [12]. As a counterpart of this possible source of inaccuracy, the method is known to be very stable. Nevertheless, in [28] numerical instabilities were observed above $Ra_q \approx 1x10^5$, in the fully developed region.

The SIMPLER (SIMPLE Revised) scheme has been adopted to deal with laminar convection in inclined isothermal tubes [30], and horizontal annuli [31]. SIMPLER was used for handling the pressure-velocity coupling in the cross section of the tube. The method proposed by Raithby and Schneider [32] was enforced to calculate the streamwise pressure gradient. Computations were performed over 22x32 (circular duct) and 22x34 (annulus) (r,θ) meshes, using a regular grid spacing in θ, and a non-uniform spacing in r. The axial step, Δz^*, varied from $1x10^{-6}$ ($1x10^{-7}$ in [31]) at the entrance, to $1x10^{-2}$ in the fully developed region. Δz^* was adjusted so that at each station the selected step size caused the bulk fluid temperature to rise by approximately 1% of maximum temperature difference $T'_w - T'_o$. About 120 axial steps were needed to reach the fully developed region. Preliminary grid refinement and accuracy checks vs. forced convection results, were reported. Results were presented up to $Ra = 1x10^6$ for $Pr = 7.65$ [30], and $Ra = 5x10^5$ for $Pr = 0.7$ [31].

An analogous SIMPLER-based solution method was used in a series of papers devoted to the analysis of combined convection in horizontal rectangular ducts, with various combinations of uniformly heated and adiabatic walls [33-36]. Note that in the last two papers, the standard Jacobi iterative solver is used, the solution procedure being fully vectorized. Grid refinement experiments were presented by Incropera and Schutt [33], showing however that grid independence was still not reached for a 26x26(xy) mesh in a duct with AR = 2. Further analyses were reported in [35], demonstrating that For AR =2, $Ra_q = 4.9x10^6$, grid independency is reached with a 30x30 (x,y) grid (with excellent agreement with results obtained with a 40x40 mesh). However, for $Ra_q = 1.6x10^7$, small but discernible differences were associated with results obtained for 30x30 and 40x40 grids. Grid-dependency seems to increase with aspect ratio, AR. Uniform (x,y)-

grid were adopted, under the argument that buoyancy-induced secondary flows necessitate fine resolution across the entire cross-section.
In [35,36] the axial step size, Δz^* was increased systematically from a prescribed minimum, 7.7×10^{-8}, to a maximum of 7.7×10^{-6}. This ensured Δz^*-independence of the results. However, marching from $z^* = 0$ to $z^* = 0.1$, demanded in excess of 13,000 longitudinal steps. Higher Δz^*-values had been used in previous studies [33,34], where it had been observed that events were artificially moved downstream, and/or the flow field was significantly modified, when the axial step size was too high. Results were presented for Pr = 6.5 (water), up to $Ra_q = 4.9\times10^6$ [35]. A common feature of the results, obtained with different combinations of **H2** B.C.'s, is that a sequence of oscillations is observed in the axial distribution of the spanwise-averaged Nu-number. These progressively damp, leading to a fully developed condition, below a critical value of Ra_q. For increasing Ra_q above that limit, a fully developed condition is no longer reached. Some evidence of this effect had previously been observed for square ducts under boundary conditions of the Benard's type, at $Ra_q = 5\times10^4$ [37].

Finite Element Method for Parabolic Flows - The same problem considered in [35,36] was also investigated in [38,39], using FEM.
The strategy adopted is a specialization of the general technique for parabolic flows described by Comini and Del Giudice [40]. This is a segregated procedure which embodies a finite element formulation of (x,y)-momentum equations in a SIMPLE-like scheme. As in SIMPLE, the solution of a pressure correction equation, here discretized with FEM, is used to correct the guessed pressure distribution over the duct cross-section, and to provide the velocity correction fields, (u',v'). All axial derivatives are estimated by a two-point backward formula.
A correction technique is employed to advance the solution axially: the z-momentum equation is solved for u* (the guessed axial velocity field at step n+1), based on known (u,v,T)-values at the previous step, n, and a guessed axial pressure gradient. This is estimated through the integral momentum equation. With symbols defined in Ch.2, this is written:

$$-\left(\frac{dP}{dz^*}\right)^{n+1} = \frac{1}{Pr}\left(\frac{dK_d}{dz^*}\right)^{n+1} - \frac{4}{\Gamma/D_h}\int\left(\frac{\partial w}{\partial n}\right)^n d(\Gamma/D_h) \qquad (3.18)$$

where K_d is the momentum flux correction factor:

$$K_d = \frac{1}{A}\int w^2 dA \qquad (3.19)$$

A three-point backward formula is used to calculate the 1st r.h.s. term, while data available at step n are used for the 2nd. Even if the u*-field does not satisfy exactly integral mass continuity, the mass flowrate error is said to be minor (generally less than 1%). Iteration not being necessary, the velocity correction is simply

based on a similarity criterion of u^{n+1} and u^*, to correct for the mass-flowrate defect.

For the sake of comparison with results in [36], all the cases considered were for AR = 2, Ra = 1.62×10^6, Pr = 6.5, Re = 500, and uniform entry velocity and temperature profiles. The standard Galerkin FE formulation was used, with rectangular 8-point parabolic elements. The mesh was uniform over the cross-section, apart from the near-wall region, where gradients are expected to be steeper. Overall, 168 elements were used over the half cross-section. The axial step size, Δz^*, was progressively increased from 3×10^{-6} at the inlet to 1×10^{-4} in the downstream region. About 1100 axial steps were needed to reach $z^* = 0.01$. The comparison with results in [36] is generally very good. In regions where oscillations are not observed the solution agree almost perfectly, with a slight underprediction of the Nu_z distribution for the side-heating case. The solutions also agree in predicting the start of the oscillating behaviour for the various heating conditions. Discrepancies are however observed in the prediction of peak intensity and position. It is interesting to note that, for bottom and side, bottom and top, and side and top heating, instabilities are observed at $z^* \cong 0.08$; 0.07; 0.045, respectively. For uniform heating the same occurs at $z^* = 0.045$. The effect was ascribed to thermal stratification occurring at the top surface, since local fluctuations of the buoyancy force, increasing upwards, are no longer damped by diffusion effects. No such effect had been observed in [36].

3.3.2 - Fully elliptic flow solutions

A specific problem of fully elliptic solutions is that conditions must be specified at the outflow boundary. The various options which have been adopted in 3DE approaches are reviewed first.
They are:

i. Dirichlet-type conditions

$$u=v=T=0 \; ; \; w = w_{fd} \qquad (3.20)$$

This condition is appropriate for boundary conditions of type **T** at the wall, when a fully developed condition is reached at the duct exit. In [41] a Dirichlet condition was however applied to a **H**-type case , using the outflow values for u,v,w,T obtained from a previous 2D marching solution.

ii. Von Neumann-type conditions
These conditions apply to any fully-developed flow problem.
For velocity they are written

$$\frac{\partial u}{\partial z^*} = \frac{\partial v}{\partial z^*} = \frac{\partial w}{\partial z^*} = 0 \qquad (3.21)$$

For b.c.s' of type **T** at the duct wall, the condition for temperature is

$$\frac{\partial T}{\partial z^*} = 0 \qquad (3.22)$$

For case H the standard formulation is

$$\frac{\partial T}{\partial z^*} = C \qquad (3.23)$$

where C is a known constant [46]
Terhmina et al.[42] suggested the alternative form:

$$\frac{\partial^2 T}{\partial z^{*2}} = 0 \qquad (3.24)$$

iii.smooth condition

$$\frac{\partial^2 u}{\partial z^{*2}} = \frac{\partial^2 v}{\partial z^{*2}} = \frac{\partial^2 w}{\partial z^{*2}} = \frac{\partial^2 T}{\partial z^{*2}} = 0 \qquad (3.25)$$

This condition is expected to ensure a smooth transition through the outflow boundary. It has been employed by Biswas et al.[43].

The numerical methods which have been applied in the context of 3DE solutions are summarized in the following.

SIMPLE - The SIMPLE procedure can be extended to 3D cases with no conceptual difficulty [13].
The round duct case was investigated by this method, under convective [44] and isothermal boundary conditions [45]. Comparison with experimental data was encouraging, in spite of the rather coarse grid used 10x16x30 (r,θ,z^*).

Nguyen and Galanis [46,47] used the SIMPLER algorithm with a Power-law scheme, to treat the case of a uniformly heated circular duct. A line-by-line (SLOR) solver was employed over a 15x18x110 (r,θ,z^*) non-uniform grid. A satisfactory agreement with experimental data by Petukhov et al.[48] was reported, over the range explored Ra_q=5x10^5-1x10^6, with Pr=7 (water). For Ra_q=3x10^6, however, Nu is underpredicted by 6.6%, and Nu_z continues to decrease slightly for increasing z^* in the asymptotic region, contrary to expectations. This effect was attributed to the grid being too coarse for large z^*.
The SIMPLE-based code PHOENIX has recently been employed to simulate an experiment in a AR=2 rectangular duct heated from below and cooled from above at uniform wall temperature [41]. Heat conduction in the vertical acrylic walls was also considered numerically, imposing a convective boundary condition at the outer surface. The computational domain covered the whole duct cross-section, without enforcing the symmetry condition at the vertical mid-plane of the duct. A regular 42x15x81 (x,y,z^*) was used, including 6 points inside each lateral wall. Results were reported for Pr=0.71 (Nitrogen), Ra = 5.3x10^4, and Re = 25, 48, and 72. The findings of this work deserve comments. It is noted first that, at z^*=0, the axial velocity profile deviates

from the fully developed isothermal distribution due to upstream diffusion of momentum. This was well simulated numerically, by extending the solution domain by a certain distance upstream. Two longitudinal rolls then form, which are expected to be symmetrical about the vertical mid-plane. However, experiments at the lowest flowrate (Re=25), showed an asymmetry in the maxima of the axial velocity. These alternated in magnitude with increasing z^*, while a symmetrical solution was found numerically. Very interestingly, however, similar spatial oscillations were obtained by considering a tilting of the duct of 2 about the z-axis. In that case, no steady solution could be obtained. Due to the cost of computations, no unsteady solution was tried. These effects were not observed at higher Re-values, where the agreement with experimental data was very good. Even in those cases, the occurrence of unsteady behaviour cannot be excluded for longer channels. Finally, the comparison of 3DE and 2DE-hdz solutions indicated that, at least for the low-Re range explored, the parabolic option slowed the development of the velocity profile, in poor agreement with experimental findings.

Marker And Cell (MAC) - MAC is a control-volume based treatment of the transient momentum and energy equations [49]. The method uses a two-step semi-implicit scheme: i. in the first step the discretized momentum equations are solved explicitly, in order to obtain the approximate velocity field at the forward time step ($t + \Delta t$), from the known field at time (t); ii. an implicit pressure-velocity iteration is used to obtain a velocity field which satisfies the continuity equation in each cell. This pressure-velocity iteration is equivalent to a SOR solution of the Poisson equation for pressure, but avoids the problem of identifying correct boundary conditions for pressure. As a final step, the energy equation is solved for T, by SOR.
The method was employed by Biswas et al. [50,51] to investigate buoyancy effects in a AR=2 rectangular duct with adiabatic upper and lateral sides, and heated from below with a uniform wall temperature. Results were presented for Pr=6.5, and $Ra = 0.96\text{-}1.93 \times 10^6$. Uniform (x,y,z) 20x22x58 grids were used. However, the comparison with alternative grid distributions (24x22x56, and 20x15x47) indicates that grid independence had not been reached. The most striking feature of the results is that, for $Ra=0.96 \times 10^6$ the distribution of Nu_z converges to an asymptotic value which is higher than the isothermal constant-property value for b.c. T. For $Ra=1.93 \times 10^6$, Nu_z increases monotonically in the downstream region. No explanation was given for those unexpected predictions.

Velocity-Pressure Method (VPM) - VPM is a FDM discretization of transient momentum and energy equations, proposed by Hishida et al. [52] to deal with an isothermally heated horizontal pipe. A Poisson-like equation for pressure is substituted for the original continuity equation, and appropriate b.c.'s derived for it. The scheme includes modified Euler and Crank-Nicholson methods. The advection terms were approximated by upwind differencing. The semi-infinite z-domain was reduced to a finite length by a coordinate transformation, thus generating a variable axial step in the natural domain. The mesh size was 26x27x26 (r,θ,ξ) (where ξ is the transformed axial coordinate).

Satisfactory grid refinement experiments were reported limited to the case of pure forced convection. Results were presented for Ra up to 5.6×10^4, with Pr=0.71. This could imply that the method has a relatively low stability limit in terms of Ra.

Velocity-Vorticity Method (VVM) - A fully 3D formulation of VVM has recently been presented by Terhmina et al.[42]. The method is an extension of the one proposed by de Vahl Davis [53] for the analysis of buoyancy driven flows in closed cavities. It requires the solution of three transient equations for vorticity, three Poisson-like equations for velocity, and the transient energy equation. In [42] VVM was employed to treat the entrance problem in an annulus having uniform, but different, temperatures at the inner and outer surfaces. Boundary conditions for vorticity were deduced from the velocity gradients at the boundaries, and a fully developed flow condition was assumed at the outlet boundary. A coordinate transformation was applied in the z^*-direction, and a uniform grid used in the transformed space. The mesh size was varied from 16x16x21 to 31x21x51 (r,θ,ξ). Ra ranges from 0 to 3.2×10^4, with Pr = 0.71, and DR=2. Even in this case, accuracy seems not to compensate for the complexity of the method, which presents seven dependent variables at each grid point. Furthermore, the stability limit of the method for increasing Ra remains to be determined.

Boundary Element Method (BEM) - A vorticity-vector potential formulation of buoyancy induced/affected problems was presented by Skerget et al.[54]. The problem was stated in terms of boundary domain integral equations, which were discretized with boundary elements. The case of an isothermal round duct, also including the effect of inclination, was considered as demonstrative of the potential of the method. Sample results were obtained for $Ra=1.25 \times 10^4$, Pr=1, using a simple 5x8x8 (r,θ,z) grid.

3.3.3 - Comments on numerical methods

From the above literature survey, and considerations presented in [11], it is possible to define the present state of the art in the field of the numerical prediction of combined convection duct flows.

The availability of modern high speed supercomputers and parallel processing facilities, allows treating combined convection as a fully elliptic 3D feature. However, high computational costs are associated with 3DE solutions, and necessitate an answer to the question of whether solutions of this type are necessary and/or useful.

Reasons for considering with favour 3DE approaches are:

- axial diffusion of momentum and heat become the more important as Re and Pe reduce. Under these circumstances the flow development can be definitely affected by upstream diffusion (see e.g. Barozzi and Nobile [55]), and a 2D-marching approach becomes incorrect. Similar effects might occur in cases where eqn.(3.2) is not

fulfilled, even if the implications of that condition are not completely clear at yet;
- under combined convection conditions, flow reversals are likely to occur in vertical and inclined ducts, with either aiding or opposing buoyancy effects. There is experimental evidence that recirculating flows can also occur at the leading edge of the entrance section [56]. These effects cannot be accommodated with a marching procedure;
- heat conduction along the solid walls (axially conjugated problems) can, in principle, be embodied in a fully 3D procedure. Iteration of the solutions over the solid and fluid domains are thus avoided, as well as problems associated with matching of the solutions at the interfaces;
- there is the need of reliable benchmark solutions, either for testing new techniques, or validating the simplified approaches. These can only be achieved by fully 3D models.

As a counterpart of the above possible advantages, fully elliptic 3D options are generally much more demanding then 2DE-hdz solutions, either in terms of memory occupation or computer time. This poses serious constraints on the mesh size which can be used, as demonstrated by the numerical experiments discussed above, and synthesized in [11](Tab.2, *ibid.*).

Other problems associated with 3DE solutions are related to inflow and outflow boundary conditions. In particular, when Re and Pe are low, there is no way to stop upstream diffusion. Conditions at z=0 are no longer known *a priori*, and, in general, the solution domain must be extended a certain distance upstream of the entrance section. The choice of outflow boundary conditions is crucial in any elliptic problem, since numerical instabilities caused by an inappropriate treatment of the outlet conditions can propagate to the upstream region and destroy the solution. All the options discussed above are expected to be viable when a fully developed condition is achieved. Numerical results in [33-36,38,39] indicate however, that this might not be the case for sufficiently high Ra-values, at least with certain combinations of geometry and thermal boundary conditions at the walls.

Control Volume discretizations, using staggered grids and primitive-variables, have in general been preferred for 3DE solutions. SIMPLE-based approaches seem to give the best performance, and, for the time being, these represent the most developed CFD tool available for the class of problems under consideration. In fact, some of the most efficient and updated CFD codes, such as Harwell-FLOW3D, and PHOENIX, are based on SIMPLE-type schemes.

In the same context, however, algorithms of the SIMPLE type present two major weaknesses:

i. with 3D features, the solution of the Poisson-like pressure and/or pressure correction equations is computationally very time-consuming. Even with SIMPLEC [57] and the use of a multigrid technique [58], under-relaxation is necessary for convergence. Optimum relaxation factors are problem-dependent, and difficult to determine by experiments;

ii. the segregated nature of the scheme implies that convergence becomes increasingly difficult, and even impossible for buoyancy-driven flows, as the leading parameters, Ra and Pr increase [59].

Alternative techniques have been developed to overcome the first difficulty. Examples are: PRIME (Pressure Implicit Momentum Explicit)[60] (recently tested on 3D buoyancy-driven cavity flows [61]), and APPLE (Artificial Pressure for Pressure-Linked Equation) [62].

As discussed by Galpin and Raithby [59], the second effect is connected with the bi-directional temperature-velocity coupling, due to the buoyancy term in the momentum equation, and the presence of the velocity components in the convective terms of the energy equation: at high Ra-values, relatively small temperature variations may induce high velocity variations, and *vice versa*, during the segregated iteration cycle. This can be the source of divergence, and, in any case, forces the use of very low under-relaxation coefficients.

An alternative strategy is to solve simultaneously the continuity-momentum-energy equation set. A few fully-coupled algorithms have been proposed in the literature, for isothermal incompressible flows [63-65]. So far, only one of them has been extended to consider buoyancy driven flows [59].

With the aim of checking the respective merits and performances of coupled algorithms, all the alternatives have been implemented, and compared for the basic case of the buoyancy driven vertical cavity. Results have been reported in a Conference paper [66]. The paper, is included in Appendix I of this Thesis (Paper [P13]). Its contents and the main findings are summarized here.

3.3.4 - The buoyancy driven cavity flow

The 2D square cavity in Fig.3.2 is considered, having the vertical walls at different temperatures (T'_h, and T'_c), and adiabatic horizontal walls.
The leading non-dimensional parameter, the Rayleigh number, Ra_c, is defined:

$$Ra_c = Gr_c\, Pr = \frac{\beta g H^3 \left(T'_h - T'_c\right)}{\nu^2} Pr \qquad (3.26)$$

According to the most up-to-date literature [67,68], two critical values of Ra exist for this problem: the first, Ra_{c1}, defines transition from steady laminar, to periodic flow; the second, Ra_{c2}, marks the passage to quasi-periodic flow (a combination of two periodic flows having non-commensurable frequencies). For further increasing Ra, the flow becomes chaotic/turbulent. Then, for the case of concern, no steady flow is possible above $Ra_{c1} = 1.7\text{-}1.93 \times 10^8$, and only a transient approach can give reliable predictions.

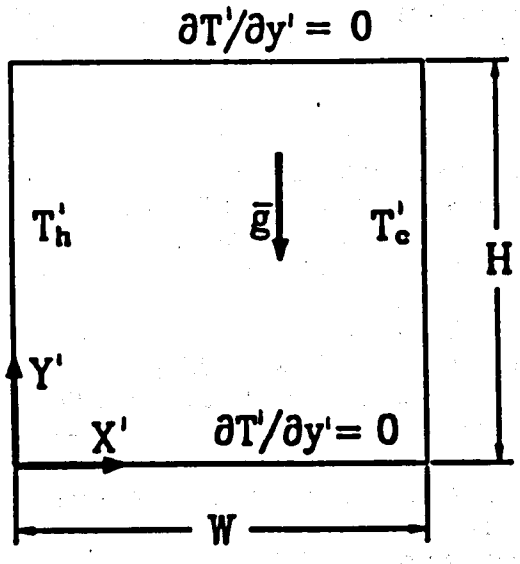

Fig.3.2 - 2D heated vertical cavity.

In this case, segregated algorithms are subject to the following stability condition over the (dimensional) time step, $\Delta t'$ [69]:

$$\Delta t' < \left(g\beta \frac{\partial T'}{\partial y'} \right)^{-\frac{1}{2}} \approx \frac{H^2}{\nu \, Gr_c^{\frac{1}{2}}} \qquad (3.27)$$

where $\partial T'/\partial y'$ indicates the vertical thermal stratification in the cavity core-zone. The condition becomes progressively more restrictive for increasing Ra_c, leading to numerical difficulties and exceedingly high costs.

Three coupled algorithms have been implemented, and tested for the buoyancy driven cavity problem. These are: Symmetrically Coupled Gauss-Seidel (SCGS), Symmetrically Coupled Alternating Line (SCAL), Coupled Equation Line Solver (CELS).

In all the methods staggered grids are used, the equations being discretized in transient conservative form. The continuity equation is left in its original form, and discretized with central differences. Convective terms in the energy equation are expressed with a Newton-Raphson expansion. This has been demonstrated to improve stability, and speed up convergence, for $Pr \geq 1$ [59]. In all the cases, use has been made of a linear multigrid accelerator of the type described by Hutchinson et al. [70].

SCGS - In this method, described by Vanka [63], and Vanka and Misegades [71], the variables associated with any scalar cell are simultaneously calculated. Including temperature, the method implies the solution of a linear system of six equations for each cell, in the course of any iteration. Note that the values of velocity are updated twice in the same iteration. Appropriate relaxation coefficients are necessary for speeding-up convergence.

SCAL - The method has been proposed by Rubin and Khosla [65] for isothermal cases. A line (row or column) is considered at a time, and all the variables associated with that line updated. The resulting system is of the tridiagonal block type. The method is applied following an alternate Zebra scheme, where alternate (odd or even) rows or columns are treated alternatively.

CELS - The method, presented by Galpin and Raithby [59,64] is a block-SLOR as SCAL, but basically differs from it in that the rows are sequentially swept. The method has the important characteristic that the continuity of mass is conserved not only at convergence, as in the above alternatives, but also in the course of iterations. However, implementation is more complex, and boundary rows demand special treatment.

Results for the lid-driven cavity flow have shown that SCALS is inferior to the other two methods in terms of velocity of convergence. Results for this method are not reported. The performances of CELS and SCGS are compared for a square heated cavity. In the figures the mass residual is plotted vs. the number of Work Units, WU, as an indication of computational efficiency. In multigrid procedures, a WU corresponds to one iteration over the finest grid.

Fig.3.3 indicates the effect of the Newton-Raphson (NR) linearization of the convective terms in the energy equation, in comparison with the standard formulation (ST). It is demonstrated that NR becomes necessary for convergence as the time step is increased.

The performances of CELS and SCGS are compared in Fig.3.4, over various grids. It is shown that the two algorithms are of comparable efficiency, even if the best result is obtained by SCGS over the finest grid (64x64).

One run was performed with a 256x256 grid, for $Ra_c=10^8$. Streamlines are shown in Fig.3.5. The results agree qualitatively and quantitatively with the best available numerical predictions in the literature [68].

a.

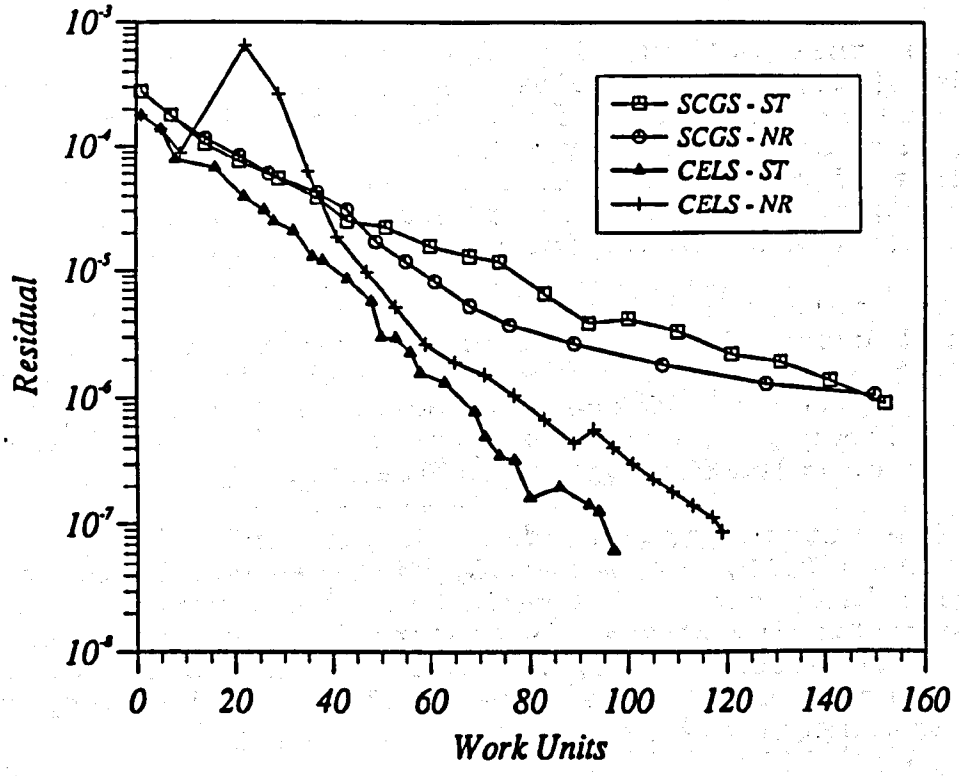

b.

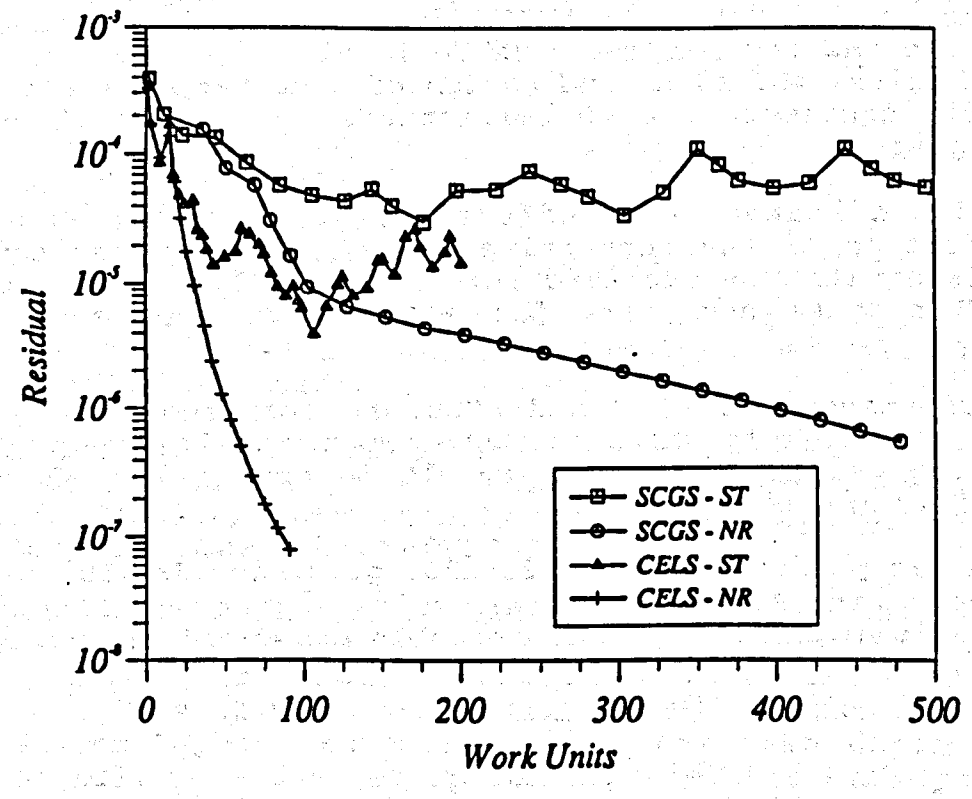

Fig.3.3 - Convergence tests for a square heated cavity; $Ra_c = 10^5$, grid (16x16). Non-dimensional time step: a.$\Delta t=2$; b.$\Delta t=10$. ST = standard; NR = Newton-Raphson.

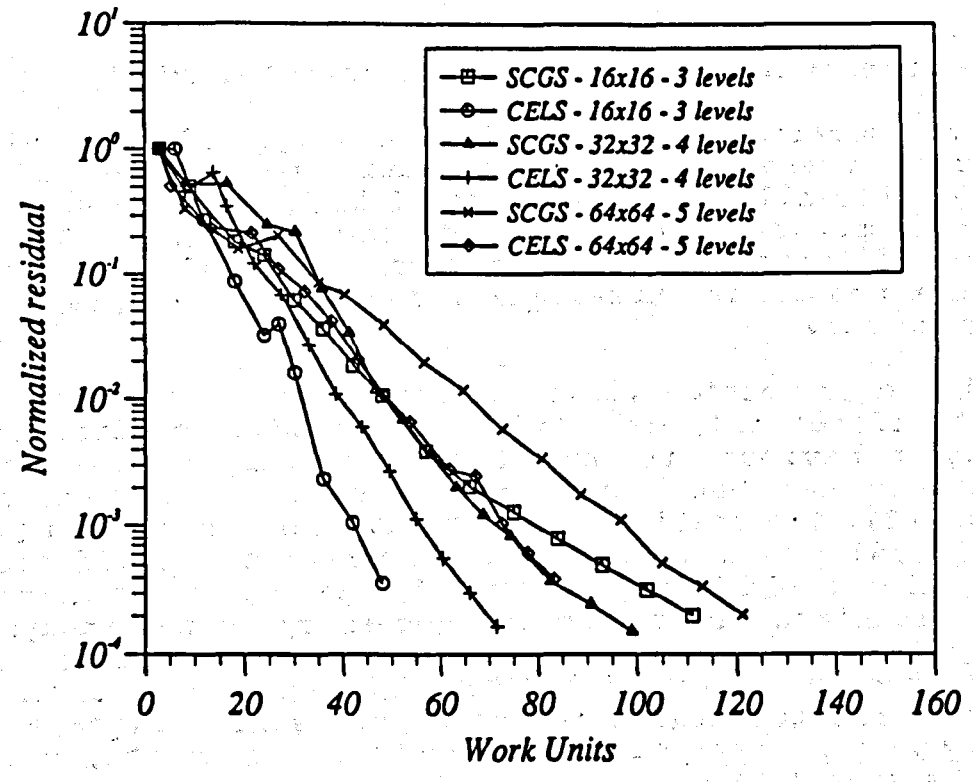

Fig.3.4 - Comparison of SCGS and CELS over various grids; $Ra_c = 10^5$, NR linearization.

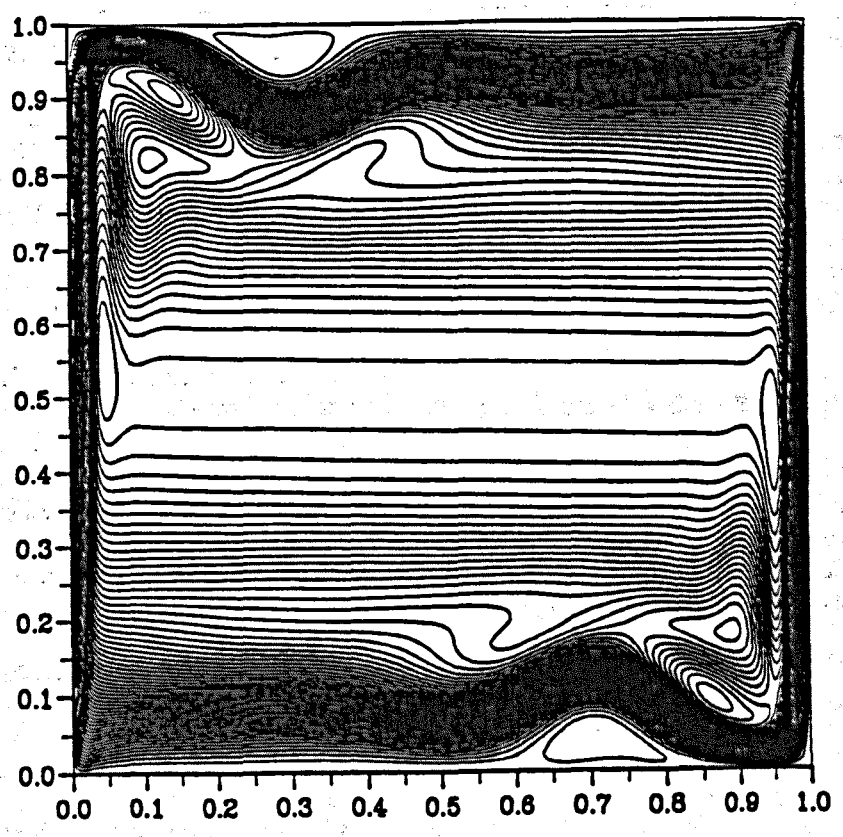

Fig.3.5 - Streamlines for a vertical heated cavity; $Ra_c = 10^8$, Pr = 0.71.

3.3.5 - Concluding remarks on numerical methods

The above numerical experiment has demonstrated that fully-coupled procedures represent a viable alternative to SIMPLE-based techniques of today. They allow the treatment of high Ra-flows with affordable cost and computational effort. This aspect becomes crucial for the modelling of intermediate flow regimes, where flow is unsteady, but turbulence models are unreliable, and direct transient approaches become necessary.

For combined convection flows the laminar stability limit is unknown for most, if not all, geometries and boundary conditions, however, unsteady behaviour is known to develop for increasing Ra. Unsteadiness has been observed experimentally, even in the low Ra-range [41]. The spatial oscillations, which have been predicted in [33-36,38,39], have received no experimental validation as yet. However, they could be indicative of some unsteady behaviour. Fully-coupled transient algorithms are necessary in the analysis of such unsteady regimes. The techniques are under development, and are likely to become an essential CFD tool in the near future.
Segregated 3DE techniques represent the state of the art. In this Thesis, the computational part has been carried out using Harwell FLOW3D, Release 3.

An acceptable compromise between accuracy and cost is represented by 2DE-tdz and 2DE-hdz solutions. However, their range of application has still to be determined for most geometries and boundary conditions. Comparison with 3DE solutions and experiments is necessary.

Asymptotic 2DE-fdz solutions can still give informative results; however they too need validation by more complete solutions, since their experimental validation is very difficult. For instance, by increasing Ra, double solutions may be found [72,73]. These have not yet been confirmed experimentally, and may in fact be indicative of unstable flow conditions.

3.4 - State of the Art

Considering that the amount of literature on combined convection in horizontal ducts is so large, and that several review papers have been published (as mentioned in § 3.2), the literature survey is presented in tabular form. The primary literature up to early 1992 is presented in Tables 3.1 - 3.6.

Letters and numbers are used to represent the different conditions, as follows:

G. GEOMETRY

1. Circular Tubes
2. Annular Tubes
3. Rectangular Ducts
4. Parallel Plate Ducts
5. Triangular Ducts
6. Semi-circular Tubes

O. ORIENTATION

1. Horizontal
2. Inclined

BC. THERMAL BOUNDARY CONDITION AT THE DUCT WALL

A. Adiabatic wall
H. Nominally uniform heat flux density (experimental papers only)
H1. Axially uniform heat flux density, and uniform temperature along the perimeter
H2. Uniform heat flux density either axially and circumferentially
Hcj. Axially uniform heat flux density, and conjugated wall effect along the perimeter
Hv. Heat flux density uniform axially, and non-uniform along the perimeter
T. Uniform wall temperature
T3. Convective boundary conditions at the outer wall surface
i,o Inner, outer surface (for annular tubes)
t,b,s Top, bottom, side surface(s) (for rectangular ducts)

DC. THERMAL AND FLOW DEVELOPMENT CONDITIONS

1. Fully developed flow
2. Thermally developing flow (fully developed inlet velocity profile)
3. Hydrodynamically developing flow (usually uniform inlet velocity profile)

PV. PROPERTY VARIATION (theoretical analyses only)

1. Variable density (Boussinesq approximation)
2. Variable density (non-linear temperature dependence, and/or non-Boussinesq effects)
3. Variable viscosity
4. Full property variation (density, viscosity, thermal conductivity, specific heat)

SM. SOLUTION METHOD (theoretical studies only)

1. Numerical, finite difference method
2. Numerical, control volume method
3. Numerical, finite element method
4. Numerical, boundary element method
5. Analytical, perturbation method
6. Analytical, boundary layer solution
7. Analytical, other

OP. OPERATING FLUID (experimental studies only)

1. Air or other gas
2. Water
3. Ethylene glycol
4. Ethyl alcohol
5. Oil
6. Sugar solutions
7. Liquid metals
8. Water glycerol solutions
9. Propylene glycol

ET. EXPERIMENTAL TECHNIQUE (experimental works only)

1. Wall temperature measurements
2. Pressure drop measurements
3. Velocity and temperature profile measurements
4. Visualization and optical methods
5. Electrochemical methods

The last column (Notes) in the tables indicates specific aspects considered or effects investigated in the solution/experiment.

TABLE 3.1 - Circular and semicircular ducts Theoretical Investigations

Author(s),Reference	G	O	BC	DC	PV	SM	Notes
Morton (1959) [74]	1	1	H2	1	1	5	
Del Casal and Gill (1962) [75]	1	1	H2	1	2	5	axial density variation
Iqbal (1966) [76]	1	2	H2	1	1	5	
Iqbal and Stachiewicz (1966) [77]	1	2	H2	1	1	5	
Iqbal and Stachiewicz (1967) [78]	1	2	H2	1	1	5	
Mori and Futagami (1967) [79]	1	1	H1	1	1	6	
Faris and Viskanta (1969) [80]	1	1	H1	1	1	5	
Siegwarth et al. (1969) [81]	1	1	H2	1	1	6	
Hwang and Cheng (1970) [82]	1	1	H2	1	1	1	BVM(*)
Newell and Bergles (1970) [83]	1	1	H1,H2	1	2(1)	1	(1) predictions for water
Siegwarth and Hanratty (1970) [84]	1	1	H1	1	1	1	
Cheng and Hong (1972) [85]	1	2	H2	1	1	1	BVM(*)
Cheng and Hong (1972) [86]	1	2	H2	1	1	1	BVM(*)
Cheng and Ou (1974) [87]	1	1	H2	2	1	1	high Pr solution
Hong et al. (1974) [88]	1	1	H2	2	1	1	high Pr solution, BVM(*)
Hieber and Sreenivasan (1974) [89]	1	1	T	2	1	7	series expansions
Hong and Bergles (1974) [90]	1	1	H2	2	1	1	high Pr solution, BVM(*)
Hong and Bergles (1974) [91]	1	1	H1,H2	1	1,3	6	
Hong and Bergles (1976) [92]	1	1	H1,H2	1	1,3	6	
Hong and Bergles (1977) [93]	1	1	H2	2	1	1	high Pr solution, BVM(*)
Ou and Cheng (1977) [94]	1	1	T	2	1	1	high Pr solution, BVM(*)
Cheng and Ou (1978) [95]	1	1	T	2	2(3)	1	(3)water density inversion
Futagami and Abe (1978) [96]	1	2	H2	1	1	7	series expansions
Patankar et al. (1978) [97]	1	1	H2t/Ab, H2b/At(2)	1	1	2	(2)half heated section

TABLE 3.1 - Circular and semicircular ducts
(continued) Theoretical Investigations

Author(s),Reference	G	O	BC	DC	PV	SM	Notes
Yao (1978) [98]	1	1	H1	3	1	5	perturbation sol. at the inlet
Yao (1978) [99]	1	1	T	3	1	5	perturbation sol. at the inlet
Hieber (1981) [100]	1	1	T	2	1		correlation of experimental data
Hieber (1982) [101]	1	1	T	2	1		correlation of experimental data
Allen et al. (1982) [102]	1	1	H(4)	2	4	1	(4)2D predictions of exp. data
Hishida et al. (1982) [52]	1	1	T	3	1	1	
Kato et al. (1982) [17]	1	1	T	2	1	1	
Swamy et al. (1983) [103]	1	1	Hv(5)	1	1	1	(5)sinusoidal heat flux distrib.
Futagami et al. (1983) [104]	1	1	Hc	1	1	1	effect of wall conduction
Hwang and Lin (1985) [105]	1	1	T	2	1	1	
Coutier and Greif (1985) [45]	1	1	T	2	1	2	
Coutier and Greif (1986) [44]	1	1	T3	2	1	2	
Nandakumar et al. (1985) [72]	1,6	1	H2	1	1	1	analysis of bifurcations
Law et al. (1987) [73]	1,6	1	H2b/At(2)	1	1	1	analysis of bifurcations
Chou and Hwang (1988) [20]	1	1	H2	2	1	1	VVM(*)
Choudhury and Patankar (1988) [30]	1	2	T	2	1	2	
Chen and Hwang (1989) [106]	1	1	Hcj	1	1	2	effect of wall conduction
Nguyen and Galanis (1987) [46]	1	1	H2	3	1	2	
Nguyen and Galanis (1989) [47]	1	1	H2	3	1	1	
Cheng and Ou (1990) [107]	1	1	T3	2	2(3)	1	(3)water density inversion
Skerget et al. (1990) [54]	1	2	T	2	1	4	
Orfi et al. (1991) [108]	1	2	H1	1	1	2	
Choi and Choi (1992) [109]	1	1	H2b/At(2)	1	1	1	analysis of bifurcations

(*) BVM: Boundary Vorticity Method
(*) VVM: Velocity Vorticity Method

TABLE 3.2 - Circular and semicircular ducts
Experimental Investigations

Author(s),Reference	G	O	BC	DC	OF	ET	Notes
Kern and Othmer (1943) [110]	1	1	T	2	5	1	
Scott et al. (1955) [111]	1	1	T	2	2,5	1	
Petukhov and Nol'de (1959) [112]	1	1,2	T	3(1)	2	1	(1)sharp entry
Iqbal (1966) [76]	1	2	H(2)	2	2	1	(2)finned tube with top heating
Ede (1961) [113]	1	1	H	1	1,2	1	laminar and turbulent data
Jackson et al. (1961) [114]	1	1	T	3(1)	1	1	(1)sharp entry
Oliver (1962) [115]	1	1	T	2	2,4,7	1	
Brown and Thomas (1965) [116]	1	1	T	2	2	1	
McComas and Eckert (1966) [117]	1	1	H	2	1	1	
Mori et al. (1966) [118]	1	1	H	1	1	1,3	laminar and transitional data
Baker (1967) [119]	1	1	H(2)	3	2	1	(2)finned tube with top heating
Kupper et al. (1969) [120]	1	1	H	2	2	1	
Shannon and Depew (1968) [121]	1	1	H	2	2	1,2	
Shannon and Depew (1969) [122]	1	1	H	2	3	1,2	effect of viscosity
Hussain and McComas (1970) [123]	1	1	H	2	1	1,2	
Petukhov and Polyakov (1967) [124,125]	1	1	H	2	2	1	
Petukhov et al. (1969) [48]	1	1	H	2,3	2	1	laminar and transitional data
Petukhov and Polyakov (1970) [126]	1	1	H	2	2	1	analysis of transition
Siegwarth et al. (1969) [81]	1	1	H	1	3	1,3	
Siegwarth and Hanratty (1970) [84]	1	1	H	1	3	3	
Bergles and Simonds (1971) [127]	1	1	H	1	2	1	
Depew and August (1971) [128]	1	1	T	2	2,4,8	1	
Lichtarowicz (1972) [129]	1	1	H	1	1	1,3	
Nagendra (1973) [130]	1	1	H	2	2	1,2	analysis of transition

TABLE 3.2 - Circular and semicircular ducts
(continued) Experimental Investigations

Author(s),Reference	G	O	BC	DC	OF	ET	Notes
Hong et al. (1974) [88]	1	1	H	1	2,3	2	glass and metal tubes
Depew et al. (1975) [131]	1	1	H	2	2	1	
Morcos and Bergles (1975) [29]	1	1	H	1	2,3	1	analysis of wall conduction
Sabbagh et al. (1976) [132]	1	2	H	1	1	1,3	
Hattori and Kotake (1978) [133]	1	1	H	2	2,6	1	
Sicardi et al. (1978) [134]	1	1	T	2	8	1,2	2D solutions
El-Hawary (1980) [135]	1	1	H	2	2	1,2	analysis of transition
Yousef and Tarasuk (1981) [136]	1	1	T	3	1	1,4	interferometric data
Yousef and Tarasuk (1982) [137]	1	1	T	3	1	1	
Kato et al. (1982) [17]	1	1	T	2	1	1	
Swamy et al. (1982) [103]	1	1	H(3)	2	1	1,3	(3)non-uniform wall thickness
Barozzi et al. (1985) [138]	1	1,2	H	3	2	1	laminar and transitional data
Coutier and Greif (1985) [45]	1	1	T	2	2,9	1,3	
Coutier and Greif (1986) [44]	1	1	T3	2	2,9	1,3	
Cheng and Yuen (1984) [139]	1	1	T	2	1	4	smoke visualizations
Cheng and Yuen (1985) [140]	1	2	T	2	1	4	smoke visualizations
Ghajar et al. (1990) [141]	1	1	H	3	2	1,2	entry geometry and transition
Lei and Trupp (1991) [142]	6	1	H	2	2	1,2	

TABLE 3.3 - Annular tubes
Theoretical Investigations

Author(s),Reference	G	O	BC	DC	PV	SM	Notes
Hattori (1977) [143]	2	1	H1i/Ao, H1,Ai/H1o	1	1	5,1	
Mojtabi & Caltagirone (1980) [144]	2	1	Ti/To	1	1	5,1	
Nguyen et al. (1983) [145]	2	1	Ti/To	1	2(1)	5,1	(1)water density inversion
Kotake (1985) [146]	2	1	H1i/Ao Ai/H1o	1	1	1	
Kotake and Hattori (1985) [147]	2	1	H1i/Ao Ai/H1o	1	1	1	
Nieckele and Patankar (1985) [148]	2	1	H2i/Ao	1	1	2	
Kaviany (1986) [149]	2	1	H2i/Ao	1	1	1	
Karki and Patankar (1989) [31]	2	1	Ti/Ao	3	1	2	
Terhmina et al. (1992) [42]	2	1	Ti/To	3	1	1	VVM(*)

(*) BVM: Boundary Vorticity Method
(*) VVM: Velocity Vorticity Method

TABLE 3.4 - Annular tubes
Experimental Investigations

Author(s),Reference	G	O	BC	DC	OF	ET	Notes
Huetz and Petit (1974) [150]	2	1	Hi/Ao	1	7	1	
Hattori and Kotake (1978) [133]	2	1	Hi/Ao, H,Ai/Ho	2	2,6	1	
Bhone and Obermeier (1986) [151]	2	2	Hi/Ao	2	2,3	1	
Ciampi et al. (1986) [152]	2	1	Hi/Ao	1	2	1	
Ciampi et al. (1987) [153]	2	1	Hi/Ao	1	2	1,4	transitional data
Ciampi et al. (1987) [154]	2	1	Hi/Ao	1	2	1,4	laminar and transitional data

TABLE 3.5 - Rectangular, triangular, and parallel plate ducts Theoretical Investigations

Author(s),Reference	G	O	BC	DC	PV	SM	Notes
Gill and Del Casal (1962) [155]	4	1	H2	1	1	7	2D solution
Mori and Uchida (1966) [156]	4	1	Tt/Tb	1	1	7	stability analysis
Cheng and Hwang (1968) [157]	3	1	H1	1	1	1	
Nakayama et al. (1970) [158]	4	1	Tt/Tb lin. var.	1	1	7	stability analysis
Hwang and Cheng (1971) [159]	4	1	Tt/Tb	1	1	1	BVM(*)
Cheng et al. (1972) [25]	3	1	H2	2	1	1	high Pr solution BVM(*)
Kiya et al. (1972) [160]	4	1	T	3	1	1	2D solution
Hwang and Cheng (1973) [161]	4	1	Tt/Tb	2	1	1	stability analysis
Ou et al. (1974) [162]	3	1	T	2	1	1	high Pr solution BVM(*)
Chang et al. (1976) [163]	3	1	H1(1)	1	1	1	(1)esothermic wall reaction
Ou et al. (1976) [164]	3	2	H2	1	1	1	BVM(*)
Matsumoto et al. (1978) [165]	4	1	H2t/H2b	1	1	1	int. heat gen. stab. analysis
Nakamura et al. (1978) [166]	3	1	H1	1	1	1	
Abou-Ellail and Morcos (1979) [26]	3	2	H2	3	1	2	
Nguyen et al. (1979) [167]	4	1	T	3	1	1	2D solution
Abou-Ellail and Morcos (1980) [27]	3	2	H2	3	1	2	
Cheng and Ou (1982) [168]	3	1	Tt/Tb/As	1	1, 2(2)	1	(2)water density inversion
Abou-Ellail and Morcos (1983) [28]	3	1	H2	3	1	2	
Cheng and Ou (1983) [37]	3	1	Tt/Tb/As	1	1	1	effect of axial tilting
Fukui et al. (1983) [169]	4	1,2	Tt/Tb	1	4	1	
Chow and Wang (1984) [170]	3	1	H1	1	1	1	
Nandakumar et al. (1985) [72]	3	1	H1	1	1	1	analysis of bifurcations
Hwang and Chou (1987) [171]	3	1	Hcj	1	1	1	effect of wall conduction

TABLE 3.5 - Rectangular, triangular, and parallel plate ducts (continued) Theoretical Investigations

Author(s),Reference	G	O	BC	DC	PV	SM	Notes
Incropera and Schutt (1985) [33]	3	1	H2t/H2b Tt/Tb	2,3	1	1	
Incropera et al. (1986) [34]	3	1	H2t/H2b Tt/Tb	2,3	1	1	
Incropera (1986) [4]	3	1	H2t/H2b	2,3	1	1	review paper
Naito (1985) [172]	4	1	T,H2	3	1	1	2D solution
Chou and Hwang (1987) [18]	3	1	H2	2	1	1	VVM(*)
Chiu et al. (1987) [173]	3	1	Tt/Tb/As	1	1	3	
Mahaney et al. (1987) [194]	3	1	Ats/H2b	3	1	2	
Muralidhar and Kulacki (1987) [205]	4	1	Tt/Tb	2	1	7	stability analysis
Law et al. (1987) [73]	3	1	H2b/At	1	1	1	analysis of bifurcations
Lavine (1988) [174]	4	2	H2	1	1	7	opposing flow
Mahaney et al. (1988) [36]	3	1	H2tbs/ Atbs(3)	3	1	2	(3)various combinations
Biswas et al. (1989) [50]	3	1	Ats/H2b	3	1	2	
Nonino et al. (1989) [38]	3	1	Ats/H2b	3	1	3	
Naito and Nagano (1989) [175]	4	2	Tt/Ab At/Tb	3	1	1	2D solution
Biswas et al. (1990) [51]	3	1	Ats/Tb	3	1	2	
Chou and Hwang (1990) [19]	3	1	H2	2	1	1	VVM(*)
Chen et al. (1990) [176]	4	2	H2	1	1	2	opposing flow
Huang et al. (1990) [177]	3	1	T	2	1	1	VVM(*); effect of gas radiation
Rheault and Bilgen (1990) [178]	4	2	Tt/Tb	3	1	1	analysis of flow reversals
Chou and Lien (1991) [206]	3	1	Hcj	2	1	1	VVM(*) effect of wall conduction
Lin et al. (1991) [207]	3	1	Tt/As/Tb Ats/Tb & T	2	1	1	VVM(*)
Nonino and Del Giudice (1991) [39]	3	1	At/H2b/As	3	1	3	
Lee and Hwang (1992) [179]	4	2	Tt/Tb	2	1	1	3D stability analysis
Lin et al. (1992) [180]	3	1	Ats/Tb(4)	2	1	1	VVM(*); (4)with mass transfer
Nyce et al. (1992) [41]	3	1	Tt/As/Tb	2	1	2	
Nakamura et al. (1977) [181]	5	1,2	H1	1	1	1	isosceles and equil. sectns.

TABLE 3.6 - Rectangular, triangular, and parallel plate ducts Experimental Investigations

Author(s),Reference	G	O	BC	DC	OF	ET	Notes
Altman and Staub (1958) [182]	3	1	H	3	1	1,2	laminar and transitional data
Mori and Uchida (1966) [156]	3	1	Tt/Tb/As	1	1	3,4	
Akiyama et al. (1971) [183]	4	1	Tt/Tb	1	1	4	
Ostrach and Kamotani (1975) [184]	4	1	Tt/Tb	1	1	1,2	
Hwang and Liu (1976) [185]	4	1	Tt/Tb	2	1	4	
Kamotani and Ostrach (1976) [186]	4	1	Tt/Tb	2	1	2	
Nakamura et al. (1978) [187]	3	1	T	2		5	electrochemical method
Kamotani et al. (1979) [188]	4	1	Tt/Tb	2	1	1,3 4	
McLarnon et al. (1982) [189]	3	1	Ats/Tb	3		4,5	interferom. and electrochem meth.
Fukui et al. (1983) [169]	4	1,2	Tt/Tb	1	1	3,4	LD velocimetry
Jorné and Labelle (1985) [190]	3	1	Ats/Tb	2		5	electrochemical method
Osborne and Incropera (1985) [191]	4	1	Ht/Hb	2	2	1,3 4	
Osborne and Incropera (1985) [192]	4	1	Ht/Hb	2	2	1,3 4	transitional and turbulent data
Incropera et al. (1986) [34]	4	1	Ht/Hb	2,3	2	1,4	
Incropera (1986) [4]	4	1	Ht/Hb	2	2		review paper
Incropera et al. (1987) [193]	4	1	At/Hb	2	2	1,4	
Maughan and Incropera (1987) [194]	4	1,2	At/Hb	2	1	1	
Chiu and Rosenberger (1987) [56]	4	1	Tt/Tb	2	1	4	LD velocimetry
Chiu et al. (1987) [173]	4	1	Tt/Tb	1	1	4	LD velocimetry
Lavine et al. (1989) [195]	4	2	Tt/Tb	2	2	4	opposing flow, flow reversal
Smith and Salman (1991) [196]	3	1	Ht/Hb	3	1	1	
Nyce et al. (1992) [41]	3	1	Tt/As/Tb	2	1	2	

(*) BVM: Boundary Vorticity Method
(*) VVM: Velocity Vorticity Method

3.5 - Circular ducts with uniform heating.

Since most of the remainder of the Thesis will be devoted to the analysis of a horizontal duct with uniform heating at the wall, this special case will be discussed in appropriate detail.

There is substantial agreement in the literature, that with this boundary condition the effect of buoyancy is stronger than with the isothermal boundary condition, since the thermogravitational effect is maintained along the duct, and does not vanish in the downstream region. Mainly for this reason case **H** has received more experimental attention than case **T**, even if this latter case is of wider practical application. Also, it is well established that the effect of buoyancy is higher for the horizontal than vertical orientation. Having been studied so widely, this case is the most appropriate for benchmarking purposes. In fact, the amount of available experimental and theoretical data should now be sufficient for creating reliable reference solutions to this combined convection problem.

The essence of the phenomenon in horizontal tubes under condition **H** is the formation of a secondary flow in the form of a double helix, caused by an upward motion of the warm fluid along the relatively hot side walls, and a downward motion in the relatively cooler and denser core. This two vortex structure has been demonstrated experimentally for a long time, and is now well documented: photographs of the flow of water at Re=150 in plan and elevation have been presented by Newell and Bergles [83]. Experimental evidence was also reported for water (refs.[1,2,4,5] in [83]) and oil (ref.[6] in [83]). Velocity and temperature profiles with air have been given by Mori et al.[118], and Lichtarowicz [129]. Siegwarth and Hanratty [84] gave temperature and velocity profiles for ethylene glycol. Mori and Futagami [79] presented visualization experiments with air.

As the fluid moves down the straight tube, the flow is symmetrical about a vertical plane along the tube axis. However, symmetry about a horizontal plane is not maintained, as shown by Hong and Bergles [90], and the eye of the circulation drops below the tube axis in the fully developed region. As a consequence, the axial velocity profile results show a modification of maximum occurring in the lower part of the section. A more important result of this auxiliary motion is to greatly enhance the convective cooling effect to the wall along the sides and at the bottom, since the secondary flow velocity components are significantly higher in the lower pipe region and lower in the upper region. In fact, a stratified flow situation develops in which a relatively hot fluid layer accumulates along the top and reduces the convective energy transfer there. The gross result is a departure from constant property predictions at some distance from the inlet section. Further downstream a fully developed condition is eventually reached, where the local average Nusselt number remains constant.
The secondary circulation can cause large variations in the circumferential wall temperature, unless the wall itself has a high conductive capability. In this latter case, however, while the wall temperature becomes uniform, the heat flux density distribution along the circumference becomes highly non-uniform.

The combination of forced and free convection leads to average heat transfer coefficients in the downstream region which are higher than pure forced convection by a factor of 2 or 3. The effect increases for increasing Rayleigh number. With uniform heating, this implies a reduction of the locally averaged wall temperature. It can be observed, however, that non-uniformities in the wall temperature may preclude taking advantage of this higher average convective capability.

The available information on case **H** is collated according to the following scheme:

A.- Entrance effects, and criteria for the onset of buoyancy.
B.- Fully developed flow.
C.- Effects of wall conduction.
D.- Temperature-dependent properties.
E.- Transition and backflow conditions.
F.- Inclination.
G.- Other H-type boundary conditions.

A.- Entrance effects, and criteria for the onset of buoyancy.

Experimental data relevant to the thermal inlet region, with a parabolic entry profile, have been presented in [117,123] for air, and in [48,121,122,124,131] for water and ethylene-glycol. Numerical results have been presented in [20,87,90,93].
It is rather difficult to extract some general conclusions from the experimental data, since most of the experiments show unexpected behaviour and a large scatter of the results. For instance, McComas and Eckert [117] data show an effect of Re which should not be present, according to dimensional analysis considerations. Hussain and McComas [123] found Nu-values lower than constant property predictions in some runs, and asymmetries in the wall temperature distribution. Shannon and Depew [121] used water initially at the ice point; the density inversion effect near the duct entrance could then have influenced the development process. The results do not indicate any fully developed behaviour, and are very scattered. Petukhov and Polyakov's [124] water data are, on the contrary, very regularly behaved. They noted that, at the upper generatrix, the local Nusselt number, Nu_l, was always lower than constant property predictions. In the lower portion of the duct, Nu_l steadily increased with z^*. For relatively low z^*, Nu_z was as for forced convection flow, but there was already an appreciable disparity in the values of Nu_l. As for the thermal entrance length, Petukhov et al.[48] found that it remained the same as in pure forced convection, when considering axial distributions of the local wall temperature. A Re-dependency of T_w was sometimes observed at the bottom of the wall.

Depew et al.[131] presented data for water in three stainless steel ducts. In some runs the bottom temperature fell below the bulk mean temperature and negative values of Nu_l were obtained.

Numerical results for the entrance region are all for boundary condition **H2**.

Hong and Bergles [90], and Hong et al. [88] used the boundary vorticity method and the high-Pr assumption. They presented axial distributions of temperature and secondary flow circulations. They observed that the centres of circulation first appeared on the radial line $\theta=\pi/2$; then, with increasing the distance from inlet, they tended first to move upward, and then downward and towards the wall.
The fully developed condition was assumed to be dT'/dz'=constant. Data for the entrance length were plotted, either based on this, or the 5% criterion (Fig.2-12 in [90]). It was noted that, when the calculation proceeded beyond the defined fully developed point, Nu_z started increasing or oscillating. The oscillation was attributed to numerical instability, in that temperature and secondary velocities continued to change downstream of the fully developed point. A similar minimum had been found in [25] with a rectangular duct. It was argued that a similar stability problem could have arisen.

Cheng and Ou [87] also used the high-Pr assumption. Their distributions for Nu_z show that the asymptotic behaviour is reached after a series of oscillations for the lowest Ra-values, while at higher Ra the results have a more regular decreasing trend.

The most recent numerical solution for the thermal inlet region has been given by Chou and Hwang [20]. The results demonstrate the effect of Pr and Ra_q on either Nu_z and fRe. In general, it was shown that the secondary circulations become the more intense as Pr decreases. More specifically, the friction factor steadily increased for increasing Ra_q. The typical trend for fRe, at constant Ra_q and Pr, is to follow the constant property prediction near the inlet, to increase with z^* up to a maximum, and then to decrease towards the asymptotic value. For increasing Ra_q (at constant Pr), the point of departure from constant property, the maximum, and the beginning of the fully developed region, all move upstream. For increasing Pr (at constant Ra_q), the maximum and fully developed points shift downstream, while the detachment from constant property curves is irregular. It is worthy of note that, for Pr=0.7, $Ra_q=1.6\times10^5$, multiple pair eddies appear at $z^*=8\times10^{-3}-1.4\times10^{-2}$, but that single pair eddies are finally obtained at $z^*\geq2\times10^{-2}$.
(Nu_z-z^*) plots for Pr=0.7,2, and 5;and $Ra_q=1.6\times10^5$, 4.8×10^5, 1.6×10^6, and 6×10^6, show an oscillating behaviour in the thermal development region. The comparison with the data of Petukhov and Polyakov [124] is satisfactory, except at $Ra_q=6\times10^6$, where experimental data are largely underpredicted.

The prediction of significant buoyancy effects is of great practical consequence. Criteria have been proposed, based on the deviation of Nu_z from constant property predictions. These all relate to the case of a fully developed (parabolic) entry velocity.

Petukhov and Polyakov [124] gave the following 5% criterion for water (Pr=2-10):

$$Ra_{q,ob} = \frac{5\times10^3}{z^*} \qquad \text{for} \quad z^* \leq 1.7\times10^{-3} \qquad (3.28)$$

$$Ra_{q,ob} = 1.8x10^4 + \frac{55}{(z^*)^{1.7}} \qquad \text{for} \qquad z^* \geq 1.7x10^{-3} \tag{3.29}$$

The following equation was given for Nu_z:

$$\frac{Nu_z}{Nu_{z,cp}} = \left[1 + \left(\frac{Ra_q}{Ra_{q,ob}}\right)^4\right]^{0.045} \tag{3.30}$$

In [48] this was completed with the following 1% correlation for the local Nusselt number, Nu_l, at the lower or the upper generatices:

$$Ra_{q,ob} = \frac{3.8x10^3}{z^*} \qquad \text{for} \quad z^* \leq 2x10^{-3} \tag{3.31}$$

$$Ra_{q,ob} = \left(2.3x10^3 + \frac{7.8}{z^{*2}}\right)\left(1 - \frac{150z^{*2}}{1 + 55x10^4 z^{*4}}\right) \quad \text{for} \quad z^* \geq 2x10^{-3} \tag{3.32}$$

Based on measurements with water [121] and ethylene-glycol [122], Shannon and Depew suggested the criterion

$$\frac{Ra_{q,ob}^{0.25}}{Nu_{z,cp}^{1.25}} = 1.75 \tag{3.33}$$

A similar criterion was suggested by Allen et al.[102], based on the departure of experimental data from numerical predictions including fully property variations (omitting buoyancy).
Chen and Ou [87], based on numerical data ($Pr \rightarrow \infty$), gave a correlation for a 2% deviation from constant property predictions:

$$Ra_{q,ob} = 52.16\, z^{*-1.61} \tag{3.34}$$

The following 1% criterion was reported by Polyakov [6] for the limiting value of Ra:

$$Ra_{q,ob} = \frac{1.1x10^3}{Nu_{z,cp}\left[1 - \exp(-100z^*)\right]^3} \tag{3.35}$$

For air in the fully developed region, according to the experimental data of Mori et al.[118], and Lichtarowicz [129], the effect of buoyancy appears in the range Ra_q~2-4x10^3.

For Pr=∞, the constant property solution is valid (within 5% accuracy) up to Ra_q<1.6x10^4, according to the numerical results of Hong and Bergles [90]. A plot for the departure from constant property predictions was presented in [90], for condition **H2** (Pr=∞).

The results by Chow and Hwang [20] show that the onset of buoyancy is anticipated for increasing Ra and Pr.

The above observations are collated and compared in Fig.3.6.
Finally, the following correlation for Nu_z was proposed by Churchill [8] for either horizontal and vertical tubes:

$$Nu_z^6 = Nu_{z,cp}^6 + Nu_N^6 \tag{3.36}$$

The asymptotic equations for forced and natural convection in horizontal ducts are:

$$Nu_{z,cp} = 5.364\left[1 + \left(\frac{\pi}{220z^*}\right)^{\frac{10}{9}}\right]^{0.3} - 1 \tag{3.37}$$

$$Nu_N = 0.847\left(Ra_q\right)^{0.177}\left[1 + \left(\frac{0.492}{Pr}\right)^{\frac{9}{16}}\right]^{-0.315} \tag{3.38}$$

This equation fits reasonably well the data for water in [124]

Data relevant to the case of uniform entry velocity are much less extensive, and no correlation has been proposed for this case.
In [126], Petukhov and Polyakov indicated that with a uniform inlet velocity, the effect of free convection manifests itself at higher values of $Ra_{q,ob}$, in respect to the case of parabolic entry. This confirms previous findings by Bergles and Simonds [127], who provided a composite plot for water also including some experimental data by Roy (ref.[15] in [127]), for the onset of significant buoyancy. Nguyen and Galanis [47] investigated the case numerically, for Pr=7; they found that, in terms of Nu_z, the forced convection region, where constant property predictions apply, extends up to $z^*\sim 2.x10^{-3}$; $1.5x10^{-3}$; and $7.2x10^{-4}$, for $Ra_q=5x10^5$; $1x10^6$; and $3x10^6$, respectively.

Non-uniform inlet velocity profiles have sometimes been used in experiments.

Ghajar et al. [141] used a square-edged, and a re-entrant entrance, over a wide Re-range (Re=200-15000). They observed some natural convection effect in the laminar regime. An Re-dependent effect on heat transfer data was observed, but data are not sufficient to clarify the effect of the entrance geometry on the onset of buoyancy.
The results of Barozzi et al. [138] were obtained with a short converging section. There too, some uncontrolled entrance effects might have been present.

▲	[6] eqn.(3.35)	1% departure from Nu_{zcp}
◊	[87] eqn.(3.34)	2% departure from Nu_{zcp}
❑	[48] eqns.(3.31/3.32)	2% departure from Nu_{lcp}
■	[124] eqns.(3.28/3.29)	5% departure from Nu_{zcp}
◆	[121] eqn. (3.33)	

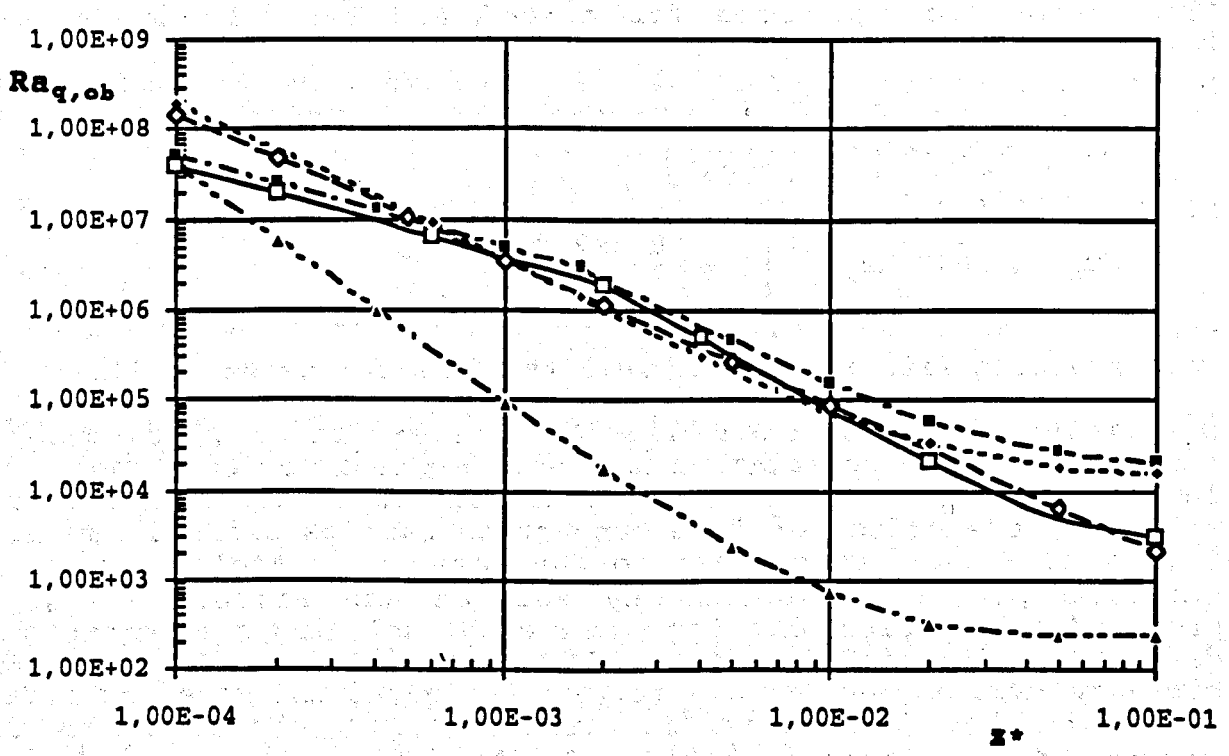

Fig.3.6 - Comparison of correlations for the onset of buoyancy, with parabolic entry velocity.

B.- Fully developed flow.

With boundary conditions of type H, a fully developed flow condition is expected to be established at a certain downstream distance. Mathematically, this implies that axial derivatives of pressure and temperature, as well as the velocity components are invariant with z*; correspondingly, the Nusselt number and the friction factor assume a constant value.
Those conditions are not always achieved in experiments. Fully developed conditions were obtained in [118,124,129,131,133,138], using different fluids and tube materials. However, no asymptotic behaviour was obtained in [121], over the range explored. The data for air in [117] behave regularly for Gr up to 500 and Re~740, but for Gr~1000, Re~200, Nu_z shows an increasing trend with z*, and almost doubles the constant property value at the end of the heat transfer section. A similarly anomalous case was observed in [138].

This behaviour cannot be explained in the light of the present knowledge of combined convection.

Fully developed combined convection has been the subject of intensive theoretical investigation. Perturbation solutions were used by Morton [74],Faris and Viskanta [80], and Del Casal and Gill [75]. These are all limited to very low values of Ra_q, and have little practical value. However, it is interesting to note that in [75], both the effects of non-uniformities in the axial pressure gradient, and minor effects involving the Froude number were considered.
The following expression was obtained for the friction factor:

$$f_z = \frac{16}{Re}\left[1 + \left(\frac{34.8}{4} Re\, Pr + \frac{0.21}{16} Re^2\, Pr^2\right)\left(\frac{1}{2}\frac{1}{2304}\frac{Ra_q}{Pe^2}\right)^2\right] \qquad (3.39)$$

Boundary layer solutions were presented by Mori and Futagami [79], Siegwarth et al [81], and Hong and Bergles [90]; these are expected to hold for large Ra-values.

Mori and Futagami [79] presented correlations for the apparent friction factor (eqn.(57) in [79]), and Nu_{fd}; the latter, for case **H1**, is:

$$\frac{Nu_{fd}}{Nu_{fd,cp}} = 0.1238 Gr_q^{0.2} \qquad \text{for } Pr = 0.72 \qquad (3.40)$$

$$\frac{Nu_{fd}}{Nu_{fd,cp}} = 0.1462 Gr_q^{0.2} \qquad \text{for } Pr = 1 \qquad (3.41)$$

These were given as appropriate for $Gr_q > 4\times10^4$. Good agreement was found with experimental data in [118].

Siegwarth et al [81] considered case **H1**, using a boundary layer approach. They showed that for $Pr=\infty$ the secondary flow has no effect on the primary flow, and the convective terms are small compared with the viscous terms over the whole cross section. Their final correlation for Nu_{fd} ($Pr=\infty$) is:

$$Nu_{fd} = 0.560(Ra)^{0.25} = 0.629\left(Ra_q\right)^{0.20} \qquad (3.42)$$

The comparison with measured temperature profiles, and Nu-values by Readal (ref.[11] in [81]), was very good. Readal's experiments for ethylene glycol ($Pr=80$) covered the range $Ra_q = 3.42\times10^8 - 3.79\times10^9$.

Hong and Bergles [90] used the boundary layer concept to analyze fully developed combined convection with variable viscosity. With constant viscosity, their correlations for Nu_{fd} ($Pr=\infty$) are:

$$Nu_{fd} = 0.5221 Ra^{0.25} = 0.5946 Ra_q^{0.20} \qquad \text{for case } \mathbf{H1} \qquad (3.43)$$

$$Nu_{fd} = 0.3950 Ra^{0.25} = 0.4756 Ra_q^{0.20} \quad \text{for case } \mathbf{H2} \tag{3.44}$$

Note that the constant 0.5221 for case **H1** is 6.8 % lower than the constant in Siegwarth et al. [81] equation.
Newell and Bergles [83] gave fully developed solutions for water for either infinite (**H1**) and zero (**H2**) wall conductivity.

The numerical results of Hong and Bergles [90] for condition **H2** ($Pr=\infty$, $Ra_q>6.4x10^4$) were correlated within 1% as:

$$Nu_{fd} = 0.4451(Ra)^{0.215} = 0.788\left(Ra_q\right)^{0.177} \tag{3.45}$$

Criteria for the thermal entrance length were also presented (as Fig.2.13, *ibid.*).

For case **H2**, Cheng and Ou [87] suggested the equations ($Pr=\infty$; $Ra_q=1.6x10^4-2.5x10^7$):

$$Nu_{fd} = 4.36 + 0.143 Ra_q^{0.25} \tag{3.46}$$

$$Nu_{fd} = 3.40 + 0.303 Ra^{0.25} \tag{3.47}$$

Mori et al.[118] correlated their experimental data for air in a brass tube, as:

$$Nu_{fd} = 0.462\left(Gr_q\right)^{0.2}\left[1 + \frac{2.38}{\left(Gr_q\right)^{0.2}}\right] \tag{3.48}$$

Petukhov and Polyakov [124] correlated their own fully developed data for water as:

$$Nu_{fd} = 4.36\left[1 + \left(\frac{Ra_q}{1.8x10^4}\right)^4\right]^{0.045} \tag{3.49}$$

The following equation was proposed by Hattori and Kotake [133], for water and sugar syrup solutions in the range $3<Pr<120$; $5x10^4<Gr_qPr^{1.4}<1.25x10^9$ (properties evaluated at film temperature):

$$Nu_{fd} = 0.5014 Ra_q^{0.2}\, Pr^{0.08} \tag{3.50}$$

Chou and Hwang [20] presented numerical data for fRe/fRe_{cp}, and Nu_{fd}, over the range: $Ra_q = 1.x10^4 - 1.x10^6$; $Pr=0.7$, 2, and 5.

C.- Effects of wall conduction.

In combined convection experiments large differences are found in the circumferential wall conduction, both in its influence and in the measurement of its effect. Depew et al.[131] commented that for gases the flow does not support a large circumferential temperature

variation; for instance, McComas and Eckert [117] with air in a Nichrome tube found a maximum top to bottom temperature difference of 0.2°C, and Mori et al. [118] obtained 0.3°C in a thin walled brass tube. However, Kupper et al. [120], using water in an inconel tube, observed wall temperature differences as high as 5°C. Hong et al [88] used Pirex E-C coated and stainless steel tubes with water and ethylene glycol, for $Ra=5x10^4-1x10^6$. The temperature difference between the top and the bottom of the tube ranged from 3 to 50°C for the glass tube and from 2 to 45°C for the metal tube. This latter result suggests that the chosen metal tube was not a good model of boundary condition **H1**. A numerical integration scheme was used to calculate the average wall temperature. A similar approach, based on a simplified 1D analysis of the wall, had been used in [124].

From dimensional analysis considerations, Hong et al. [88] and Morcos and Bergles [29] deduced that an appropriate correlating parameter for the effect of the wall is the ratio between the convective and circumferential heat conductances. The wall parameter is defined:

$$Pw = \frac{h_{fd}D}{k_w}\frac{D}{t} \tag{3.51}$$

where, t is the wall thickness. A modified wall parameter was also defined as:

$$Pw^* = \frac{k_f}{k_w}\frac{D}{t} \tag{3.52}$$

Hong et al. [88] correlated 92% of their data within ±10% with the equations (all properties evaluated at film temperature):

$$Nu_{fd} = \frac{0.378Gr^{0.28}\,Pr^{0.33}}{Pw^{0.12}} \tag{3.53}$$

$$Nu_{fd} = \frac{0.42Gr^{0.25}\,Pr^{0.30}}{Pw^{*0.12}} \tag{3.54}$$

Morcos and Bergles [29] correlated most of the available experimental data for water, ethylene glycol, and air, with different tube wall materials, with the equations (properties evaluated at film temperature):

$$Nu_{fd} = \left\{(4.36)^2 + \left[0.055\left(\frac{Gr\,Pr^{1.35}}{Pw^{0.35}}\right)^{0.40}\right]^2\right\}^{0.5} \tag{3.55}$$

$$Nu_{fd} = \left\{(4.36)^2 + \left[0.145\left(\frac{Gr_q\,Pr^{1.35}}{Pw^{*0.35}}\right)^{0.265}\right]^2\right\}^{0.5} \tag{3.56}$$

Those correlations were given for $3x10^4<Ra<10^6$; $4<Pr<175$; and $2<Pw<66$. Good agreement was found with all the available experimental data apart for the results by Ede [113] and Sigwarth et al. [81]. Those data are for thick, highly conductive walls; they extend several decades beyond the above Ra-range, and Nusselt numbers are considerably lower than predicted by the correlations. Both tubes have high axial conduction, which generally has the effect of making calculated Nu-values too low and calculated Gr-values too high. However, this does not seem to be a major cause of disagreement. The experiments of Barozzi et al.[138], for water in a thick walled copper tube ($Pw = 2.6x10^{-2} - 4.7x10^{-2}$), were in good agreement with Morcos and Bergles' equations.

Morcos and Bergles [29] also correlated all the available experimental data in terms of the apparent friction factor. Their equation, with properties estimated at film temperature, is:

$$\frac{f_{app}}{f_{app,cp}} = \left\{1 + \left(0.195Ra^{0.15}\right)^{15}\right\}^{\frac{1}{15}} \qquad (3.57)$$

It was observed that the experimental data do not reflect the large difference in friction factor between the two extreme boundary conditions predicted in [83], even if the data are generally some compromise between them.

The effects of peripheral wall conduction on fully developed combined convection were investigated numerically by Futagami et al.[104] and Chen and Hwang [106].
Two wall conditions were considered in [104]: a uniform heat flux at the outer wall surface; and, a uniform heat generation inside the wall, with an adiabatic outer wall surface. The relevant wall parameters were: $DR = D_{out}/D_{in}$, and $K = k_w/k_f$. The numerical experiment covered the range $Ra_q=4x10^3-3.2x10^7$, $Pr=5$. The effects of peripheral wall conduction were found to become substantial for $Ra_q>4x10^5$. In both cases, the temperature and heat flux density distributions were observed to approach condition **H2** for reducing K and DR, and condition **H1** for increasing K and DR.
The expression for peripherally averaged Nusselt number, including the effect of heat conduction in the wall, is:

$$\frac{Nu_{fd}}{Nu_{fd,cp}} = \frac{Nu_{\infty}}{Nu_{fd,cp}} - \left(\frac{Ra_q}{14.4x10^6}\right)^{0.51}\left[1 - \exp\left(-0.8532\left(Pw^*\right)^{0.33}\right)\right] \qquad (3.58)$$

where Nu_{∞} designates Nu-values for $K = \infty$ (ie, case **H1**), as calculated from equation:

$$\frac{Nu_{\infty}}{Nu_{fd,cp}} = 0.198X\left(1 - 1.57X^{-1} + 17.59X^{-2} - 62.68X^{-3} + 139.17X^{-4}\right) \qquad (3.59)$$

where $X = \left(\frac{Ra_q}{4}\right)^{0.2}$

The Prandtl number does not appear as an independent parameter in these equations, which should be valid for Pr=5 (water). The comparison with experimental data in [88] indicates that metal tube data are underpredicted, while glass tube data are slightly overpredicted.

Chen and Hwang [106] considered the range Gr = 10^3-$4x10^4$; Pr = 0.72-10. They investigated the influence of the wall to fluid conductivity ratio, $K = k_w/k_f$, on the friction factor: fRe was found to increase with Gr, Pr, and K. At equal Gr and Pr, the increase of fRe becomes almost negligible for Pr≥10 (changing K from 10 to 10^4 had a minimum effect). For decreasing K from 10 to 0.1, the decrease of fRe is important (eg, for Gr=$4x10^4$, Pr=10, the friction factor ratio dropped from 1.55 to 1.27). In the ranges K =10-10^4 and 0.1-0 the effect of the wall is less than 1%. It was concluded that conditions **H1** and **H2** are approximated for K ≥10, and K ≤0.1, respectively.

The effects of K and Pr on Nu are moderate at high K, but increase at relatively low K-values; the important range for K being 0.1≤K≤10.

Chen and Hwang [106] suggested a new correlation for the effect of the wall:

$$Nu_{fd} = \left\{(4.36)^2 + \left[0.23(RaF)^{0.32}\right]^2\right\}^{0.5} \qquad (3.60)$$

where: $$F = \frac{Pr + 0.06}{Pr + 0.6}\,\frac{Pw + 200}{5Pw + 200} \qquad (3.61)$$

The range suggested for this equation is: $10^3 \le Ra \le 10^5$; $.72 \le Pr < \infty$; $Pw = 0-\infty$.

All the above is concerned with circumferential conduction under fully developed flow conditions. The combined effects of both peripheral and axial wall conduction in the entrance region, still remain unexplored.

D.- Temperature-dependent properties.

As noted by Bergles [2] the thermodynamic properties of most fluids vary with temperature and, thus, vary over the cross-section of the tube. The temperature-dependent problem is further complicated by the fact that the properties of different fluids behave differently with temperature. For gases, the specific heat varies only slightly with temperature, but μ and k increase with about the 0.8 power of the absolute temperature. The net result is that Pr does not vary significantly with temperature.

For most liquids, c_p and k are relatively independent of temperature, but μ varies markedly, and Pr thus varies with temperature in the same manner. When heating, the viscosity at the wall decreases. This could be the cause of flow instability and transition to turbulence.

The effects of temperature-dependent viscosity have been widely investigated in the absence of buoyancy. Martin and Fargie [197], and Test[198] considered the effect of viscosity in the inlet region. Test indicated errors of more than 50% on fRe and Nu, if radial viscosity variation is overlooked. Newell and Bergles [83] discussed the effect of the variable viscosity of water on a fully developed laminar flow without buoyancy. They stated that the radial viscosity variations result in deviations in Nu from the Poiseuille flow of less than 5%, subject to the fulfillment of the condition:

$$\frac{D_h q'_w}{k T'_m} < 1.74 \tag{3.62}$$

After Sieder and Tate [199], the viscosity correction factor $\left(\frac{\mu_m}{\mu_w}\right)^m$ has been commonly used to account for temperature-dependent viscosity for liquids; the temperature ratio $\left(\frac{T_m}{T_w}\right)^n$ can be used for gases.

For the case of fully developed flow with temperature-dependent viscosity, there is a general agreement that the effect of this on Nu_{fd} can be accounted for by using the viscosity ratio, with m = 0.14 (Deissler [200], Shannon and Depew [122], Joshi and Bergles [201]).

In the thermally developing region, however, the correct value to be given to the exponent is still a matter of discussion: Shannon and Depew [122], concluded that the exponent m is a function of z^*, and decreases from 0.3 at the entrance to 0.14 in the fully developed region. However, Yang [202] found that the correlation for fully developed flow holds also for developing flow. For case **H**, the latter conclusion was also reached by Joshi and Bergles [201], and confirmed that the exponent m can be assumed constant and equal to 0.14 all along the heat transfer section.

The only analysis of the combined effect of buoyancy and temperature-dependent viscosity was performed by Hong and Bergles [90], using the boundary layer concept in the fully developed region. Both boundary condition **H1** and **H2** were considered.
The appropriate non dimensional group for variable viscosity was recognized to be the Bergles number, Be:

$$Be = \kappa\left(T'_w - T'_m\right) \tag{3.63}$$

where

$$\kappa = -\frac{1}{\mu}\left(\frac{d\mu}{dT'}\right) \tag{3.64}$$

Be is negative for most gases; for liquids Be is positive for heating and negative for cooling.

The following correlations for Nu_{fd} were given:

Case **H1**

$1.5 \geq Be \geq 0$

$$Nu_{fd} = \left(0.5246 + 0.0091Be + 0.0881Be^2\right) (Ra)^{0.25} \quad (3.65)$$

$0 \geq Be \geq -1.0$

$$Nu_{fd} = (0.521 + 0.0319Be) (Ra)^{0.25} \quad (3.66)$$

Case **H2**

$2.0 \geq Be \geq 0$

$$Nu_{fd} = \left(0.393 + 0.0832Be - 0.0058Be^2 + 0.027Be^3\right) (Ra)^{0.25} \quad (3.67)$$

$0 \geq Be \geq -1.0$

$$Nu_{fd} = \left(0.394 + 0.0527Be - 0.00313Be^2\right) (Ra)^{0.25} \quad (3.68)$$

It was observed that constant property predictions are valid only for $Be<0.5$.

Allen et al.[102] considered the effect of property variation for horizontal ducts, by comparing numerical predictions with experiments. The onset of transverse circulations could not be accommodated in the 2D analysis. However, full consideration was given to all temperature-dependent properties: thermal conductivity, viscosity, density, and specific heat. Experimental data for glycerol/water mixtures from Butterworth and Hazell [203], Mobil 600 oil from Martin and Fargie [197], and data for water from Shannon and Depew [121] were used for comparison. The predictions indicated that allowance for k variation always results in a rather small increase in heat transfer. Allowance for the variation of μ results in a relatively large increase in heat transfer, while allowance for other property changes, including k, gives a further increase in heat transfer. Viscosity variations give the most significant heat transfer effect, where the variation of k happens to be much smaller.

E.- Transition and backflow conditions.

The stability problem of combined convection flows is far from being re-solved. For the case of horizontal round ducts, in particular, conclusions from the present knowledge are rather confused. In practice, there are four phenomena which are, or could be, relevant to the stability of laminar flow and the transition to turbulent flow. They are:
- backflow;
- occurrence of bifurcations;
- thermal instability;
- hydrodynamic instability.

For boundary conditions of type **H**, the non-dimensional quantities governing those effects are Ra_q, Pr, and Re.

The flow reversal, or backflow effect was first observed experimentally by Mikesell (ref.[4] in [81]). The phenomenon, according to the analysis of Del Casal and Gill [75], is linked to changes of the average density in the axial direction. These produce changes in the axial velocity profile by variations of the axial pressure gradient over the cross section of the tube. If the axial density gradient is large enough the fluid in the top part of the tube will eventually flow backwards, under heating conditions. The effect has recently been discussed by Lavine et al. [195].
Del Casal and Gill [75] observed that the variation in the axial pressure gradient superimposes an additional effect which is independent, to the first order, of the intensity of the secondary circulations. The relative importance of the effect increases as the Peclet number decreases. Dispersion experiments by Reejhsinghani et al.[204] seem to confirm that at low Pe (<100) more axial mixing (higher dispersion coefficients) occurs, while for high Pe radial mixing increases and depresses axial dispersion.
According to Gill [Discussion to [117]] the circulation and pressure gradient effects are roughly of the same order of magnitude when:

$$Re^2\,Pr \approx 650 \tag{3.69}$$

Siegwarth et al [81] gave the following criteria for neglecting axial density variations:

$$0.84\,\frac{NuGr}{(Gr\,Pr)^{0.25}} << 1 \qquad \text{for} \quad Pr \to 1 \tag{3.70}$$

$$\frac{1}{2}\,\frac{NuGr}{Pr\,Re^2} = \frac{1}{2}\,\frac{Ra_q}{Pe^2} << 1 \qquad \text{for} \quad Pr \to \infty \tag{3.71}$$

It is to be noted that the axial density variation becomes particularly important for small Re.
According to Siegwarth and Hanratty [84], a more accurate assessment can be obtained by using the solution presented by Del Casal and Gill [75] for the case of negligible effects due to secondary flow. From there, the velocity gradient at the wall will be affected by the axial temperature gradient by less than 10% if:

$$\frac{Ra_q}{Pe^2} < 3.2 \tag{3.72}$$

Shannon and Depew [121] reported from Mikesell the two following conditions, under which backflow should not occur:

$$\left(\frac{Ra_q}{Pr^2\,Re^2}\right) < 150 \tag{3.73}$$

and

$$\left(\frac{NuGr}{Pr\,Re^2}\right)\left(\frac{Pr}{Gr}\right)^{0.25} < 12 \tag{3.74}$$

Shannon and Depew [122] indicated that water data in [121] were actually critical for backflow.
Based on an order of magnitude analysis, Polyakov [6] indicated the following alternative condition under which backflow cannot occur:

$$Ra_q < 4\,Pr^2\,Re^3 \qquad (3.75)$$

According to the above observations, it seems reasonable to conclude that backflow can be important only in the case of very low Re flows and/or low Pr-fluids.

Nandakumar et al.[72] demonstrated numerically that double bifurcated solutions are possible for fully developed combined convection flows in horizontal rectangular, semicircular and circular ducts, under boundary condition **H1**. The observation, if confirmed by either careful experimentation, or the use of advanced numerical methods, could be of great value for predicting the route to turbulence in combined convection flows.
The starting point was the observation that the equations governing the mixed convection problem are very similar to those of laminar flow in helical tubes (the Dean problem), and Couette flow between rotating cylinders (the Taylor problem). Flow bifurcation in the Taylor problem is known to exist. Some of its essential characteristics are: i. it can exhibit profuse multiplicity; ii. certain anomalous and asymmetric modes of flow behaviour are possible; iii. the end effects are important, no matter how large the aspect ratio is. For the Dean problem, dual solutions have been observed in both experimental and numerical studies (see [72] for references). For the circular duct, Nandakumar et al.[72] explored the range $Gr_q = 4x10^2$-$4x10^6$ for Pr=5 and 0.7. They predicted that, above a critical Gr-number, two different solutions coexist, one characterized by two vortices, and the other by four vortices over the cross-stream section. Critical Gr-values for bifurcated solutions were:

$Gr_q=8.0x10^5$ ($Ra_q=5.60x10^5$), for Pr=0.7,
$Gr_q=2.5x10^5$ ($Ra_q=1.24x10^6$), for Pr=5.0.

It was expected that, above a second critical Gr-value, the four vortex structure was the only one possible, as observed in the case of rectangular and semicircular ducts. This upper limit of the double solution region was not reached, however, due to instabilities in the numerical solution. The effect of the four or two vortex solutions on both f_zRe and Nu_z was seen to be moderate for the circular duct, but very significant for the other geometries considered.
As for the effect on the Prandtl number, it was observed that the strength of the secondary flow was weakened considerably with an increase in Pr. However, dual solutions were present for both cases. Bifurcated solutions were also observed in [73] and [109] for other **H**-type boundary conditions.

Newell and Bergles [83] commented that, under adiabatic conditions, when all possible sources of disturbance are eliminated, laminar

flow may exist at Re~10^5. When no special care is exercised to prevent external disturbances, these will be attenuated only for Re<1000. Visualization studies by Newell (ref.[1] in [83]) indicated that for Re<1000 flow is stable; for 1000<Re<2000 a locally time-dependent sinuous motion ensues, and at Re~2000 the first disturbance eddy breaks away.

Earliest attempts to correlate the available transitional data for both vertical/horizontal ducts were made by Metais and Eckert [1]. Extensive investigations with water were made by Petukhov and Polyakov [126], Nagendra [130], and El-Hawary [135], all under uniform heating conditions. Their results can be summarized as follows:

- beyond transition two types of turbulence are possible [130]: i. hydrodynamic turbulence, where fluctuations are predominantly in velocity, and, ii. thermal turbulence, where fluctuations are predominantly in temperature. For large Re and Ra_q-values these can no longer be distinguished, and give rise to turbulent combined convection;
- according to El-Hawary [135], the transition process can be more strictly distinguished as: i. hydraulic transition, and, ii. thermal transition.
  Hydraulic transition was first observed in experiments at constant heating power, where, starting from a stable laminar flow, the flow rate was progressively increased. In those cases, the apparent friction factor $f_{app}Re$ behaved as for isothermal flows, i.e. no fluctuation was observed in the laminar region (up to Re~3000), then the transition region was reached, where periods of laminar and turbulent flows alternated, and simultaneous oscillations of temperature, velocity, and pressure drop were observed.
  Thermal transition was observed at constant flow rate with increasing heating power. Even in this case, the fluid experienced a laminar-turbulent transition, but some temperature and velocity fluctuations were detected at a heating power smaller than required to produce turbulent-like friction factor values. This laminar regime, with local oscillations and laminar-like friction factors, was termed 'disturbed' laminar flow. A rough estimate from El-Hawary [135] plot (Fig. 7, *ibid.*), gives the following criterion for stable laminar flow:

$$\frac{Ra_q}{Re} < 250 \qquad (3.76)$$

- two critical values of Re are commonly defined for hydraulic transition: i. Re_{cr1} defines the limit between laminar and transitional regimes; ii. Re_{cr2} indicates the passage from transitional to turbulent flow. El-Hawary [135] found that both increase slightly with Ra_q. As for Re_{cr1}, this agrees with findings of Petukhov et al. [48] for water, and Mori et al. [118] for air, under perturbed entrance conditions. Polyakov reported the following correlation equation for Re_{cr1}:

$$Re_{cr1} = 2300 + 4000 \log\left(1 + Ra_q x 10^{-5}\right) \qquad (3.75)$$

valid for $Ra_q < 10^8$; $0.6 < Pr < 10$.

When the inlet turbulence level is low, however, the buoyancy induced secondary flow seems to have a destabilizing effect [118,126];

- the effect of 'disturbed' and transitional conditions on heat transfer have not yet been identified clearly. According to El-Hawary [135], Nu_z is definitely higher for thermal transition, i.e. Nu_z is much higher than it would be expected by extrapolation of the laminar trend; also, Nu_z is definitely higher than for laminar disturbed flow in the hydraulic transition region, at equal Ra_q. In the 'disturbed' laminar region, Nu_{fd}-values were found not to be distinguishable from laminar data. However, Barozzi et al. [138] found that one single run for water in this region presented very high heat transfer data. They also noticed that, over the range Re=1660-2330; Ra_q=2.1-3.5x10^5, heat transfer results had some turbulent characteristics: Nu_z was well above laminar predictions both in the entrance and the downstream regions, where an independent effect of Re was evident.

F.- Inclination.

For inclined tubes, the available information for combined convection flows appears to be limited to the theoretical contributions of Iqbal [76], Iqbal and Stachiewicz [77,78], Cheng and Hong [85,86], and Orfi et al. [108], and the experimental work of Sabbagh et al. [132], and Barozzi et al. [138]. All the theoretical work referred to fully developed conditions, with aiding flow. Numerical solutions [85,86,108] demonstrated that an optimum inclination angle does not exist, contrary to what is demonstrated by perturbation solutions [77,78]. This seems to be confirmed by the small amount of available experimental data for water [138], and for air [132], where Nu_z was observed to decrease regularly for increasing the inclination angle over the horizontal. An independent, but very moderate effect, of Re on Nu_z was noticed in [138].
No consideration seems to have been given to the case of opposing flow, or to stability effects with inclined orientation.

G.- Other H-type boundary conditions.

As mentioned by Petukhov et al.[5], practical cases are encountered where neither condition **H** nor condition **T** can be attained. Examples where the heat flux density is distributed asymmetrically over the perimeter are solar collector tubes, and thermodynamic light guides (gas lenses). Solutions for cases with axially uniform, but sinusoidal peripheral distribution of the heat flux were given by Swamy et al.[103], other were reported in [5] (refs. [21,22], *ibid.*).

The case of uniform heating over a half duct section, either top or bottom, was investigated numerically by Patankar et al. [97], under fully developed flow conditions. The bottom heating case was later investigated by Law et al. [73], and by Choi and Choi [109].
Bottom heating was demonstrated to be much more effective than top heating, in terms of the strength of secondary circulations, and the increase of Nusselt numbers and friction factors, over constant property values [97]. This can be explained by the fact that the top heated case is a relatively stable configuration which tends to weaken the secondary flow. In the case of bottom heating, the configuration is much less stable, and natural convection becomes dominant. In the latter case, a change in the flow structure was observed (at $Gr_q = 2.4x10^5$, Pr=0.7, and $Gr_q = 1.6x10^5$, Pr=5), with a passage from a two- to a four-vortex structure over the duct cross section. It was pointed out that with such a complex structure it is possible that, in reality, the flow exhibits a steady-periodic behaviour rather than a totally time-invariant one. Law et al.[73] also investigated the bottom heating case, but were unable to find any transition to multiple vortex structures over the range $Gr_q = 4x10^2$-$8x10^7$, Pr=5 and 0.7. However, Choi and Choi [109] repeated the prediction with much finer grids, and double solutions were found for Pr=5 and $Gr_q>2.12x10^4$, i.e., the two-vortex or four-vortex patterns were found to be both possible. The upper limit of the double solution region could not be determined in terms of Gr_q; it was still present at the highest limit ($Gr_q=4x10^8$; Pr=5.0) of the calculation. Note that a coarser computational grid gave a much higher Gr_q-value for the occurrence of a four-vortex structure. It was shown that double solutions were possible over all the Pr-range explored (Pr=0.2 - 10). Reformulating the transition data in terms of Ra_q, rather than Gr_q, one finds that a common value of order $1x10^5$, holds for $0.7 \leq Pr \leq 10$.
How the flow reaches the two different final states is still in question. It is expected that, to shed some light on the subject, the entrance region of the tube must be examined.

References

1 - B. Metais, and E.R.G. Eckert - Forced, Mixed and Free Convection Regimes - ASME, J. Heat Transfer, 86, 1964; 295-296.

2 - A.E. Bergles - Experimental Verification of Analyses and Correlation of the Effects of Temperature-Dependent Fluid Properties on Laminar Heat Transfer - in '*Low Re Number Heat Exchangers*', S. Kacac, R.K. Shah, and A.E. Bergles, ed., Hemisphere, Washington D.C., 1983; 473-486.

3 - A.E. Bergles - Prediction of the Effect of Temperature-Dependent Fluid Properties on Laminar Heat Transfer - in '*Low Re Number Heat Exchangers*', S. Kacac, R.K. Shah, and A.E. Bergles, ed., Hemisphere, Washington D.C., 1983; 451-471.

4 - F.P. Incropera - Buoyancy Effects in Double-Diffusive and Mixed Convection Flows - *Procs. 8th Heat Transfer Conference*, S. Francisco, Cal., U.S.A., 1986; Vol. 3; 121-130.

5 - B.S. Petukhov, A.F. Polyakov, and O.G. Martynenko - Buoyancy Effects on Heat Transfer in Forced Channel Flows - *Procs. 7th Int. Heat Transfer Conf.*, Munich, 1982, Hemisphere, Washington D.C., 1982, Vol. 1; 343-362.

6 - A.F. Polyakov - Mixed Convection in Single-Phase Flows - in '*Heat Transfer: Soviet Reviews*', Vol. 1 - *Convective Heat Transfer* - O.G. Martynenko, and A.A. Zukauskas, eds., Hemisphere Pub. Co., New York, N.Y., 1989; 1-95.

7 - B. Gebhart, Y. Jaluria, R.L. Mahajan, and B. Sammakia - Mixed Convection - Chap. 10 in *"Buoyancy-Induced Flows and Transport"*, Hemisphere Pub. Co., Washington, 1989, 467-545.

8 - S.W. Churchill - Combined Free and Forced Convection in Channels - in '*Heat Exchanger Design Handbook*', D.B. Spalding Ed., Vol. 2, Fluid Mechanics and Heat Transfer, Hemisphere pub. Corp., Washington D.C., 1983; 2.5.10 - 1-12.

9 - W. Aung - Mixed Convection in Internal Flow - in '*Handbook of Single-Phase Convective Heat Transfer*', S. Kakac, R.K. Shah, and W. Aung, eds., J. Wiley & Sons, NY, 1987.

10 - Y. Jaluria, T.S. Chen, and O.A. Plumb - Mixed Convection - in '*Procs. of a Workshop on Natural Convection*', K.T. Yang, and J.R. Lloyd, eds., Beaver Run, Breckenridge, Co, 1982; 47-63.

11 - G.S. Barozzi, and M.W. Collins - Mixed Convection in Horizontal Ducts: an Overview of Numerical Methods - *Atti 9° Congresso Nazionale U.I.T.*, Pisa, I, June 1991; 45-60.

12.- P.J. Roache - '*Computational Fluid Dynamics*' - Hermosa Publishers, Albouqueque, NM, 1976.

13.- S.V. Patankar - '*Numerical Heat Transfer and Fluid Flow*' - Hemisphere pub Co., Washington, 1980.

14 - W.J. Minkowycz, E.M. Sparrow, G.E. Schneider, and R.H. Pletcher - '*Handbook of Numerical Heat Transfer*' - J. Wiley & Sons, Inc., NY, 1988.

15.- T.M. Shih - '*Numerical Heat Transfer*' - Hemisphere pub. Co., Washington, 1984.

16 - C. Brebbia - '*Topics in Boundary Element Research. Basic Principles and Applications*' - Spriger-Verlag, Berlin, 1984.

17 - K. Kato, E. Watanabe, T. Ogura, and T. Hanzawa - Effect of Natural Convection on Laminar Flow Heat Transfer in Horizontal Circular Tubes - J. Chem. Eng. Japan, 15 (5), 1982; 355-361.

18 - F.C. Chou, and G.J. Hwang - Vorticity-Velocity Method for the Graetz Problem and the Effect of Natural Convection in a Horizontal Rectangular Channel with Uniform Wall Heat Flux - ASME, J. Heat Transfer, 109, 1987; 704-710.
19 - F.C. Chow, and G.J. Hwang - Buoyancy Effects on Laminar Forced Convection in the Thermal Entrance Region of Horizontal Rectangular Channels - ASME, J. Heat Transfer, 112, 1990; 250-253.
20 - F.C. Chou, and G.J. Hwang - Numerical Analysis of the Graetz Problem with Natural Convection in a Uniformly Heated Horizontal Tube - Int. J. Heat Mass Transfer, 31, 1988; 1299-1308.
21 - K. Ramakrishna, S.G. Rubin, and P.K. Khosla - Laminar Natural Convection Along Vertical Square Ducts - Num. Heat Transfer, 5,1982; 59-79.
22 - B. Farouk, and T. Fusegi - A Coupled Solution of the Vorticity- Velocity Formulation of the Incompressible Navier-Stokes Equations - Int. J. Num. Meth. Fluids , 5, 1985; 1017-1034.
23 - T. Fusegi, B. Farouk, and K.S. Ball - Mixed-Convection Flows within a Horizontal Concentric Annulus with a Heated Rotating Inner Cylinder - Num. Heat Transfer, 9, 1986; 591-604.
24 - B. Farouk, and T. Fusegi - Predictions of Fluid and Heat Transfer Problems by the Vorticity-Velocity Formulation of the Navier-Stokes Equations - J. Comp. Phys., 65, 1986; 227-243.
25- K.C. Cheng, S.W. Hong, and G.J. Hwang - Buoyancy Effects on Laminar Heat Transfer in the Thermal Entrance Region of Horizontal Rectangular Channels with Uniform Heat Flux for Large Prandtl Number Fluid - Int. J. Heat Mass Transfer, 15, 1972; 1819-1836.
26 - M.M.M. Abou-Ellail, and S.M. Morcos - A Prediction Procedure for Combined Forced and Free Laminar Convection in the Entrance Region of an Inclined Rectangular Channel Solar Collector - '*Izmir Int. Symp.- II on Solar Energy Fundamentals and Applications*', Izmir, Turkey, Aug. 1979.
27 - M.M.M. Abou-Ellail, and S.M. Morcos - Combined Forced and Free Laminar Convection in the Entrance Region of Inclined Rectangular Channels - Procs. Int. Conf. *'Numerical Methods for Non-Linear Problems'* , C. Taylor, E. Hinton, and D.R.J. Owen, eds., Swansea, UK, Sept. 1980; Pineridge Press, Swansea, UK, 1980; 807-820.
28 - M.M.M. Abou-Ellail, and S.M. Morcos - Buoyancy Effects in the Entrance Region of Horizontal Rectangular Channels - ASME, J. Heat Transfer, 105, 1983; 924-928.
29 - S.M. Morcos, and A.E. Bergles - Experimental Investigation of Combined Forced and Free Laminar Convection in Horizontal Tubes - ASME, J. Heat Transfer, 97, 1975; 212-219.
30 - D. Choudury, and S.V. Patankar - Combined Forced and Free Laminar Convection in the Entrance Region of an Inclined Isothermal Tube - ASME, J. Heat Transfer, 110, 1988; 901-909.
31 - K.C. Karki, and S.V. Patankar - Laminar Mixed Convection in the Entrance Region of a Horizontal Annulus - Numerical Heat Transfer, 15, 1989; 87-99.

32 - G.D. Raithby, and G.E. Schneider - Numerical Solution of Problems in Incompressible Fluid Flow: Treatment of the Velocity-Pressure Coupling - Num. Heat Transfer, 2, 1979; 417-440.
33 - F.P. Incropera, and J.A. Schutt - Numerical Simulation of Laminar Mixed Convection in the Entrance Region of Horizontal Rectangular Ducts - Num. Heat Transfer, 8, 1985; 707-729.
34 - F.P. Incropera, A.L. Knox, and J.A. Schutt - Onset of Thermally Driven Secondary Flow in Horizontal Rectangular Ducts - '*Procs. 8th Heat Transfer Conference*', S. Francisco, Cal., 1986; Vol. 3; 1395-1400.
35 - H.V. Mahaney, F.P. Incropera, and S. Ramadhyani - Development of Laminar Mixed Convection Flow in a Horizontal Rectangular Duct with Uniform Bottom Heating - Num. Heat Transfer, 12, 1987; 137-155.
36 - H.V. Mahaney, F.P. Incropera, and S. Ramadhyani - Effect of wall Heat Flux Distribution on Laminar Mixed Convection in the Entrance Region of a Horizontal Rectangular Duct - Num. Heat Transfer, 13, 1988; 427-450.
37 - K.C. Cheng, and J.-W. Ou - Buoyancy and Tilt Angle Effect on Graetz Problem in Horizontal Rectangular Channels - '*Procs. ASME-JSME Thermal Eng. Joint Conf.*', Honolulu, Ha, 1983; Vol. 3 ; 141-147.
38 - C. Nonino, S. Del Giudice, and G. Comini - Forced and Mixed Convection in Three-Dimensional Parabolic Flows - in '*Finite Element Analysis in Fluids*', T.J. Chung, and G.R. Karr, eds., UAH Press, Dept. Mech. Eng., Univ. Alabama, Huntsville, USA, 1989; 1507-1512.
39 - C. Nonino, and S. Del Giudice - Laminar Mixed Convection in the Entrance Region of Horizontal Rectangular Ducts - Int. J. Num. Meth. Fluids, 12, 1991;.33-48.
40 - G. Comini, and S. Del Giudice - Parabolic Systems: Finite Element Method - in '*Handbook of Numerical Heat Transfer*', W.J. Minkowycz, G.E. Schneider, and R.H. Pletcher, eds., J. Wiley and Sons, New York, 1988; 155-181.
41 - T.A. Nyce, J. Ouazzani, A. Durand-Daubin, and F. Rosemberg - Mixed Convection in a Horizontal Rectangular Channel - Experimental and Numerical Velocity Distributions - Int. J. Heat Mass Transfer, 35, 1992; 1481-1494.
42 - O. Terhmina, A. Mojtabi, and B. Roux - A Numerical Procedure for Three-Dimensional Mixed Convection Developing in an Axisymmetric Geometry - Eur. J. Mech., B/Fluids, 11, 1992; 21-38.
43 - G. Biswas, H. Laschefski, N.K. Mitra, and M. Fiebig - Numerical Investigation of Mixed Convection Heat Transfer in a Horizontal Channel with a Built-in Square Cylinder - Num. Heat Transfer, 18, 1990; 173-188.
44 - J.P. Coutier, and R. Greif - Mixed Laminar Convection in a Horizontal Tube with Natural Convection around its Boundaries - Int. J. Heat Mass Transfer, 29, 1986; 391-402.
45 - J.P. Coutier, and R. Greif - An Investigation of Laminar Mixed Convection inside a Horizontal Tube with Isothermal Wall Conditions - Int. J. Heat Mass Transfer, 28, 1985; 1293-1305.

46 - C.T. Nguyen, and N. Galanis - Combined Forced and Free Convection in the Developing Laminar Flow in Horizontal Tubes under Uniform Heat Flux - in '*Numerical Methods in Thermal Problems*', Pineridge Press, Swansea, UK, Vol.5, part 1, 1987; 414-425.
47 - C.T. Nguyen, and N. Galanis - Investigation of Rayleigh Number Effects on Combined Forced and Free Convection for Developing Laminar Flow in Uniformly Heated Horizontal Tubes - ASHRAE Trans., 95, part 1, 1989; 171-178.
48 - B.S. Petukhov, A.F. Polyakov, and B.K. Strigin - Heat Transfer in Tubes with Viscous-gravity Flow - Heat Transfer-Sov. Res., 1 (1), 1969; 24-31.
49 - C.W. Hirt, B.D. Nichols, and N.C. Romero - SOLA, A Numerical Solution Algorithm for Transient Fluid Flows - Los Alamos Sc. Lab. Rep. LA-5652, 1975.
50 - G. Biswas, T. Pelster, J.S. Cornelius, N.K. Mitra, and M. Fiebig - Three Dimensional Computations of Laminar Mixed Convection Flows in a Horizontal Rectangular Duct with a Uniformly Heated Bottom Wall - Procs. 6rd. Int. Conf. *'Numerical Methods in Thermal Problems'* , R.W. Lewis, and K. Morgan, eds., Swansea, UK, Jul. 1989; Pineridge Press, Swansea, UK, 1989; 1721-1731.
51 - G. Biswas, N.K. Mitra, M. Fiebig, and J.S. Cornelius - Numerical Investigation of Laminar Mixed Convection Flows in Rectangular Horizontal Ducts - '*Procs. 9th. Int. Heat Transfer Conf.*', G. Hestroni, ed., Jerusalem, Israel, 1990; Vol.2; 435-439.
52 - M. Hishida, Y. Nagano, and M.S. Montesclaros - Combined Forced and Free Convection in the Entrance Region of an Isothermally Heated Horizontal Pipe - ASME, J. Heat Transfer, 104, 1982; 153-159.
53 - G. De Vahl Davis - Program FRECON for the Numerical Solution of Free Convection in a Rectangular Cavity, Univ. N.S.W. School of Mech. and Ind. Eng., Rept. FMT 1, April 1976.
54 - P. Skerget, I. Zagar, and A. Alujevic - Combined Forced and Free Laminar Convection in the Inclined Tube by BEM - in '*Advanced Computational Methods in heat Transfer*', L.C. Wrobel, C.A. Brebbia, and A.J. Nowak, eds., Spriger-Verlag, Berlin, 1990; Vol. 2, 3-17.
55 - G.S. Barozzi, and E. Nobile - Low Reynolds Number Heat Transfer and Fluid Flow in the Inlet Region of Parallel Plates - '*Atti 6° Congresso Nazionale U.I.T.*', Bari, I, June 1988; 141-152.
56 - K.C. Chiu, and F. Rosemberger - Mixed Convection between Horizontal Plates - I. Entrance Effects - Int. J. Heat Mass Transfer, 30, 1987; 1645-1654.
57 - J.P. Van Doormaal, and G.D. Raithby - Enhancements of the SIMPLE Method for Predicting incompressible Fluid Flows - Numerical Heat Transfer, 7, 1984; 147-163.
58 - V.M. Theodossiou, and A.C.M. Sousa - An Efficient Algorithm for Solving the Incompressible Fluid Flow Equations - Int. J. Num. Meth in Fluids, 9, 1986; 557-572.

59 - P.F. Galpin, and G.D. Raithby - Numerical Solution of Problems in Incompressible Fluid Flow: Treatment of the Temperature-Velocity Coupling - Numerical Heat Transfer, 10, 1986; 105-129.
60 - C.R. Maliska, and G.D. Raithby - Calculating 3-D Fluid Flows Using Non-Orthogonal Grid - '*Proc. 3rd Int. Conf. on Numerical Methods in Laminar and Turbulent Flows*', Seattle, 1983; 656-666.
61 - C.-Y. Perng, and, R.L. Street - Three-Dimensional Unsteady Flow Simulations: Alternative Strategies for a Volume-Averaged Calculation - Int. J. Num. Meth. in Fluids, 9, 1989; 341-362.
62 - S.L. Lee, and R.Y. Tzong - Artificial Pressure for Pressure-Linked Equation - Int. J. Heat Mass Transfer, 35, 1992; 2705-2716.
63 - S.P. Vanka - A Calculation Procedure for Three Dimensional Steady Recirculating Flows Using Multigrid Methods - Comp. Meth. in Appl. Mech. Eng., 55, 1986; 321-338.
64 - P.F. Galpin, and G.D. Raithby - Treatment of non-Linearities in the Numerical Solution of the Incompressible Navier-Stokes Equations - Int. J. Num. Methods in Fluids, 6, 1986; 409-426.
65 - S.G. Rubin, and P.K. Khosla - Navier-Stokes Calculations with a Coupled Strongly Implicit Method. I - Computers and Fluids, 9, 1981; 163-180.
66 - E. Nobile, and G.S. Barozzi - Un Approccio Numerico ai Problemi di Convezione Naturale e Mista ad Elevati Valori del Numero di Rayleigh - '*Procs. 47th ATI Nat. Conf.*', Parma, I, 1992.
67 - S. Paolucci, and D.R. Chenoweth - Transition to Chaos in a Differentially Heated Vertical Cavity - J. Fluid Mech., 201, 1989; 379-410.
68 - P. Le Quéré - Transition to Unsteady Natural Convection in a Toll Water-Filled Cavity - Phys. Fluids, Ser. A, 2, 1990; 503-515.
69 - I.P. Jones - The Convergence of a Simple Iterative Strategy for Strongly Stratified Flows - Procs. 4th. Int. Conf. *'Numerical Methods in Thermal Problems'* , R.W. Lewis, and K. Morgan, eds., Swansea, UK, Jul. 1985; Pineridge Press, Swansea, UK, 1985; 733-740.
70 - B.R. Hutchinson, P.F. Galpin, and G.D. Raithby - Application of Additive Correction Multigrid to the Coupled Fluid Flow Equations - Num. Heat Transfer, 14, 1988; 133-147.
71 - S.P. Vanka, and K.P. Misegades - Vectorized Multigrid Fluid Flow Calculations on a CRAY X-MP/48, Int. J. Num. Meth. in Fluids, 7, 1987; 635-648.
72 - K. Nandakumar, J.H. Masliyah, and H-S. Law - Bifurcation in Steady Laminar Mixed Convection Flow in Horizontal Ducts - J. Fluid Mech., 152,1985; 145-161.
73 - H-S. Law, J.H. Masliyah, and K. Nandakumar - Effect of Nonuniform Heating on Laminar Mixed Convection Flow Ducts - ASME, J. Heat Transfer, 109, 1987; 131-137.
74 - B.R. Morton - Laminar Convection in Uniformly Heated Horizontal Pipes at Low Rayleigh Numbers - Quart. J. Mech. Appl. Math., 12, 1959; 410-419.

75 - E. Del Casal, and W.N. Gill - A Note on Natural Convection Effects in Fully Developed Horizontal Tube Flow - AIChE J., 8, 1962; 570-575.
76 - M. Iqbal - Free-Convection Effects Inside Tubes of Flat-Plate Solar Collectors - Solar Energy, 10, 1966; 207-211.
77 - M. Iqbal, and J.W. Stachiewicz - Influence of Tube Orientation on Combined Free and Forced Laminar Convection Heat Transfer - ASME J. Heat Transfer, 88, 1966; 109-116.
78 - M. Iqbal, and J.W. Stachiewicz - Variable Density in Combined Free and Forced Convection in Inclined Tubes - Int. J. Heat Mass Transfer, 10, 1967; 1625-1629.
79 - Y. Mori, and K. Futagami - Forced Convective Heat Transfer in Uniformly Heated Horizontal Tubes (2nd report, theoretical study) - Int. J. Heat Mass Transfer, 10, 1967; 1801-1813.
80 - G.N. Faris, and R. Viskanta - An Analysis of Laminar Combined Forced and Free Convection Heat Transfer in a Horizontal Tube - Int. J. Heat Mass Transfer, 12, 1969; 1295-1309.
81 - D.P. Siegwarth, R.D. Mikesell, T.C. Redal, and T.J. Hanratty - Effect of Secondary Flow on the Temperature Field and Primary Flow in a Heated Horizontal Tube - Int. J. Heat Mass Transfer, 12, 1969; 1535-1552.
82 - G.J. Hwang, and K.C. Cheng - Boundary Vorticity Method for Convective Heat Transfer with Secondary Flow - Application to Combined Free and Forced Laminar Convection in Horizontal Tubes - '*4th Int. Heat Transfer Conf.*', Paris, 1970; Vol. 4, pap. No. NC3.5
83 - P.H. Newell, and A.E. Bergles - Analysis of Combined Free and Forced Convection for Fully Developed Laminar Flow in Horizontal Tubes - ASME, J. Heat Transfer, 92, 1970; 83-93.
84 - D.P. Siegwarth, and T.J. Hanratty - Computational and Experimental Study of the Effect of Secondary Flow on the Temperature Field and Primary Flow in a Heated Horizontal Tube - Int. J. Heat Mass Transfer, 13, 1970; 27-42.
85 - K.C. Cheng, and S.W. Hong - Effect of Tube Inclination on Laminar Convection in Uniformly Heated Tubes for Flat-Plate Solar Collectors - Solar Energy, 13, 1972; 363-371.
86 - K.C. Cheng, and S.W. Hong - Combined Free and Forced Laminar Convection in Inclined Tubes - Appl. Sci. Res., 27, sec. A, 1972; 19-38.
87 - K.C. Cheng, and J-W. Ou - Free Convection Effects on Graetz Problem for Large Prandtl Number Fluids in Horizontal Tubes with Uniform Wall Heat Flux - '*5th Int. Heat Transfer Conf.*', Tokyo, 1974; Vol. 4, pap. No. NC4.7;159-163.
88 - S.W. Hong, S.M. Morcos, and A.E. Bergles - Analytical and Experimental Results for Combined Forced and Free Laminar Convection in Horizontal Tubes - *5th Int. Heat Transfer Conf.*, Tokyo, 1974; Vol. 4, pap. No. NC4.6;154-158.
89 - C.A. Hieber, and S.K. Sreenivasan - Mixed Convection in an Isothermally Heated Horizontal Pipe - Int. J. Heat Mass Transfer, 17, 1974; 1337-1348.
90 - S.W. Hong, and A.E. Bergles - Analysis of Combined Forced and Free Laminar Convection in Horizontal Tubes - Engineering Res. Inst. Iowa State Univ., Ames, Iowa, Tech. Rep. HTL-4, ISU-ERI-Ames-74155, Nov. 1974.

91 - S.W. Hong, and A.E. Bergles - Analysis of Combined Forced and Free Laminar Convection in Horizontal Tubes - Engineering Res. Inst. Iowa State Univ., Ames, Iowa, Tech. Rep. HTL-4, ISU-ERI-Ames-74155, Nov. 1974.

92 - S.W. Hong, and A.E. Bergles - Theoretical Solutions for Combined Forced and Free Convection in Horizontal Tubes with Temperature-Dependent Viscosity - ASME, J. Heat Transfer, 98, 1976; 459-465.

93 - S.W. Hong, and A.E. Bergles - Analysis of Combined Forced and Free Laminar Heat Transfer in the Entrance Region of Horizontal Tubes - '*Procs. 14th Annual Meeting of the Society of Engineering Science*', Lehigh University, Nov. 1977; 453-469.

94 - J-W. Ou, and K.C. Cheng - Natural Convection Effects on Graetz Problem in Horizontal Isothermal Tubes - Int. J. Heat Mass Transfer, 20, 1977; 953-960.

95 - K.C. Cheng, and J-W Ou - Maximum Density Effect on Forced Laminar Convection in Horizontal Water Pipes with Near Freezing Wall Temperature - '*Proc. 6th Int. Heat Transfer Conf.*', Toronto, Canada, Vol. 1, MC12, 1978; 67-72

96 - K. Futagami, and F. Abe - Combined Forced and Free Convective Heat Transfer in an Inclined Tube (1st report, laminar region) - Trans. JSME, 38, 1978; 1799-1811.

97 - S.V. Patankar, S. Ramaghyani, and E.M. Sparrow - Effect of Circumferentially Nonuniform Heating on Laminar Combined Convection in a Horizontal Tube - ASME, J. Heat Transfer, 100, 1978; 63-70.

98 - L-S Yao - Entry Flow in a Straight Tube - J. Fluid Mech., 88,1978; 465-483.

99 - L.S. Yao - Free-Forced Convection in the Entry Region of a Heated Straight Pipe - ASME, J. Heat Transfer, 100, 1978; 212-219.

100 - C.A. Hieber - Mixed Convection in an Isothermal Horizontal Tube: Some Recent Theories - Int. J. Heat Mass Transfer, 24, 1981; 315-322.

101 - C.A. Hieber - Laminar Mixed Convection in an Isothermal Horizontal Tube: Correlation of Heat Transfer Data - Int. J. Heat Mass Transfer, 25, 1982; 1737-1746.

102 - P.H.G. Allen, O. Szpiro, and M.W. Collins - Prediction Methods for Entry Length Heat Transfer by Combined Laminar Convection in Horizontal Tubes - Inst. Mech. Eng., Vol. 196, No. 33, 1982;409-415, and S55-S59 (discussion).

103 - B. Swamy, V. Seshagiri, and M.V. Krishna Murthy - Effect of Secondary Flow on Heat Transfer in Solar Collector Tubes - Procs. 7th Int. Heat Transfer Conf., Munich, 1982, Hemisphere, Washington D.C., 1982, Vol. 6; 515-520.

104 - K. Futagami, Y. Aoyama, T. Kohno - Effects of Heat Conduction in Tube Wall on Combined Free and Forced Convective Heat Transfer in a Horizontal Tube - '*Procs. ASME-JSME Thermal Eng. Joint Conf.*', Honolulu, Ha., 1983; Vol. 3 ; 119-123.

105 - G.J. Hwang, and M.J. Lin - Natural Convection Effects on Laminar Heat Transfer in the Thermal Entrance Region of Horizontal Isothermal Tubes - J. Chinese Inst. Eng., 8, 1985; 343-355.

106 - R.S. Chen, and G.J. Hwang - Effect of Wall Conduction on Combined Free and Forced Laminar Convection in Horizontal Tubes - ASME, J. Heat Transfer, 111, 1989; 581-585.
107 - K.C. Cheng, and J.W. Ou - Graetz Problem with Maximum Density effect in Convectively Cooled Horizontal Water Pipes - Heat Transfer Characteristics Preceding the Onset of Ice Formation - '*Procs. 9th. Int. Heat Transfer Conf.*', G. Hestroni, ed., Jerusalem, Israel, 1990; Vol.3; 291-296.
108 - J. Orfi, N. Galanis, and C.T. Nguyen - Mixed Convection for the Fully-Developed Laminar Flow in Inclined Uniformly Heated Tubes - Procs. 7th. Int. Conf. '*Numerical Methods in Thermal Problems* ', R.W. Lewis, J.H. Chin, and G.M. Homsy, eds., Stanford, Jul. 1991, Pineridge Press, Swansea, UK, 1991; Part 1, 545-555.
109 - D.K. Choi, and D.H. Choi - Dual Solution for Mixed Convection in a Horizontal Tube under Circumferentially Non-Uniform Heating - Int. J. Heat Mass Transfer, 35, 1992; 2053-2056.
110 - D.G. Kern, and D.F. Othmer - Effect of Free Convection on Viscous Heat Transfer in Horizontal Tubes - Trans. AIChE, 39, 1943; 517-555.
111 - C. Scott, G.E. Eggleston, and W.L. Sibbitt - Local and Average Coefficients of Heat Transfer for Horizontal Laminar motion of Fluids in a Circular Tube - ASME Paper No. 55-SA-17, 1975.
112 - B.S. Petukhov, and L.D. Nol'de - Heat Transfer During the Viscous-Gravitational Flow of a Liquid through Pipes - Teploenergetika, 6 (1), 1959; 72-80.
113 - A.J. Ede - The Heat Transfer Coefficient for Flow in a Pipe - Int. J. Heat Mass Transfer, 4, 1961; 105-110.
114 - T.W. Jackson, J.M. Spurlock, and K.R. Purdy - Combined Free and Forced Convection in a Constant Temperature Horizontal Tube - AIChE J. - 7, 1961; 38-41.
115 - D.R. Oliver - The Effect of Natural Convection on Viscous-Flow Heat Transfer in Horizontal Tubes - Chem. Eng. Sci., 17, 1962; 335-350.
116 - A.R. Brown, and M.A. Thomas - Combined Free and Forced Convection Heat Transfer for Laminar Flow in Horizontal Tubes - J. Mech. Eng. Sci., 7, 1965; 440-448.
117 - S.T. McComas, and E.R.G. Eckert - Combined Free and Forced Convection in a Horizontal Circular Tube - ASME, J. Heat Transfer, 88, 1966; 147-153.
118 - Y. Mori, K. Futagami, S. Tokuda, and N. Nakamura - Forced Convective Heat Transfer in Uniformly Heated Horizontal Tubes (1st report - experimental study of the effect of buoyancy) - Int. J. Heat Mass Transfer, 9, 1966; 453-463.
119 - L.H. Baker - Film Heat-Transfer Coefficients in Solar Collector Tubes at Low Reynolds Numbers - Solar Energy, 11, 1967;78-85.
120 - A. Kupper, E.G. Hauptmann, and M. Iqbal - Combined Free and Forced Convection in a Horizontal Tube under Uniform Heat Flux - Solar Energy, 12, 1969; 439-446.
121 - R.L. Shannon, and C.A. Depew - Combined Free and Forced Laminar Convection in a Horizontal Tube with Uniform Heat Flux - Trans. ASME, J. Heat Transfer, 89, 1968; 353-357.

122 - R.L. Shannon, and C.A. Depew - Forced Laminar Convection in a Horizontal Tube with Variable Viscosity and Free Convection Effects - Trans. ASME, J. Heat Transfer, 90, 1969; 251-258.
123 - N.A. Hussain, and S.T. McComas - Experimental Investigation of Combined Convection in a Horizontal Circular Tube with Uniform Heat Flux - '*Proc. 4th Int. Heat Transfer Conf.*', Paris, 1970; Vol. 4, pap. No. NC3.4.
124 - B.S. Petukhov, and A.F. Polyakov - Experimental Investigation of Viscogravitationaal Fluid Flow in a Horizontal Tube - High Temperature, 5, 1967; 75-81.
125 - B.S. Petukhov, and A.F. Polyakov - Effect of Free Convection on Heat Transfer During Forced Flow in a Horizontal Pipe - High Temperature, 5, 1967; 348-351.
126 - B.S. Petukhov, and A.F. Polyakov - Flow and Heat Transfer in Horizontal Tubes under Combined Effect of Forced and Free Convection - '*Proc. 4th Int. Heat Transfer Conf.*', Paris, 1970; Vol. 4, pap. No. NC3.7.
127 - A.E. Bergles, and R.R. Simonds - Combined Forced and Free Convection for Laminar Flow in Horizontal Tubes with Uniform Heat Flux - Int. J. Heat Mass Transfer, 14, 1971; 1989-2000.
128 - C.A. Depew, and S.E. August - Heat Transfer due to Free and Forced Convection in a Horizontal and Isothermal Tube - Trans. ASME, J. Heat Transfer, 93, 1971; 380-384.
129 - A. Lichtarowicz - Combined Free and Forced Convection Effects in Fully Developed Laminar Flow in horizontal Tubes - in '*Heat and Mass Transfer by Combined Forced and Free Convection*', Ins. Mech. Eng., London, 1972.
130 - H.R. Nagendra - Interaction of Free and Forced Convection in Horizontal Tubes in the Transition Regime - J. Fluid Mech., 57, 1973; 269-288.
131 - C.A. Depew, J.L. Franklin, and C.K. Ito - Combined Free and Forced Convection in Horizontal, Uniformely Heated Tubes - ASME Paper, No. 75-HT-17 , 1975.
132 - J.A. Sabbagh, A. Aziz, A.S. El-Ariny, and G. Hamand - Combined Free and Forced Convection in Inclined Circular Tubes - ASME, J. Heat Transfer, 98, 1976; 322-324.
133 - N. Hattori, and S. Kokake - Combined Free and Forced Convection Heat Transfer for Fully Developed Laminar Flow in Horizontal Tubes (Experiments) - Bull. Jap. Soc. Mech. Eng., 21, 1978; 861-868.
134 - S. Sicardi, G. Baldi, and A. Gianetto - Non Isothermal Pressure Drop and Heat Transfer for Steady and Pulsed Laminar Flow in Horizontal Pipes - Ing. Chim. Ital., 14 (1-2), 1978; 9-13.
135 - M.A. El-Hawary - Effect of Combined Free and Forced Convection on the Stability of Flow in a Horizontal Tube - ASME, J. Heat Transfer, 102, 1980; 273-278.
136 - W.W. Yousef, and J.D. Tarasuk - An Interferometric Study of Combined Free and Forced Convection in a Horizontal Isothermal Tube - ASME, J. Heat Transfer, 103, 1981; 249-256.
137 - W.W. Yousef, and J.D. Tarasuk - Free Convection Effects on Laminar Forced Convective Heat Transfer in a Horizontal Isothermal Tube - ASME, J. Heat Transfer, 104, 1982; 145-152.

138 - G.S. Barozzi, E. Zanchini, and M. Mariotti - Experimental Investigation of Combined Forced and Free Convection in Horizontal and Inclined Tubes - Meccanica, 20, 1985; 18-27.
139 - K.C. Cheng, and F.P. Yuen - Flow Visualization Studies on Secondary Flow Patterns in Curved Tubes and Isothermally Heated Horizontal Tubes - ASME Paper 84-HT-62, 22nd Nat. Heat Transfer Conf., Niagara Falls, NY, 1984.
140 - K.C. Cheng, and F.P. Yuen - Flow Visualization Studies on Secondary Flow Pattern for Mixed Convection in the Thermal Entrance Region of Isothermally Heated Pipes - in '*Fundamentals of Forced and Mixed Convection*', ASME HTD-Vol. 42, 1985; 121-130.
141 - A.J. Ghajar, D.T. Stickland, and S. Kuppuraju - Forced and Mixed Convective Heat Transfer Measurements in a Circular Tube with Different Inlets - in '*Mixed Convection and Environmental Flows*', ASME, HTD-Vol. 152, 1990; 37-45.
142 - Q.M. Lei, and A.C. Trupp - Experimental Study of Laminar Mixed Convection in the Entrance Region of a Horizontal Semicircular Duct - Int. J. Heat Mass Transfer, 34, 1991; 2361-2372.
143 - N. Hattori - Combined Free and Forced-Convection Heat Transfer for Fully Developed Laminar Flow in Horizontal Concentric Annuli - Heat transfer - Jap. Res., 8(4), 1977; 27-48.
144 - A. Mojtabi, and J.-P. Caltagirone - Analyse du Transfert de Chaleur en Convection Mixte Laminaire Entre Deux Cylindres Coaxiaux Horizontaux - Int. J. Heat Mass Transfer, 23, 1980; 1369-1375.
145 - T. Hung Nguyen, P. Vasseur, L. Robillard, and B. Chandra Shekar - Combined Free and Forced Convection of Water Between Horizontal Concentric Cylinders - ASME, J. Heat Transfer, 105, 1983; 498-504.
146 - S. Kotake - Numerical Studies of Combined Forced and Free Convection in Horizontal Annular Flows - Procs. 4th. Int. Conf. '*Numerical Methods in Thermal Problems*' , R.W. Lewis, and K. Morgan, eds., Swansea, UK, Jul. 1985; Pineridge Press, Swansea, UK, 1985; 365-375.
147 - S. Kotake, and N. Hattori - Combined Forced and Free Convection Heat Transfer for Fully-Developed Laminar Flow in Horizontal Annuli - Int. J. Heat Mass Transfer, 28, 1985; 2113-2120.
148 - A.O. Nieckele, and S.V. Patankar - Laminar Mixed Convection in a Concentric Annulus With Horizontal Axis - ASME, J. Heat Transfer, 107, 1987; 902-909.
149 - M. Kaviany - Laminar Combined Convection in a Horizontal Annulus Subject to Constant Heat Flux Inner Wall and Adiabatic Outer Wall - ASME, J. Heat Transfer, 108, 1986; 392-397.
150 - J. Huetz, and J.P. Petit - Natural and Mixed Convection in Concentric Annular Spaces - Experimental and Theoretical Results for Liquid Metals - '*Proc. 5th Int. Heat Transfer Conf.*', Tokyo, Vol. 3, 1974, 169-172.
151 - D. Bohne, and E. Obermeier - Combined Free and Forced Convection in a Vertical and Inclined Cylindrical Annulus - '*Procs. 8th Int. Heat Transfer Conf.*', S. Francisco, Cal., 1986; Vol. 3; 1401-1406.

152 - M. Ciampi, S. Faggiani, W. Grassi, F.P. Incropera, and G. Tuoni - Experimental Study of Mixed Convection in Horizontal Annuli for Low Reynolds Numbers - '*Procs. 8th Int. Heat Transfer Conf.*', S. Francisco, Cal., 1986; Vol. 3; 1413-1418.

153- M. Ciampi, S. Faggiani, W. Grassi, G. Tuoni, and F.P. Incropera - Mixed Convection Heat Transfer in Horizontal, Concentric Annuli for Transitional Flow Conditions - Int. J. Heat Mass Transfer, 30, 1987; 833-841.

154- M. Ciampi, S. Faggiani, W. Grassi, and G. Tuoni - Remarks on Mixed Convection in Horizontal Concentric Annuli - Heat & Technol., 5, 1987; 38-48.

155 - W.N. Gill, and E. Del Casal- A Theoretical Investigation of Natural Convection Effects in Forced Horizontal Flows - AIChE J., 8, 1962; 513-518.

156 - Y. Mori, and Y. Uchida - Forced Convective Heat Transfer Between Horizontal Flat Plates - Int. J. Heat Mass Transfer, 9, 1966; 803-817.

157 - K.C. Cheng, and G.J. Hwang - Numerical Solution for Combined Free and Forced Laminar Convection in Horizontal Rectangular Channels - Trans. ASME, J. Heat Transfer, 90, 1969; 59-66.

158 - W. Nakayama, G.J. Hwang, and K.C. Cheng - Thermal Instability in Plane Poiseuille Flow - Trans. ASME, J. Heat Transfer, 92, 1970; 61-68.

159 - G.J. Hwang, K.C. Cheng - A Boundary Vorticity Method for Finite Amplitude Convection in Plane Poiseuille Flow - Developments in Mechanics, '*Procs. 12th Midwestern Mechanics Conf.*', Vol. 6, 1971; 207-220.

160 - M. Kiya, S. Fukusako, and M. Arie - Effect of Buoyancy on Laminar Developing Flow Between Parallel Plates - Bull. JSME, 15, 1972; 735-746.

161 - G.J. Hwang, and K.C. Cheng - Convective Instability in the Thermal Entrance Region of Horizontal Parallel-Plate Channel Heated from Below - Trans. ASME, J. Heat Transfer, 95, 1973; 72-77.

162 - J-W. Ou, K.C. Cheng, and R-C. Lin - Natural Convection Effects on Graetz Problem in Horizontal Rectangular Channels with Uniform Wall Temperature for Large Pr - Int. J. Heat Mass Transfer, 17, 1974; 835-843.

163 - C.Y. Chang, J.A. Guin, and L.D. Roberts - Surface Reaction with Combined Forced and Free Convection - AIChE J., 22, 1976; 252-259.

164 - J-W. Ou, K.C. Cheng, and R-C. Lin - Combined Free and Forced Laminar Convection in Inclined Rectangular Channels - Int. J. Heat Mass Transfer, 19, 1976; 277-283.

165 - R. Matsumoto, T. Nakajima, and M. Jamaguchi - Effect of Thermal Instability on Fully Developed Laminar Flow with Internal Heat Generation Between Two Horizontal Parallel Plates - '*Proc. 6th Int. Heat Transfer Conf.*', Toronto, Canada, Vol. 1, MC11, 1978; 61-66

166- H. Nakamura, A. Matsuura, J. Kiwaki, S. Hiraoka, and I. Yamada - Numerical Solutions for Combined Free and Forced Laminar Convection in Horizontal Rectangular Ducts by Conjugate Gradient Method - J. Chem. Eng. Japan, 11, 1978; 354-360.

167 - T.V. Nguyen, I.L. Maclaine-Cross, and G. de Vhal Davis - Combined Forced and Free Convection Between Parallel Plates - in '*Numerical Methods in Thermal Problems*', R.W. Lewis, and K. Morgan, eds., Pineridge Press, Swansea, UK, 1979; 269-278.
168 - K.C. Cheng, and J.W. Ou - Convective Instability and Finite Amplitude Convection in the Thermal Entrance Region, of Horizontal Rectangular Channels Heated from Below - '*Proc. 7th Int. Heat Transfer Conf.*', Munich, 1982, Hemisphere, Washington D.C., 1982, Vol. 2; 189-194.
169 - K. Fukui, M. Nakajima, and H. Ueda - The Longitudinal Vortex and its Effects on the Transport Processes in Combined Free and Forced Convection between Horizontal and Inclined Parallel Plates - Int. J. Heat Mass Transfer, 26, 1983; 109-120.
170 - F.C. Chou, and G.J. Hwang - Combined Free and Forced Convection in Horizontal Rectangular Channels for High ReRa - Can. J. Chem. Eng., 62,1984; 830-836.
171 - G.J. Hwang, and F.C. Chou - Effect of Wall Conduction on Combined Free and Forced Laminar Convection in Horizontal Rectangular Channels- ASME, J. Heat Transfer, 109, 1987; 936-942.
172 - E. Naito - The Effect of Buoyancy on Laminar Flow and Heat Transfer in the Entrance Region between Horizontal, Parallel Plates - Int. Chem. Eng;, 25, 1985; 315-323.
173 - K.C. Chiu, J. Ouazzani, and F. Rosemberger - Mixed Convection between Horizontal Plates - II. Fully Developed Flow - Int. J. Heat Mass Transfer, 30, 1987; 1655-1662.
174 - A.S. Lavine - Analysis of Fully Developed Opposing Mixed Convection between Inclined Parallel Plates - Warme-Stoff., 23, 1988; 249-257.
175 - E. Naito, and Y. Nagano - Combined Forced and Free Upward-Flow Convection in the Entrance Region Between Inclined Parallel Plates - ASME, J. Heat Transfer, 111, 1989; 675-682.
176 - S.S. Chen, A.S. Lavine, and J.M. McDonough - Computations of Three-Dimensional Opposing Mixed Convection Between Inclined Heated Plates - '*Proc. 9th. Int. Heat Transfer Conf.*', G. Hestroni, ed., Jerusalem, Israel, 1990; Vol.3; 321-326.
177 - J.M. Huang, J.D. Lin, and F.C. Chou - Combined Radiation and Laminar Mixed Convection in the Thermal Entrance Region of Horizontal Isothermal Rectangular Channels - Num. Heat Transfer, 18, 1990; 113-125.
178 - S. Rheault, and E. Biligen - Mixed Convective Developing Flow with Flow Reversal in Open-Ended Inclined Channels - in '*Mixed Convection and Environmental Flows*', ASME, HTD-Vol. 152, 1990; 9-14.
179 - F.S. Lee, and G.J. Hwang - A Time-Dependent Analysis of the Vortex Instability in the Thermal Entrance Region of an Inclined Parallel-Plate Channel - ASME, J. Heat Transfer, 114, 1992; 761-764.
180 - J.N. Lin, P.Y. Tzeng, F.C. Chou, and W.M. Yan - Convective Instability of Heat and Mass Transfer for Laminar Forced Convection in the Thermal Entrance Region of Horizontal Rectangular Channels - Int. J. Heat and Fluid Flow, 13, 1992; 250-258.

181 - H. Nakamura, A. Matsuura, J. Kiwaki, S. Hiraoka, and I. Yamada - Combined Free and Forced Laminar Convection in Triangular Ducts - J. Chem. Eng. Japan, 10, 1977; 109-115.
182 - M. Altman, and F.W. Staub - The Effect of Superimposed Forced and Free Convection in Horizontal and Vertical Rectangular Ducts - '*Proc. 2nd Nat. Heat Transfer Conf. AIChE-ASME*', Chicago, Ill., 1958. (83)
183 - M. Akiyama, G.J. Hwang, and K.C. Cheng - Experiments on the Onset of Longitudinal Vortices in Laminar Forced Convection Between Horizontal Plates - ASME, J. Heat Transfer, 93, 1971; 335-341.
184 - S. Ostrach, and Y. Kamotani - Heat Transfer Augmentation in Laminar Fully Developed Channel Flow by Means of Heating From Below - ASME, J. Heat Transfer, 97, 1975; 220-225.
185 - G.J. Hwang, and R-C. Lin - An Experimental Study of Convective Instability in the Thermal Entrance Region of a Horizontal Parallel-Plate Channel Heated from Below - Can J. Chem. Eng., 54, 1976; 521-525.
186 - Y. Kamotani, and S. Ostrach - Effect of Thermal Instability on Thermally Developing Laminar Channel Flow - ASME, J. Heat Transfer, 98, 1976; 62-66.
187 - H. Nakamura, A. Matsuura, J. Kiwaki, S. Hiraoka, and I. Yamada - Experimental Study on Heat Transfer of Combined Free and Forced Laminar Convection in Thermal Entrance Region of Horizontal Rectangular Ducts - J. Chem. Eng. Japan, 11, 1978; 438-443.
188 - Y. Kamotani, S. Ostrach, and H. Miao - Convective Heat Transfer Augmentation in Thermal Entrance Regions by means of Thermal Instability - ASME, J. Heat Transfer, 101, 1979; 222-226.
189 - F.R. McLarnon, R.H. Muller, and C.W. Tobias - Interferometric Study of Combined Forced and Natural convection - J. Electrochem. Soc., 129, 1982; 2201-2206.
190 - J. Jorné, and D. Labelle - Combined Natural and Forced Convection in a Horizontal Flow Channel - Chem. Eng. Commun., 38, 1985; 347-356.
191 - D.G. Osborne, and F.P. Incropera - Laminar, Mixed Convection Heat Transfer for Flow Between Horizontal Parallel Plates with Asymmetric Heating - Int. J. Heat Mass Transfer, 28, 1985; 207-217.
192 - D.G. Osborne, and F.P. Incropera - Experimental Study of Mixed Convection Heat Transfer for Transitional and Turbulent Flow Between Horizontal, Parallel Plates - Int. J. Heat Mass Transfer, 28, 1985; 1337-1344.
193 - F.P. Incropera, A.L. Knox, and J.R. Maughan - Mixed-Convection Flow and Heat Transfer in the Entry Region of a Horizontal Rectangular Duct - J. Heat Transfer, 109, 1987; 434
194 - J.R. Maughan, and F.P. Incropera - Experiments on Mixed Convection Heat Transfer for Airflow in a Horizontal and Inclined Channel - Int. J. Heat Mass Transfer, 30, 1987; 1307-1318. (175)
195 - A.S. Lavine, M.Y. Kim, and C.N. Shores - Flow Reversal in Opposing Mixed Convection in Inclined Pipes - ASME, J. Heat Transfer, 111, 1989; 114-120.

196 - R. Smyth, and Y.K. Salman - Combined Free and Forced Convection Heat Transfer in a Rectangular Duct - Int. Comm. Heat Mass Transfer, 18, 1991; 669-680.
197 - B.W. Martin, and D. Fargie - Effect of Temperature Dependent Viscosity on Laminar Forced Convection in the Entrance Region of a Circular Pipe - Proc. Ins. Mech. Eng., 186, 1972; 307-316.
198 - F.L. Test - Laminar Flow Heat Transfer and Fluid Flow for Liquids with Temperature Dependent Viscosity - Trans. ASME, J. Heat Transfer, 90, 1968; 415-420.
199 - E.N. Sieder, and G.E. Tate - Heat Transfer and Pressure Drop of Liquids in Tubes - Ind. Eng. Chem., 28, 1936; 1429-1435.
200 - R.G. Deissler - Analytical Investigation of Fully Developed Laminar Flow in Tubes with Heat Transfer with Fluid Properties Variable Along the Radius - NACA TN 2410, 1951.
201 - S.D. Joshi, and A.E. Bergles - Analytical Study of Heat Transfer to Laminar In-Tube Flow of Non-Newtonian Fluids - AIChE Symp. Series, 76, No.199, 1980; 270-281.
202 - K.T. Yang - Laminar Forced Convection of Liquids in Tubes with Variable Viscosity - Trans. ASME, J. Heat Transfer, 84, 1962; 353-362.
203 - D. Butterworth, and T.D. Hazell - Forced Convective Laminar Flow Heat Transfer in the Entrance Region of a Tube - Report AERE R6057, Chem. Eng. Div., AERE Harwell, UK, 1969.
204 - N.S. Reejhsinghani, W.N. Gill, and A.J. Barduhn - Part III. Experiments in Horizontal Tubes Including Observations on Natural Convection effects - AIChE J., 12, 1966; 916-921.
205 - K. Muralidhar, and F.A. Kulacki - Stability of Mixed Convection Flow - Heat and Fluid Flow, 8, 228-234; 1987.
206 - F.-C. Chou, and W.-Y. Lien - Effect of Wall Heat Conduction on Laminar Mixed Convection in the Thermal Entrance Region of Horizontal Rectangular Channels - Warme und Stoffbertragung, 26, 1991; 121-127.
207 - J.N. Lin, F.C. Chou, and P.Y. Tzeng - Theoretical Prediction of the Onset of Thermal Instability in the Thermal Entrance Region of Horizontaal Rectangular Channels - Int. J. Heat and Fluid Flow, 12, 1991; 218-224.

COMBINED CONVECTION AND OTHER EFFECTS IN HEAT TRANSFER IN HORIZONTAL FLOWS

CHAPTER 4: SYNTHESIS OF CANDIDATE'S PUBLISHED WORK ON CONVECTION

4.1 - Introduction

In Chapter 1.1 it has been explained that combined convection is the most general convective heat transfer case, of which what are termed forced and natural convection become almost limiting cases.
Further, in Chapter 1.1, other effects may well be present in combined convection which should either be eliminated beforehand (by design of experiment, say) or accommodated. Specifically, the issues of axial diffusion, conduction conjugate with the convection, and variable properties were raised.

Over the period of this work, studies have been made of all the above, and the work has been published as shown in Table 4.1. In Appendix I the papers are listed, together with a complete set.
It will be noted that a number have been published in International Journals, or equivalent Conference Proceedings.

In this Chapter the material is synthesized in the order described above, and the relevance to the remaining specific combined convection study is explained.

4.2 - Forced Convection (Refs. [P1,P2,P3,P4,P8,P11,P12])

Papers [P1], [P2], [P8], and [P12], will be better presented under the 'conjugate problems' heading, paper [P4], under the 'axial diffusion heading', and [P11] under the 'variable property' heading.

Paper [P3] deals with the prediction of forced convection flows in a round duct, with an axially exponential heat flux distribution. The method is an improved version of the original one by Collins [1,2]. The algorithm is based on a finite difference discretization of the governing equations in the 2D axis-symmetric elliptic form. The method utilizes a marching procedure, where the discretized momentum and energy equations are solved at the same time at a single axial position. An original feature of the algorithm is that continuity is enforced in an integral, rather than differential, form. The mass-flow is automatically conserved in this manner. The drawback is that the coefficient matrix is very sparse, and the solution correspondingly very slow. This could be accommodated in [P3], by the introduction of an auxiliary variable (the stream function), so as to obtain a band-diagonal matrix. Very efficient library-routines could then be used, and, overall, a 95% reduction of the computer time was obtained.
The analysis covers the thermal inlet region, the combined effect of hydraulic and thermal inlet, and the asymptotic region, for constant property fluids. Analytical solutions in the literature [3], are for the asymptotic region; they cover the range ($-70 \leq m \leq 40$). Numerical predictions agree very well (within 0.6 % in terms of the Nusselt number) with analytical solutions, for m in the range -20 to +40. However, for $m \leq -50$, negative asymptotic Nu-values would be theoretically predicted, while, numerically, the Nusselt number systematically converges to zero. No explanation of the inconsistency has been found. As for entrance effects, the results indicate that the value of the exponent m definitely affects the Nusselt number, and the thermal inlet length: both increase for increasing m.
It is interesting to note that all (Nu-z*) curves, irrespective of m, coincide with the relevant prediction for the uniform heat flux boundary condition, **H**, up to $z^* \sim 1 \times 10^{-3}$.
With constant property, the asymptotic Nu-value is a increasing monotonic function of m, independent of inlet conditions.

Buoyancy effects have also been considered in this work, for the case of water in a vertical tube. It is shown that the effect of redistribution of heat flux, compared with the uniform heating case, has a possible influence on the stability of flow, under variable property conditions. This is a conclusion of some general relevance, since it qualitatively extends to conjugate conduction and convection situations.

The Candidate was responsible for the entire study, except for the actual computational work, that is approximately 67%.

4.3 - Natural Convection (Refs. [P5,P6,P9,P13])

Papers [P5], [P6], and [P9], are discussed together, since they mark the development of control volume based numerical techniques for the analysis of buoyancy driven flows in a 2D differentially heated cavity, the implementation in it of k-ε turbulence models, and the validation process.

The numerical scheme is a modification of the SIMPLEC procedure, based on previous work of Theodossiou and Sousa [4], and Barozzi and Nobile [P8], and the implementation of the k-ε model proposed by Ozoe et al. [5]. The method has been demonstrated to be robust, in that stable results could be obtained at values of the Rayleigh number (based on the cavity height) as high as 10^{10}, with air in a square cavity. However, heavy under-relaxation is always necessary to provide convergence, due to the large variations of the source terms in the equations for turbulent kinetic energy (k), and for dissipation of turbulent kinetic energy (ε). Except for the coefficient in the buoyant term of the ε equation (adopted from [5]), the empirical constants were as from Launder and Spalding [6]. The method is validated in [P5], where numerical results for a 48x48 stretched grid, are compared with some other numerical prediction in the literature. In [P6] and [P9], the validation process is extended to the comparison with experimental data for water in a 10:1 vertical cavity, by Giel and Smith [7]. Numerical results are found to compare reasonably well with experimental findings, but also point out the limitations of the segregated procedure, becoming rapidly inadequate for an increase in the cavity Ra-number, and the drawbacks of k-ε modeling. In particular, k-ε models are not physically appropriate in the transition region.

All of this led to the conclusion that a direct approach is the much better tool for investigating buoyancy driven flows in the transitional region, thus avoiding turbulence modeling. To this aim a research activity has been initiated to provide a robust coupled (ie non-segregated) algorithm. This led to the production of paper [P13],where very accurate convergent solutions have been obtained up to $Ra=10^8$. This has already been discussed in some detail in Ch.2.

This research has provided clear evidence of the basic physical aspects of buoyancy dominated flow, and their numerical implications, both of utmost importance in the present context.

In all the above, the Candidate was responsible for approximately 25%.

4.4 - Axial Diffusion (ref.[P4])

This specific paper reports new data on laminar heat transfer in parallel plate ducts. The program, written by Nobile, treats the complete 2D equations using the SIMPLEC approach, over a staggered rectangular grid. Results cover the laminar flow range Re = 400 to 2000, for Pr = 0.71. The computational domain extends well upstream of the duct inlet. In this way, the effects of heat and momentum diffusion can be modelled correctly. In fact, there is no way of stopping their upstream propagation at $z^* = 0$.
The study demonstrates that, for this geometry, diffusive effects may be important. In fact, due to the influence of upstream diffusion of momentum, both the velocity and pressure profiles are not perfectly uniform at the entry section, not even at the highest Re-value. Further downstream, the results indicate that axial

diffusion of momentum influences all the relevant fluid-dynamic parameters, such as the distributions of axial velocity and pressure, and the friction factor, and, as Re reduces, the solution increasingly diverges from boundary layer considerations. In particular, the (non-dimensional) hydrodynamic development length slowly increases with Re (for Re > 300). Also, there is evidence of a rapid progressive increase of the hydrodynamic length at low Re (Re <40). The results of boundary layer-type solutions are approximated only for Re > 1000. Corresponding original heat transfer data are presented, allowing for axial heat conduction.

The Candidate was responsible for the entire study, except for the actual computational work, that is approximately 67%.

While these results relate to forced convection, they demonstrate the effect of axial diffusion under laminar flow conditions. A consideration relevant to the present combined convection study is that, while upstream diffusion has been found to affect the flow and temperature fields all over the laminar range with parallel-plate geometry, the effects have been found to be much more limited in the case of round ducts [8,9].

4.5 Conjugate Convection/Conduction (Refs. [P1,P2,P8,P12])

In the first paper, a simple, but fast and quite general procedure is presented to deal with forced convection heat transfer problems, including the effect of axial conduction in the wall. The method is a combination of the superposition principle at the wall boundary, and the numerical solution of the conduction equation within the wall. The accuracy of the solution has been checked carefully, by comparison with the available literature on conjugate heat transfer (which is the object of a complete review, also reported in this paper). A specific finding of the work, is that the convection equation is to be preferred to the simple matching of the heat flux, or temperature, at the solid-to-fluid interface. In fact, this is a 'soft' way for transmitting thermal effects from one phase to the other, in the iterative process.

The method is applied to the case of fully developed laminar flow in a round duct of finite length, under uniform heating conditions at the outer duct surface. The non-dimensional parameters relevant to the conjugate problem are identified as: the heat transfer length and the wall thickness (made dimensionless with the pipe diameter), the wall to fluid conductivity ratio, and the Peclet number (other than the axial coordinate, z^*).

The effects of heat conduction along the wall are discussed, as well as the heat flux, the interfacial temperature, the bulk temperature of the fluid, and the Nusselt number. It is found that a major effect of wall conduction is to redistribute heat flux at the inner wall surface. This progressively approaches the distribution typical of uniform wall temperature, for increasing wall conduction.

The Candidate was equally involved in the entire study, that is 50%.

This study is of special relevance here, in that it gives guidance in the estimate of wall conduction effects, whether in forced or combined convection circumstances.

Paper [P12] is an extension of [P1] to the case of countercurrent heat exchangers, again including the effects of conduction in the wall separating the two streams. The method is in fact the same as the one mentioned above. Thermal coupling of the two streams through a conductive wall is shown to have a definite effect on heat transfer performance. These are either estimated in terms of effectiveness, or using a 'second law approach'. Taking a practical point of view, it is demonstrated that an optimum value of wall conductivity exists, for any specific application.
The Candidate was equally involved in the entire study, that is 50%.

Paper [P2] represents an early attempt to predict numerically an experiment for combined convection, taking account of the duct wall effect. Experiments used a thick-wall vertical copper tube, under uniform heating. Forced convection data had previously [10] been simulated with good success using the method given in [P1]. This however does not apply to combined convection circumstances. A slightly modified version of the code written by Collins [1] was then tried, using a spline-fitting of experimental wall temperatures as the thermal boundary conditions. Results were only partially satisfactory, both due to limitations in the step size of the numerical scheme, and the 'stiffness' of the boundary condition imposed.
The study is relevant to this work, however, since it demonstrated that a complete numerical approach must be used to deal with conjugate combined convection problems.

The Candidate was equally involved in the entire study (50%), being specifically concerned with the predictive part.

Conjugate conduction and convection are also dealt with in paper [P8], in the framework of an electronic cooling problem. In this case, forced laminar flow is investigated in a parallel-plate channel, with protruding heating blocks. The method, is an improved version of the one used in [P4]. It is based on a Control Volume discretization of convection-diffusion equation, over a staggered rectangular grid. The SIMPLEC procedure is used for pressure-velocity decoupling. It is a specific feature of the algorithm (described with more detail, and tested in [P10]) the use of the ALZR (Alternate Line Zebra Relaxation) scheme. The technique is adapted here to non-staggered grids.

The thermal-fluid problem is considered of a plate cascade (simulating electronic wire-boards), and cross-stream periodic boundary conditions are applied. The effects of blockages on the velocity and temperature fields are demonstrated, and the influence of the entry velocity (flat or fully developed) estimated in terms of total head loss through the device.
A major result of the investigation, also relevant here, is that high conductivity solid domains present serious difficulties in

terms of convergence. In fact, strong anisotropy in the coefficient matrix correspond to large conductivity variation. In the case of concern, not only a very fine grid is used near the solid-fluid interfaces, but also a specific block correction procedure is applied to overcome this difficulty.

The Candidate was responsible for the entire study, except for the actual computational work, that is approximately 50%.

4.6 - Variable Properties (Refs.[P2,P3,P11])

Papers [P2] and [P3] have already been discussed in the context of conjugate problems, and forced convection, respectively. We just specify here that, in the former case, full property variation has been allowed in numerical predictions, while the more standard Boussinesq approximation has been used in the latter case.

Paper [P11] actually represents the conclusion of a long research activity [11,12] dealing with the effects of the non-Newtonian properties of blood on head losses, residence times, and heat transfer in the circulation. Numerical predictions have been produced by an original finite difference program by Barozzi and Dumas [8]. In the analysis, the possible presence of a cell-depleted plasma layer in the proximity of the vessel wall is accounted for. This is actually found to produce a remarkable enhancement of heat transfer rates in small vessels. When compared to this, the influence of blood rheological properties is found to be minor. The analysis covers the entire vessel size range of the circulation, also considering entrance effects.

The Candidate was again equally involved in the entire study, that is 50%.

4.7 - Computational Methods (Ref.[P7])

In paper [P7] an enhanced form of the SIMPLEC segregated algorithm used in [P8] was presented and validated, for the solution of the Navier-Stokes equations. This was fully coded in PARFOR77, a parallel structured extension of FORTRAN77. The implementation was for the CRAY X-MP/48 parallel computer, here used with one, two or four CPUs. Results showed that a considerable speed-up could be achieved by using two rather than one CPU, while little advantage was gained using four CPUs. The result is consistent with the structure of the already mentioned ALZR algorithm.

The Candidate acted mainly as the coordinator of this research activity, with an estimated personal contribution of 25%.

4.8 - Review (Ref.[P10])

While the review has been subsumed in Ch.3, in fact to produce [P10] required a considerable effort over a number of years. This effort

involved collaboration with the Supervisor, and required careful analysis of the widely varying parameter definitions used in the literature. The fruits of this analysis are apparent in Ch.3.

The Candidate's contribution was approximately 75%.

4.9 - Preliminary Combined Convection Study (Ref.[P14])

This study involved a not insubstantial collaborative exercise between the Candidate (who integrated the activity) and two of the authors, S. Piva, and G. Scarcella. The former performed the numerical predictions, and the latter the actual reading of the experimental data. The rational of the study was completely agreed beforehand with the Supervisor. It is important to realize that the results presented in [P14] explicitly, are only summarized in Chs.5 and 6.

The Candidate composed the paper, with an approximate contribution of 35%.

TOPICS Authors	FORCED CONVECTION	NATURAL CONVECTION	AXIAL DIFFUSION HEAT & Momentum	CONJUGATE CONDUCTION & Convection	VARIABLE PROPERTIES	JOURNALS (DETAILS) OR conference (c)
P1 Barozzi& Pagliarini	♦			♦		J.Heat Transfer 1985
P2 Barozzi, Pagliarini & Sousa	♦			♦	♦	C 1987
P3 Barozzi & Nobile	♦				♦	C 1987
P4 Barozzi & Nobile	♦		♦			C 1988
P5 Nobile, Sousa & Barozzi		♦				C, Heat & Technol. 1989
P6 Nobile, Sousa & Barozzi		♦				C 1989
P7 Nobile, Russo & Barozzi	COMPUTATIONAL METHODS					C 1989
P8 Barozzi & Nobile	♦			♦		C, BOOK 1990
P9 Nobile, Sousa & Barozzi		♦				C, 9th IHTC 1990
P10 Barozzi & Collins	REVIEW					C 1991
P11 Barozzi & Dumas	♦				♦	J.Biomech. Eng. 1992
P12 Pagliarini & Barozzi	♦			♦		J.Heat Transfer 1992
P13 Nobile & Barozzi		♦				C 1992
P14 Piva, Scarcella Barozzi & Collins	PRELIMINARY COMBINED CONVECTION RESULTS					C 1993

Table 4.1 - Synthesis of candidate's published work in chronological order.

List of Candidate's published work

P 1 - G.S. Barozzi, and G. Pagliarini - A Method to Solve Conjugate Heat Transfer Problems: the Case of Fully Developed Laminar Flow in a Pipe - ASME, J. of Heat Transfer, 107, 1985; 77-83.

P 2 - G.S. Barozzi, G. Pagliarini, and A.C.M. Sousa - Conjugate Heat Transfer in Vertical Tubes: Experimental and Numerical Study - Procs. 11th *Canadian Conference on Applied Mechanics*, Edmonton, Alberta, Canada, June 1987; Vol. 2, C 58-59.

P 3 - G.S. Barozzi, and E. Nobile - Scambio Termico Convettivo in Condotti con Distribuzione Esponenziale del Flusso Termico alla Parete - Procs. 5th U.I.T. Nat. Conf., Torino (I), June 1987; A 170-184.

P 4 - G.S. Barozzi, and E. Nobile - Low Reynolds Number Heat Transfer and Fluid Flow in the Inlet Region of Parallel Plates - Procs. 6th U.I.T. Nat. Conf., Bari (I), June 1988; 141-152.

P 5 - E. Nobile, A.C.M. Sousa, and G.S. Barozzi - Turbulence Modelling in Confined Natural Convection - Procs. 7th U.I.T. Nat. Conf., Firenze (I), June 1989; 85-96.; and 'Int. J. Heat and Technology', 7, 1989; 24-35.

P 6 - E. Nobile, A.C.M. Sousa, and G.S. Barozzi - Accuracy of Two-Equation Turbulence Modelling in Free Convection - in *Numerical Methods in Thermal Problems*, Procs. 6th Int. Conf., Swansea (UK), July 1989; Pineridge Press, Swansea (UK.), 1989, Vol. 6, Part 1; 600-610.

P 7 - E. Nobile, T. Russo, and G.S. Barozzi - An Efficient Parallel Algorithm for the Numerical Solution of Navier-Stokes Equations Using Fortran Structured Multiprogramming - *Applications of Supercomputers in Engineering, ASE 89* , 1st Int. Conf., Southampton (UK), Sept. 1989, C.A. Brebbia, and A. Peters, eds.; Elsevier, Amsterdam (NL), 1989, Vol.1; 3-14.

P 8 - G.S. Barozzi, and E. Nobile - Conjugate Heat Transfer in Forced Convection Cooling of Chip Arrays - Procs. 20th Int. Symp. *Heat Transfer in Electronic and Microelectronic Equipment*, A.E. Bergles, ed., Hemisphere pub. Co., New York, 1990; 709-723.

P 9 - E. Nobile, A.C.M. Sousa, and G.S. Barozzi - Turbulent Buoyant Flows in Enclosures - in *Heat Transfer 1990* , Procs. 9th Int. Heat Transfer Conf., G. Hetsroni, ed., Hemisphere pub. Co., New York, 1990; Pap. 5-NC-11, Vol. 2; 543-548.

P10 - G.S. Barozzi, and M.W. Collins - Mixed Convection in Horizontal Ducts: an Overview of Numerical Methods - Procs. 9th U.I.T. Nat. Conf., Pisa (I), June 1991; 45-60.

P11 - G.S. Barozzi, and A. Dumas - Convective Heat Transfer Coefficients in the Circulation - ASME, J. of Biomechanical Engineering, 113, 1991; 308-313.

P12 - G. Pagliarini, and G.S. Barozzi - Thermal Coupling in Laminar Double Pipe Heat Exchangers - ASME, J. of Heat Transfer, 113,.1991; 526-534.

P13 - E. Nobile, and G.S. Barozzi - Un Approccio Numerico ai Problemi di Convezione Naturale e Mista ad Elevati Valori del Numero di Rayleigh - Procs. 47th ATI Nat. Conf., Parma (I), 1992, Vol. I; 567-578.

P14 - S. Piva, G. Scarcella, G.S. Barozzi, and M.W. Collins - Comparison of Predictive and Experimental Data for Combined Convection in Horizontal Duct Flow - Procs. '*CMEM93 6th Intl. Conf. on Computational Methods and Experimental Measurements*', Siena (I), May 1993, C.A. Brebbia, and G.M. Carlomagno, eds., Comp. Mech. Pub., Southampton Boston (UK); Vol.1, 169-182.

References

1 - M.W. Collins - An Analysis of Combined Natural and Forced Convection and Other Problems in Internal Laminar Flow - Ph.D. Thesis, The City University, London, Oct. 1975.

2 - M.W. Collins - Finite Difference Analysis for Developing Laminar Flow in a Circular Tube Applied to Forced and Combined Convection - Int. J. Num. Meth. Eng., 15, 1980; 381-404.

3 - R. Shah, and A.L. London - '*Laminar Forced Convection in Ducts*' - Academic Press, NY., 1978.

4 - V.M. Theodossiou, and A.C.M. Sousa - An Efficient Algorithm for Solving the Incompressible Fluid Flow Equations - Int. J. Num. Meth. Fluids, 6, 1986; 557-572.

5 - H. Ozoe, A. Mauri, M. Ohmuro, S.W. Churchill, and N. Lior - Numerical Calculations of Laminar and Turbulent Natural Convection in Water in Rectangular Channels Heated and Cooled Isothermally on the Opposing Vertical Walls - Int. J. Heat Mass Transfer, 28, 1985; 125-138.

6 - B.E. Launder, and D.B. Spalding - The Numerical Computation of Turbulent Flows - Comp. Meth. Appl. Mech., 3, 1974; 269-289.

7 - P.W. Giel, and F.W. Schmidt - Natural Convection Heat Transfer in Cavities and Cells - Procs. 7th Int. Heat Transfer Conference, Munich (G), 1982; Vol. 1, 365-379.

9 - G. Pagliarini - Steady Laminar Heat Transfer in the Entry region of Circular Tubes with Axial Diffusion of Heat and Momentum - Int. J. Heat Mass Transfer, 32, 1989; 1037-1052.

8 - A. Dumas, and G.S. Barozzi - Laminar Flow Heat Transfer with Axial Conduction in a Circular Tube: a Finite Difference Solution - in '*Numerical Methods in Thermal Problems*', Vol. II - R.W. Lewis, K. Morgan and B.A. Schrefler, edrs., Pineridge Press, Swansea (UK.), 1981; 1111-1121.

10 - G.S. Barozzi, and G. Pagliarini - Experimental Investigation of Coupled Conduction and Laminar Convection in a Circular Tube - Int. J. Heat and Mass Transfer, 27, 1984; 72-91.

11 - S. Salvigni, M. Mariotti, and G.S. Barozzi - Red Cells Residence Time Distribution in the Circulation - Procs. 1st '*Mediterranean Conf. on Medical and Biological Engineering*', Sorrento, I, September 1977; Vol. I, 3.9-3.12.

12 - A. Dumas, and G.S. Barozzi - Laminar Heat Transfer Coefficients to Blood Flowing in a Circular Duct - Int. J. Heat and Mass Transfer, 27, 1984; 391-398.

CHAPTER 5: EXPERIMENTAL WORK

5.1 - Experimental Arrangements

An experimental strategy was devised to investigate the effects of combined convection in a uniformly heated horizontal duct.

As stated in the premises, the primary objective of the experimental part was to obtain data under controlled conditions, to be compared with numerical predictions, in a cross-validation process. When designing the experiment, then, care has to be taken to avoid any possible source of uncertainty, which could compromise the reliability of the simulation. More specifically, inlet effects are virtually eliminated by providing a fully developed entry velocity profile; experimental conditions are maintained within a range of Re, and Pe, where stable laminar flow conditions are expected, and the axial diffusion of heat and momentum has no significant effect; Ra_q-values are limited to the stable laminar region; all the test section is heavily insulated to provide a uniform distribution of the heat supply along the duct outer surface.

Distilled and de-ionized water was used in the course of the experiments.

The layout of the experimental rig is shown in Fig.5.1; three main parts can be distinguished:

- hydraulic circuit;
- test section
- measuring and data acquisition facilities.

5.1.1 - Hydraulic circuit

With reference to Fig.5.1, a constant head reservoir, A (30 liters), feeds the circuit. Before reaching the test section, water is cooled at a constant temperature in a compact heat exchanger, B (Alfa-Laval heat exchanger, with 15 elements). A constant temperature bath, H (Colora WK30), provides the cooling fluid (water) to the heat exchanger. This arrangement has been found satisfactory in terms of stability, and no adjustment of the water temperature is necessary before the inlet of the test section. As a unique artifice, the heat exchanger is operated concurrently. In fact, previous experiments by Piva [1] on a similar rig, had shown that, with a countercurrent arrangement, the switching cycles of the bath could be detected by

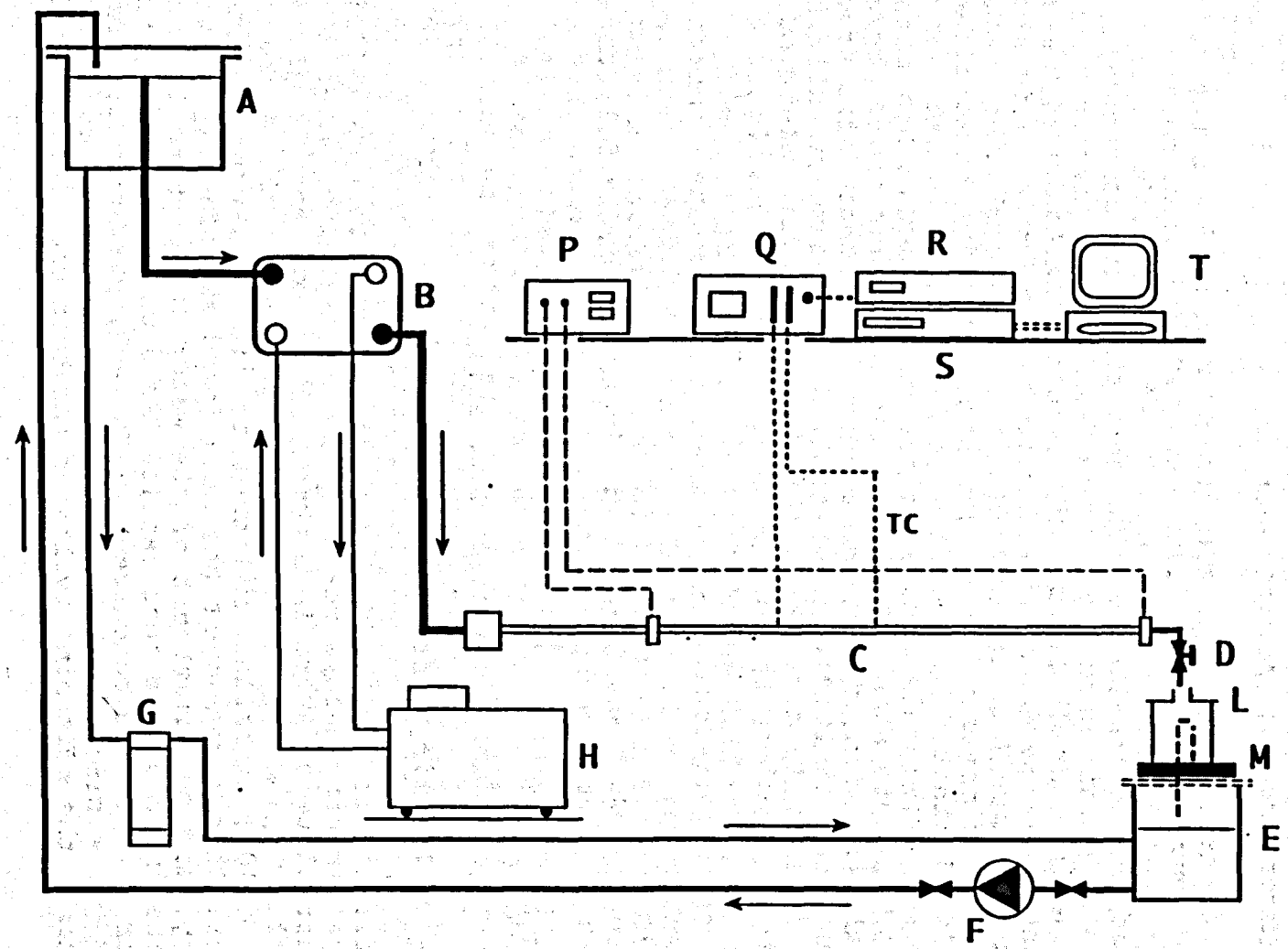

LEGEND

A	constant head tank
B	heat exchanger
C	test section
D	control valve
E	receiving tank
F	pump
G	filter
H	constant temperature bath
L	flask for flow rate measurements
M	electronic balance
P	DC or AC power supply
Q	thermoelectric reference point
R	data-logger (control unit)
S	digital multimeter
T	personal computer
TC	thermocouples

Fig. 5.1 - Lay-out of the experimental rig

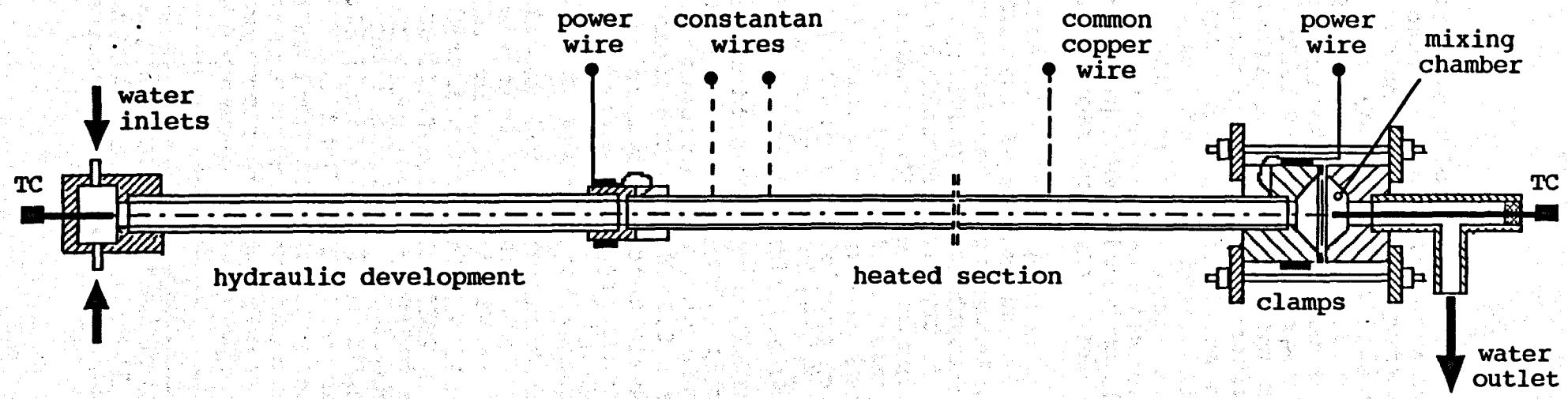

Fig. 5.2 - General view of the test section

the inlet thermocouple. The stability of the bath has been checked in the course of preliminary runs; its temperature always remained constant within 0.1 °C. Polypropylene tubing from B to the test section, C, was thermally insulated by cellular rubber. A micrometric control valve, D, regulates the water flow rate. At the exit of the test section, water is passed through the measuring flask, M, and discharged in the collecting tank, E. A centrifugal pump, F, brings the fluid back to reservoir A. Water filtering is operated by a rope-type filter, G, inserted on the overflow line.

5.1.2 Test Section

Essential parts of the test section are: the heat transfer measurement section; the hydrodynamic development length; the entry, exit, and connection blocks. The test section is schematically represented in Fig. 5.2.

The hydraulic development length is made with a 1318 mm long Perspex tube (16 mm ID./20 mm OD). According to recent numerical predictions of Pagliarini [2], this length should provide a fully developed velocity profile (99% of the fd centreline velocity) up to Re ~ 1450. This agrees quite well with the prediction based on the Chen's equation [3]

$$\frac{L_{hy}}{D} = \frac{0.72}{0.04\,Re + 1} + 0.061\,Re \qquad (5.1)$$

The hydraulic development section is connected to the heated section by a properly designed acrylic (Perspex) joint, sealed with silicone rubber. Perspex has favourable mechanical and thermal characteristics (k_p = 0.17 - 0.25 W/m°C). The arrangement provides a firm alignment of the development and measuring sections, and a smooth connection of the two parts. The entry and exit blocks are also made with acrylic material.

Water from the feeding tank enters a cylindrical mixing chamber (Ø 50 mm) in the entry block, through four radial inlets (90° apart). Annular tubing distributes the flow-rate to the four entries. The inlet fluid temperature is measured in this mixing chamber. The bulk fluid temperature is also measured in a mixing chamber at the exit of the heated section. As shown in Fig 5.2, the mixing chamber, in the end block, is divided into two parts by a circular diaphragm, leaving a 3 mm wide passage along its contour. Initially, a small mechanical stirrer had been inserted in the upstream volume of the chamber, further to improve mixing. However, preliminary tests showed the provision had no appreciable effect on mixing; the stirrer has not been used in the experiments. The two parts of the end block are clamped, with a rubber lining in between, for sealing.

The core of the test section is a commercial copper pipe, 2757 mm long, 16 mm ID, 18 mm OD. The thermal conductivity of the material (k_w = 334.2 W/m°C) had been measured very precisely by Piva and Pagliarini [4].

Heating is provided by six thin constantan wires (Ø 0.036 mm), with silk insulation, wound in spirals on the outer surface of the duct. Six constant pitch helices were machined on the tube surface to guide the heating wires. Each wire is 6.4 m long and the pitch of each helix is 30 mm, giving a distance of 5 mm between two consecutive spirals. A dielectric coating (3M/Scotchkote) provides the electrical insulation of the surface. The same product is used to glue the heating wires to the wall. Both the connection and the end joints have six longitudinal grooves (60° apart) to permit the passage of the heating wire terminations through the Perspex blocks. Those passages, in the part overlapping the metal tube, are carefully sealed with silicone rubber. Each wire termination is soldered to a low resistance copper wire, whose other extremity is screwed on a copper collar, at the pipe end joints. The two copper collars provide connections for power leads and voltage measurement.

The wall temperature is measured by 22 copper-constantan thermocouples. These have been built up, by soldering constantan wires (Ø 0.15 mm), and a common copper wire, directly on the duct wall. The measuring extremity of each constantan wire is soldered in a cut (max. depth 0.20 mm) traced on the duct wall, and orthogonal to the duct axis. To reduce the conduction error along the wires, these are wound around the duct at least once. Wall thermocouples are mounted at 12 axial positions, as indicated in Table 5.1. Note that the measuring stations are closer in the entry region, and but more spaced in the fully developed region. Upstream stations are provided with only one thermocouple (at the top of the duct section, $\theta = 0°$); from position 7, the wall temperature is also measured at the side ($\theta = 90°$) and/or the bottom ($\theta = 180°$) of the duct section.

Table 5.1 - Axial and peripheral positioning of wall thermocouples ($\theta = 0°$ at the top generatrix, positive clockwise)

Thermocouple number & position				Axial position, z' (mm)	Relative distance, Δz' (mm)
$\theta = 0°$	$\theta = 180°$	$\theta = 90°$	$\theta = -90°$		
2.0				42.0	-
3.0				69.0	27.0
4.0				118.0	49.0
5.0				198.5	80.5
6.0				298.5	100.0
7.0	7.1			498.0	199.5
8.0	8.1			843.0	345.0
9.0	9.1			1198.0	355.0
10.0	10.1			1501.0	303.0
11.0	11.1	11.2		1809.0	308.0
12.0	12.1	12.2	12.3	2300.0	491.0
13.0	13.1	13.2		2750.0	450.0

Thermocouples of type K (Philips Thermocoax TI, Ø1.5) are used to measure the fluid temperature at inlet and outlet of the test section, as well as air temperature in the neighbourhood of the test section. These had been calibrated in advance, by a constant temperature bath, a reference platinum thermoresistance (type PT100, Minco Prods., mod. S 7924 PD180), and a precision bridge (Leeds & Nothrup 8078). The thermometer calibration is certified with 0.01 °C accuracy (NIST Test Report 240072/236856, Aug. 1988). Before calibration, the resistance at 0°C of the reference thermometer has been checked according to ASTM E563-87 Standard.
Over the range 15-65 °C, individual 2nd order calibration curves have been obtained for the three thermocouples, by a least square technique. The calibration parameters have been implemented in the program for automated data processing.

Wall thermocouples were calibrated as follows: water was circulated in the test section at the maximum flowrate, and inlet/outlet temperatures measured by the above K-thermocouples. The test section had been carefully insulated before starting the calibration runs. The circuit was operated at 6 different inlet temperatures, in the range 20-60 °C. The inlet-outlet temperature drop was subdivided linearly along the test section, and used to correct temperature readings of wall thermocouples for heat losses to the environment. This gave individual second order calibration equations, which are used in the data processing.

The complete test section, including the hydraulic development length, and Perspex end-parts, were thermally insulated with cellular rubber. From the Manufacturer's spreadsheets, the thermal conductivity of the material is k_i = 0.032 W/m°C. The thickness of the insulation is 40 mm all along the heated section.

5.1.3 Instrumentation and data acquisition

Electrical power supply and regulation are provided by an autotransformer (Iskra TRN 140-IT). AC current is stabilized (AROS SEM415 voltage stabilizer), and a 220/220 V transformer is used as a net-separator.
An initial test of the DC power supply proved unsatisfactory, since effects due to water polarization interfered with wall temperature measurements.

The voltage drop through the heating resistances is measured by a precision digital multimeter (Hewlett Packard HP3478A). Current intensity is measured by an ammeter (CGS C-0.5).

The reference point for thermocouples is provided by a thermoelectric ice point (Kaye K170), with 50 built-in junctions (25 for K-thermocouples, and 25 for T-thermocouples). This is certified to reproduce the ice point of water with a typical stability of ± 0.01 °C. The input panel of the joint has been carefully insulated to eliminate parasitic thermoelectric forces due to variations of the ambient temperature.
Electromotive forces of thermocouples are measured by a precision voltmeter (Hewlett Packard 3458A; maximum sensitivity 10 nV). This

is provided with an auto-calibration facility, which can be used to minimize the effect of environmental temperature variations on the uncertainty of the measurements.
For automatic data collection, the sequence of temperature readings is driven by a switch/control unit (HP 3488A). The equipment is provided with 50 input channels, which can be swept according to any programmed sequence. The unit is driven by a Personal Computer (Compaq ProLinea 3/25s), through an interface board (IEEE488 Standard, N.I.).

With minor adaptations, the data acquisition software is essentially the same which had been designed, and successfully used, by Piva [1], to investigate convection heat transfer in ducts with exponential heat flux distributions. A detailed description of the program is given in [1]. Briefly, the program data-base is made up with thermocouple numbers, positions, and calibration constants; the measuring sequence can freely be selected, as well as channel switching time, sampling frequency (time for one individual reading), the number of individual readings of the probe during the measuring (closed switch) period, number of valid readings (usually the first two readings are eliminated before averaging, to avoid the effect of switching). At any cycle, the software automatically provides the arithmetic mean of valid readings of each thermocouple, and converts it into Celsius degrees.
Other options of the software are: graphical display of the temperature distribution along the test section; automatic acquisition of the results in ASCII format, for successive elaborations; statistical treatment of the data.

The mass flow-rate is measured automatically using a computerized gravimetric method, set up by Piva and Carlino [5]: water from the test section is continuously discharged into the measuring tank (10 lt) which is fitted with a precision electronic balance (Gibertini Europe 8000, accuracy ± 0.1 g). The measuring process is fully controlled by computer, through a RS232 interface (apart from the start and stop of the sampling periods, which are operated manually) by an electric switch. A siphoning system periodically discharges the contents of the measuring tank into the receiving tank.
One sampling sequence is made of five individual measurements. After each of them, the program displays the sampling time, based on the computer internal clock, the weight of water collected within the sampling time, the mass flow-rate, and the Reynolds number, at the entry conditions, Re_o. The entry temperature, T'_o, is part of the input for the program. Correlations for computing the water properties at T'_o are implemented in the software. At the end of a measuring cycle, averaged Q_m and Re_o values are displayed, with their precision index, computed in accordance with ANSI/ASME PTC 19.1-1985 Standard [6].

In the preliminary runs the flow rate had been measured manually, by a calibrated flask and a stop-watch.

5.1.4 Test method and precautions

The testing procedure is as follows, and described in an 'instruction' mode:

a. Preliminaries: switch on the measuring instruments, the constant temperature bath, the pump; check the electrical resistance of the heating wires; actuate the heating circuit at the voltage needed to obtain the wanted Ra_q value; fix the bath temperature; regulate the flow-rate at the wanted Re_o-value, by adjusting the control valve; check for the presence of air bubbles (by visual observation, after removing the thermal insulation of the perspex joints), and eventually eliminate them (air drainages are provided at the test section extremities); set the sampling parameters of the data acquisition system.

   In the present runs the sampling parameters for temperature readings were:

sampling frequency	10 s^{-1}
total number of readings	12
number of valid readings	10

   The digital voltmeter has always been operated in the auto-calibration mode.

   In the final runs the bath temperature has been fixed a few degrees above the ambient air temperature at the start. This provision is intended to obtain an almost perfect balance (within 2-3 °C) of the water temperature at the test section inlet, and the environmental temperature in the lab at the time of reaching steady conditions (this typically increases by about 3 °C from morning to afternoon). The final goal of this is to eliminate the need for correcting T'_o for heat exchange along the hydraulic development section. The correction would anyway be minimal, but, of course, rather uncertain.

b. Transient following: check at intervals the time evolution of fluid, ambient, and wall temperatures (this can either be done automatically, or manually); check the constancy of flow-rate, voltage and current. Typically, the checking procedure is repeated every 30 minutes at the beginning of the run, and more frequently in the proximity of steady state conditions.

c. Steady state control: steady state conditions are stated to be reached when four complete measurement cycles of wall and fluid temperatures, executed at intervals of two minutes or more (up to 5), give unchanged results within 0.1 °C, the maximum deviation from the average of the four readings is within 0.03 °C, and the wall temperature variations are randomly positive and negative from one sample to another. A computer screen printout of an acceptable sequence is shown in Fig.5.3.
   A typical time period to reach steady conditions is 5-6 hours.

d. Final measurements: complete the set of temperature sampling up to five readings or more (a maximum of 15 has been reached), and

save on hard-disk; execute the final measuring cycle for the flow-rate; repeat five readings of current and voltage; immediately after the power shut-off, check the value of the heating resistance network.

30 Giu 1993	Automatic Data Logger - rel 2.55	17:45:48

	17:35:20		17:38:20		17:41:35		17:44:20	
2)	29.00°C	0.01	29.01°C	0.01	29.00°C	-0.01	29.01°C	0.01
3)	29.05°C	-0.01	29.07°C	0.02	29.06°C	-0.01	29.07°C	0.01
4)	29.21°C	-0.01	29.22°C	0.01	29.21°C	-0.01	29.22°C	0.01
5)	29.32°C	-0.02	29.34°C	0.02	29.31°C	-0.03	29.33°C	0.02
6)	29.46°C	-0.02	29.47°C	0.01	29.47°C	0.00	29.46°C	-0.01
7)	29.59°C	0.00	29.59°C	0.00	29.59°C	0.00	29.59°C	0.00
71)	29.56°C	-0.02	29.56°C	0.00	29.56°C	0.00	29.57°C	0.01
8)	29.70°C	-0.03	29.71°C	0.01	29.71°C	0.00	29.70°C	-0.01
81)	29.65°C	-0.01	29.65°C	0.00	29.65°C	0.00	29.65°C	0.00
9)	29.84°C	-0.01	29.86°C	0.02	29.84°C	-0.02	29.84°C	0.00
91)	29.70°C	-0.01	29.71°C	0.01	29.71°C	0.00	29.71°C	0.00
10)	29.93°C	-0.02	29.97°C	0.04	29.94°C	-0.03	29.94°C	0.00
101)	29.75°C	-0.02	29.75°C	0.00	29.75°C	0.00	29.76°C	0.01
11)	29.96°C	-0.02	29.97°C	0.01	29.96°C	-0.01	29.97°C	0.01
111)	29.84°C	-0.01	29.84°C	0.00	29.84°C	0.00	29.85°C	0.01
112)	29.86°C	-0.02	29.87°C	0.01	29.86°C	-0.01	29.87°C	0.01
12)	30.21°C	-0.01	30.21°C	0.00	30.20°C	-0.01	30.21°C	0.01
121)	30.03°C	-0.01	30.03°C	0.00	30.02°C	-0.01	30.03°C	0.01
122)	30.09°C	-0.02	30.09°C	0.00	30.09°C	0.00	30.10°C	0.01
123)	30.14°C	0.00	30.14°C	0.00	30.12°C	-0.02	30.13°C	0.01
131)	30.50°C	-0.01	30.50°C	0.00	30.50°C	0.00	30.51°C	0.01
132)	30.44°C	-0.01	30.45°C	0.01	30.45°C	0.00	30.46°C	0.01
402)	28.28°C	0.00	28.27°C	-0.01	28.27°C	0.00	28.27°C	0.00
403)	29.08°C	-0.03	29.14°C	0.06	29.09°C	-0.05	29.14°C	0.05
400)	27.23°C	0.01	27.14°C	-0.09	27.21°C	0.07	27.15°C	-0.06

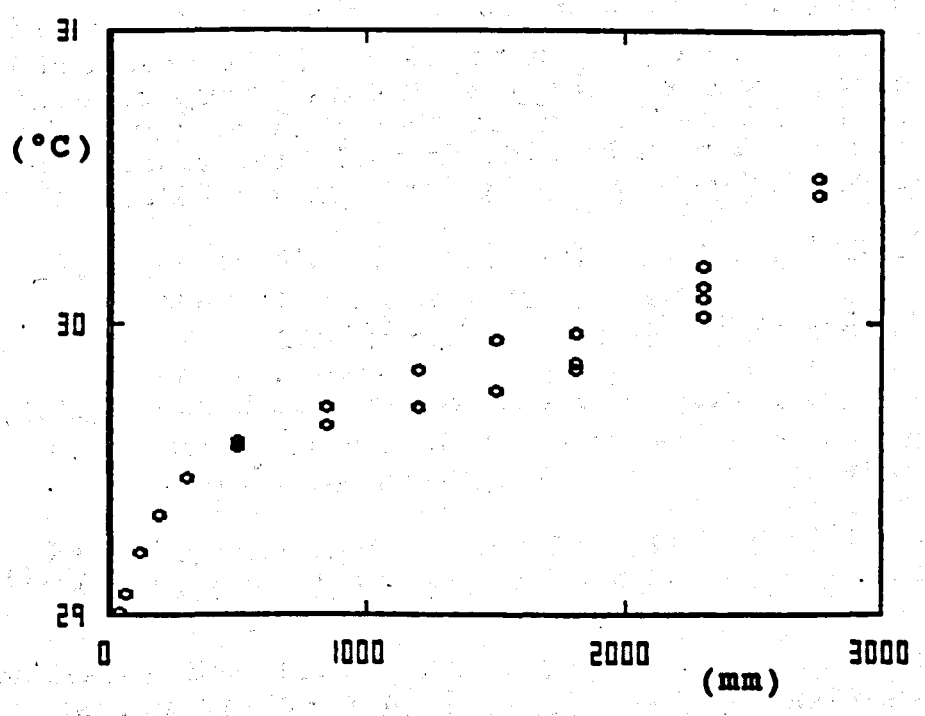

Fig. 5.3 - Typical computer screen printout of temperature sequences at steady state.

5.2 - Data Reduction and Uncertainty Considerations

The following data are available at the end of an experimental run:

- voltage drop at the ends of the heating wires, V [V];
- electric current through the heating circuit, I [A];
- electrical resistance of the heating circuit, R_{el} [Ω];
- inlet fluid temperature, T'_o [°C];
- outlet fluid temperature, T'_{out} [°C];
- ambient temperature, T'_a [°C];
- local wall temperatures, T'_{wl} [°C];
- mass flow-rate, Q_m [kg/s];

Data reduction proceeds as follows:

a. <u>wall temperature averaging</u>

The mean wall temperature at the general axial station i, $T'_{wz,i}$, is calculated as:

$$T'_{wz,i} = \frac{\sum_1^4 T'_{wl,i}}{4} \qquad (5.2)$$

For stations where only one temperature is measured, the measured value is used as the average; for stations where temperature is not measured at $\theta = \pm 90°$, the missing temperatures are assumed equal to the mean of the measured top and bottom values; where only one lateral temperature is available, this is counted twice in the average. This simple averaging procedure has been considered reliable, since top-to-bottom temperature differences are limited (max. 1-2°C).

b. <u>effective heat supply rate</u>

The total electrical power supplied, $\dot{Q}_{el}$, is:

$$\dot{Q}_{el} = VI \qquad (5.3)$$

or, alternatively:

$$\dot{Q}_{el} = \frac{V^2}{R_{el}} \qquad (5.4)$$

The comparison of results of equations (5.3) and (5.4) has always shown convergence within 2%. This check is necessary, since the ammeter used is only class 0.5 (Range 2.5 or 5 A); on the other hand, wire resistance is not measured under operative conditions. Therefore, the two methods are expected to have a comparable level of uncertainty.

The electrical power must be reduced for heat losses. These can either be estimated from the water energy balance, $\dot{Q}_{lt,w}$, or by calculating heat leakages through the insulation, $\dot{Q}_{lt,is}$.
In the first case we have:

$$\dot{Q}_{lt,w} = \dot{Q}_{el} - Q_m c_p \left(T'_{out} - T'_o\right) \tag{5.5}$$

In the second case, the following summation is executed:

$$\dot{Q}_{lt,is} = \sum_{i=1}^{13} \frac{\left(T'_{wz,i} - T'_a\right)\left(z'_i - z'_{i-1}\right)}{R_{T,i}} \tag{5.6}$$

Here, z'_i is the axial distance of station i from the inlet section ($z'_{13} = L_{ht}$); $z'_{13} = L_{ht}$; $T'_{wz,13} = T'_{wz,12}$; and, $R_{T,i}$ is the radial (wall to air) thermal resistance of the section from z'_{i-1} to z'_i, per unit length. $R_{T,i}$ is written:

$$R_{T,i} = R_{w-is} + R_{is-a,i} \tag{5.7}$$

with:

$$R_{w-is} = \frac{\ln\left(D_{is}/D_{out}\right)}{2\pi k_{is}} \tag{5.8}$$

$$R_{is-a} = \frac{1}{\pi D_{is} h_a} \tag{5.9}$$

Quantities in eqns.(5.8),(5.9) are:

D_{is}, outer diameter of insulation (0,098 m);
k_{is}, thermal conductivity of insulation (0,035 W/m°C, inclusive of a 10% increase for the effect of connections and moisture content);
D_{out}, outer diameter of the tube (0,018 m);
h_a, convection coefficient at the outer surface of the insulation ($W/m^2°C$).

Assuming the ambient air is still, h_a has to be determined by correlations for natural convection. The Churchill and Chu [7] equation for isothermal horizontal cylinders, is used:

$$Nu_a^{0.5} = 0.60 + \frac{0.387 Ra_a^{0.167}}{\left[1 + \left(0.559/Pr_a\right)^{0.563}\right]^{0.296}} \tag{5.10}$$

In eqn.(5.10) suffix a indicates that quantities are estimated for air.
Equations by McAdams [8] and Morgan [9] have also been tested; over the range used, (Ra_a ~ 7000-18000) these agree with eqn.(5.10), within 20 %.
Solving for eqns.(5.7-5.10) demands an iteration to determine compatible values of two variables (h_a, T'_{is}). This is accomplished automatically on an electronic table (MS Excel 3.0). An average value of h_a for this experiment is 7.3 W/m^2°C, leading to estimate R_{is-a} as about 6% of R_{w-is}. Overall, $\dot{Q}_{lt,is}$ is within about 2% of $\dot{Q}_{el}$, a very reasonable figure.
However, the comparison of $\dot{Q}_{lt,w}$ and $\dot{Q}_{lt,is}$ was always unsatisfactory: eqn.(5.5) leads to very unreliable estimates of the heat loss, which sometimes became higher than 30% of $\dot{Q}_{el}$. A bias error in the outlet temperature measurement seems to be at the origin of this large overestimate. However, attempts to correct it have failed. It is possible that a new mixing section, with turbulence promoters could satisfactory reduce the effect.

The net power input, $\dot{Q}_w$, is thus calculated as:

$$\dot{Q}_w = \dot{Q}_{el} - \dot{Q}_{lt,is} \qquad (5.11)$$

The nominal heat flux at inner duct surface is finally obtained as:

$$q'_w = \frac{\dot{Q}_w}{\pi D L_{ht}} \qquad (5.12)$$

c. Fluid bulk temperature and Nusselt number

The bulk temperature of water, $T'_{m,z}$, is assumed to increase linearly with z', as from equation

$$T'_{m,z} = T'_o + \frac{q'_w \pi D z'}{Q_m c_p} \qquad (5.13)$$

The mean Nusselt number at z', Nu_z , is calculated in correspondence with the twelve measuring stations, by the equation

$$Nu_z = \frac{q'_w D}{(T'_{wz} - T'_{mz})k} \qquad (5.14)$$

d. Properties and non-dimensional quantities

The important non-dimensional parameters are: Ra_q, Gr_q, Pr, Re, Pe, and z*.

These are either estimated at the inlet temperature, at the local fluid bulk temperature, or at the local film temperature. The properties of water, density, specific heat, thermal conductivity, thermal expansion coefficient, viscosity, are computed by the following general equation [10]:

$$\Xi(T') = C_A + C_B T' + C_C T'^2 + C_D T'^3 \qquad (5.15)$$

The constants and standard deviation from tabulated data are listed in Table 5.2

Table 5.2 - Constants for the temperature variation of water properties using eqn.(5.15)

Ξ	C_A	C_B	C_C	C_D	Standard deviation
273.15 < T'<373.15 K					
ρ	766.17	1.80396	-3.4589 E-3		0.5868
c_p	5.6158	-9.0277 E-3	14.177 E-6		4.142 E-3
k	-0.4806	5.84704 E-3	-0.733188E-5		0.481 E-3
273.15 < T'<320 K					
$\mu x 10^6$	0.239179 E6	-2.23748 E3	7.03318	-7.40993E-3	4.0534 E-6
$\beta x 10^6$	-57.2544 E3	530.421	-1.64882	1.73329 E-3	1.1498 E-6
320 < T'<373.15 K					
$\mu x 10^6$	35.6602 E3	-272.757	0.707777	-0.618833E-3	1.0194 E-6
$\beta x 10^6$	- 11.1377 E3	84.0903	-0.208544	0.183714 E-6	1.2651 E-6

Source: R.S. Figliola, and D.E. Beasley, *Theory and Design for Mechanical Measurements*, J. Wiley & Sons, N.Y., 1991.

To determine the uncertainty of heat transfer results is a formidable task. When declared, the accuracy of the measurements is usually presented as a range of uncertainty, in percentage terms, of the Nusselt number, with no specification of the type of errors embodied, and the error sources. In those terms, the uncertainty of results in convection heat transfer is typically ± 20%.

In the present case, an error estimate analysis has been made on one of the experimental runs (run FA), following ANSI/ASME standards [6]. The procedure is very complex and lengthy; only the essence and the meaning of the results are presented here.

As far as precision (random) errors are concerned, the number of readings executed for each sample (at least 5 readings per sample) allows the statistical treatment of the error. This leads to a relative variance of the heat flux density (also considering uncertainties in the determination of heat leakages through the insulation) of ~ 1%. The relative uncertainty of wall temperature measurements as estimated from at least 5 samples of 10 valid readings, results ~ 0.1 % (± 0.03 °C at 30°C). Random errors in bulk fluid temperature embody the effect of flow-rate measurements. The

analysis has shown that random errors of the latter are very low and have no practical influence on T'_{mz}. Wall and fluid temperatures thus have the same level of accuracy. Overall, the relative variance of Nu_{zm} ranges from 7 to 4% along the test section (higher values correspond to the entry part, where temperature differences are the lowest).

A bias (fixed) error estimate is extremely uncertain in itself, since, according to ANSI/ASME standards, it must be based on judgment and experience. The quality of the instrumentation leads to an estimate of a relative bias limit of 4% for the value of the heat flux density; the bias limit of temperature measurements mainly derives from calibration of K tc's. In fact these have been used to calibrate wall tc's. Considering the bias of the error chain, including errors in the reference resistance thermometer, and its measuring bridge, long term stability of the instruments (ice point reference, and voltmeter), and bias errors deriving from the different placement of the probes in operation, in respect to calibration, as well as fitting errors, it is probably optimistic to define the bias error range of the K tc's as ± 0.1 °C. As a consequence a probable bias range for wall tc's is not less than ± 0.2 °C. However, when calculating the difference $T'_{wz} - T'_{mz}$, the bias error on T'_o should cancel out, and only the bias of wall temperature would be important. One source of bias in the calibration of wall tc's is the temperature gradient from the fluid to the wall (outer) where tc's are placed. Since this effect had not been accounted for in the calibration, it had to be included in the bias. It can be estimated with relative ease, considering that calibration has been performed under fully turbulent conditions (Re = 5000-10000). Using the Dittus and Boelter equation for determining the convective thermal resistance, the temperature drop from fluid to the inner duct wall can be computed. This comes out as a range between 0,01 and 0,04 °C (water temperature range 25 - 50°C). The temperature drop in the duct wall is negligible either in calibration or measurement.

Overall, it is unlikely that the bias limit on the wall to fluid temperature difference can be fixed at a level lower than 0.1-0.2°C. This leads to a general estimate of about 15% for the bias range of Nu_z; this increases to a maximum of 20% at the first station (z'=46 mm). Correspondingly, the uncertainty interval providing a 95% coverage is ± 16% for the generality of the results, and increases up to ± 28% close to the entrance. Those uncertainty intervals reduce for increasing Ra_q.

The comparison of experimental Nu_z-values with the reference solutions and experimental data in the literature is more encouraging than shown by the above analysis. Comparison with Shah and London [11] constant property solution is possible in the entrance region, before the onset of buoyancy. In general the percentage deviation of Nu_z is within 10%, in the various runs, with a maximum of 20% (Run FC). The comparison with available correlations for fully developed flow is also satisfactory, as will be shown in the following.

The uncertainty analysis shows that the Nusselt number is very sensitive to the value of the inlet temperature, especially at low Ra_q values. This has been verified by using as input slightly modified values of the inlet temperature: at $Ra_q \sim 9x10^5$ (Run FC), changing T'_o of 0.1 °C produced a changes in Nu_z of ~ 10 %. The sensitivity to T'_o reduces for increasing Ra_q. This provides a useful indication for the future, in that new provisions must be taken to reduce uncertainties in the measurement of the entry temperature. Possibly, two or more high quality thermocouples should be provided at the entrance section.

5.3 - Heat Transfer Results

Experimental results are subdivided into a preliminary and a final series. The former has been reported in a recent Conference paper [12], enclosed in Appendix I of this Thesis. More details of this part of the work may be found in [13].

5.3.1 - Preliminary tests

The preliminary experimentation had the advantage of pointing out possible weak points and deficiencies of the rig, and showing the reliability and the limits of the test method.
In those experiments the test section was 2.8 m long, with a 43 mm unheated part at the end. Five runs, demonstrative of the performance of the apparatus, are reported in [12]. These are further assessed here to extract the information needed and changes for the final part of the work. The most important non-dimensional quantities at the entry temperature, and their variations along the test section, are presented in Table 5.3.

Table 5.3 - Preliminary runs: entry and exit values of the leading non-dimensional parameters.

Run No.	PA	PB	PC	PD	PE
Re_o	904	952	1005	184	151
Re_e	909	993	1244	187	189
Pr_o	7.07	7.09	6.88	7.10	7.10
Pr_e	7.03	6.76	5.41	6.95	5.50
Ra_{qo}	1.04 E5	8.83 E5	5.06 E6	8.90 E4	9.04 E5
Ra_{qe}	1.05 E5	9.95 E5	8.45 E6	9.41 E4	1.58 E6
Ra_o	5.92 E3	5.83 E4	3.59 E5	7.03 E3	1.08 E5
Ra_e	1.19 E4	8.31 E4	3.45 E5	7.09 E3	9.57 E5
Gr_{qo}	1.47 E4	1.25 E5	7.35 E5	1.25 E4	1.27 E5
Gr_{qe}	1.50 E4	1.47 E5	1.56 E6	1.35 E4	2.88 E5
Gr_o	8.37 E2	8.22 E3	5.22 E4	9.90 E2	1.52 E4
Gr_e	1.70 E3	1.23 E4	6.37 E4	1.02 E3	1.74 E4
Pe_o	6391	6749	6914	1306	1072
Pe_e	6390	6713	6730	1300	1039

N.B.: index o designates entry conditions; index e indicates the last measuring station.

Three runs (PA, PB, PC) are characterized by Re-values of order 1000, while the two last runs (PD, and PE) have Re ~ 100. This second figure represents the lower limit of the apparatus in terms of flow-rate stability. On the other hand, $Ra_{qo} \sim 6x10^5$ has been (rather arbitrarily) assumed as a conservative stability limit for horizontal flows.
It can be observed that temperature-dependent properties, particularly viscosity, can have a certain effect on heat transfer results at relatively high heat flux densities ($Ra_q > 5x10^5$); in all the cases, the Peclet number is above one thousand, and then conduction effects along the fluid have no practical effect.

At high Re-numbers, the distribution of wall temperature at the upper generatix, follows the expected trend, in the sense that the wall temperature increases rapidly in the inlet section, then assuming a linear trend, parallel to the one of the bulk fluid temperature. For increasing Ra_q, the transition to linearity occurs earlier. The wall temperature of the last station (z' = 2.75 m) regularly falls below the linear trend. This was also to be expected, since those thermocouples sense the fin-effect of the unheated final part. Bottom temperatures are less regularly distributed; in fact, at stations 8 and 9, a temperature inversion is systematically observed, the bottom wall temperature overcoming that at the top. This effect has no physical explanation, and is interpreted as an unwanted artifact. In all the cases, either in the low- and high-Re ranges, the intermediate temperatures ($\theta = \pm 90°$) regularly fall in between the top and bottom values. This deserves mention, since, in low Ra_q-runs, top to bottom temperature differences can be as low as 0.05 °C. As from Fig.3a, in [12], the locally averaged Nusselt number, Nu_z, initially follows the descending trend of constant property predictions. After the onset of buoyancy, a minimum is observed, and, further downstream, the plots assume a rather clear asymptotic behaviour. Slight increases in Nu_z in this region are presumably due to property variations. When compared with available experimental and theoretical correlations for Nu_{fd} (case H1), the results in the asymptotic region (excluding station No.13) agree satisfactorily, as shown in Figs. 5.11, and 5.12.

Temperature distributions of the two low-Re runs (PD, and PE), indicate a much more pronounced effect of wall conduction. Temperature gradients are practically absent in the circumferential direction (maximum top-to-bottom temperature difference is 0.15 °C). In the axial direction, the wall temperature tends to assume a linear trend from the very beginning of the heated section. In the downstream region, however, the wall and bulk fluid temperature lines tend to converge, rather than to become parallel. As a consequence, no asymptotic behaviour is found in the distributions of Nu_z. This steadily increases with the downstream distance, as shown in [12] (Fig.3.b. *ibid.*). Fig.5.11 shows that Nu_z is higher than predicted, in the downstream region. As discussed in Ch.3, this behaviour was not totally unexpected, having been observed in other experiments. The present data suggest that conduction in the wall

might play a role, since the relative importance of axial wall conduction increases for a reduction in the Peclet number [14].

In conclusion, the preliminary experiments gave the following information relevant to the final set of tests:

a. the rig provides very stable results over the range explored (neither temperature nor flow-rate unsteadiness were observed);
b. some artifact might be present in wall temperature measurements at two axial positions. Also, the thermocouple at station No.2 did not work properly. This suggested a complete check of wall thermocouples;
c. the short unheated end affects data at the last measuring station. It is opportune to eliminate that unheated part, since its temperature is not controllable (no thermocouple had been mounted in that part);
d. heat transfer results are satisfactory in terms of accuracy; however low-Re runs have no asymptotic behaviour, and there is no sound explanation for this effect. For the sake of the comparison with numerical predictions, this range is not advisable, since sources of possible discrepancies are not controllable on a physical basis.

5.3.2 - Final results

Based on the experience gained with preliminary runs, a set of four final runs have been performed. For the purpose of numerical cross-validation, inlet values of the relevant non-dimensional parameters have been chosen: Ra_{qo} ~ $8x10^5$, and $5x10^6$, Re_o ~ 500 and 1000, and Pr_o~ 5 (Runs FA-FD). An additional test (Run FE) has been done to check the limits of the rig performance at low Ra_q.

With the aim of obtaining a better control of the end part of the test section, the unheated terminal part (43 mm) has been removed. However, this precaution had a very limited success. In actual facts, only one run (Run FA) has been executed under the desired conditions, since a water leakage through the silicon sealing short-circuited the heating wires, and forced to a reduction in the heated length again to 2715 mm.
Wall thermocouples have been carefully checked, and TC No.2 repaired, before the final runs. Unfortunately, TC No. 13.0 ceased to operate during the preparation of the final session, and TC No.13.2 ceased to work during Run FC. It was likely that thermocouples at station No.13 might have been compromised when inserting the end Perspex block, and/or by water leakages. Results at station No.13 have to be taken with caution.

Relevant data and results for the five final runs are displayed in Tables 5.4-5.8. Results are also presented in terms of local wall temperatures, and mean Nusselt numbers, in Figs. 5.4-5.8. In the reduction of the data, the fluid properties have been assumed constant, at the entry temperature value T'_o.

The following comments apply to the experimental data:

Run FA - The run is performed with a moderate heat flux density (Ra_{qo}~$8x10^5$), and Re_o~1000. The evolution of wall temperatures is in qualitative agreement with expectations based on constant property predictions: we see a very regular increasing trend in the entry region, and a very clear tendency to assume a linear trend in the downstream region. Circumferential temperature gradients are detectable at position No.8 (the top-to-bottom temperature difference is ~ 0.1°C). This corresponds to z^*= $9.2x10^{-3}$. This is linked to the presence of buoyancy driven secondary circulations, and clearly indicates their presence. We point out that the detection of a circumferential temperature gradient in the wall is a sufficient condition for the onset of buoyancy, but not a necessary one. As shown in Fig.5.4b, the departure from constant property predictions occurs well upstream of the detection of a gradient in wall temperature. The gradient increases with the downstream distance, even if the top-to-bottom temperature differences still remains of the order of 0.2 °C. In the entry region, the measured Nu_z agree reasonably well with the Shah and London [14] constant property solution. In the downstream region Nu_z increases slightly, possibly assuming an asymptotic value, as predicted by the current theories. However, this trend is interrupted by an intermediate peak at position No.11. The relatively low value of Nu_z at station No.13 is also contrary to expectations. It corresponds to an overshoot of $T'_{w,z}$ at the end section, which does not lend itself to physical explanation. For the reasons given above, it has not been possible to confirm the observed behaviour experimentally.

Run FB - This run is similar to Run FA as for Ra_{qo} (~ $9x10^5$), but here (Re_o ~ 500) the non-dimensional heat transfer length is about double. The general trend of the results is also similar to Run FA; the agreement with the constant property solution is less good near the entrance; a circumferential temperature gradient is already detectable at station No.7 (which however corresponds to z^*~ $1x10^{-2}$, again in very good agreement with Run FA); a temperature inversion is observed at position No.8; station No.13, in the final unheated length, indicates a wall temperature decay, consistent with expectation. Even in this case, Nu_z has a peak, now in correspondence with station No.12.

Run FC - Input data for this run correspond to Run FA as for Re_o (~1000), and Pr_o, but Ra_{qo} (~ $5x10^6$) is about sixfold. The general trend of T'_w differs from the one observed in Runs FA and FB, in that the mean wall temperature shows a more linear trend from the very beginning of the heat transfer section. The top-to-bottom temperature difference is now relatively large already at station No.7 (~0.5 °C); further downstream it increases up to ~1.2 °C. Consistent with T'_w, Nu_z is lower than predicted by the constant property solution, in the inlet

region; it has an increasing trend in the downstream part, with a peak at station No.11.

Run FD - This run corresponds almost perfectly to Run FC as for Ra_{qo} and Pr_o, but Re_o is reduced to ~ 500. Comments to these results are practically the same as for Run FC. An inversion in wall temperature is noted at position No.8, not present in Run FC.

Run FE - This final run is meant to check the reliability of the rig at low Ra_{qo}, and intermediate Re_o values. Comments on Run FE are twofold: on one side T'_w presents a very regular increasing trend, and undetectable circumferential temperature gradients. This should indicate that the effects of buoyancy are minor in this run. The prediction is confirmed by the plot of Nu_z in Fig.5.8b, where the trend of Nu_z conforms to constant property predictions. On the other hand, wall temperature at the first measuring point (station No.2), falls unreliably close to $T'_{m,z}$, giving an unreasonably high Nu_z-value, and the constant property solution overpredicts (of about 8%) the experimental data in Fig.5.8b, while the present knowledge of horizontal flows means that buoyancy effects should be evident on Nu_z at $Ra_{qo} = 1x10^5$. One possible source of error is the already mentioned sensitivity of the data to T'_o. Minor variations in the value of the inlet temperature (just some hundredths of Celsius degrees) can actually produce very large variations in Nu_z. Overall, Run FE indicates that $Ra_{qo} = 1x10^5$, and $Re_o = 1000$, are at the border of the reliability domain of the experimental rig in its present configuration. This further corroborates the need for improving the accuracy of inlet temperature measurement.

Data for Ra_{qo} ~ $8x10^5$, and, ~ $5x10^6$, both from the preliminary, and the final series, are compared in Figs.5.9, and 5.10, respectively. These figures demonstrate that measurements have a good repeatability: excluding end effects, the agreement between the results of the three runs in Fig.5.9 is extremely good; a band of ±10% from the average contains 91% of the data. Results in Fig.5.10 have a larger, but still acceptable, spread, indicating increasing difficulties in obtaining good results for increasing heat flux density. Discrepancies are particularly evident close to the entrance.
In Fig.5.11, Nusselt number results at stations No.10, 11, and 12 are compared with the numerical predictions by Newell and Bergles [15] and the theoretical correlation by Siegwarth *et al.* [16], eqn.(3.42), both for fully developed combined convection (case **H1**). A comparison with Morcos and Bergles [17] semi-empirical correlation, eqn. (3.56), is presented in Fig.5.12. Results of preliminary runs at stations No.11, and 12, have also been included. Experimental data reported in Figs.5.11, and 5.12 have been estimated at the local bulk fluid temperature, and at the local film temperature, respectively. We observe that the agreement with the Newell and Bergles theoretical solution is good, but not impressive, with a maximum 30% deviation. This increases to 54% for one of the

low-Re preliminary runs (Run PD). The comparison with the Morcos and Bergles correlation leads to similar conclusions.

Overall, it is concluded that experimental results are sufficiently accurate and reliable for providing the data base for numerical predictions, even if some inconsistencies are observed, especially at the extremities of the test section.

The experience gained in the experiment suggests new provisions to be taken to improve the results in terms of accuracy and reliability, and to broaden the experimental range. These are:

- the measurement of the inlet temperature should be extremely precise;
- mixing of the fluid at the exit must be very effective, so as to permit the energy balance of the fluid to be checked, and eventually used to define the nominal heat flux density;
- the number of wall thermocouples should be increased, particularly near the extremities of the test section;
- the insertion of the duct terminations in the end Perspex blocks provide inhomogeneous thermal conditions to those, very delicate, parts; new joints and connections should be designed.

A final comment is concerned with the influence of wall conduction: the inspection of wall temperature distributions in the various runs, suggests that conduction along the duct wall may have some influence on heat transfer results. If confirmed by numerical predictions, this observation would imply that the effect of a highly conductive wall should not be overlooked under combined convection circumstances, even for relatively long and thin-walled tubes.

References

1 - S. Piva - Scambio Termico Coniugato: Effetti di Pre- e Post Riscaldamento in Condotti Circolari (Conjugated Heat Transfer : Pre- and Post-Heating Effects in Round Ducts) - Tesi di Dottorato di Ricerca, Università di Bologna, Italy, October 1991.

2 - G. Pagliarini - Steady Laminar Heat Transfer in the Entry Region of Circular Tubes with Axial Diffusion of Heat and Momentum - Int. J. Heat and Mass Transfer, 32, 1989; 1037-1059.

3 - R. Y. Chen - Flow in the Entrance Region at Low Reynolds Numbers - J. Fluid Eng., 95, 1973; 153-158.

4 - S. Piva, and G. Pagliarini - Experimental Investigation on Exponential Heating of a Laminar Flow - '*Procs. 3rd World Conference on Experimental Heat Transfer, Fluid Mechanics and Thermodynamics*', Honolulu, Ha., USA, November 1993; to be presented.

5 - S. Piva, and C.M. Carlino - personal communications, November 1992.

6 - ASME - Measurement Uncertainty, Part 1 - ANSI/ASME PTC 19.1-1985.

7 - S.W. Churchill, and H.H.S. Chu - Correlating Equations for Laminar and Turbulent Free Convection from a Horizontal Cylinder - Int. J. Heat Mass Transfer, 18, 1975; 1049-1053.
8 - W.H. McAdams - *'Heat Transmission'* - McGraw-Hill, N.Y., 1954.
9 - V.T. Morgan - The Overall Convective Heat Transfer from Smooth Circular Cylinders - in *'Advances in Heat Transfer'*, T.F. Irvine, and J.P. Hartnett, eds., Vol. 16, Academic Press, N.Y., 1975; 199-264.
10 - F.P. Incropera, and D.P. DeWitt - *'Fundamentals of Heat and Mass Transfer'* - Wiley, N.Y., 1985.
11. R.K. Shah, and A.L. London - *'Laminar Flow Forced Convection in Ducts'*, Supplement 1 - Advances in Heat Transfer, T.J. Irvine, Jr., and J.P. Hartnett,eds., Academic Press, N.Y., 1978.
12 - S. Piva, G. Scarcella, G.S. Barozzi, and M.W. Collins - Comparison of Predictive and Experimental Data for Combined Convection in Horizontal Duct Flow, Procs. *'CMEM93 6th Intl. Conf. on Computational Methods and Experimental Measurements'*, Siena, May 1993, C.A. Brebbia, and G.M. Carlomagno, eds., Comp. Mech. Publ., Southampton Boston, U.K., Vol.1; 169-182.
13 - G. Scarcella - Analisi Sperimentale sullo Scambio Termico Convettivo in Regime di Convezione Mista entro un Condotto Cilindrico Orizzontale (Experimental Analysis on Convective Heat Transfer with Mixed Convection in a Cylindrical Horizontal Duct) - Tesi di Dottorato di Ricerca, Università di Bologna, Italy, October 1992.
14 - G.S. Barozzi, and G. Pagliarini - A Method to Solve Conjugate Heat Transfer Problems: the Case of Fully Developed Laminar Flow in a Pipe - ASME, J. of Heat Transfer, 107, 1985; 77-83.
15 - P.H. Newell, and A.E. Bergles - Analysis of Combined Free and Forced Convection for Fully Developed Laminar Flow in Horizontal Tubes - ASME, J. Heat Transfer, 92, 1970; 83-93.
16 - D.P. Siegwarth, R.D. Mikesell, T.C. Redal, and T.J. Hanratty - Effect of Secondary Flow on the Temperature Field and Primary Flow in a Heated Horizontal Tube - Int. J. Heat Mass Transfer, 12, 1969; 1535-1552.
17.- S.M. Morcos, and A.E. Bergles - Experimental Investigation of Combined Forced and Free Laminar Convection in Horizontal Tubes - ASME, J. Heat Transfer, 97, 1975; 212-219.

Table 5.4 - Run FA: data and experimental results.

RUN	FA	DATE	30.06.1993	NOTES	2757 mm heated length				
Reo =	1023	Pro =	5,60	Raqo =	7,75E+05	Grqo =	1,38E+05	Peo =	5728

WALL TEMPERATURES			
TC No	Tw (°C)		
2.0	29,02		
3.0	29,09		
4.0	29,23		
5.0	29,34		
6.0	29,48		
7.0	29,61		
7.1		29,58	
8.0	29,72		
8.1		29,66	
9.0	29,85		
9.1		29,71	
10.0	29,95		
10.1		29,77	
11.0	29,96		
11.1		29,84	
11.2			29,87
12.0	30,2		
12.1		30,03	
12.2			30,09
12.3			30,13
13.1		30,5	
13.2			30,45

WATER and AMBIENT TEMPERATURES		
To =	28,48	°C
Tout =	29,15	°C
Tamb =	27,31	°C

INPUT DATA	
I (A) =	2,7
V (V) =	16,33
Qm (kg/s) =	0,0106
ELECTRIC POWER	
Qel (W) =	44,09
POWER LOSSES	
Qlt,b(W) =	14,39
Qlt,is(W) =	0,88
NET POWER GAIN	
Qb (W) =	29,70
Qw (W) =	43,21
HEAT FLUX DENSITY	
qw(W/m2)	311,83
WATER PROPERTIES (To)	
To (°C) =	28,48
To (K) =	301,63
RO (kg/m3) =	995,61
Cp (J/kgK) =	4182,61
K (W/mK) =	0,61598
B (1/K) =	291,56E-6
Mi (kg/ms) =	824,27E-6
Ni (m/s2) =	827,91E-9
Pr =	5,5969

RESULTS			
ST No	z' (m)	Twz (°C)	Tmz (°C)
2.	0,042	29,02	28,49
3.	0,069	29,09	28,50
4.	0,118	29,23	28,52
5.	0,199	29,34	28,55
6.	0,299	29,48	28,59
7.	0,498	29,60	28,66
8.	0,843	29,69	28,78
9.	1,198	29,78	28,90
10.	1,501	29,86	29,01
11.	1,809	29,88	29,12
12.	2,300	30,11	29,29
13.	2,750	30,48	29,45

ST No	z*	Nuz
2.	0,000458	15,427
3.	0,000750	13,832
4.	0,001287	11,437
5.	0,002164	10,256
6.	0,003255	9,056
7.	0,005437	8,629
8.	0,009200	8,884
9.	0,013073	9,243
10.	0,016380	9,539
11.	0,019740	10,688
12.	0,025098	9,887
13.	0,030009	7,921

a.

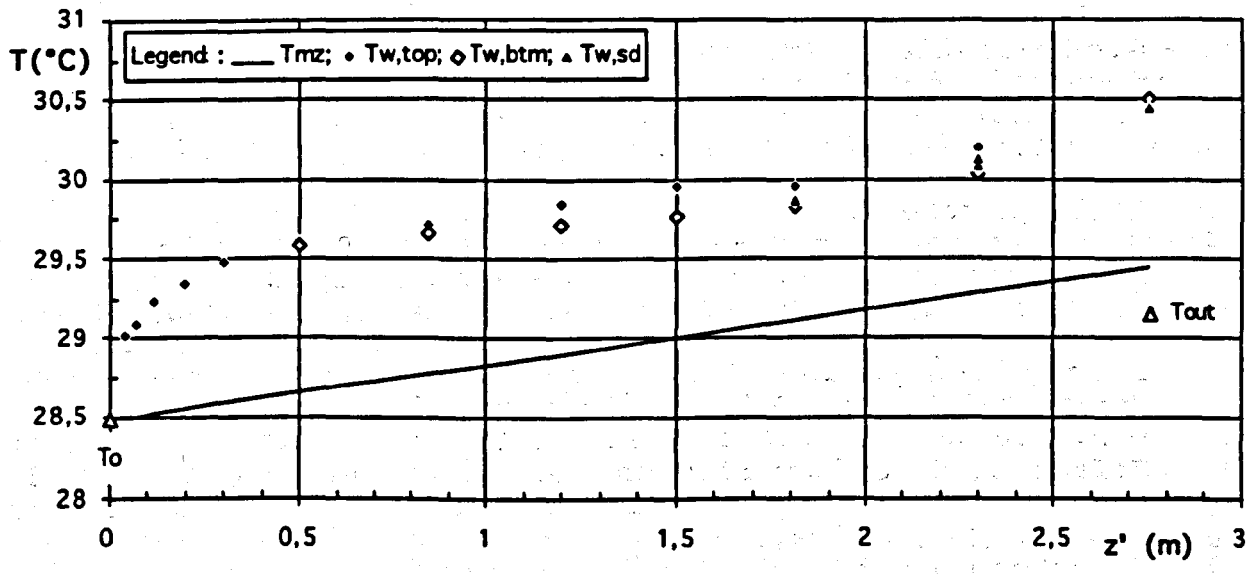

b.

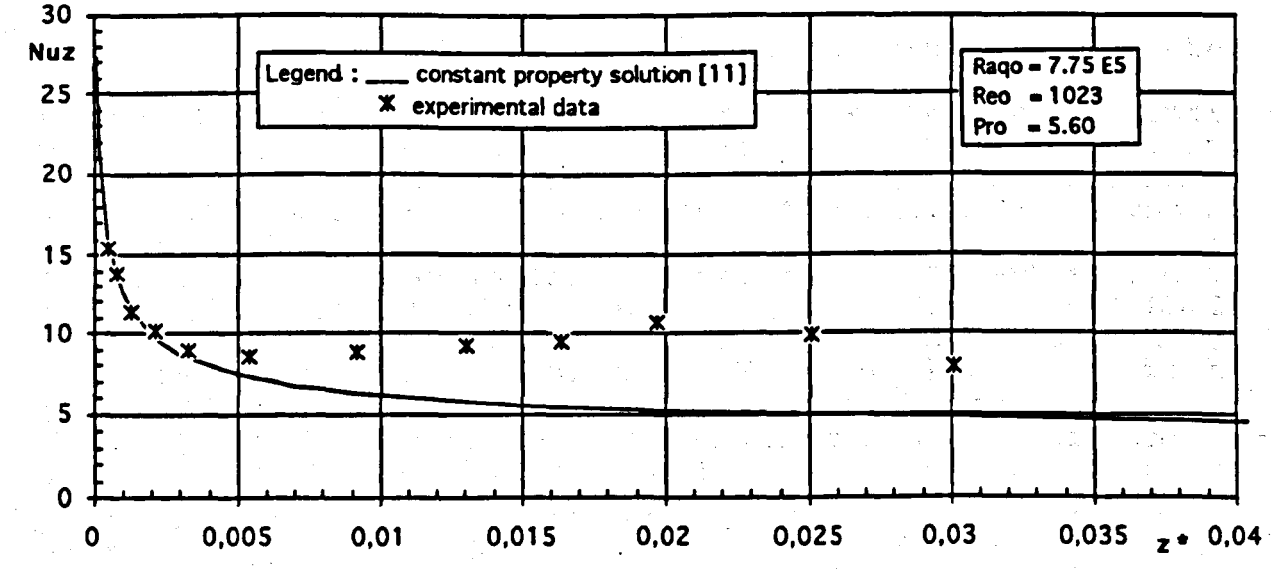

Fig.5.4 - Run FA: a. local wall and fluid temperatures; and, b. mean Nusselt number vs. non-dimensional distance.

Table 5.5 - Run FB: data and experimental results.

RUN	FB	DATE	02.07.1993	NOTES	2715 mm heated length				
Reo =	518	Pro =	5.62	Raqo =	9.35E+05	Grqo =	1.66E+05	Peo =	2911
WALL TEMPERATURES				INPUT DATA		RESULTS			
TC No	Tw (°C)			I (A) =	3.26	ST No	z' (m)	Twz (°C)	Tmz (°C)
2.0	29.01			V (V) =	16.430	2.	0.042	29.01	28.36
3.0	29.18			Qm (kg/s)=	0.005385	3.	0.069	29.18	28.38
4.0	29.35			ELECTRIC POWER		4.	0.118	29.35	28.42
5.0	29.46			Qel (W) =	53.48	5.	0.199	29.46	28.49
6.0	29.56			POWER LOSSES		6.	0.299	29.56	28.57
7.0	29.73			Qlt,b(W) =	14.74	7.	0.498	29.69	28.74
7.1		29.64		Qlt,is(W)=	0.94	8.	0.843	30.00	29.03
8.0	29.94			NET POWER GAIN		9.	1.198	30.17	29.33
8.1		30.05		Qb (W) =	38.74	10.	1.501	30.40	29.59
9.0	30.24			Qw (W) =	52.54	11.	1.809	30.56	29.85
9.1		30.1		HEAT FLUX DENSITY		12.	2.300	31.07	30.27
10.0	30.5			qw(W/m2)	379.13	13.	2.750	30.73	
10.1		30.29		WATER PROPERTIES (To)		ST No	z*	Nuz	
11.0	30.67			To (C) =	28.32	2.	0.000902	15.053	
11.1		30.52		To (K) =	301.47	3.	0.001477	12.287	
11.2			30.54	RO (kg/m3) =	995.65	4.	0.002532	10.591	
12.0	31.19			Cp (J/kgK) =	4182.68	5.	0.004259	10.133	
12.1		30.96		K (W/mK) =	0.61576	6.	0.006405	9.975	
12.2			31.05	B (1/K)=	290.15E-6	7.	0.010698	10.442	
12.3			31.08	Mi (kg/ms) =	827.02E-6	8.	0.018103	10.245	
13.1		30.7		Ni (m/s2) =	830.63E-9	9.	0.025723	11.779	
13.2			30.75	Pr =	5.6178	10.	0.032230	12.239	
WATER and AMBIENT TEMPERATURES						11.	0.038842	13.838	
To =	28.32	C				12.	0.049384	12.254	
Tout =	30.04	°C				13.	0.059047		
Tamb =	27.58	°C							

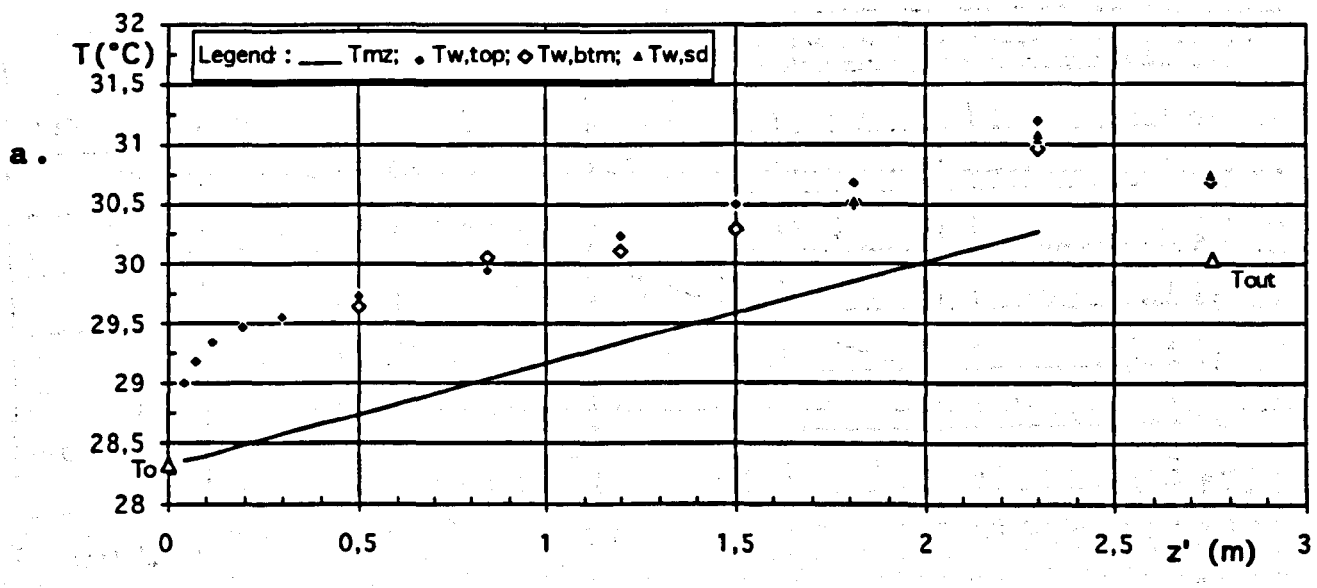

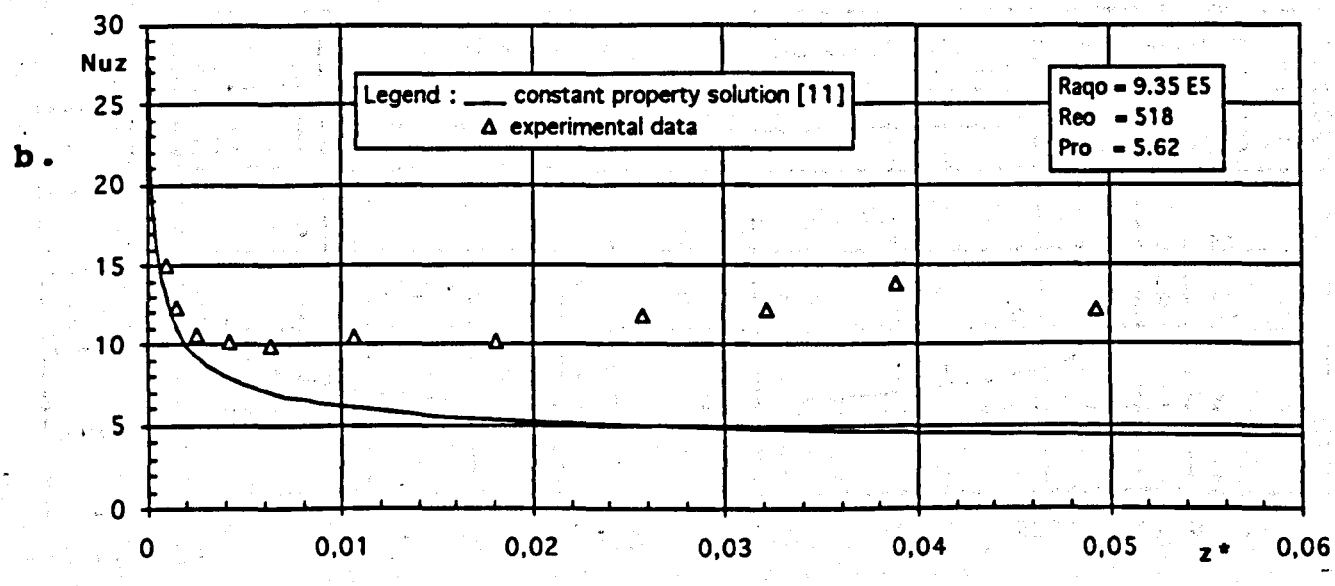

Fig.5.5 - Run FB: a. local wall and fluid temperatures; and, b. mean Nusselt number vs. non-dimensional distance.

Table 5.6 - Run FC: data and experimental results.

RUN FC		DATE 05.07.1993		NOTES 2715 mm heated length /TC No 13.2 not working			
Reo = 958		Pro = 5.57		Raqo = 4,98E+06	Grqo = 8,94E+05		Peo = 5335
WALL TEMPERATURES				INPUT DATA	RESULTS		
TC No	Tw (°C)			I (A) = 7,44	ST No	z' (m)	Twz (°C)	Tmz (°C)
2.0	33,25			V (V) = 37,319	2.	0,042	33,25	28,80
3.0	33,40			Qm (kg/s)= 0,009879	3.	0,069	33,40	28,87
4.0	33,96			ELECTRIC POWER	4.	0,118	33,96	28,98
5.0	34,10			Qel (W) = 277,65	5.	0,199	34,10	29,18
6.0	34,44			POWER LOSSES	6.	0,299	34,44	29,42
7.0	34,97			Qlt,b(W) = 24,24	7.	0,498	34,70	29,90
7.1		34,42		Qlt,is(W)= 2,59	8.	0,843	35,78	30,74
8.0	35,45			NET POWER GAIN	9.	1,198	35,92	31,59
8.1		36,12		Qb (W) = 253,41	10.	1,501	36,51	32,32
9.0	36,29			Qw (W) = 275,07	11.	1,809	36,85	33,07
9.1		35,55		HEAT FLUX DENSITY	12.	2,300	38,44	34,25
10.0	37,07			qw(W/m2) 1984,85	13.	2,750	36,51	
10.1		35,95		WATER PROPERTIES (To)	ST No	z*	Nuz	
11.0	37,35			To (°C) = 28,7	2.	0,000492	11,591	
11.1		36,61		To (K) = 301,85	3.	0,000806	11,360	
11.2			36,82	RO (kg/m3) = 995,54	4.	0,001382	10,351	
12.0	39,09			Cp (J/kgK) = 4182,50	5.	0,002324	10,478	
12.1		37,88		K (W/mK) = 0,61630	6.	0,003495	10,270	
12.2			38,33	B (1/K)= 293,50E-6	7.	0,005837	10,750	
12.3			38,48	Mi (kg/ms) = 820,52E-6	8.	0,009877	10,212	
13.1		36,51		Ni (m/s2) = 824,19E-9	9.	0,014035	11,900	
13.2			36,51	Pr = 5,5685	10.	0,017585	12,313	
WATER and AMBIENT TEMPERATURES					11.	0,021192	13,643	
To =	28,70	C			12.	0,026944	12,299	
Tout =	34,83	C			13.	0,032216		
Tamb =	28,76	C						

a.

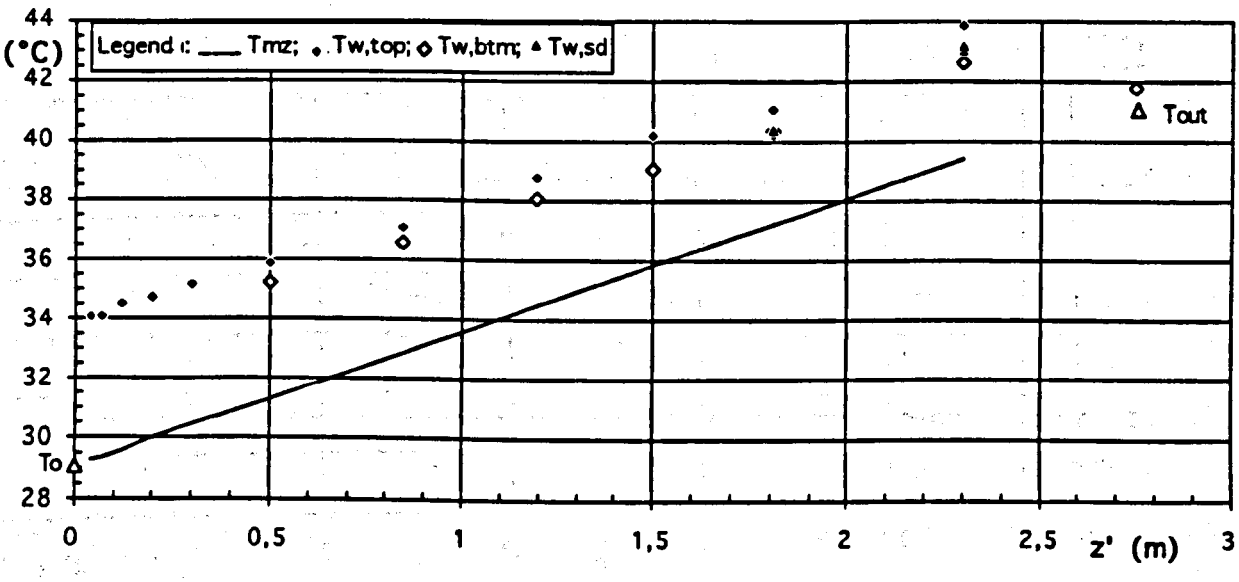

b.

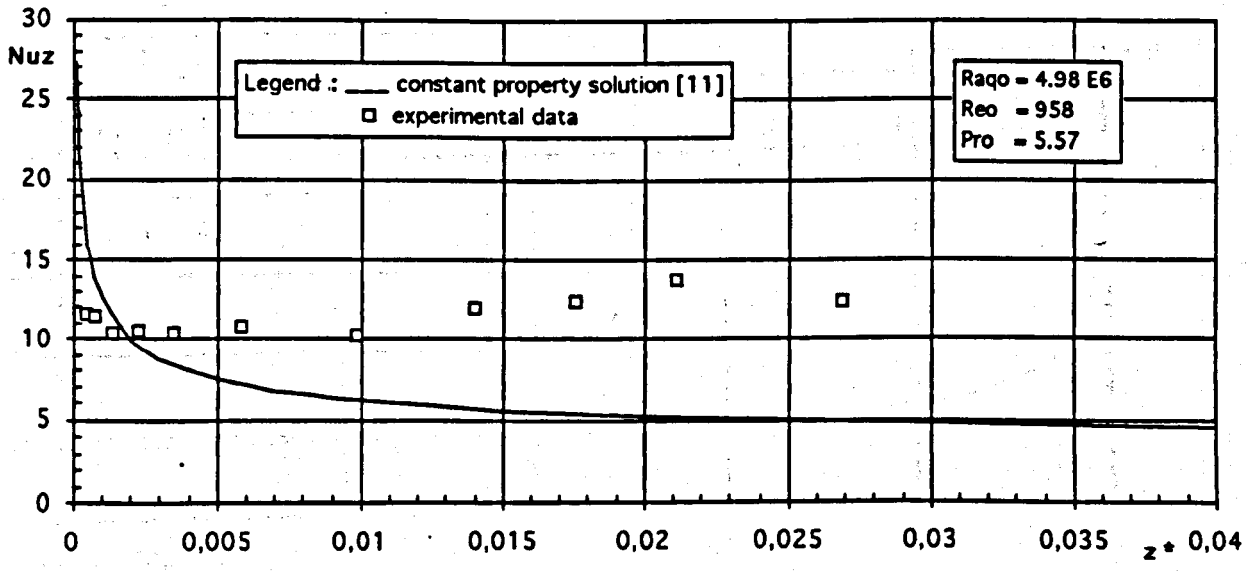

Fig.5.6 - Run FC: a. local wall and fluid temperatures; and, b. mean Nusselt number vs. non-dimensional distance.

Table 5.7 - Run FD: data and experimental results.

RUN FD		DATE 05.07.1993		NOTES 2715 mm heated length / TC No 13.2 not working			
Reo = 518		Pro = 5,52		Raqo = 5,05E+06	Grqo = 9,16E+05	Peo = 2856	
WALL TEMPERATURES				INPUT DATA		RESULTS	
TC No	Tw (°C)			I (A) = 7,45	ST No	z' (m)	Twz (°C)	Tmz (°C)
2.0	34,08			V (V) = 37,28	2.	0,042	34,08	29,28
3.0	34,06			Qm (kg/s)= 0,005293	3.	0,069	34,06	29,40
4.0	34,54			ELECTRIC POWER	4.	0,118	34,54	29,62
5.0	34,73			Qel (W) = 277,70	5.	0,199	34,73	29,99
6.0	35,16			POWER LOSSES	6.	0,299	35,16	30,43
7.0	35,87			Qlt,b(W) = 12,43	7.	0,498	35,54	31,33
7.1		35,20		Qlt,is(W)= 3,52	8.	0,843	36,83	32,88
8.0	37,06			NET POWER GAIN		1,198	38,41	34,48
8.1		36,60		Qb (W) = 265,27	10.	1,501	39,65	35,84
9.0	38,78			Qw (W) = 274,18	11.	1,809	40,57	37,22
9.1		38,04		HEAT FLUX DENSITY	12.	2,300	43,16	39,43
10.0	40,21			qw(W/m2) 1978,45	13.	2,750	41,78	
10.1		39,09		WATER PROPERTIES (To)	ST No	z*	Nuz	
11.0	41,09			To (°C) = 29,09	2.	0,000919	10,708	
11.1		40,37		To (K) = 302,24	3.	0,001505	11,010	
11.2			40,46	RO (kg/m3) = 995,43	4.	0,002581	10,449	
12.0	43,83			Cp (J/kgK) = 4182,32	5.	0,004341	10,824	
12.1		42,60		K (W/mK) = 0,61685	6.	0,006529	10,859	
12.2			43,03	B (1/K)= 296,96E-6	7.	0,010905	12,209	
12.3			43,18	Mi (kg/ms) = 813,88E-6	8.	0,018452	12,997	
13.1		41,78		Ni (m/s2) = 817,62E-9	9.	0,026219	13,053	
13.2			41,78	Pr = 5,5182	10.	0,032852	13,465	
WATER and AMBIENT TEMPERATURES					11.	0,039591	15,303	
To =	29,09	C			12.	0,050336	13,740	
Tout =	41,08	°C			13.	0,060186		
Tamb =	29,13	°C						

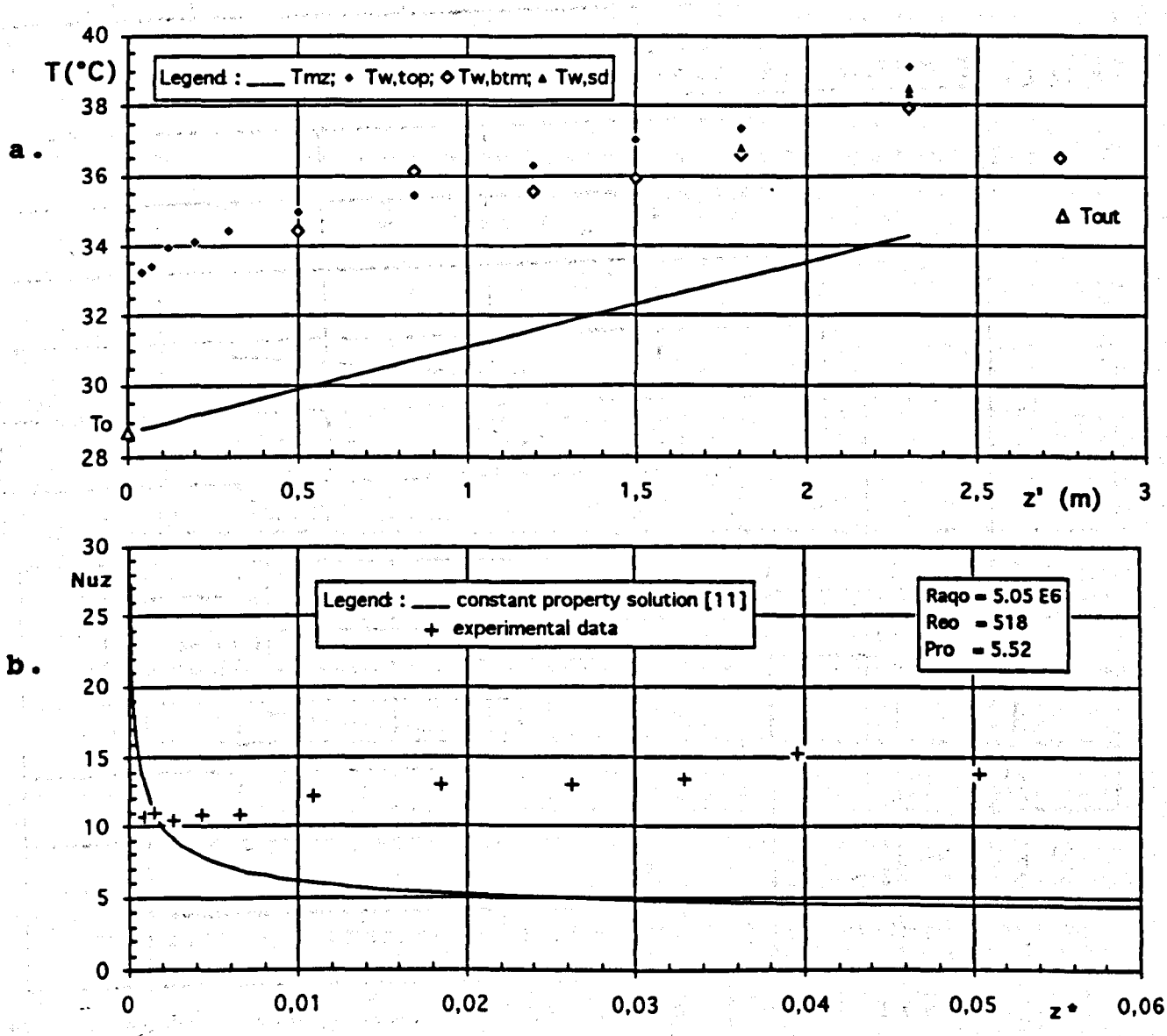

Fig.5.7 - Run FD: a. local wall and fluid temperatures; and, b. mean Nusselt number vs. non-dimensional distance.

Table 5.8 - Run FE: data and experimental results.

RUN	FE	DATE	06.07.1993	NOTES	2715 mm heated length / TC No 13.2 not working			
Reo =	949	Pro =	5.73	Raqo =	8,57E+04	Grqo =	1,50E+04	Peo = 5438

WALL TEMPERATURES			
TC No	Tw (°C)		
2.0	27,49		
3.0	27,56		
4.0	27,57		
5.0	27,59		
6.0	27,61		
7.0	27,66		
7.1		27,64	
8.0	27,69		
8.1		27,71	
9.0	27,75		
9.1		27,74	
10.0	27,77		
10.1		27,76	
11.0	27,79		
11.1		27,76	
11.2			27,76
12.0	27,83		
12.1		27,80	
12.2			27,81
12.3			27,80
13.1		27,74	
13.2			27,74

WATER and AMBIENT TEMPERATURES		
To =	27,48	°C
Tout =	27,50	°C
Tamb =	24,48	°C

INPUT DATA	
I (A) =	1,12
V (V) =	5,46
Qm (kg/s) =	0,01004
ELECTRIC POWER	
Qel (W) =	6,11
POWER LOSSES	
Qlt,b(W) =	5,36
Qlt,is(W) =	1,10
NET POWER GAIN	
Qb (W) =	0,76
Qw (W) =	5,01
HEAT FLUX DENSITY	
qw(W/m2)	36,14
WATER PROPERTIES (To)	
To (°C) =	27,48
To (K) =	300,63
RO (kg/m3) =	995,88
Cp (J/kgK) =	4183,10
K (W/mK) =	0,61455
B (1/K) =	282,64E-6
Mi (kg/ms) =	841,73E-6
Ni (m/s2) =	845,21E-9
Pr =	5,7295

RESULTS			
ST No	z' (m)	Twz (°C)	Tmz (°C)
2.	0,042	27,49	27,482
3.	0,069	27,56	27,483
4.	0,118	27,57	27,485
5.	0,199	27,59	27,489
6.	0,299	27,61	27,493
7.	0,498	27,65	27,502
8.	0,843	27,70	27,516
9.	1,198	27,74	27,532
10.	1,501	27,76	27,545
11.	1,809	27,77	27,558
12.	2,300	27,81	27,579
13.	2,750	27,74	

ST No	z*	Nuz
2.	0,000483	77,239
3.	0,000790	13,065
4.	0,001355	11,632
5.	0,002280	9,012
6.	0,003428	8,248
7.	0,005726	6,492
8.	0,009690	5,100
9.	0,013768	4,499
10.	0,017251	4,296
11.	0,020790	4,418
12.	0,026433	4,109
13.	0,031605	

a.

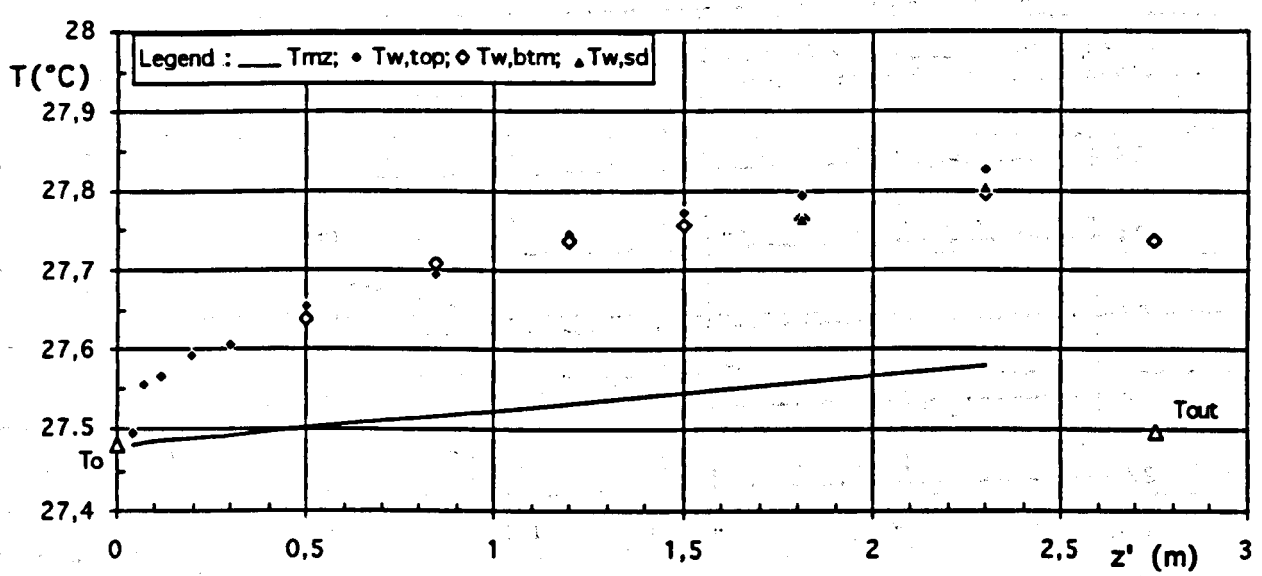

b.

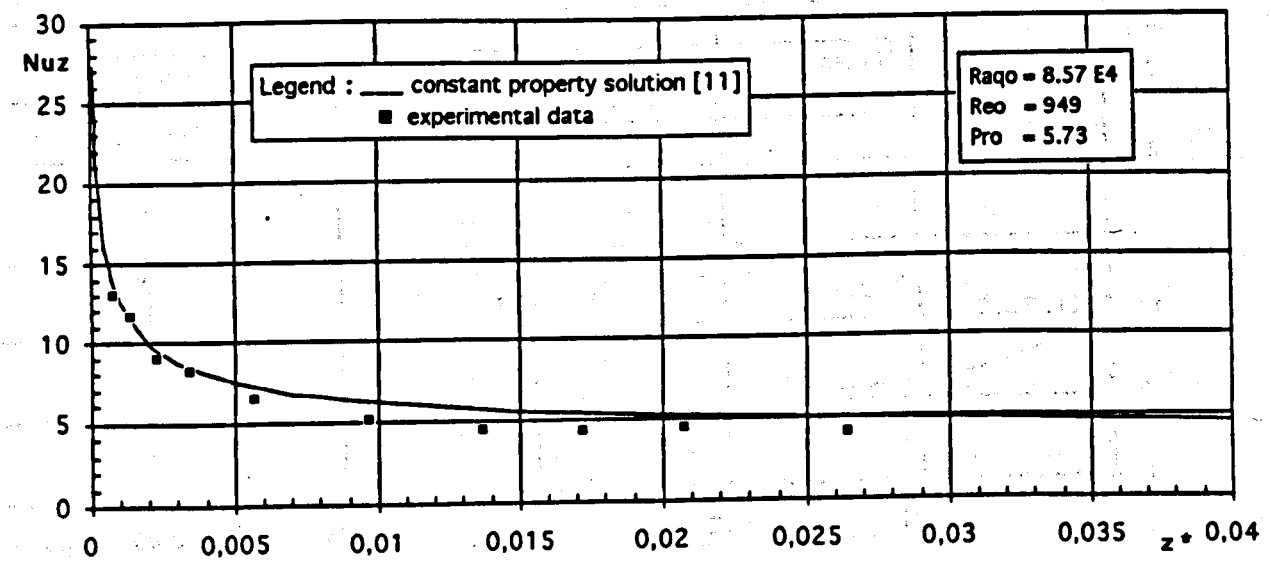

Fig.5.8 - Run FE: a. local wall and fluid temperatures; and, b. mean Nusselt number vs. non-dimensional distance.

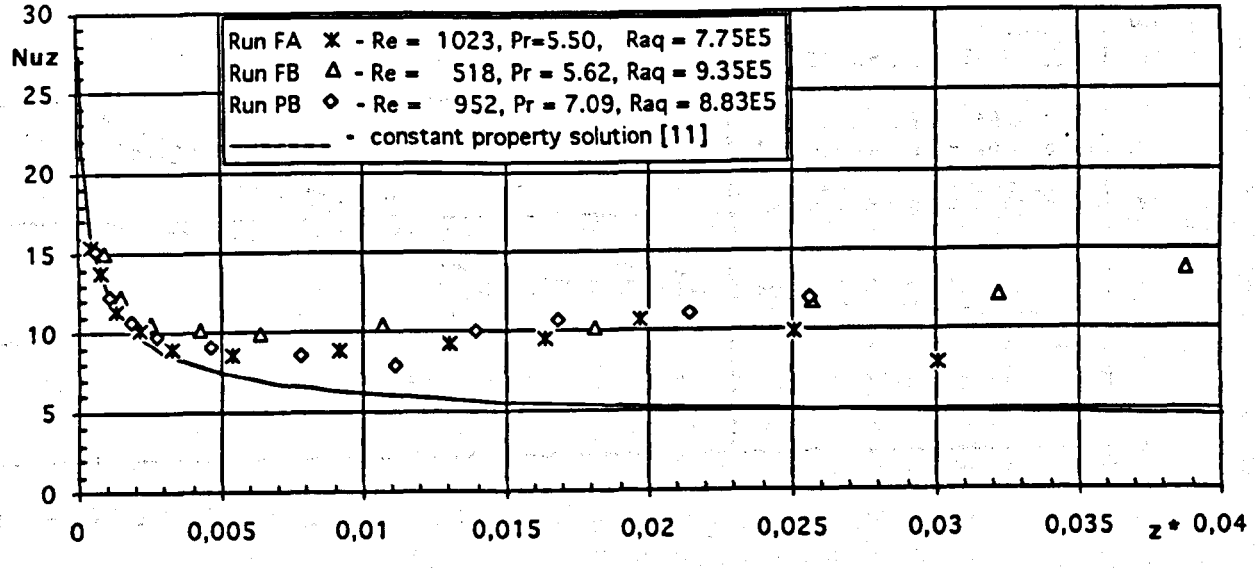

Fig.5.9 - Comparison of experimental Nu_z-values for $Ra_{qo} \sim 8x10^5$ (final and preliminary results).

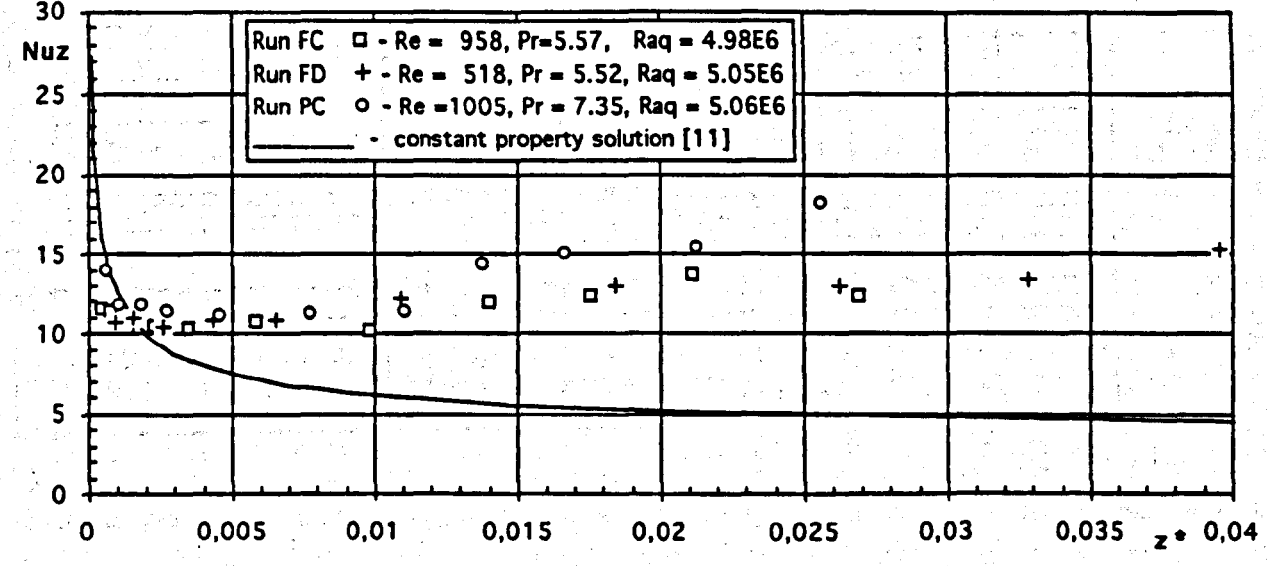

Fig.5.10 - Comparison of experimental Nu_z-values for $Ra_{qo} \sim 5x10^6$ (final and preliminary results).

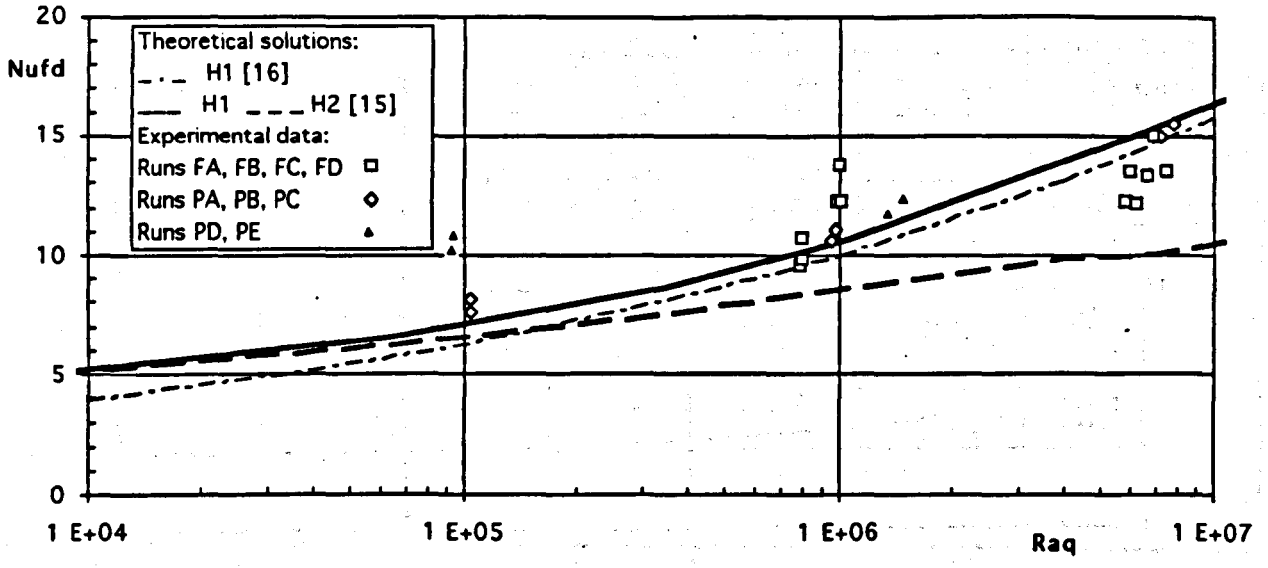

Fig.5.11 - Comparison of final (No.10, 11, and 12) and preliminary (No. 11 and 12) results with theoretical correlations, for fully developed combined convection; (properties at local bulk fluid temperature).

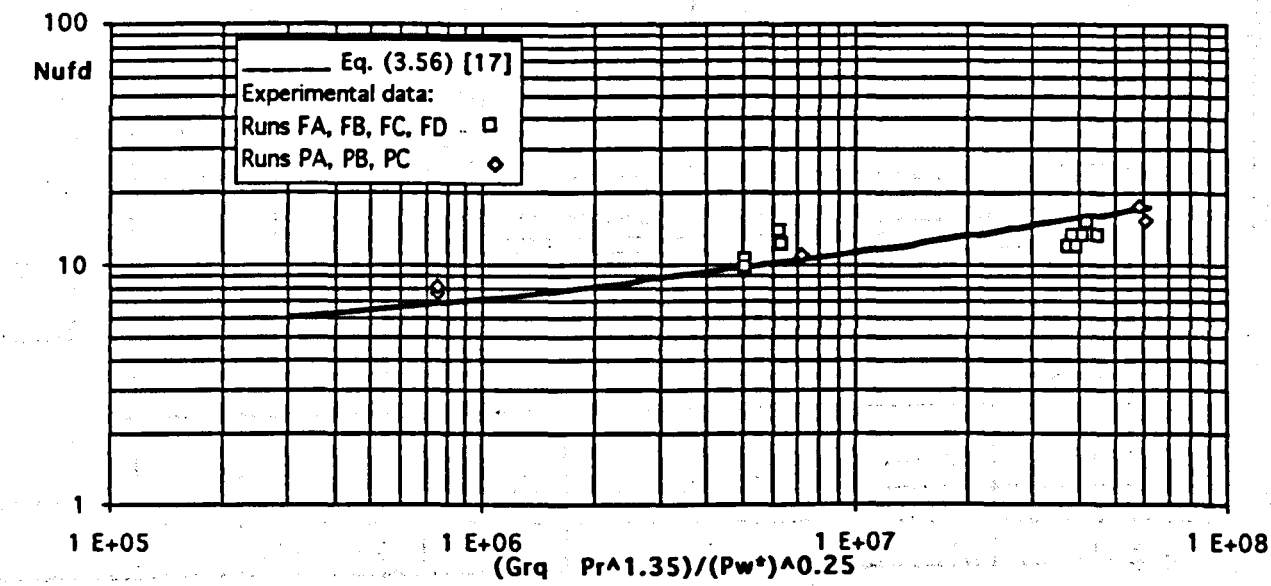

Fig.5.12 - Comparison of final (No.10, 11, and 12) and preliminary (No. 11 and 12) results with Morcos and Bergles [17] correlation, for fully developed combined convection; (properties at local film temperature).

CHAPTER 6: COMPUTATIONAL WORK

6.1 - FLOW3D Computer Program

Numerical methods which have been used in the context of combined convection in duct flows, were reviewed by Barozzi and Collins [1] (see Ch.3 and Appendix I). The main conclusion of that survey was that accurate predictions of combined convection duct flows could only be achieved by treating the inherently three-dimensional, and elliptic nature of the problem. The adoption of the computer program FLOW3D, from Harwell Laboratory, UK., then followed as a direct and natural consequence. This choice is also particularly well suited to the present circumstances, where computing is seen more as an integral part of the experiment, rather than an autonomous activity. FLOW3D seems in fact to have the potential for being fully integrated into heat transfer experiments.

FLOW3D is a distinguished member of the family of Computational Fluid Dynamics (CFD) software. This family is continuously widening and rapidly evolving; it nowadays comprises very sophisticated computer codes, which not only embody the numerical algorithms (for finite elements, control volume, or boundary element discretizations), but also advanced turbulence models, grid generators, and graphics facilities. Various options also account for many different effects possibly present in thermal-fluid problems, such as buoyancy, compressibility, temperature-dependent properties, conductive and radiative boundaries.
In particular, FLOW3D is based on control-volume discretizations and makes use of a general non-orthogonal body-fitted gridding system; it has a polyalgorithmic structure whereby options are available for the user to select from different discretization schemes and solvers. The program has been under continuous evolution since 1985 (Release 1), and has now reached its third revision (Release 3.2 is the most recent updating), through the progressive integration of new structures, facilities and algorithms [2-7]. It has been tested in many heat transfer and fluid flow applications, both under laminar and turbulent flow conditions. Meaningful examples, among many, are: turbulent flow predictions for recirculating flows,

[8,9], the study of fluid flow with heat transfer in coiled tubes [10], the analysis of swirl flow in nuclear reactors [11],and of cross-corrugated rotary regenerators [12].

In this work, Releases 3.1, and 3.2 have been used, the former at the Istituto di Fisica Tecnica, Università di Bologna, I, and the latter at CINECA (Centro Interuniversitario di Calcolo dell' Italia Nord Orientale), Bologna, I.

A brief discussion of the main features of FLOW3D appropriately precedes the description of the numerical work.

6.1.1 - Structure of the software

In its present format, the common name FLOW3DE Computer Program designates a cluster of modules, with specific tasks. The basic modules are:

- the Grid Generator,
- the Front-End Module,
- the Solution Module,
- the Graphics Module.

The Grid Generator may optionally be used. In the present case, grids have all been generated by the interactive grid generator, SOPHIA, which is also an optional module of FLOW3D. In this module, rectangular (x,y,z) geometries are constructed. The physical problem is defined in a single data file (Command Language data file). The Front-end Module (Command Language Front-end) transforms the user's input specifications into a form suitable for efficient solution. The Solution Module solves the discretized form of the governing p.d.e.'s, and provides an output file which can be post-processed by the Graphics Module. Interfaces to other post-proc software are available. An Interactive Front-end is also provided with Release 3.2.
For technical reasons, only the interactive grid generator and the solution module could be used in this study.

The route to the solution of a general CFD problem comprises the following logical steps, to which various FLOW3D options correspond:

Geometry definition and grid generation - The program operates on structured rectangular grids, in the transformed computational space. Then, having defined the geometry of the problem, a structured grid has to be built-up in the physical (natural) space, by identifying the vertices of the cells. In the natural domain, grids are restricted to be topologically rectangular (they can be bent or stretched to a uniform grid without tearing or folding) to allow conversion into cubical volumes in the transformed space. In this way, a uniform mesh in the transformed space is equivalent to one which follows the boundaries in the physical space. The coordinates in physical space are referred as body- or boundary-fitted coordinates.

As for the coordinate system in the natural domain, the basic FLOW3D option is Cartesian (x,y,z); the cylindrical option is available.

An original feature of Rel.3 is the possible resort to multi-block grids. These are constructed by patching together a number of simple blocks of cells (obviously parallelepipeds in the transformed space). The natural grid does not need to be topologically rectangular, even if each single block is still restricted to be so. A multi-block grid permits a reduction in the memory occupation in cases where large inactive solid portions are present, to produce local grid refinement (FLOW3D has no grid-embedding option), and to fit complex geometries. In this latter case the grid is built up by connecting a number of simple grids. The three most commonly used single-block topologies are the H-grid (rectangular in the natural space), the O-grid (annular), and the C-grid (a horseshoe shaped grid, whose prongs can be bent at will, and eventually 'glued' together). The former two have been utilized in this work.
Use of the multi-block option is particularly recommended when employing vector computer facilities [13].

Once the fluid domain has been treated, the boundary characteristics are to be defined. Each block may contain solid or porous blockages, inlet, outlets, at arbitrary internal locations. To this end, rectangular sub-arrays of control cells or faces are created in the computational space, to form 2D (surface), or 3D (volume) 'patches', where boundary conditions, or material characteristics are defined. 2D patches are used to define thin surfaces, entry and exit sections, symmetry planes, and inter-block connections; 3D patches, usually define conductive solid, or porous regions. These also are connected to the fluid regions by 2D patches (in the case of a conducting solid, a 'conducting boundary' patch).
In the present context, 'conducting solid' patches have been used to define the duct wall.

Mathematical modelling - A set of partial differential equations, constitutive equations, property values, and boundary conditions are chosen, so as to describe in the best way the underlying physical problem. It should be borne in mind that FLOW3D works with dimensional quantities (SI units).

The basic equations of the code are the general conservative forms of Navier-Stokes equations for Newtonian fluids, and the energy equation. Following Patankar [14], these are all expressed as a scalar advection-diffusion equation of the conservative form:

$$\frac{\partial(\rho'\varphi')}{\partial t'} + \nabla \bullet (\rho'\mathbf{u}'\varphi' - \sigma\nabla\varphi') = S \qquad (6.1)$$

Here, φ' is a general variable, σ the appropriate diffusion coefficient, and S the source term representing creation or destruction of φ'. The energy equation presents some peculiarities, in that it is solved for enthalpy, rather than for temperature. Eqn. (6.1) is written in time-dependent form, since transient as well as steady problems can be approached by the code.

Further to the basic equations, a number of options are available to model buoyancy driven flows, compressible fluids, turbulent flows, mass transfer, chemical kinetics, combustion, radiation, multi phase flows, and particle transport.

For buoyancy driven flows, the standard option is to formulate the momentum equations assuming the Boussinesq approximation (see Ch.2). In this case all properties are held constant, except density, for which a meaningful reference temperature is supplied by the user (in our case this was the entry temperature). Full property variation is however possible, by means of user-defined temperature-dependent properties.

Conductive solid regions are also defined by the user in terms of thermophysical properties. A specific and original feature of FLOW3D (Rel.3.1 and 3.2), is that it can treat thermally non-isotropic walls, since it accepts the conductivity of a solid in the form of a tensor.

Many options are also available in the code for setting boundary conditions. Here we only consider those relevant to the present work.

For open boundaries, a Dirichlet boundary condition may apply, where local values of the velocity component normal to the inlet section are specified point by point (at the centroids of the elemental surfaces). This condition is typical of inlet sections, but it can also be used at outlet sections, provided that the distribution of the variable under consideration is known. Scalar variable distributions may also be specified; under incompressible flow circumstances, however, pressure is extrapolated from the internal field. Note that boundary conditions for non-isothermal flows are specified in terms of temperature, not enthalpy.

Von Neumann boundary conditions are treated by FLOW3D under the general name of 'Mass Flow Boundaries'. These are typical of outlet sections, where a fully developed situation is expected to occur. The same option can also be used to produce a fully developed velocity profile at inlet sections. In that case, the mass flow boundary option is a simpler alternative to a the Dirichlet boundary condition, since only the global mass flow-rate needs to be specified. However, convergence tends to be better if the inflow velocity distribution is assigned [13].

The mass flow boundary option has been used in this simulation experiment both at the inlet and outlet sections of the duct.
It should be pointed out here that scalar variables, except pressure, can be set at any desired value at an inlet mass flow boundary. For an outlet mass flow boundary, however, normal derivatives of scalars are subject to a zero gradient condition, by default. This does not fit the commonly stated outlet boundary condition on temperature in uniformly heated ducts, which is in fact a constant axial derivative. As will be discussed, this fully

developed condition can not be achieved in a conjugate circumstance, and it is doubtful it has ever been approximated experimentally.

At solid surfaces, the non-slip boundary condition is set by default on velocities. Tangential velocities or/and shear stresses may however be defined.

Three basic boundary conditions may apply at non-conducting solid/fluid, and conducting/non-conducting solid interfaces, or at the boundary edge of a conducting solid. They are:
constant temperature, constant heat flux, or a linear combination of the two (mixed boundary condition).

The general boundary condition for temperature is:

$$A_T T' + B_T q'_w = C_T \qquad (6.2)$$

where, A_T, B_T, and C_T, are user-defined constants.

Temperature conditions need not be specified at the interface between a conducting solid and a fluid. FLOW3D automatically adjusts for continuity of temperature and heat flux through such interfaces. Planes of periodicity and symmetry also do not need explicit treatment.

Discretization schemes and solution algorithms - A characteristic of FLOW3D is that it uses co-located grids, i.e. all variables are stored and computed at the cell centroids, as opposite to standard control volume formulations, where staggering is used for velocity components. To do this, yet avoiding the chequerboard oscillations of pressure and velocity (see e.g. [14,15]), the code uses the Rhie and Chow [16] interpolation procedure. This is generalized to three dimensional non-orthogonal grids, and, in Rel.3, improved, to guarantee second order accuracy in pressure gradient approximations (on a non-uniform rectangular grid), and reduce nodal continuity errors which had been observed in previous versions (specifically in the context of with variations in the body force).

FLOW3D embodies a variety of differencing options for the treatment of advective terms in the general convection-diffusion equation, eqn.(6.1),.and solution schemes for pressure-velocity decoupling.
The advection terms may be treated using hybrid differencing [17], higher-order upwind (HUW) [18], or quadratic upwind (QUICK) [19], other than standard central and first order upwind differencing. Although the accuracy of HUW and QUICK schemes is higher, they are less robust and slower to converge than the hybrid differencing scheme. The hybrid scheme has, therefore, been preferred in this work. In all schemes, diffusive terms are treated by central differences.

FLOW3D gives options for three basic schemes, to accommodate the velocity-pressure coupling, viz.: SIMPLE by Patankar and Spalding [29], SIMPLEC, by Van Doormal and Raithby [20], and (up to Rel.2.6) PISO, by Issa [21]. All are segregated algorithms, where a pressure

correction equation is derived from the continuity equation. Here SIMPLEC has been preferred, since it has proven to be less sensitive to under relaxation, and demands less under-relaxation, compared with SIMPLE. The more complex procedure of PISO seems not to give any specific advantage in cases where strong body forces are present (see e.g. [10]).

As for the solution of discretized equations, various options are offered by the code. Here, the standard combination of pre-conditioned conjugate gradient (ICCG) [22], and Stone's [23] methods has been adopted, for solving the Poisson-like pressure correction equation, and convection-diffusion equations, respectively.

6.2 - Problem Statement and Numerical Options

As already noted, the ultimate objective of the computational work is the direct numerical simulation of the experiment, including wall conduction effects. As a consequence, the numerical model is intended to be none other than a detailed mathematical description of the test section described in Ch.6. In fact, the actual achievement could better be described as 'a reasonable approximation of reality', as will be shown in the following.

6.2.1 - Problem statement

The problem has been addressed according to the following prescriptions:

a. - A duct is considered of the same geometry as the heat transfer section used in the experiments (L_{ht} = 2757 mm, D = 16 mm, with a 1 mm thick wall);
b. - The gravity force acts along the vertical direction (axis y'), orthogonal to the main direction of the flow (axis z'). This dictates the horizontal orientation of the duct;
c. - Flow is steady, and laminar;
d. - Distilled water is the working fluid, with properties defined according to Table 5.2. Fluid properties are estimated at the inlet section temperature, T'_o, and held constant, except for density;
e. - The Boussinesq approximation is enforced in the x- y-momentum equations. The reference temperature for density is T'_o; the reference temperature for enthalpy is T'_{ref} = 280 K, i.e. the default value in FLOW3D;
f. - The duct is isotropically conductive with k_w = 334.2 W/mK.

Boundary conditions are as follows:

A. - Inlet section: fully developed (Hagen-Poiseuille) velocity profile; uniform temperature $(T' = T'_o)$;
B. - Outlet section: fully developed velocity and temperature profiles;

C. - Inner duct wall: zero velocity (no-slip condition); continuity of temperature and normal component of the heat flux density vector;
D. - Outer duct wall: uniform heat flux density;
E. - End surfaces of the duct walls: zero heat flux density.

As anticipated in § 6.1, condition A. is achieved using the FLOW3D 'mass flow boundary' option. The same holds true at the outlet section. In this case, however, the imposition of a zero axial gradient on temperature does not fit the commonly stated outlet boundary condition on temperature in uniformly heated ducts. In the absence of any wall effect, this is in fact a constant derivative. As noted in the literature survey, Ch.3, there is no previous knowledge about the conjugate effect of wall conduction and combined convection. However, results relevant to forced convection circumstances [24] allow the inference that the heat flux density is influenced by conduction along the wall, specifically at the duct extremities. A fully developed condition, for temperature, therefore, can not be achieved exactly. It can be approximated, but to an extent not predictable 'a priori'. With combined convection, the same becomes obviously true for velocity. On those bases, the constant gradient option seems quite unrealistic, when simulating real engineering experiments, and becomes the more so as the conductivity of the wall increases (the limit in that case is a uniform wall temperature at the inner wall surface).
For the time being, the above zero-gradient boundary conditions have been considered preferable, as a provisional, numerically attainable, option.
Other boundary conditions are straightforward, and do not need to be discussed further at this stage.

6.2.2 - Grid description and numerical options

Due to the symmetry of the problem about the vertical mid plane, only one half of the duct cross-section is considered. The grid is obtained by 'patching' a uniform orthogonal (H-grid) with an external annular grid (O-grid). The latter is subdivided into three blocks, as shown in Figure 6.1. The wall is modeled correspondingly, using two radial steps.

This multi-block arrangement has been preferred to the more conventional cylindrical grid, not only for the reasons given in the previous section, but also because it allows the grid to be easily fitted to the specific features of the secondary flow, while removing the singularity at the duct axis.

The half duct section is subdivided into 50 square volumes in the central block, Block 1 in the figure, and 10 rings in the O-grid, for a total of 182 elements, in the fluid region, plus 30 elements in the solid region.

In the preliminary phase, the wall was omitted, and 50 steps were spaced axially, increasing with a constant ratio of 1.3, starting from an initial step $\Delta z' = 0.0215$ mm. A total length of about 300 tube diameters was obtained in this way.

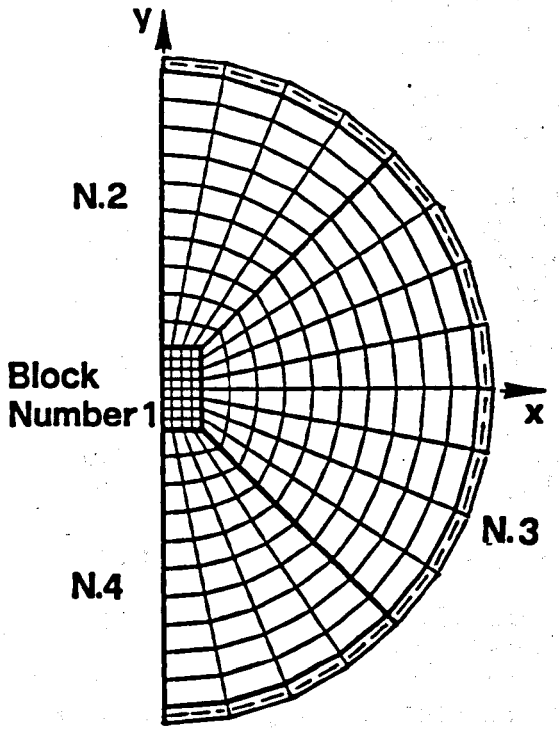

Fig. 6.1 - Multi-block and control-volume arrangement over the duct cross-section.

In the final sequence of simulations, on account of the steeper temperature gradients expected at the duct wall extremities, an axial grid symmetrical with respect to the half tube length has been preferred. The following rule is used to define the position of volume vertices in the axial direction:

$$z'_n = \frac{L_{ht}}{2}\left(1 - \cos\left(\frac{n\pi}{50}\right)\right) \quad \text{with} \quad n = 1, \ldots, 50 \qquad (6.3)$$

Overall, 10600 control volumes are used.

Procedural and solving options used throughout are as follows: convective terms in momentum and energy equations are discretized according to the hybrid scheme; the SIMPLEC algorithm is used for velocity-pressure coupling; the discretized momentum and energy equations are solved with the Stone's method, the Incomplete Cholewsky Conjugate Gradient (ICCG) method is used in the solution of the Poisson-like pressure-correction equation. The multigrid option, also available in FLOW3D, has been given an initial trial (using Rel.3.1) but with no relevant advantage in terms of computer time.

6.3 - Accuracy Considerations (preliminary tests)

The preliminary numerical activity has already been reported in a Conference paper [25], which is a part of this Thesis (Appendix I, paper P14).

With the aim of checking the adequacy of the grid, and validate the procedure, an axially and peripherally uniform heat flux was specified at the wall/fluid boundary, boundary condition **H2**.
The program was run with input data corresponding to one of the preliminary experimental cases, namely, Run PB (Re_o = 952; Pr_o = 7.09; Ra_{qo} = 8.83×10^5), for both forced and combined convection conditions.

In these preliminary runs, the restart option has not been used. Solutions have been initialized with zero velocity and uniform temperature fields. The convergence behavior of the solution is shown in Fig.6.2. Convergence is controlled by the absolute mass residual (Euclidean norm of local dimensional residuals of the continuity equation). The trend of the residuals with the number of outer iterations, similar in the two cases, indicates a monotonic convergent behavior. About 2000 outer cycles are needed to reduce the residual to 3×10^{-4} kg/s. The corresponding computer times are 2.2×10^4, and 1.2×10^3 CPU seconds, with SG IRIS Indigo WS, and CRAY YMP/432, (two processors) respectively.
Under-relaxation factors (URF) have been left fixed at their default values, namely, URF = 0.65 for the velocity components, and URF = 1.0 for pressure and temperature.

Preliminary results are presented in [25] (Fig. 5 *ibid.*). It can be noted that forced convection results compare well with the Shah and London [26] reference solution. In terms of Nu_z, the deviation from the reference is inside 3% for $z^* > 1 \times 10^{-3}$. However, the numerical solution becomes inaccurate in the proximity of the inlet section and in the asymptotic region. In both cases, the use of smaller axial steps is expected to cure the effect.
The results for the combined convection case are also presented in [25]. Direct comparison with experimental data is clearly inappropriate in this case, since the numerical results refer to boundary condition **H2**, while the experiment approximates the infinite conductivity case, **H1**, as already discussed. Even so, the onset of buoyancy is well predicted, and the agreement remains quite satisfactory up to $z^* = 0.01$. Further downstream, the experimental data are underpredicted; this is consistent with the expected effect of wall conduction.

Overall, preliminary results have been encouraging, in that they have demonstrated the feasibility of the proposed simulation program.

With the intention of validating further the solution strategy, and checking the appropriateness of the new grid (including the wall), the program has been run using the entry data of Run FD, but reducing the flow-rate to half (Re_o = 258.8), omitting the buoyancy

effect, and reducing the wall conductivity to k_w = 1.0 W/mK. This solution should, in principle, be a good approximation of the standard constant property case. Comparison with the reference solution [26] resulted, in actual fact, in a more satisfactory result than the preliminary assessment. In terms of the local Nusselt number the deviation reduces from 4% at $z^* \sim 3 \times 10^{-4}$, to less than 1% at $z^* \sim 0.1$, where the asymptotic value 4.364 is to be expected.

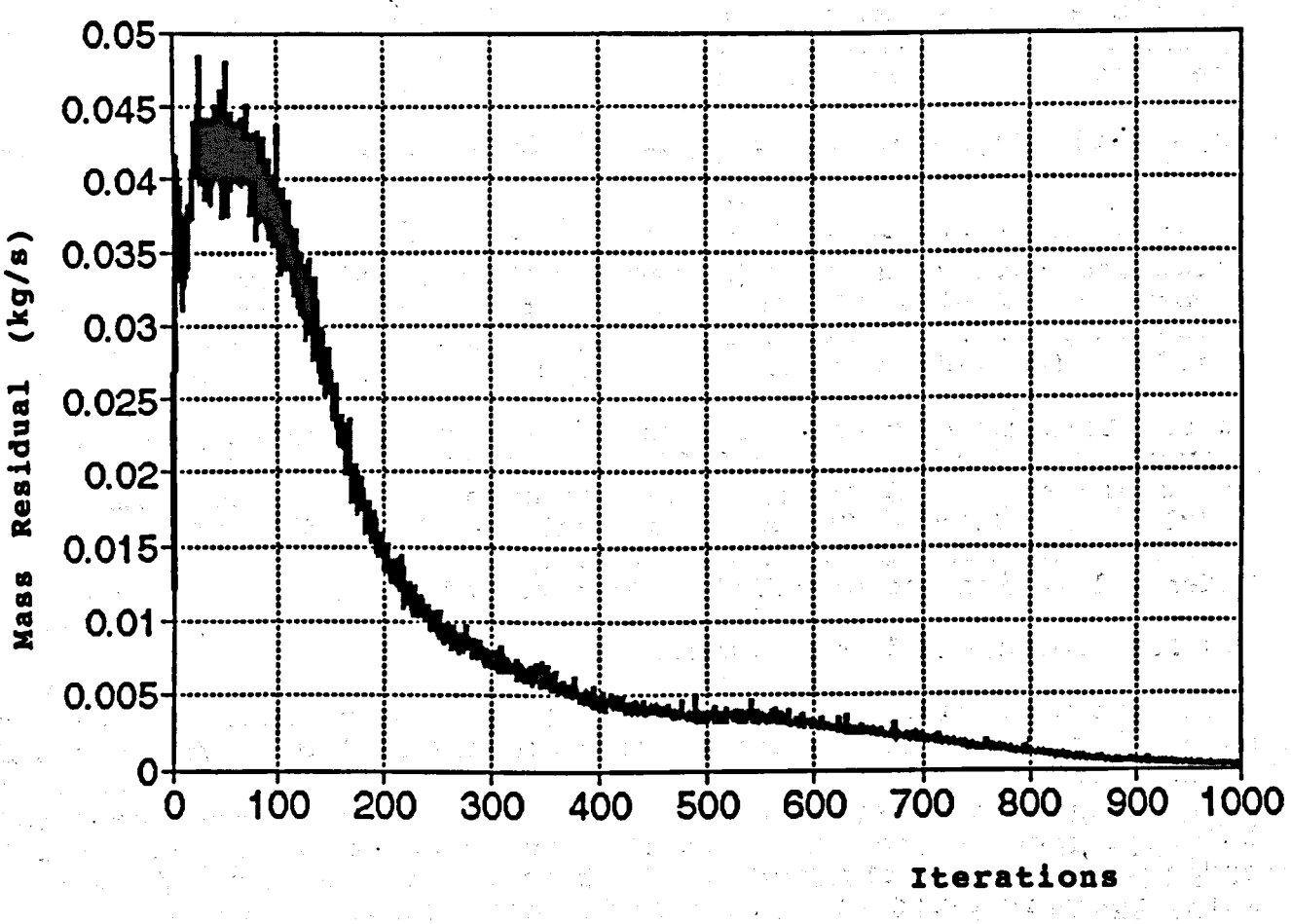

Fig. 6.2 - Convergence behavior of the numerical solutions. Total mass residual vs. number of outer SIMPLEC cycles.

It is observed further, that the deviation remains negative along most of the computational domain, and changes sign only at z^* = 0.1126 (z' = 2.527 m).
A careful check of the axial distribution of the bulk fluid temperature reveals that, except at the first axial position, this steadily overpredicts the linear distribution of the reference case, and converges to it only at the end section. This is recognized as typical of the behavior of conjugate conduction and convection [24]. The obvious conclusion can be driven that the effects of axial conduction remain still perceptible even in the case of a long, thin-walled duct. This, in turn, gives motivation for undertaking the parametric analysis described below.

6.4 - Comparison of Predictions and Experimental Data

Numerical results have been obtained for the entire set of five experimental runs. Entry data (mass flow-rate, temperature, heat flux density), as well as the fluid and wall properties have been set at the same values as used in the data reduction (see tables in Ch.6).
For each experimental run, the results of numerical simulations are reported, and compared, together with the results for two modified conditions, namely: i. the case of no buoyancy, obtained by reducing the gravity acceleration to virtually zero ($g = 1x10^{-5}$ m/s^2); and, ii. the low wall conductivity case, obtained by reducing the conductivity of the wall to 1/100 of its original value (k_w = 3.3 W/mK).

A few comments on numerical aspects of the solution precede the presentation of the actual results.

6.4.1 - Numerical details

Final numerical simulations have been carried out on the CRAY YMP/434 (4-CPU mode), at CINECA Computer Centre, using FLOW3D Rel.3.2.
All the computational activity, including initial adjustments, had to be performed in 'batch' mode, since no interactive facilities were available on a workstation at the time of computing.

The restart facility has been used on all possible occasions, in that a converged solution of one case was always used to start the next case. The restart option has also been employed to control convergence, converged solutions being in fact obtained by launching successive blocks of 500 iterations.
In all cases, the CPU time per Work-Unit has been around one second.

For all runs the criterion for convergence has been to accept a maximum tolerance of $1x10^{-6}$ kg/s, on the total mass source residual.
For the test-case, Run FA, the first to be processed, a converged solution has been achieved within 1700 outer iterations, starting with a zero-velocity, uniform temperature initial guess.

Computer runs for cases FA, and FE, all converged with success using default under-relaxation factors, i.e. URF = 0.65 for velocity, and URF = 1.0 for temperature (the pressure-correction equation has never been relaxed). Passing to Run FB (thus, in practice, halving Re_o), the resulting convergence was very slow, using the same parameters.
It has been considered that the double velocity-temperature link between momentum and energy equations (as discussed in Ch.2) could be only one of the sources of inconvenience. In fact, the case with no buoyancy also converged with difficulty. It has been hypothesized further, that the thermal coupling between the wall and the thermo-fluid field was mainly responsible for the instability. As a consequence, the program was run using a lower under-relaxation coefficient in the energy equation, and leaving it unchanged for

velocity. Converged solutions were in fact obtained setting URF = 0.7, for cases FB, and FC. For case FD, however, the under-relaxation factor on temperature had to be set as low as URF=0.3 to achieve convergence. Results for the parametric study, also related to Run FD, have been obtained in the same way.

It is interesting to observe that stability problems increase for reducing Re_o, and for increasing Ra_{qo}, as would be expected, but also for reducing wall conductivity.

6.4.2 - Numerical results, and comparison

Numerical results for the five data-sets (three runs each) are presented in Figs. 6.3 - 6.7, in terms of the axial distributions of: a. mean pressure, p', (averaged over the duct cross-section); b. peripherally averaged wall temperature, T'_{wz}; and, c. locally averaged Nusselt number, Nu_z.

It is important to stress that, here and in the following, the definition of the Nusselt number is consistent with the one used in experimental data-reduction. Thus, we are actually dealing with an 'apparent' Nusselt number, as judged by an experimentalist (ie, defined on the basis of an axially uniform heat input, a consistently predicted (linear) distribution of the bulk temperature, and the measured wall temperatures).
Reasons for this choice are: i. the prime objective of this analysis is to compare experiments with predictions; ii. the knowledge of 'true' Nusselt number values is of no practical use in itself. In the prediction of a conjugate heat transfer circumstance, the quantity must in fact be complemented with some other data (usually not available), such as the 'true' bulk temperature, and the 'true' heat flux density.

The figures can either be read with respect to the Reynolds number (Figs.6.3, 6.5, and 6.7 are for $Re_o \sim 1000$, Figs. 6.4, and 6.6, for $Re_o \sim 500$), or with respect to the Rayleigh number (Figs. 6.3 and 6.4 are for Ra_{qo} in the range $8 - 9\times10^5$; Figs. 6.5, and 6.6, for $Ra_{qo} \sim 5\times10^6$, and Fig.6.7 is for $Ra_{qo} \sim 1\times10^5$).

Pressure - In Figs.6.3-6.7a, the zero-level for pressure is set at the outlet section. Pressure distributions indicate a total pressure loss of the order 15 Pa, at $Re_o \sim 1000$, in the absence of buoyancy. The effect of buoyancy on the total head loss is shown quite clearly by the graphs. While, in fact, the inlet pressure remains practically the same for all conditions in Fig.6.7a ($Ra_{qo} = 1\times10^5$), it increases by 9%, passing from the constant property to the buoyancy affected cases of Run FA (Fig.6.3a). The effect is more evident for Run FD (Fig.6.5a), with a 22% increase. In this case, the slope of the graphs is modified by buoyancy, and the results for high and low conductivity walls can also be distinguished. The total pressure drop is obviously lower for runs at $Re_o \sim 500$, but the above effects are of the same order of magnitude.

Wall temperature - T'_w is the 'natural' parameter to investigate the effect of buoyancy, with the general boundary condition **H**.

In Fig.6.7b, it can be seen that, for Ra_{qo} as low as $1x10^5$ (Run FE), the deviation from constant property predictions is detectable (~ 0.1 °C) in the downstream part of the tube. The effects of buoyancy become quite well evident in all the other cases (Figs.6.4-6.6b). As expected, these increase for increasing Ra_{qo}.

In general terms, the comparison with constant property results indicates that the effect of buoyancy on T'_w is as below.
Buoyancy does not affect appreciably the temperature of the wall up to a certain distance from the inlet. This decreases for increasing heat flux, and, using dimensional quantities, for reducing flow rate. In our case this length is of the order of 25, 13, 10, and 6 duct diameters, for runs FA, FB, FC, and FD, respectively. Further downstream, the prediction of the wall temperature is definitely lower than constant property predictions. Again the effect is more marked for higher Ra_{qo}, and lower Re_o. This is the expected trend following the onset of buoyancy.

The effect of conduction in the wall can be observed by comparing the results for high and for low wall conductivity (both affected by buoyancy) in the above figures. Axial wall conduction always appears as an increase in wall temperature in the initial part of the heated section, and a reduction further downstream. Again this is consistent with the findings referring to forced convection flows, discussed in Ch.4. Differences in the average wall temperatures remain however very small, even for Runs FC and FD. This could lead to the judgment that axial conduction in the wall could actually play only a marginal role. In fact, the *opposite* holds true as will be demonstrated. For the time being, we just note that, in no case is a linear asymptotic behavior obtained; in all buoyancy affected circumstances, in particular, $T'_{w,z}$ happens to assume an 'almost' linear trend in the downstream region. To a careful observation, this actually presents a, more or less pronounced, waviness. The presence of a maximum, with zero derivative, is also noted at the end section; it is the direct consequence of the adiabatic boundary condition employed in the model.

Nusselt number - The above effects are also evident from the diagrams (Nu_z-z^*), where the constant property solution by Shah and London [26], has also been reported for reference purposes. The onset of significant buoyancy, and the effects of upstream heat diffusion can now be observed quite clearly. The downstream part is, however, not clearly distinguishable using those coordinates. The effects of buoyancy are in any case well evident in all the Runs, except for FE (Fig.6.7c). For example, in Runs FA, and FB (Figs.6.3, and 6.4c), at $z^* = 2x10^{-2}$, Nu_z is 72% higher than the constant property reference; the relative difference becoming as high as 150% with Runs FC and FD (Figs.6.5, and 6.6c). The relative effect of the wall in the downstream region results one order of magnitude lower: passing from the low- to the high-conductivity case, Nu_z increase of 14% in Runs FC and FD; this reduces to about 4% in Runs FA and FB.

Parametric study - As already indicated in § 6.3, a parametric study on the cumulative effects of combined convection and wall conduction has been performed, limited to a single case-study (Run FD). In this analysis, the conductivity of the wall, k_w, is progressively reduced from 300 to 1 W/mK, in steps of fifty. Results are only presented in terms of Nusselt numbers; they are collated in Fig.6.8.
We note that the effects of axial conduction remain discernible in the immediate proximity of the entrance, even at the lowest k_w-value. In this case, however, the effect rapidly disappears, the curve converges to the reference solution, and then assumes an almost perfect asymptotic (i.e., horizontal) trend, in the downstream region. This conforms with expectations based on boundary condition **H2**. For increasing k_w, all other relevant parameters remaining constant, convergence to the reference solution reduces to a very short length. All the curves for $k_w \geq 50$ W/mK do not overlap the reference solution, but rather have a definite crossing point with the reference solution. This is shown more clearly in Fig.6.8b, where the crossing point region has been enlarged. It is noted further that Nu_z-graphs for different values of k_w have a tendency towards a common crossing point at $z^* \sim 9x10^4$.
All of this is of some relevance when judging the onset of buoyancy in terms of percentage deviation over the constant property reference (see Ch.3), as it will be discussed further in the next section.

Comparison of experimental and predicted results - Numerical results and experimental data are compared in Figs.6.9-6.13, in terms of: a. wall temperatures, and b. average Nusselt number distributions.
It is recognized here that the two quantities give exactly the same information. Since, in fact, $T'_{m,z}$ is just an 'apparent' fluid temperature, Nu_z simply reflects the trend of $T'_{w,z}$. It nonetheless is very useful for this comparison exercise, since it emphasizes the deviation of the experimental data from predictions, and, in virtue of its non-dimensional nature, makes it easier to generalize the results. We also note that the only difference in the treatment of experimental and numerical data, is that, in the latter case, $T'_{w,z}$ is a weighted average with the elemental surface areas, while the simple arithmetic mean of wall temperature measured values is taken in the experiments.

Overall, the agreement between the two assessments is well above expectation. For example, the deviation of the (mean) experimental temperature from predictions is always within ± 0.1 °C, in Run FA (Fig.6.9a). Experiment and predictions for Run FA also agree extremely well in terms of Nu_z, up to $z^* \sim 0.018$, (Fig.6.9b), with both the predictions and the experimental data following a slightly ascending trend in the downstream region. The maximum in Nu_z, observed in the experiment at $z^* \sim 0.02$, is however not captured. As can be seen in the other figures, this is a common feature of all the experimental set, irrespective of the different heating conditions applied in the terminal part of the test section.

The first experimental point in Fig.6.9b is noteworthy. Fitting the prediction almost perfectly, it indicates that the deviation of (measured) Nu_z from the reference solution at the first measuring point (noted in Ch.5) is not a reliable estimate of the experimental error at that position. It is rather a consequence of the fact that the constant property curve (not including wall effects) is not the correct reference in our case.

The measured wall temperature is slightly overpredicted, and Nu_z correspondingly underpredicted, in Run FB (Fig.6.10). This is most probably to be ascribed to some error in the measurement of the inlet fluid temperature. The trend of Nu_z found in the experiment, is nevertheless, in very good agreement with predictions. Similar considerations also apply to Run FC (Fig.6.11), where Nu_z is overpredicted.
Run FD is modeled extremely well in terms of the wall temperature (Fig.6.12a), less accurately, but still satisfactorily, in terms of Nu_z (Fig.6.12b).
Note that in Figs.6.11a, and 6.12a, the predicted top and bottom temperatures have also been plotted. This is motivated by the fact that the circumferential temperature gradient is relatively high in Runs FC and FD. Measured temperature differences are correspondingly more meaningful, and useful for validation purposes. In our case, the predicted temperature differences are, in general, quite well consistent with measurements.

As for Run FE (Fig.6.13), Nusselt number results are in poor agreement with the numerical data, as expected (see discussion of experimental data in Ch.5). However, also in this case, the wall temperature is well predicted (within 0.1°C).

The relative deviation of experimental Nu_z-values from numerical predictions, expressed in relative terms, is shown in Fig.6.14, for Runs FA to FD.

Overall, the comparison experiment can be considered successful.
Disagreements have however been noted in the comparison exercise. These may as well have a random character (e.g., Run FB is underpredicted, and Run FC overpredicted in terms of the Nusselt number), or have systematic features (the peak of Nu_z observed in the experiments at $z^* \sim 2\text{-}4\text{x}10^{-2}$ is not reflected in the simulation).
In the first case, the most likely cause of disagreement is the uncertainty in the measurement of the inlet fluid temperature, as discussed in Ch.5.
The systematic effect seems however be caused by some, still unclear, physical effect. Note that the peak in Nu_z: i. is in coincidence with different measuring stations, in the various runs; ii. is present both when the entire heat transfer length is heated (Run FA), and when a short end length is left unheated (Runs FB, FC, and FD); iii. is more pronounced for low Re_o-runs, and hardly detectable at low Ra_{qo} (Run FE). Note, further, that peaks of that kind are quite a common occurrence in combined convection experiments (see e.g..[27]). Possible causes of the observed disagreement could be: the effect of temperature-dependent properties (mainly viscosity), not considered in the numerical

model, or some inaccuracy in modeling 'true' boundary conditions at the end section of tube.

6.5 - Significance of the Results

The problem of horizontal combined convection under 'entry length' conditions has been studied both experimentally and predictively with some care, and in an integrated manner.

Firstly, the candidate's past experience in combined convection (both with vertical and horizontal orientations) has been used in designing a rig capable of producing reliable results of quantitative accuracy. Possible circumferential effects have been investigated. Secondly, the CFD code FLOW3D has been proved to be very appropriate to the combined convection problem, since it properly accommodates the generally elliptic nature of this type of flow. Finally, the *comprehensive* characteristics of the code have made a true (predictive) *simulation* of the experiments to be effected.

The candidate's previous work on conjugate conduction/convection has been utilized in allowing (i) for the effect of wall conduction in a proper manner, and (ii) investigating how a range of conductivities could have affected the results. By so doing, it has proved possible to isolate with some confidence the effects of buoyancy itself.

The novelty of the present approach mainly stems from the fact that combined convection in horizontal ducts, has been approached as a fully 3D conjugate feature.
The problem offers, in principle, formidable mathematical difficulties. While, in fact, the elliptic thermo-fluid problem is only weakly so in many practical circumstances (this allows a 2D marching approach to be applied), the presence of wall conduction requires the energy equations, in the solid and fluid regions, to be solved at the same time. In a combined convection circumstance, the pressure-velocity field is, in turn, linked to the temperature field. All of this makes of the problem a 'strongly' elliptic one, and, except for a vertical orientation, three-dimensional.

Fully 3D solutions of combined convection problems have been reported, and fully developed predictions of conjugate wall effects also given, in the literature (see Ch.2, and paper P1, Appendix I, for references). However, the fully 3D conjugate problem had never been attacked before, neither numerically, nor analytically. The CFD code FLOW3D has been demonstrated to be very effective in addressing such a problem. Results have been obtained with relative ease and affordable computational effort.

Specifically, the analysis indicates the following:

- the general features of laminar combined convection in horizontal ducts, as described in Chs.1 and 3, are confirmed, in their essence;

- in the low Ra_q-range, the thin metal wall approximates the expected behavior for high circumferential conduction, top-to-bottom temperature differences remaining very small (~ 0.4 - 0.5 °C, maximum). For increasing Ra_q, however, the temperature difference in the wall becomes quite well evident, thus demonstrating an increased interaction between the circumferential conduction, and convection (i.e. a progressive departure from the infinite conductivity boundary condition, **H1**). This behavior is consistently found in both the experiments and the numerical predictions;

- buoyancy is found to produce increased head loss and heat transfer coefficients, in comparison with constant property predictions, again consistent with expectations;

- the numerical data indicate that axial conduction in the wall may have a definite influence on heat transfer, even for a long heat transfer section with a thin wall. Its effect is to increase the wall temperature in the initial part of the heat transfer length, and, to reduce it in the downstream region (the wall temperature tends to become axially uniform). Nu_z (apparent) has the opposite trend. After the onset of buoyancy, Nu_z tends to increase with the axial distance. This trend is again linked with axial conduction in the wall. In fact, the wall temperature is lower than it would be in the absence of the wall effect, in the downstream region. This derives from the combined (in this case synergetic) action of buoyancy (increased heat transfer coefficient), and axial conduction (reduced heat flux supply to the fluid). The latter effect increases with distance, and is maximum near the end section of the duct;

- the parametric study on the wall conductivity shows that axial conduction will always be present in practical occurrences. Only for k_w of order one, it can be overlooked, in a long (L_{th}/D ~ 170) tube (also in this case its influence can still be detected with appropriate numerical tools). The effect of conduction obviously increases for increasing k_w (as it has been shown here), as well as for increasing the wall thickness, and for reducing L_{th}, and the Peclet number (as shown in [24]). We can now add that, in a combined convection circumstance, its extent will also be influenced by the Rayleigh, and Prandtl numbers;

- general consequences of the above statements are that neither the infinite conductivity boundary condition, **H1**, nor a fully developed flow condition, will be approximated in experiments and applications, when the effects of axial conduction are remarkable. Whether or not this is the case in a practical circumstance, still remains largely undefined. A first quantitative estimate is given by the present results and data;

- as stated by Allen et al [28], the effect of buoyancy on experimental data should correctly be estimated by comparison with fully variable-property predictions. The insertion of variable properties in the software is not difficult, and is, in fact

scheduled in future activity. We point out here that the same assertion holds true for wall conduction effects. The above statement can therefore be complemented with the following one: experimental data in combined convection should be compared with predictions including the axial effect of the wall (conjugate constant property reference, or, better, conjugate temperature-dependent property reference). This corroborates the need for intensive numerical modeling in the experimental activity. A step in that direction has been done here;

- as for criteria for the onset of buoyancy, our numerical results including the effect of buoyancy and the wall, indicate that the conductive effect in the entry region can actually mask it in experiments. In fact, an increase over the constant-property reference solution is usually ascribed to the onset of buoyancy. It is shown here that it is, *actually*, mainly a result of wall conduction, which would be present anyway even in the absence of any buoyancy. Based on the above considerations, it can be stated that criteria for the onset of buoyancy based on experimental data in the literature (see Ch.3 for references), are, most likely, affected by axial conduction in the heat transfer section. They should then be regarded with some caution;

- It is expected that the Peclet or the Reynolds number really take-up an autonomous influence on heat transfer (not included into z*). This has not been quantified or completely checked, but is indicated with some evidence by the numerical results, and is consistent with dimensional analysis considerations [24];

- The observed trends of experimental and predicted data agree satisfactorily; the results are also quite consistent in quantitative terms, on account of the difficulties inherent in performing accurate measurements in convection heat transfer. This allows the conclusion that the experiments have been made properly, and are sufficiently accurate. On the other hand, it also indicates that experiments are well modeled, even if some additional effect should be embodied in the model to improve the agreement. Then, the reliability of the simulation is validated;

- FLOW3D has been demonstrated to be the appropriate tool for approaching this class of combined convection problems.
  Both the procedure and the grid seem to be adequate to the present circumstances.
  The model is flexible enough to allow different conditions to be considered with relative ease; it can then be extended to other cases. In particular, the range of Ra_{qo} should be increased, and Re_o reduced, to reach the stability limit of laminar flow (yet not clearly defined), and to check the uniqueness of the 'true' combined convection problem (fully 3D and conjugate), as an alternative to using highly idealized cases (such as fully developed flow). Stability problems are likely to occur for increasing Rayleigh number. Much refined grids will be therefore be necessary to those aims.

References

1 - G.S. Barozzi, M.W. Collins - Mixed Convection in Horizontal Ducts: an Overview of Numerical Methods - Procs. 9th U.I.T. Nat. Conf., Pisa (I), June 1991; 45-60.

2 - I.P. Jones, J.R. Kightley, C.P. Thompson, and N.S. Wilkes - FLOW3D, a Computer Code for the Prediction of Laminar and Turbulent Flow and Heat Transfer: Release 1 - UKAEA Report No. AERE R11825, Harwell Lab., Harwell (UK), 1985.

3 - A.D. Burns, N.S. Wilkes, I.P. Jones, and J.R. Kightley - FLOW3D: Body Fitted Coordinates - UKAEA Report No. AERE R12262, Harwell Lab., Harwell (UK), 1986.

4 - A.D. Burns, and N.S. Wilkes - A Finite Difference Method for the Computation of Fluid Flow in Complex Three Dimensional Geometries - UKAEA Report No. AERE R12342, Harwell Lab., Harwell, UK, 1987.

5 - N.S. Wilkes, and D.S. Clarke - Turbulent Flow Predictions Using Algebraic Stress Models - UKAEA Report No. AERE R12694, Harwell Lab., Harwell (UK), 1989.

6 - D.S. Clarke, and N.S. Wilkes - The Calculation of Turbulent Flow in Complex Geometries Using a Differential Stress Model - UKAEA Report No. AERE R13428, Harwell Lab., Harwell (UK), 1989.

7 - D.S. Clarke, and N.S. Wilkes - The Calculation of Turbulent Flow in Complex Geometries Using a Differential Flux Model - AEAInTec-0216, AEA Ind. Tech., Harwell Lab., Harwell (UK), 1991.

8 - M.W. Collins - Heat Transfer Predictions for Turbulent Flow Downstream of an Abrupt Pipe Expansion, Report HTFS RS477, July 1983.

9 - M. Ciofalo, and M.W. Collins - K-ε Predictions of Heat Transfer in Turbulent Recirculating Flows Using an Improved Wall Treatment, Num. Heat Transfer, part B, 15, 1989; 21-47.

10 - S. Jayanti - Contribution to the Study of non-Axisymmetrical Flows - Ph.D. Thesis, Imperial College, Univ. of London, 1990.

11 - M.W. Collins, and F.S. Henry - Swirling Flow and Heat Transfer over AGR Fuel Elements Using the FLOW3D Code - '*Anglo-Soviet Seminar on Heat Transfer Modeling*', Univ. of Manchester, UK, April 1990.

12 - M. Ciofalo, G. Perrone, J. Stasiek, and M.W. Collins - Numerical and Experimental Study of Flow and Heat Transfer in Cross-Corrugated Rotary Regenerators - Procs. '*10th U.I.T. Nat. Conf. on Heat Transfer*', Genova (I), June 1992.

13 - AEA - FLOW3D Release 3.2: User Manual - CFD Dept., AEA Ind. Tech., Harwell Laboratory, Oxfordshire (UK), Oct. 1992.

14 - S.V. Patankar, '*Numerical Heat Transfer and Fluid Flow*', Hemisphere pub. Co., Washington DC., 1983.

15 - W.J. Minkowycz, E.M. Sparrow, G.E. Schneider, and R.H. Pletcher, '*Handbook of Numerical Heat Transfer* ', J. Wiley & Sons, Inc., N.Y., 1988.

16 - C.M. Rhie, and W.L. Chow - Numerical Study of the Turbulent Flow Past an Aerofoil with Trailing Edge Separation - AIAA J., 21, 1983; 1527-1532.

17 - N.S. Wilkes, and C.P. Thompson - An Evaluation of Higher-Order Upwind Differencing for Elliptic Flow Problems - UKAEA Report No. CSS137, 1983.

18 - C.P. Thompson, and N.S. Wilkes - Experiments with Higher-Order Finite Difference Formulae - UKAEA Report No. AERE R10493, Harwell Lab., Harwell (UK), 1982.
19 - B.P. Leonard - A Stable Accurate Convective Modeling Procedure Based on Quadratic Upstream Interpolation - Comp. Meth. Appl. Mech. Eng., 19, 1979; 59-98.
20 - J.P. Van Doormal, and G.D. Raithby - Enhancements of the SIMPLE Method for Predicting Incompressible Fluid Flows - Num. Heat Transfer, 7, 1984; 147-163.
21 - R.I. Issa - Solution of the Implicitly Discretized Fluid Flow Equations by Operator Splitting - J. Comp. Phys., 61, 1985; 40-55.
22 - J.R. Kigthtley, and I.P. Jones - A Comparison of Conjugate Gradient Preconditioning for Three Dimensional Problems on a CRAY-1 - Comp. Phys. Comm., 37, 1984; 205-214.
23 - H.L. Stone - Iterative Solution of Implicit Approximations of Multi-Dimensional Partial Differential Equations - SIAM J. Num. Anal., 5, 1968; 530-558.
24 - G.S. Barozzi, and G. Pagliarini - A Method to Solve Conjugate Heat Transfer Problems: the Case of Fully Developed Laminar Flow in a Pipe - ASME, J. Heat Transfer, 107, 1985; 77-83.
25 - S. Piva, G. Scarcella, G.S. Barozzi, and M.W. Collins - Comparison of Predictive and Experimental Data for Combined Convection in Horizontal Duct Flow, Procs. '*CMEM93 6th Intl. Conf. on Computational Methods and Experimental Measurements*', Siena, May 1993; C.A. Brebbia, and G.M. Carlomagno, eds., Comp. Mech. Pub., Southampton Boston (UK), Vol.1; 169-182.
26 - R. Shah, and A.L. London, '*Laminar Forced Convection in Ducts*', Academic Press, NY., 1978.
27 - G.S. Barozzi, E. Zanchini, and M. Mariotti - Experimental Investigation of Combined Forced and Free Convection in Horizontal and Inclined Tubes - Meccanica, 20, 1985; 18-27.
28 - P.H.G. Allen, O. Szpiro, and M.W. Collins - Prediction Methods for Entry Length Heat Transfer by Combined Laminar Convection in Horizontal Tubes - Inst. Mech. Eng., Vol. 196, No. 33, 1982;409-415, and S55-S59 (discussion).
29 - S.V. Patankar, and D.B. Spalding - A Calculation Procedure for Heat and Momentum Transfer in Three-Dimensional Parabolic Flows - Int. J. Heat Mass Transfer, 15, 1972; 1787-1806.

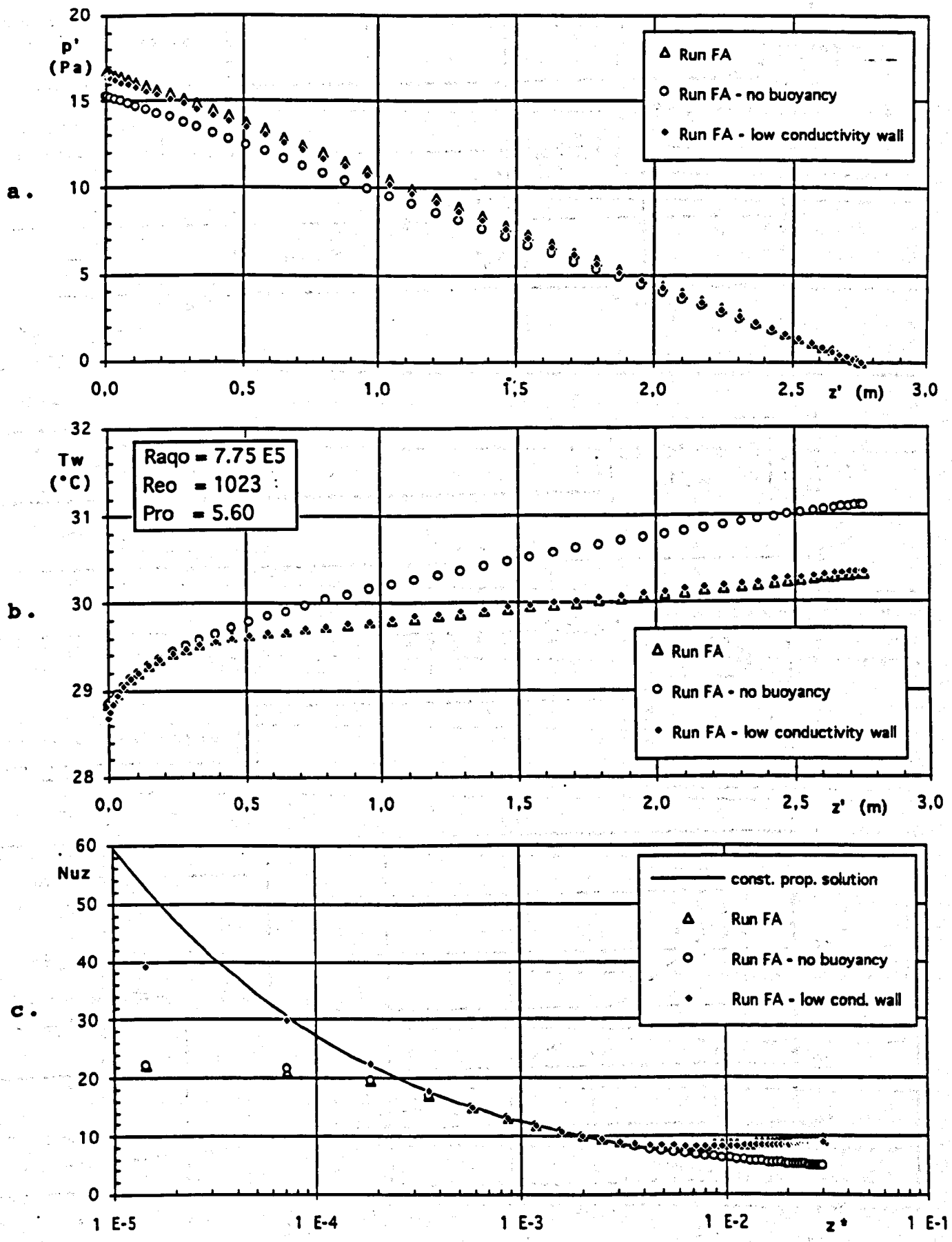

Fig. 6.3 - Numerical predictions (data as for Run FA):
a. Mean pressure distributions, vs. axial distance;
b. Mean wall temperature distributions, vs.axial distance;
c. Mean Nusselt number distributions vs. non-dimensional axial distance.

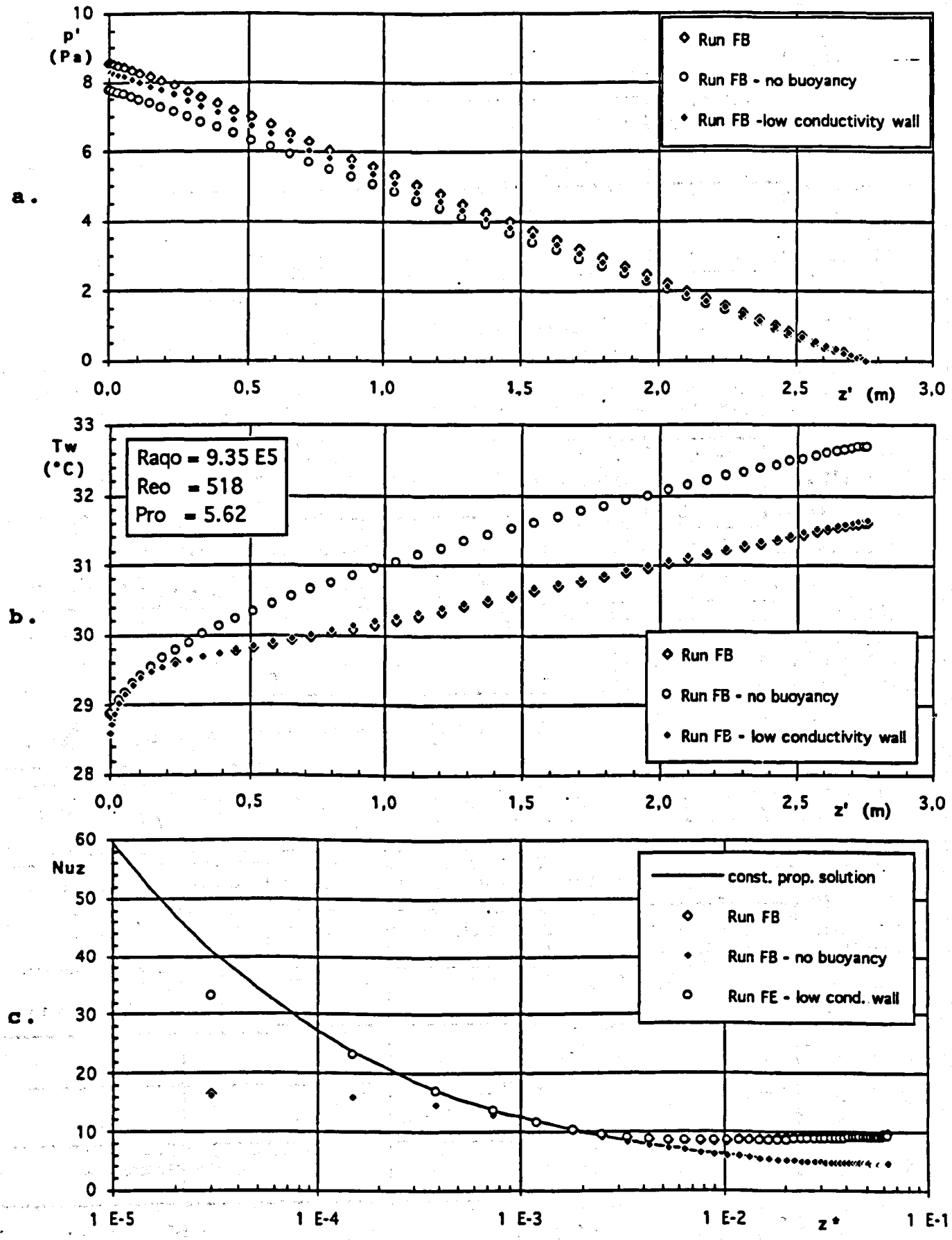

Fig. 6.4 - Numerical predictions (data as for Run FB):
a. Mean pressure distributions, vs. axial distance;
b. Mean wall temperature distributions, vs.axial distance;
c. Mean Nusselt number distributions vs. non-dimensional axial distance.

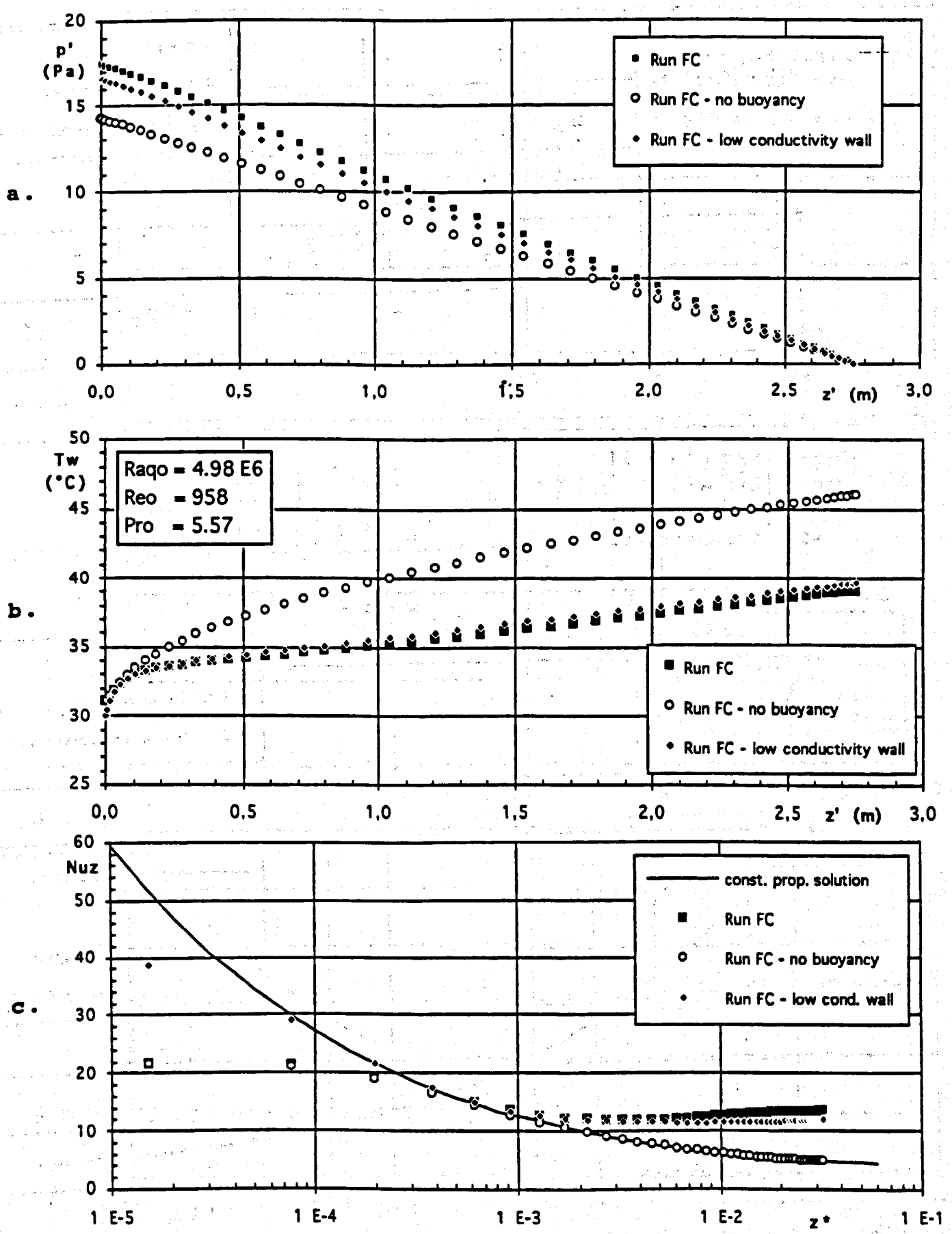

Fig. 6.5 - Numerical predictions (data as for Run FC):
a. Mean pressure distributions, vs. axial distance;
b. Mean wall temperature distributions, vs.axial distance;
c. Mean Nusselt number distributions vs. non-dimensional axial distance.

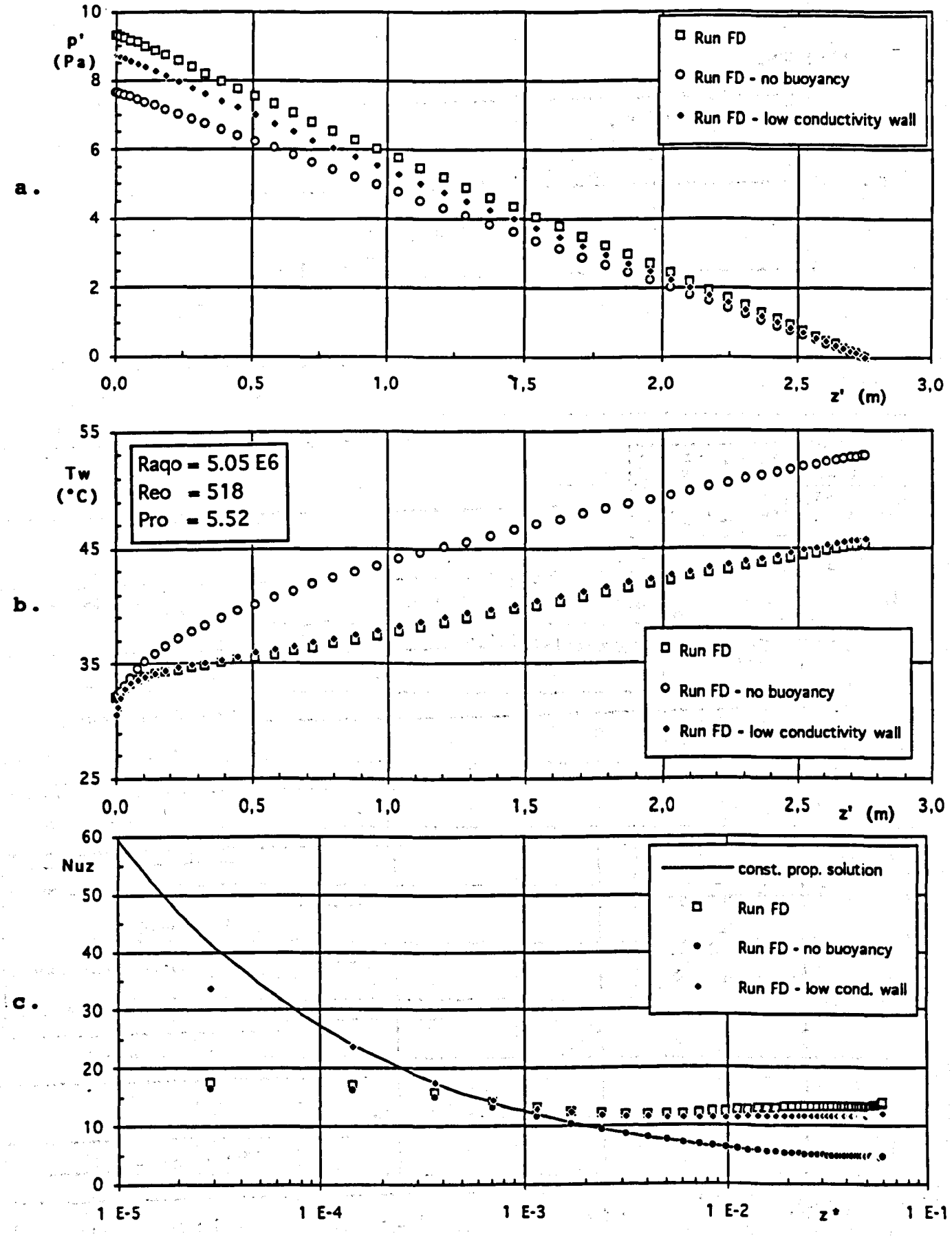

Fig. 6.6 - Numerical predictions (data as for Run FD):
a. Mean pressure distributions, vs. axial distance;
b. Mean wall temperature distributions, vs.axial distance;
c. Mean Nusselt number distributions vs. non-dimensional axial distance.

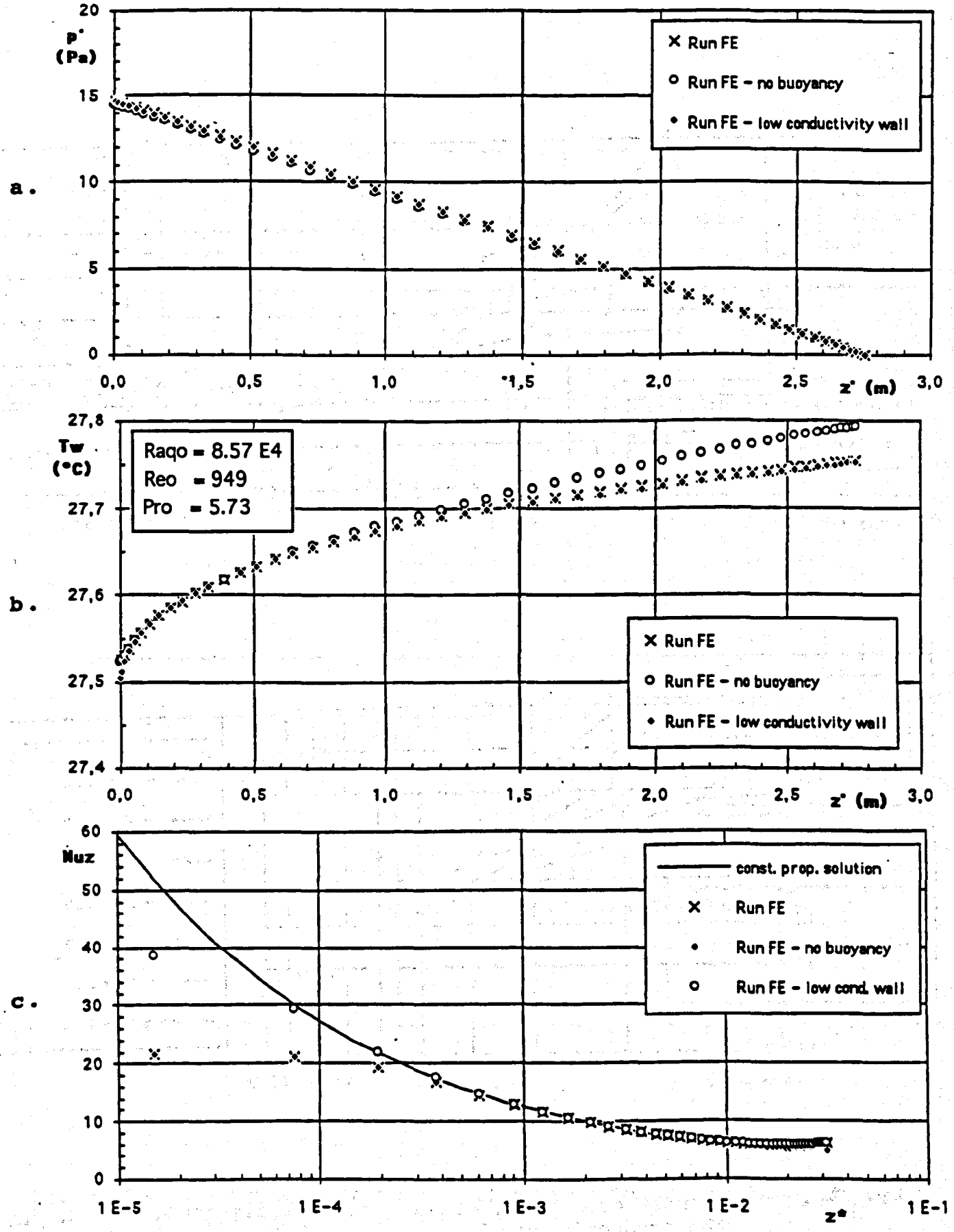

Fig. 6.7 - Numerical predictions (data as for Run FE):
a. Mean pressure distributions, vs. axial distance;
b. Mean wall temperature distributions, vs.axial distance;
c. Mean Nusselt number distributions vs. non-dimensional axial distance.

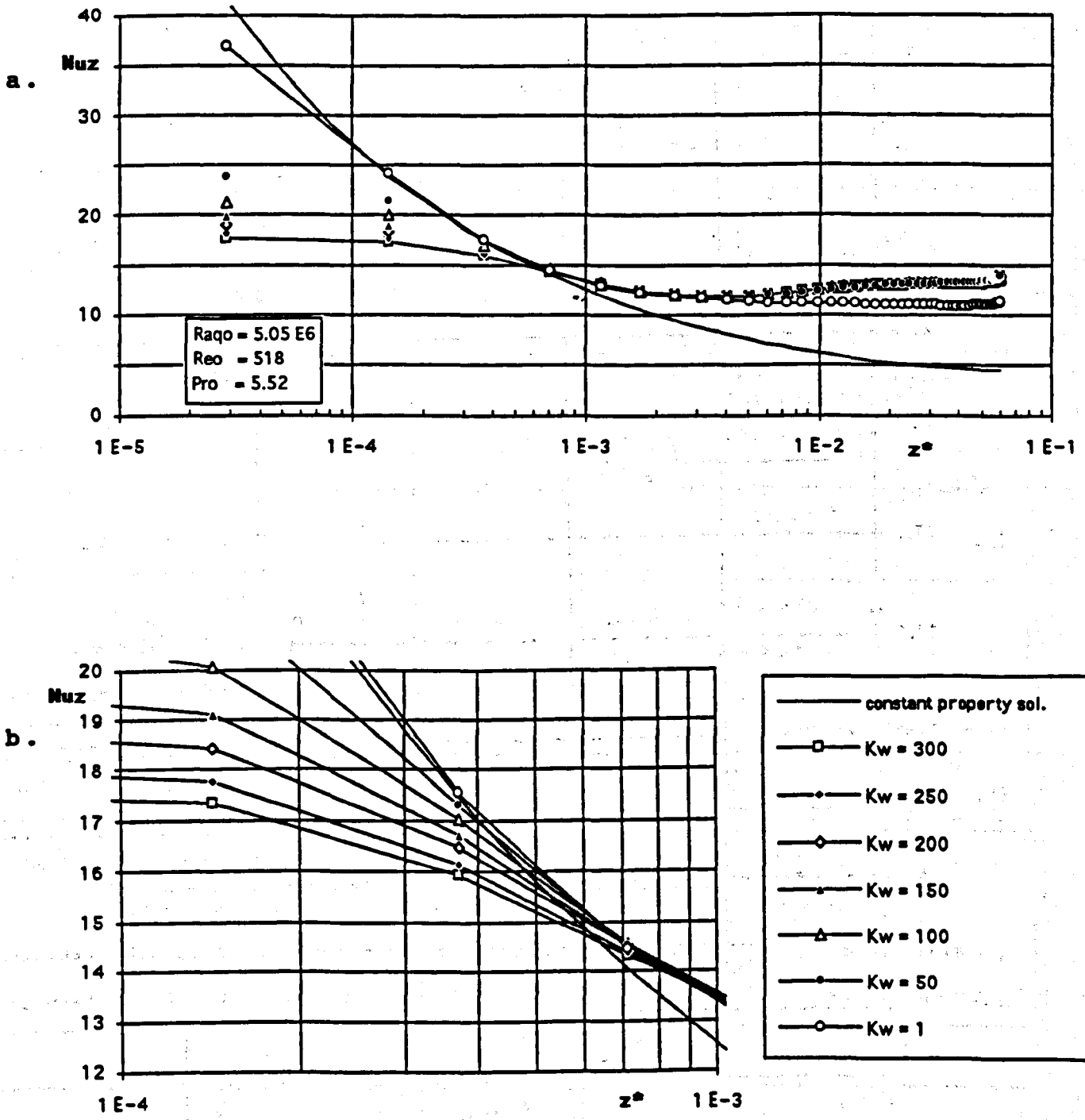

Fig. 6.8 - Nusselt number vs. non-dimensional distance, for varying the conductivity of the duct wall (data as for Run FD):
a. General view;
b. Enlarged view in the thermal inlet region.

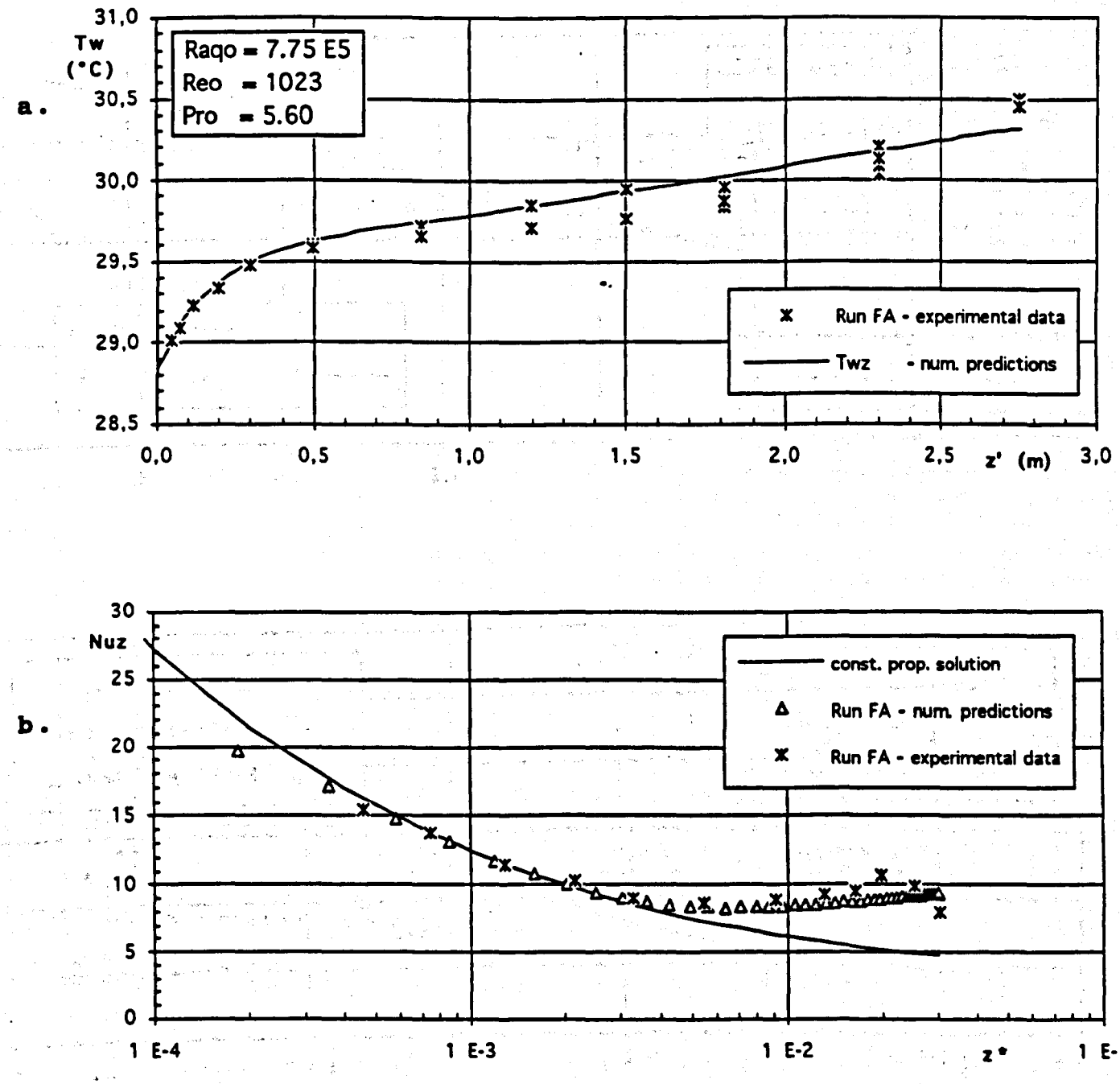

Fig. 6.9 - Comparison of numerical predictions, and experimental data for Run FA:
a. Measured wall temperatures as compared with the predicted distribution of mean wall temperature;
b. Measured and predicted Nusselt number distributions.

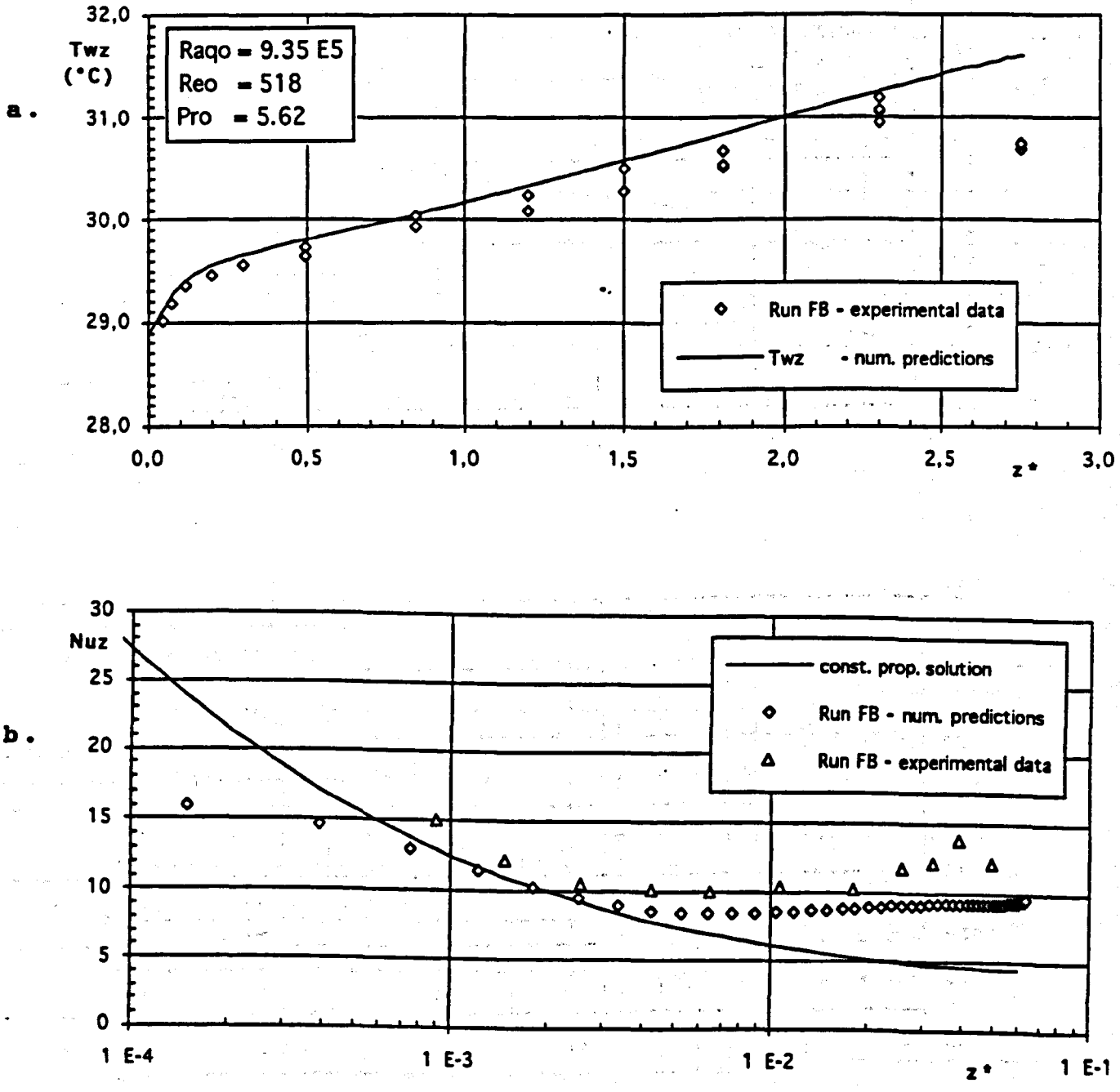

Fig. 6.10 - Comparison of numerical predictions, and experimental data for Run FB:
a. Measured wall temperatures as compared with the predicted distribution of mean wall temperature;
b. Measured and predicted Nusselt number distributions.

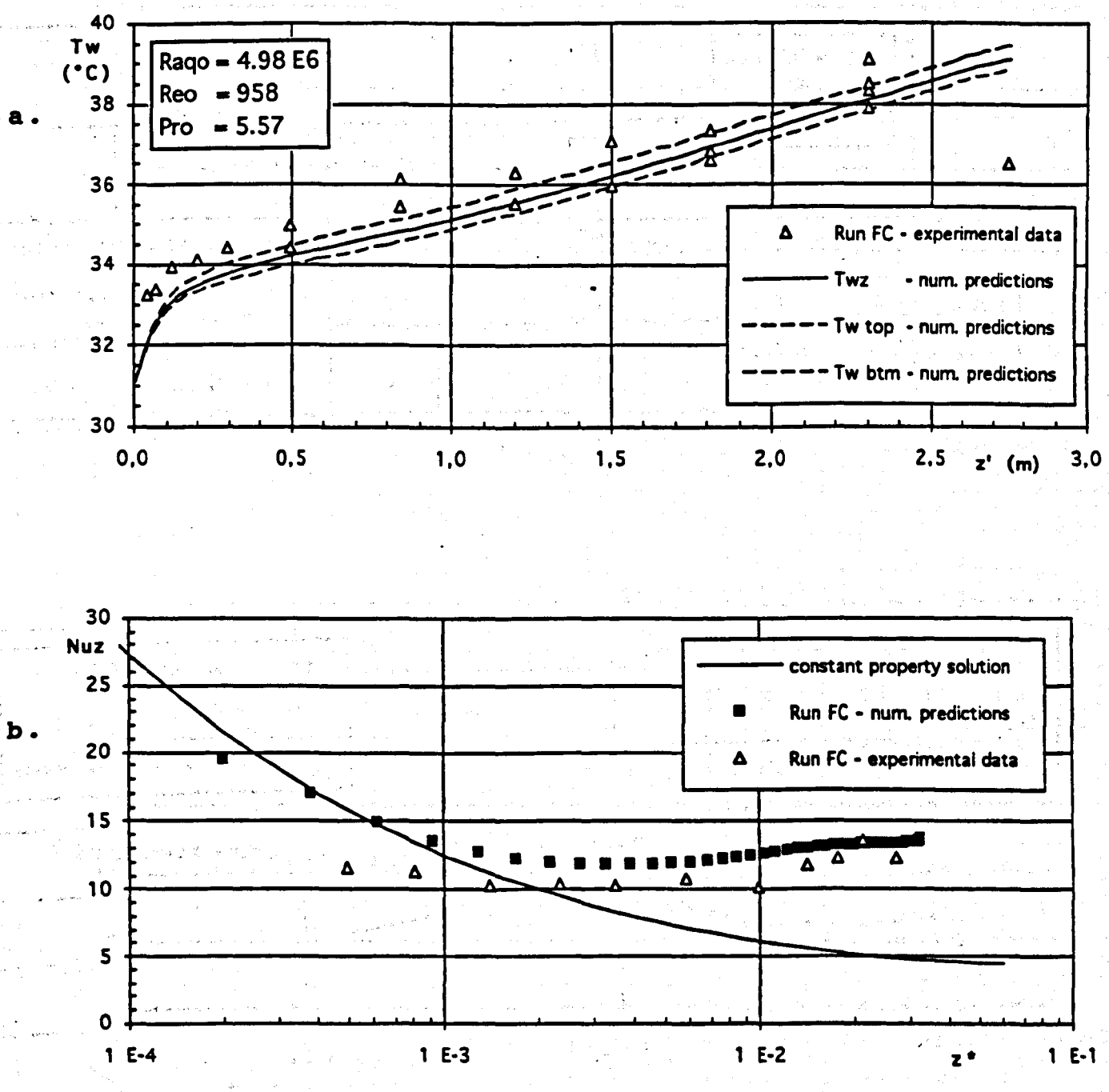

Fig. 6.11 - Comparison of numerical predictions, and experimental data for Run FC:
a. Measured wall temperatures as compared with predicted mean, top, and bottom wall temperature distributions;
b. Measured and predicted Nusselt number distributions.

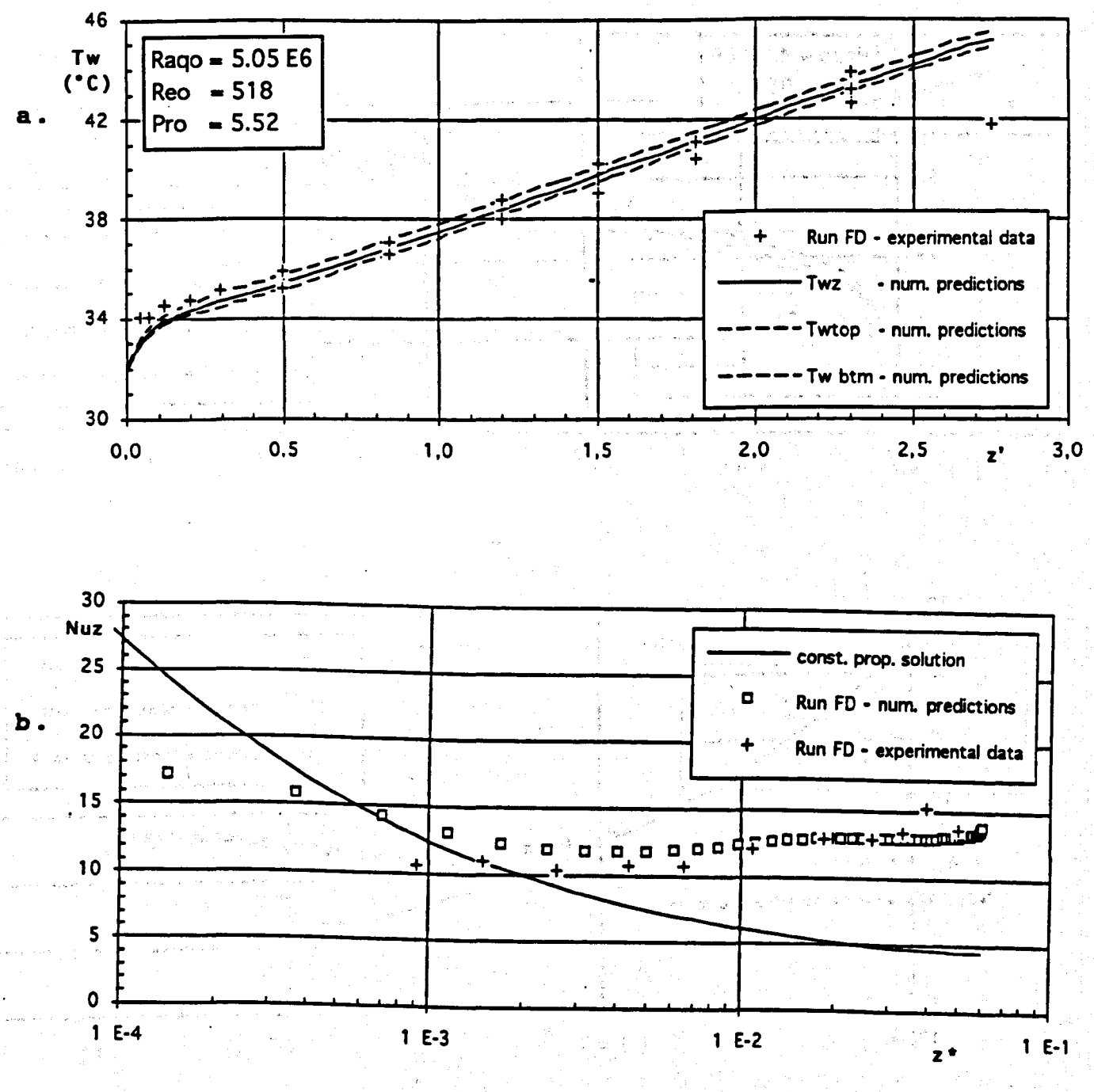

Fig. 6.12 - Comparison of numerical predictions, and experimental data for Run FD:
a. Measured wall temperatures as compared with predicted mean, top, and bottom wall temperature distributions;
b. Measured and predicted Nusselt number distributions.

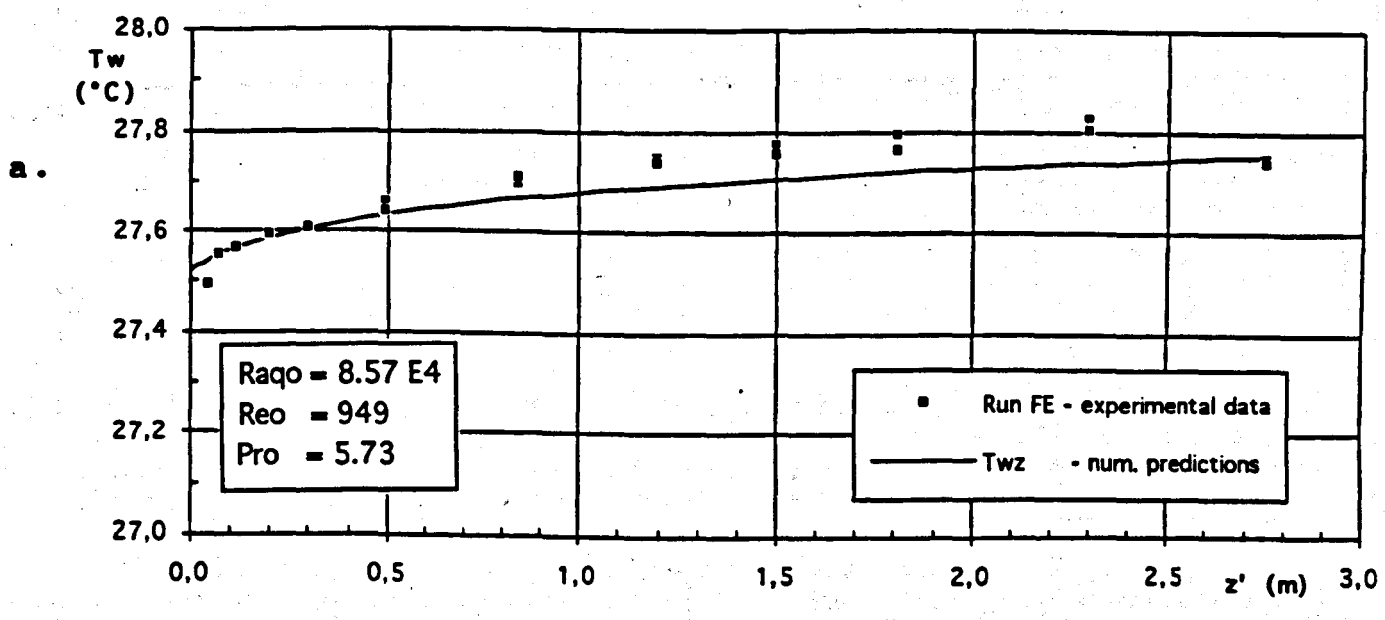

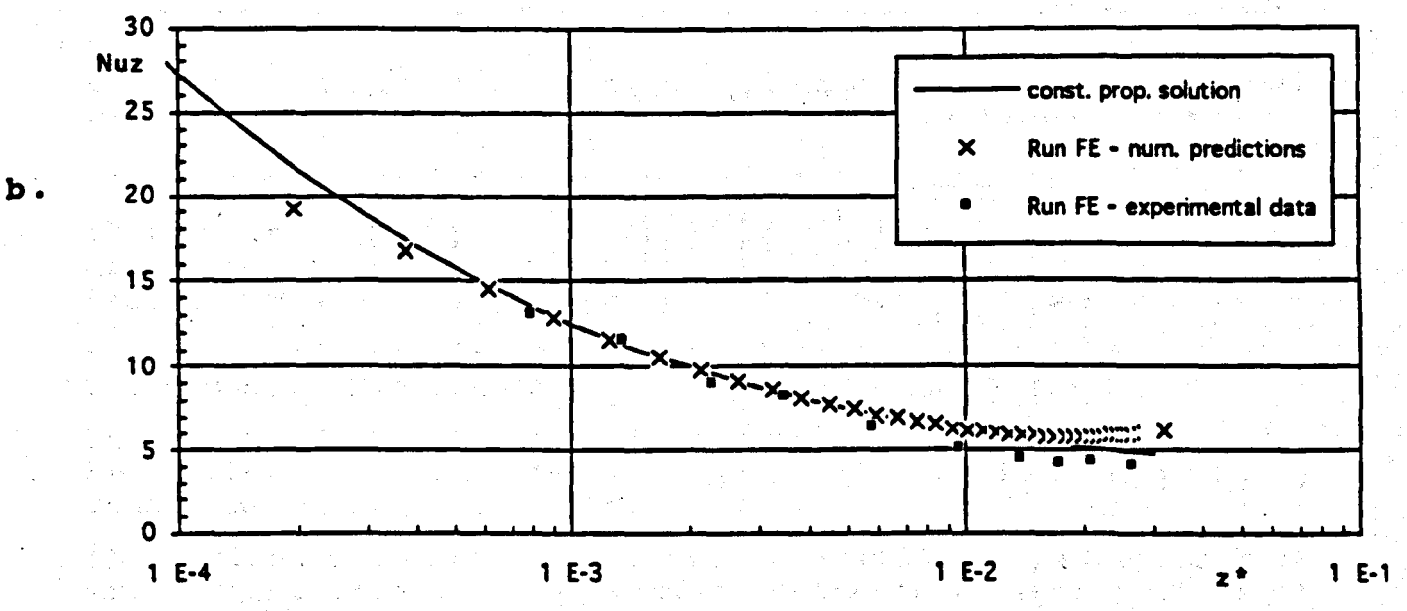

Fig. 6.13 - Comparison of numerical predictions, and experimental data for Run FE:
a. Measured wall temperatures as compared with the predicted distribution of mean wall temperature;
b. Measured and predicted Nusselt number distributions.

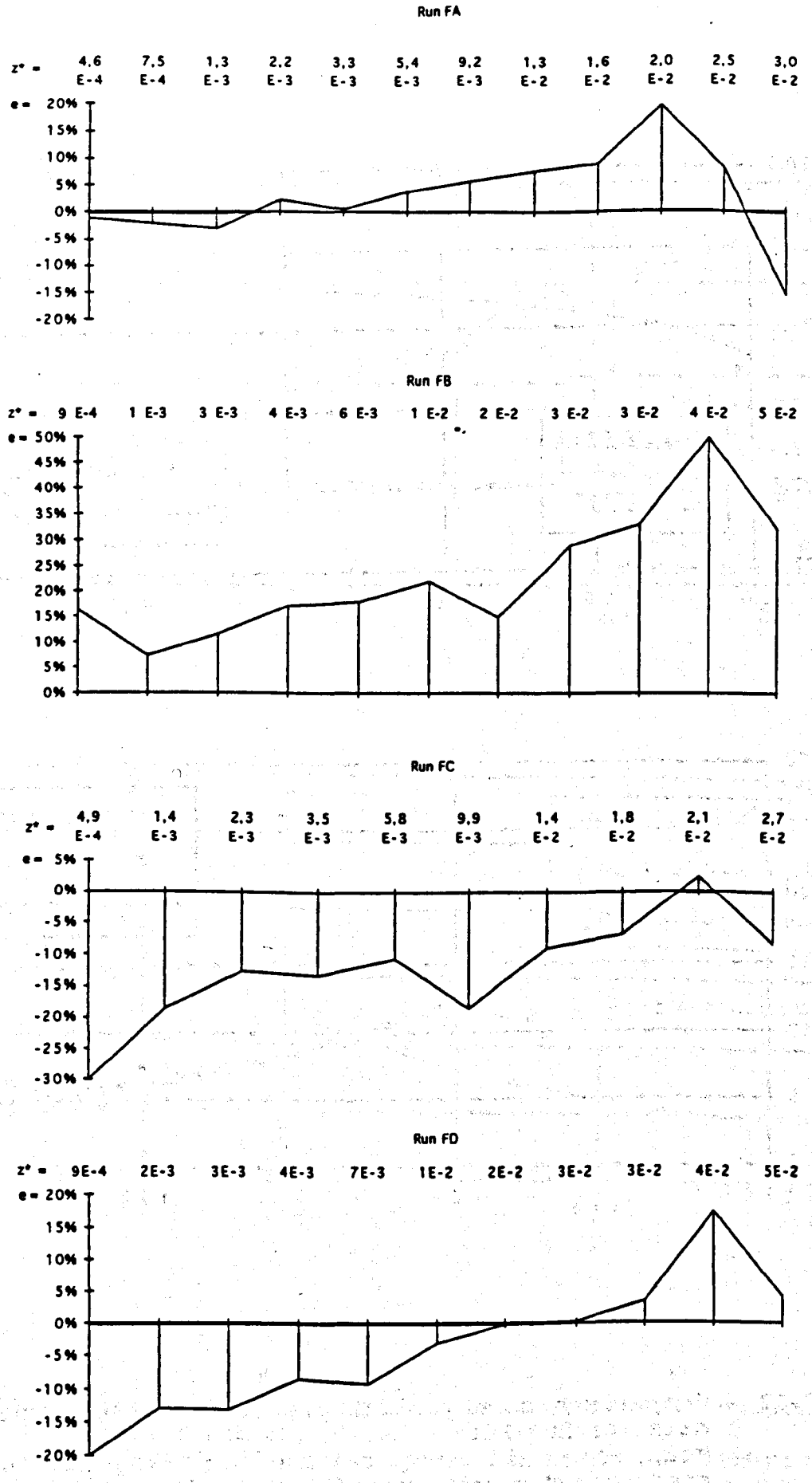

Fig. 6.14 - Percentage deviation of experimental data from numerical predictions; Runs FA, FB, FC, and FD.

CHAPTER 7: CONCLUSIONS

7.1 - Review of Main Findings

Main achievement of this work is to have treated combined convection in a horizontal duct, as a truly three-dimensional problem, accounting for all relevant effects. Previously, especially with predictive methods, this had not been done.

Steady laminar flow of water in a long, but finite, duct, has been considered as the case study, using the basic boundary condition of uniform heat flux at the outer duct surface.
Apart from consideration of boundary condition effect *per se*, the buoyancy effects have been treated for values of the modified Rayleigh number, Ra_q, up to $5x10^6$; the forced convection contribution has been for two values of the entry Reynolds number, Re_o = 1000, and 500.
The conjugate effects of convection, and conduction in the duct wall (either peripheral and axial), have been given special emphasis.

In synthesis, the following has been treated:

- thermal inlet region with forced convection flow (the standard Graetz problem), and with axial wall conduction (the conjugate Graetz problem);
- buoyancy effects with the standard (axially and peripherally) uniform heat flux boundary condition (case **H2**);
- buoyancy effects with a high conductivity wall, and a uniform heat flux at the outer duct surface (conjugate boundary condition)
- the influence of wall conductivity on combined convection heat transfer, over a range encompassing the thermal properties of all the materials of practical use in heat transfer applications.

The last two items are specific to this Thesis, in that no previous numerical investigation had treated combined convection in ducts (of any orientation, or geometry) as a fully 3D conjugate feature.

The main findings are as below.

i. General effects of buoyancy are confirmed, in that both the total pressure loss, and the heat transfer coefficients are found to increase for increasing Ra_{qo}. At the highest

Ra_{qo}-value, the head loss has been predicted to increase up to 22%, over the appropriate constant property reference. However, the Nusselt number increases up to 150% in the downstream region.

ii. The wall conductivity value has little effect on the pressure drop. The sensitivity of Nu_z to the variation of wall conductivity is also moderate, but well evident over the range considered here. It increases for increasing Ra_{qo}.

iii. Peripheral wall conduction tends to reduce the local mean wall temperature, and to increase the Nusselt number, in comparison with the standard solution of the Graetz problem. As the intensity of buoyancy increases, convection becomes comparable with wall conduction, and the peripheral temperature gradient in the wall becomes significant. Temperature is higher at the top of the duct cross-section, indicating the occurrence of vertical temperature stratification in the fluid.

iv. Conduction also tends to equalize the wall temperature in the axial direction (the boundary condition of uniform wall temperature, **T**, would be approximated at the inner duct wall, for increasing the wall conductivity up to infinite). This results in lower Nu_z-values in the initial part of the duct, and enhanced heat transfer in the downstream region.
Even with a long heat transfer section, and a relatively thin wall, axial conduction have a remarkable influence on heat transfer. This increases in the presence of buoyancy.

v. With forced flow, the Nusselt number never presents the well known asymptotic trend of standard constant property cases, provided that the wall is sufficiently conductive. The same holds true in corresponding buoyancy affected circumstances.

vi. A fully developed condition is commonly used in the numerical modeling of combined convection. It represents, however an highly idealized situation, seldom occurring in practical applications. This conclusion can be of some value when interpreting experimental heat transfer results.

vii. The wall conduction problem being elliptic in nature, then end effects have a definite importance. Then, the non-dimensional length of the heat transfer section comes to play a definite role. Dimensional analysis indicates further that, in a circumstance of conduction conjugate with convection, either forced or combined, the Peclet number is an independent parameter, whose effect is not completely accounted for by the non dimensional axial coordinate, z^*.

viii. All the above arguments lead to the general conclusion that standard constant property predictions are not the correct reference to judge the onset and/or the extent of buoyancy effects. A forced convection, conjugate reference should rather be used.

Experimental runs have been modeled with the inclusion of wall effects. The agreement between predictions and measurements is found to be satisfactory. In particular, measured temperatures are in general, quite well consistent with predictions, both as for the trend, and the range of the temperature differences encountered in the downstream part of the test section. It can then be concluded that the above observations are corroborated with experimental evidence.

FLOW3D was one of the many possible alternatives for CFD modeling. Here it has been proved that the Code, not only has the potential to approach the three-dimensional conjugate combined convection problem, as, virtually, other CFD software, but can actually solve it reliably, and with affordable computational effort.

Various other items have been the considered in the frame of this Thesis. Most of them have been the subject of publications in Conference Proceedings, and in International Journals. A total of 14 research papers are presented in Appendix I, and demonstrate the Candidate's research activity in the context of convection.
Results encompass the effects of axial diffusion of heat and momentum in the fluid, conjugate conduction and convection, the influence of different thermal boundary conditions, the effect of property variations, and the case of purely natural convection, and of purely forced convection, the latter for Newtonian and non-Newtonian fluids. The study, implementation, and validation of standard, ie segregated, as well as novel, ie fully coupled, iterative algorithms, directed to treat the velocity-temperature coupling, is also part of this research.

This activity has been synthesized, and the main significance pointed out, in Ch.4.

The basic equations governing combined convection had initially been reviewed and extensively discussed, together with their related boundary conditions. An original non-dimensional form has been derived for the equations. This is presented in Ch.2.

Finally, the result of a massive literature survey is reported in Ch.3. This was the result of a very long-term work, and took a very substantial part of the Candidate's effort. Overall, more than 200 papers have been collate and reviewed, all relevant to laminar combined convection. The survey encompasses the effects of thermal boundary conditions, geometry, inclination, wall conduction, variable properties, and extends to consider flow stability problems, and of transitional regimes. The circular geometry and the uniform heat flux boundary condition have been considered with special care, in that context.

The literature survey has served to furnish the necessary background for all the successive, numerical and the experimental, work; more then that, however, it provides a comprehensive, updated and detailed synthesis of the present knowledge on combined convection flows.

7.2 - Suggestions for Further Work

The numerical predictions have demonstrated to be in very good agreement with the experiments, however, some of the observed experimental trends could not be found in the simulation, especially in the final part of the test section. It is argued that the disagreement in this region possibly derives from the omission of some, apparently non-significant, physical detail of the test section.

To improve the agreement further, the following short-term activity has been planned on the numerical side:

- design a new grid, with much higher refinement in the proximity of the wall, and increase, at least doubling, the number of the axial steps;
- include unheated lengths both upstream and downstream of the heated section, so as to achieve a more secure statement of the boundary conditions. Also, provide a model of both the geometry, and the thermal properties of the end blocks;
- consider the effect of temperature-dependent properties in full. This is of prime importance, also in the view of extending the range of the Rayleigh, Reynolds, and Prandtl numbers.

As for the experimental activity, (i) a new design of the outlet mixing chamber, should be provided, and (ii), most important, new high precision sensors used for measuring the inlet and outlet fluid temperature. The insertion of additional wall thermocouples is also in the frame of a short-term experimental program.

No attempt has been done here to generalize the results, in the sense that the range over which the various effects observed here are important or can be overlooked, has not been identified. This would of great practical importance, and remains to be done.

Other possible extensions of this study are the analysis of aiding and opposing flows in inclined and vertical ducts, and the consideration of other non-circular geometry, and boundary conditions.

A longer term, and more ambitious, program would include a detailed numerical analysis of the route to instability, for combined convection flows. This would imply the prediction of possible bifurcated solutions, using a '*true*' model (ie three dimensional, conjugate, and with variable-properties), so as to complement the scarce and incomplete information of today on this fundamental aspect of combined convection flows.

We conclude by indicating the practical implications of the work. They are twofold:

- on the predictive side, there is an increasing need for improved fluid dynamic and heat transfer predictions in high technology applications, such as the cooling of electronic equipment. The

present benchmarking exercise, supported by experimental validation, demonstrates the reliability of advanced numerical tools of today in the modelling of complex thermal-flow situations;

- on the applicative side, the performance of heat exchanger devices can only be improved on account of real-world complexity. This may imply the inclusion of *'secondary'* effects such as axial diffusion, buoyancy, conjugate conduction and convection, and variable-properties. In this context, the present work specifically contributes to identifying the interaction of wall conduction and combined convection effects, and forms the basis for establishing quantitative criteria for the optimization of wall size and material, to be embodied in the design procedure.

"COMBINED CONVECTION AND OTHER EFFECTS IN HEAT TRANSFER IN HORIZONTAL FLOWS"

APPENDIX I

LIST AND SET OF CANDIDATE'S PUBLISHED WORK

LIST OF CANDIDATE'S PUBLISHED WORK

P 1 - G.S. Barozzi, and, G. Pagliarini - A Method to Solve Conjugate Heat Transfer Problems: the Case of Fully Developed Laminar Flow in a Pipe - ASME, Journal of Heat Transfer, 107 (1), 1985; 77-83.

P 2 - G.S. Barozzi, G. Pagliarini, and, A.C.M. Sousa - Conjugate Heat Transfer in Vertical Tubes: Experimental and Numerical Study - Procs. '*11th Canadian Conference of Applied Mechanics*'., Edmonton, Alberta, Canada, June 1987; Vol. 2, C 58-59.

P 3 - G.S. Barozzi, and, E. Nobile - Scambio Termico Convettivo in Condotti con Distribuzione Esponenziale del Flusso Termico alla Parete - Atti 5° '*Congresso Nazionale U.I.T.*', Torino, I, June 1987; A 170-184.

P 4 - G.S. Barozzi, and, E. Nobile - Low Reynolds Number Heat Transfer and Fluid Flow in the Inlet Region of Parallel Plates - Atti 6° '*Congresso Nazionale U.I.T.*', Bari, I, June 1988; 141-152.

P 5 - E. Nobile, A.C.M. Sousa, and G.S. Barozzi - Turbulence Modeling in Confined Natural Convection - Atti 7° '*Congresso Nazionale U.I.T.*', Firenze, June 1989; 85-96.; *and*, International Journal of Heat and Technology, 7,(3-4), 1989; 24-35.

P 6 - E. Nobile, A.C.M. Sousa, and, G.S. Barozzi - Accuracy of Two-Equation Turbulence Modeling in Free Convection - in *Numerical Methods in Thermal Problems*, Procs. 6th Int. Conf., Swansea, UK., July 1989; Pineridge Press, Swansea, UK., 1989, Vol. 6, Part 1; 600-610.

P 7 - E. Nobile, T. Russo, and G.S. Barozzi - An Efficient Parallel Algorithm for the Numerical Solution of Navier-Stokes Equations Using FORTRAN Structured Multiprogramming - *Applications of Supercomputers in Engineering, ASE 89* , 1st Int. Conf., Southampton, UK., Sept. 1989, C.A. Brebbia, and, A. Peters, eds.; Elsevier, Amsterdam, 1989, Vol.1; 3-14.

P 8 - G.S. Barozzi, and, E. Nobile - Conjugate Heat Transfer in Forced Convection Cooling of Chip Arrays - in '*Heat Transfer in Electronic and Microelectronic Equipment*', Procs. 20th ICHMT Int. Symp., A.E. Bergles, ed., Hemisphere Pub. Co., New York, 1990; 709-723.

P 9 - E. Nobile, A.C.M. Sousa, and, G.S. Barozzi - Turbulent Buoyant Flows in Enclosures - in '*Heat Transfer 1990* ', Procs. 9th Int. Heat Transfer Conf., G. Hetsroni, ed., Hemisphere Pub. Co., New York, 1990; Pap. 5-NC-11, Vol. 2; 543-548.

P10 - G.S. Barozzi, and, M.W. Collins - Mixed Convection in Horizontal Ducts: an Overview of Numerical Methods - Atti 9° '*Congresso Nazionale U.I.T.*', Pisa, I, June 1991; 45-60.

P11 - G.S. Barozzi, and, A. Dumas - Convective Heat Transfer Coefficients in the Circulation - ASME, Journal of Biomechanical Engineering, 113, 1991; 308-313.

P12 - G. Pagliarini, and, G.S. Barozzi - Thermal Coupling in Laminar Double Pipe Heat Exchangers - ASME, Journal of Heat Transfer, 113 (2),.1991; 526-534.

P13 - E. Nobile, and, G.S. Barozzi - Un Approccio Numerico ai Problemi di Convezione Naturale e Mista ad Elevati Valori del Numero di Rayleigh - *Procs. 47th ATI Nat. Conf.*, Parma, I, Sept. 1992; Vol. I; 567-578.

P14 - S. Piva, G. Scarcella, G.S. Barozzi, and M.W. Collins - Comparison of Predictive and Experimental Data for Combined Convection in Horizontal Duct Flow - Procs. '*CMEM93 6th Intl. Conf. on Computational Methods and Experimental Measurements*', Siena, I, May 1993, C.A. Brebbia, and, G.M. Carlomagno, eds., Computational Mech. Pub., Southampton, Boston, UK; Vol.1, 169-182.

PAGE 179 ONWARDS

NOT DIGITISED BY REQUEST OF THE UNIVERSITY